Characterisation of the roles of Poz1 and Stn1 at *Schizosaccharomyces pombe* telomeres

A thesis submitted to the University of Sussex for the degree of Doctor of Philosophy

By

Jubed Omee Ahmed

September 2013

Declaration

I hereby declare that this thesis has not been and will not be submitted in whole or in part to another university for the award for any other degree. The work described herein is my own work except where otherwise stated.

Jubed Omee Ahmed

September 2013

Acknowledgements

UNIVERSITY OF SUSSEX

JUBED OMEE AHMED

A thesis submitted for the degree of DPHIL BIOCHEMISTRY

CHARACTERISATION OF THE ROLES OF POZ1 AND STN1 AT *SCHIZOSACCHAROMYCES POMBE* TELOMERES

SUMMARY

Telomeres protect the ends of chromosomes from the activity of DNA repair machinery and provide a solution to the end-replication problem. In humans, the core protein complex located at telomeres is known as shelterin and consists of six protein subunits. Although variation is seen in the telomeric complex between species, in fission yeast the complex has notable similarities to that of humans. Separately to shelterin, the CST complex (Cdc13/Stn1/Ten1) is conserved in budding yeast, plants and mammals and is thought to negatively regulate telomerase, in addition to being required for telomere protection. However, unlike Stn1 and Ten1, Cdc13 has not yet been identified in fission yeast.

Poz1 is a bridging molecule equivalent to TIN2 in human shelterin, which links the Taz1-Rap1 and the Pot1-Tpz1-Ccq1 sub-complexes, respectively bound to double- and single-stranded DNA at telomeres. Poz1 is required for the regulation of telomerase activity, and it has been hypothesised that it might do so by playing a structural role in the switching of telomeres from an open to a closed state. In this study, a reverse-2-hybrid approach was used to generate Poz1 alleles unable to interact with Rap1 or Tpz1 specifically. These alleles were subjected to phenotypic and biochemical analysis which indicated that neither individual interaction is sufficient to maintain telomere homeostasis. With telomere lengths similar to a Poz1 deletion, it is proposed that negative regulation cannot occur without the ability to form a closed complex.

Given that Cdc13 is currently the only missing component in fission yeast, a second study was initiated aiming to identify a homologue by yeast-2-hybrid screening of a cDNA library, using Stn1 and Ten1 as baits. However, this approach did not yield any positive candidates. In an alternative approach, Stn1 temperature-sensitive (ts) alleles were generated and characterised. These were used to screen a genomic library for suppressors of the Stn1 ts phenotype. Several candidates were identified that require further examination while the ts allele analysis indicated that telomeres are lost in their entirety at non-permissive temperatures and that survivors of this process did so by chromosome circularisation, similar to Pot1 mutants.

Table of Contents

Table of Figures

Table of Tables

List of Abbreviations

Δ: Gene deletion

3-AT   3-Amino-1,2,4-triazole

5-FOA: 5-Fluoroorotic Acid

APS: Ammonium persulphate

bp: base pairs

BSA: Bovine Serum Albumin

CFU: Colony Forming Unit

ChIP: Chromatin Immuniprecipitation

DDR: DNA Damage Response

DMSO: Dimethyl Sulfoxide

DNA: Deoxyribonucleic acid

dNTP: deoxyribonucleotide triphosphate

DSB: Double Strand Break

dsDNA: double-stranded DNA

EDTA: Ethylenediamine tetraacetic acid

g: Gram

GAD: Gal4 Activating Domain

GBD: Gal4 Dna Binding Domain

GFP: Green Fluorescent Protein

HR: Homologous Recombination

Hs: *Homo sapiens*

HU: Hydroxyurea

IP: Immuniprecipitation

kb: Kilobases

kDa: Kilodalton

L: Litre

M: Molar

ml: millilitre

mM:	millimolar
MMS:	Methyl Methane Sulphonate
NHEJ:	Non-homologous End Joining
ORF:	Open Reading Frame
PBS:	Phosphate Buffered Saline
PCR:	Polymerase Chain Reaction
PMSF:	Phenylmethanesulfonyl fluoride
RCF:	Relative Centrifugal Force
RMCE:	Recombinase-mediated Cassette Exchange
RPA:	Replication Protein A
RPM:	Revolutions Per Minute
RT:	Room Temperature
Sc:	*Saccharomyces cerevisiae*
SDS:	Sodium Dodecyl Sulphate
SDS-PAGE:	Sodium Dodecyl Sulphate Polyacrylamide Gel Electrophoresis
Sp:	*Schizosaccharomyces pombe*
SSB:	Single Strand Break
ssDNA:	single-stranded DNA
TBE:	Tris/Borate/EDTA Buffer
TBS:	Tris-Buffered Saline
TCA:	Trichloroacetic Acid
TE:	Tris/EDTA
TEMED:	Tetramethyl-ethylenediamine
YES:	Yeast Extract/Supplements
YNG:	Yeast Nitrogen/Glutamate
YPAD:	Yeast extract/Peptone/Adenine/Dextrose
Sc:	Synthetic complete (*S. cerevisiae* media)
Wt:	Wild-type

Chapter 1

Introduction

1.1 *Schizosaccharomyces pombe* as a model organism

Fission yeast, *S. pombe*, when compared to brewer's yeast *S. cerevisiae* may not be so widely known in the general public, but it plays a key role in research as a model organism. Though fission yeast is as evolutionarily distinct from mammals as they are from budding yeast, the levels of homology in areas such as DNA replication, damage repair and, in this case, telomere maintenance are remarkable (Sipiczki, 2000). As a result, fission yeast has become a widely used model organism in the study of various aspects of human biology. The similarities in form and function of telomeres in particular, combined with the ease of genetic manipulation, have made it a useful tool in the study of telomere biology (Dehé and Cooper, 2010, Forsburg, 1999, Wixon, 2002).

1.1.1 *S. pombe* characteristics

Schizosaccharomyces pombe is a rod-shaped single-celled eukaryote in the phylum Ascomycota which divides by medial cell division, as opposed to the budding in *S. cerevisiae*. Originally isolated in the 1920's, the laboratory strains used as model organisms today can be grown vegetatively as haploids but also as diploids with the appropriate selection. Typical wild-type haploid cells are 8-14µm in length at division and 4µm wide (Sabatinos and Forsburg, 2010). Throughout the 2-5 hour cell cycle, which varies dependent on the culture conditions, the width tends to remain constant while the length increases until cell division occurs. Diploid cells can be identified as proportionally larger cells and can be grown vegetatively through the use of complementing alleles such as *ade6-210* and *ade6-216*. Individually, these produce an Ade⁻ phenotype but together produce an Ade⁺ phenotype. Diploids, however, can be unstable and a proportion of cells in each generation tend to sporulate, regardless of selection

(Forsburg and Rhind, 2006). The *S. pombe* genome, originally published in 2002 (Wood *et al.*, 2002), is 13.8 Mb in size, spread across three chromosomes, I (5.7 Mb), II (4.6 Mb) and III (3.5 Mb) (Wixon, 2002) and currently consists of 5123 catalogued protein coding genes. The names of genes and proteins used herein reflect the updated names in the PomBase database, which now conform with the names of homologous proteins in human cells, where available (Wood *et al.*, 2012).

1.1.2 The *S. pombe* cell cycle

The *S. pombe* haploid cell cycle is divided into several phases, as is consistent with other organisms. In S-phase, the genome is duplicated while in M-phase it is divided for distribution to two daughter cells. As with other eukaryotes, two gap phases, G1 and G2, are present. However, in this case, the cells largely favour remaining in G2 for the majority of the cycle. The proportions of each phase are: G1 (10%), S (10%), G2 (70%) and M (10%). In wild-type cells, nuclear division occurs early in the cycle, such that the nuclei enter G1 and S-phase before cell division occurs. As a result, unlike *S. cerevisiae*, daughter cells are formed already in G2 phase (Sabatinos and Forsburg, 2010). Most cells, therefore, contain 2C DNA, either due to being in G2 phase, or already having two nuclei in G1 and S-phase.

These phases of the cell cycle, as in other eukaryotes, are controlled by cyclin-dependent kinases (CDKs) which phosphorylate target proteins in response to changing cellular levels of cyclins. Higher eukaryotes have multiple CDK proteins while fission and budding yeast only contain one each. The *S. pombe* CDK, Cdc2, and *S. cerevisiae* Cdc28, were the first CDKs identified (Nurse, 1997). Cdc2 functions in complex with a cyclin protein component, the degradation of which results in Cdc2 deactivation. During S-phase, as well as early M-phase, cyclin levels and, therefore, Cdc2 activity are modulated to initiate DNA replication and chromosome segregation respectively.

During G1 phase, Cdc2 is in complex with the cyclin Cig1. This complex deactivates Rum1, an inhibitory protein, which results in increasing levels of the complex. When a threshold level of Cdc2-Cig1 is passed, entry into S-phase is triggered. The complex then disassembles as levels of the Cig1 cyclin decrease. Cdc2 then forms complexes with the Cdc13 cyclin, which not to be confused with the *S. cerevisiae* Cdc13 telomere protein. Levels of Cdc2-Cdc13 complex increase until, once again, a threshold is reached. This triggers entry into M-phase (Legouras *et al.*, 2006). Additional control of Cdc2-Cdc13 is exerted by the regulatory kinases, Wee1 and Mik1, and phosphatase, Cdc25. Phosphorylation of Cdc2 by Wee1 or Mik1 results in deactivation while phosphatase action by Cdc25 results in reactivation (Nurse, 1997). These processes occur as part of an overriding mechanism which regulates progression from one cell cycle phase to the next.

1.2 DNA replication in *S. pombe*

1.2.1 Overview of replication

All eukaryotic genomes go through a complete and accurate duplication during S-phase; indeed it is the initiation of replication that defines the beginning of S phase. A semi-conservative replication mechanism is present in eukaryotes which ensures the genome is duplicated accurately and only once (Takeda and Dutta, 2005). Unlike bacteria, which initiate replication from a specific point in the genome, eukaryotes use multiple origins of replication. In *S. pombe*, as well as higher eukaryotes, the origins of replications are not defined by a specific sequence but do consist of AT-rich sequences that can vary from 500bp to 1500bp in length (Legouras *et al.*, 2006, Segurado *et al.*, 2003). This is in contrast to *S. cerevisiae* which has smaller, specific origin sequences (Palzkill and Newlon, 1988). The number of origin sequences present in eukaryotes is also degenerate, in that there are many potential origins of which only a subset are used to initiate replication in any one passage through S phase.

In *S. pombe*, a pre-replication complex forms at origins in late M phase and G1 which initially consists of the ORC complex, containing 6 subunits (Orc1-6), followed by MCM, a replicative helicase, also containing 6 subunits (Mcm2-7), that is initially loaded in an inactive form (Blow and Dutta, 2005). The loading of ORC and MCM is termed licensing, where potential origins are selected for activation. In *S. pombe* this is thought to at least party consist of the Orc4 subunit interaction with the AT-rich origin sequences. The timing of this licensing is dependent on the proteins Cdc18 and Cdt1 which are only present during late M phase and G1 (Legouras *et al.*, 2006).

In S phase, MCM helicase activation and maturation of the pre-replication complex to the pre-initiation complex, depends on phosphorylation by two kinases, DDK (composed of Hsk1 and Dpf1) and Cdc2 (Labib, 2010). A number interactions between these and other factors results in the recruitment of Cdc45 and GINS, which are thought to form the active helicase complex

with MCM as well as recruitment of the replication polymerase, Pol-ε. This leads to the subsequent initiation of replication (Moyer *et al.*, 2006).

Replication is bidirectional, consisting of two replication forks travelling in opposite directions, where Pol-ε is continuously synthesising DNA in the 5'-3' direction away from the origins. This refers to the leading strand. The lagging strand is synthesised in fragments in the 5'-3' direction. As the replicative helicase, MCM, unwinds the DNA, the heterotrimeric RPA complex (Ssb1-3) coats the exposed single-stranded DNA. Controlled by Pol-α/primase, RNA primers are synthesised and used to initiate replication on this strand, which is then completed in short stretches (200bp to 1000bp) by Pol-δ (Miyabe *et al.*, 2011, Stillman, 2008). These Okazaki fragments require more processing than the leading strand (Okazaki *et al.*, 1968). On reaching the RNA primer of the previous fragment, Pol-δ removes the primer, fills-in the resulting gap and generates a 5' flap of DNA. This flap is removed by the endonucleases, Rad2 and Dna2 and the adjacent Okazaki fragments are ligated to complete synthesis (Burgers, 2009).

If progression is unhindered, replication will be terminated when one fork encounters another fork from a neighbouring origin or replication reaches the telomeres at the chromosome termini. This would normally complete synthesis of this section of DNA. However, if fork progression is stalled due to an encounter with a DNA secondary structure, damage or other Protein-DNA complexes, all of which can hinder progression, the obstacle must be removed or bypassed before replication can be completed. Stalled forks, where the replication complex is still present, and collapsed forks, where the replication complex has disbanded, result in an arrest in the cell cycle. Once the barrier to progression has been removed, the replication forks can be rescued and cell cycle progression continued (Lambert and Carr, 2005). Telomeres are notorious for being fragile sites with secondary structures that impede replication in this manner (Ishikawa, 2013). In addition to this, telomeres have to compete with the end-replication problem, as explained in a following section.

1.3 Responses to DNA damage in *S. pombe*

1.3.1 Checkpoints

For long term survival, cells must withstand DNA lesions, including double-strand and single-strand breaks, during S phase replication and throughout the rest of the cell cycle. Signal cascades, known as checkpoints, triggered on the detection of damage at various stages halt the progression of the cell cycle until the damage is suitably repaired. These checkpoints are well conserved between humans, fission yeast and budding yeast (Carr, 2002, Zegerman and Diffley, 2009).

Though several different checkpoints can be defined, the ones that respond to replication stress and DNA damage specifically have essentially the same outcome; arrest of the cell cycle and activation of the most suitable repair pathway (Carr, 2002). Typically, exposure of single-stranded DNA or double-strand breaks can initiate a checkpoint response. As previously mentioned, in *S. pombe*, single-stranded DNA (ssDNA) is coated with RPA as part of the usual replication process. When a replication fork encounters a DNA lesion or other replication stress, however, the helicase may continue unwinding the DNA to form longer stretches of ssDNA which result in accumulation of RPA (Sogo *et al.*, 2002). In the case of exposed double-strand breaks (DSBs), 5'-3' exonuclease activity which, mediated by MRN^{MRN} (Mre11-Rad50-Nbs1), $Ctp1^{CtIP}$ and $Exo1^{Exo1}$, exposes ssDNA, leading to the same accumulation of RPA as replication stalling. MRN also recruits $Tel1^{ATM}$ to activate signalling of damage through phosphorylation of various substrates as part of the response to repair the break (Raji and Hartsuiker, 2006).

The $Rad26^{ATRIP}$ protein and its partner, the $Rad3^{ATR}$ kinase, are recruited to the RPA-coated ssDNA. Independently, the $Rad17^{RAD17}$ clamp loader and associated proteins, Rfc2-5, as well as the 9-1-1 complex, $Rad9^{RAD9}$-$Rad1^{RAD1}$-$Hus1^{HUS1}$, are recruited (Caspari *et al.*, 2000). These bind to the ssDNA-dsDNA junction. Recruitment of $Rad4^{TopBP1}$ by $Rad9^{RAD9}$ leads to activation of

Rad3^{ATR}. A phosphorylation signal cascade is then initiated, passed from Rad3^{ATR} through Crb2^{53BP1} at DSBs or Mrc1^{Claspin} in replication stress and leads to activation of either Chk1^{CHK1} or Cds1^{CHK2} respectively. These then activate cell cycle arrest through either Wee1 or Mik1 and inhibition of Cdc25 resulting in deactivation of the CDK, Cdc2 and, therefore, prevention of the transition to M phase (Carr, 2002, Caspari and Carr, 2002, Xu *et al.*, 2006).

1.3.2 Repair

When a cell cycle arrest is triggered by the detection of DNA damage, be it during replication or otherwise, appropriate repair pathways are activated. Depending on the type of lesion, one of the following repair processes would be employed: Base Excision Repair (BER), Nucleotide Excision Repair (NER) and Mismatch Repair (MMR) for single-strand lesions and Non-Homologous End Joining (NHEJ) or Homologous Recombination (HR) for double-strand breaks (Hoeijmakers, 2001, Li *et al.*, 2012, Raji and Hartsuiker, 2006).

1.3.2.1 The single-strand lesion repair pathways: BER, NER and MMR

Lesions affecting one strand of the DNA helix are corrected by one of three main pathways, Base Excision Repair (BER), Nucleotide Excision Repair (NER) or Mismatch Repair (MMR).

1.3.2.1a BER

Damaged bases, as a result of oxidation, alkylation or deamination, are repaired though BER, a conserved mechanism across prokaryotic and eukaryotic species (Robertson *et al.*, 2009). DNA glycosylases remove the damaged base to produce an apurinic or apyrimidinic site (AP sites). These become the target of repair proteins, including AP endonucleases that cleave the phosphodiester backbone as well as polymerases, helicases and ligases that replace either a single (short patch repair) or at least two (long patch repair) nucleotides and ligate the newly synthesised section (Mol *et al.*, 2000, Robertson *et al.*, 2009).

1.3.2.1b NER

Bulky lesions that distort the DNA double helix, such as pyrimidine dimers, are repaired through the NER pathway. This is divided between global genome repair (GGR) and transcription coupled repair (TCR) (Hoeijmakers, 2001). Both GGR and TCR excise the affected nucleotides then synthesise and ligate the new DNA, however, as the names indicate, unlike GGR, TCR is specifically linked to repair of actively transcribed genes. Although the mechanisms are fairly well conserved, the number of proteins required does vary between species.

1.3.2.1c MMR

In the case of MMR, mismatched nucleotides, which are inserted during synthesis despite the high fidelity and proofreading ability of the polymerases, are repaired through this highly conserved mechanism. The strand containing the mismatched nucleotides is recognised by the Msh2-Msh6 heterodimer, which bind to mismatches, small insertions and deletions while the Msh2-Msh3 heterodimer binds larger loops that are a result of insertions or deletions. These incorrect bases are degraded by the exonuclease action of Exo1 and resynthesised by Pol-δ to complete repair (Fleck and Nielsen, 2004, Hoeijmakers, 2001).

1.3.2.2 The double-strand break repair pathways: NHEJ and HR

Damage events that result in breaks in both strands of the DNA double helix are highly cytotoxic and can be caused by a variety of internal and external factors. Internal factors include collapsed replication forks, reactive oxygen species (ROS) and meiotic recombination. The latter being a programmed series of double-strand breaks induced to bring about genetic diversity. External factors include ionising radiation and chemicals that damage DNA. The repair of these falls under the scope of two major mechanisms, Non-Homologous End Joining (NHEJ) and Homologous Recombination (HR) (Raji and Hartsuiker, 2006, Sung and Klein, 2006).

1.3.2.2a NHEJ

Non-Homologous End Joining is a potentially error-prone mechanism which essentially takes the two free ends of the double-strand break and ligates them to complete repair. Depending on the nature of the break, this can result in the loss of several nucleotides due to end processing. For example, should the break leave single-stranded overhangs, these would be removed before re-joining the ends (Fleck and Nielsen, 2004). As a result, this method tends to only be preferred when a sister chromatid or other homologous template is not available. In fission yeast, although the prevalent repair mechanism is HR, during the short time when only 1C DNA is present NHEJ becomes the prevalent mechanism. Indeed, lab strains held in G1 by nitrogen starvation use NHEJ 10-fold more than HR (Ferreira and Cooper, 2004). In human cells, due to sister chromatid availability only during late S and G2 phase, NHEJ remains the major pathway for repair (Radhakrishnan *et al.*, 2014).

The mechanism for NHEJ is well conserved. In *S. pombe* the ends of the double-strand break are bound by the Ku70/Ku80 heterodimer. In mammals, the DNA-PKcs and XRCC4, which are involved in processing of the ends, are also recruited (Mahaney *et al.*, 2009). No homologues of either DNA-PKcs or XRCC4 have yet been identified in *S. pombe*. XLF and Ligase IV, however, are conserved as Xlf1 and Lig4 and work to complete the ligation of the two ends (Cavero *et al.*, 2007). If additional processing of the ends is required, such as in the presence of overhangs or secondary structures that are prohibitive to ligation, additional factors can be recruited. In human cells these include the nucleases Artemis and APLF for removal of overhangs by exonuclease and endonuclease activity, Polymerases µ and λ for gap filling, PNK for 3'-phosphatase and 5'-kinase action on non-ligatable nucleotides and the RecQ helicase, WRN, for unwinding of secondary structure (Mahaney *et al.*, 2009). In *S. pombe*, Pol4 has been shown to be required for gap filling while Ctp1 and Exo1 may be used in exonuclease activity (Li *et al.*, 2012).

1.3.2.2b HR

Homologous Recombination is, in theory, an error-free mechanism. It requires a homologous sequence, such as a sister chromatid, as a template to complete repair without loss of nucleotides. The availability of a homologous sequence can depend on the cell cycle stage. For example, in *S. pombe* the long G2 phase means a homologous sequence is available for most of the cell cycle. As a result, HR is the primary mechanism of repair (Ferreira and Cooper, 2004, Raji and Hartsuiker, 2006).

The classical Szostak model of HR is a highly conserved mechanism that has been well studied (Szostak *et al.*, 1983). In *S. pombe*, on detection of the double-strand break by the MRN complex, as described earlier, a checkpoint signal is activated through Tel1. MRN, in combination with Ctp1, initially resect the ends of the double-strand break in the 5'-3' direction (Limbo *et al.*, 2007, Williams *et al.*, 2010). This is followed by further resection by Exo1 and Dna2 such that RPA is able to coat the exposed single-stranded overhangs (Langerak *et al.*, 2011). The RPA is replaced by Rad51, facilitated by Rad52, to generate a 3'-nucleoprotein filament that is able to invade a homologous template (Krogh and Symington, 2004). Invasion of a homologous strand by one of the overhangs, displacement loop (D-loop) generation and subsequent strand extension is dependent on Rad54 DNA-dependent ATPase activity. Extension of the invading strand is conducted by Pol-δ, recruited by PCNA, as with standard DNA replication (Li *et al.*, 2009). In the Szostak model, the second Rad51-coated overhang is then able to invade, using the D-loop as a template for extension. When the 3' invading strands are sufficiently extended, they are able to ligate to the 5' ends of the double-strand break to generate a double Holliday junction (Szostak *et al.*, 1983). The Mus81 and Eme1 resolvases, which cleave the double Holiday junction, then generate a crossover or non-crossover resolution, completing repair (Krogh and Symington, 2004, Raji and Hartsuiker, 2006).

1.3.2.3 Other repair mechanisms

In addition to this standard NHEJ and HR pathways described, additional mechanisms have also been identified. These include Microhomology-Mediated End Joining (MMEJ), Single-Strand Annealing (SSA) and Synthesis-Dependent Strand Annealing as variations to the NHEJ and HR mechanisms (McVey and Lee, 2008, Radhakrishnan *et al.*, 2014, Raji and Hartsuiker, 2006).

1.3.2.3a MMEJ

The MMEJ mechanism repairs double-strand breaks through the use of microhomology, typically 5-25 nucleotides on each side of the break, and results in a loss of the intervening sequence. As a result, this mechanism, which has been observed in both yeast and human cells, can contribute to genome instability. It could be considered as a fall-back mechanism in some circumstances as it is observed when key NHEJ proteins, such as Ku70/Ku80, are absent but has also been observed in V(D)J recombination, indicating it does have a physiological purpose (McVey and Lee, 2008, Truong *et al.*, 2013).

The initial steps in MMEJ appear to be the same as for HR, that is, recruitment of and resection of the DNA ends by the MRN complex. Further resection may be carried out by other exonucleases, such as Exo1, until sufficient microhomology is exposed on each side of the break. These can then anneal. Repair is completed by flap-trimming of any excess nucleotides, polymerase extension to fill in any remaining gap and, finally, ligation. It is likely that this method would produce some nucleotide mismatches and so the repaired sequence may also be a substrate for the mismatch repair pathway (McVey and Lee, 2008).

1.3.2.3b SSA

The SSA mechanism has been studied in *S. pombe*, *S. cerevisiae* and also in human cells. It is somewhat similar to MMEJ in that it relies on resection of the double-strand break ends to expose regions of homology. There is also a loss of the intervening sequence. However, unlike

MMEJ, it requires Rad52 for strand annealing, making it a distinct pathway (Rudin and Haber, 1988, Truong *et al.*, 2013).

Similar to the initial processes in Homologous Recombination, MRN and Ctp1-dependent resection occurs in the 5'-3' direction on the two ends of the double-strand break. Unlike HR, however, rather than using a homologous sequence on a sister chromatid, resection continues until direct repeats of complementary sequence are exposed on the 3' resected strands (Raji and Hartsuiker, 2006). Studies in *S. cerevisiae* indicate that the size of the sequences need only be a few nucleotides but larger sequences increase efficiency (Sugawara *et al.*, 2000). These direct complimentary repeats anneal in a manner that is dependent on Rad52, leaving long single-stranded DNA flaps. Removal of these DNA flaps is dependent on Rad16 and Swi10 endonuclease action in *S. pombe* as well as Msh2-Msh3 in *S. cerevisiae* (Raji and Hartsuiker, 2006, Sugawara *et al.*, 1997, Wang and Baumann, 2008). This results in repair of the break.

1.3.2.3c SDSA

The SDSA mechanism is, once again, similar to HR in the initial stages and has been proposed as an alternative to the classical Szostak model for non-crossover repair. MRN and Ctp1-dependent resection, followed by more extensive resection by Exo1, occur on the ends of the double-strand break. However, after initial strand displacement to a homologous template sequence takes place to create a D-loop, sufficient extension of the invading strand results in a second strand displacement event. This time, the newly synthesised 3' strand anneals back to the other exposed 3' overhang from the initial resection. Any gaps left in the sequence can then be filled by Pol-δ using the newly synthesised DNA as a template. The result is repair without the formation of a double Holliday junction or crossovers (Pâques and Haber, 1999, Raji and Hartsuiker, 2006).

1.4 Telomeres

The structure of eukaryotic chromosomes enables a vast amount of DNA to be compacted into the nucleus of each cell. These linear structures are composed of a tightly packed arrangement of chromatin, made up of DNA wrapped around histone octamers, which is in a constant state of flux. During the cell cycle, transcription, replication and repair factors require access to the DNA and the chromatin packing is modified accordingly. Active regions, referred to as euchromatin, are more loosely packaged while less active regions, referred to as heterochromatin, are more tightly packaged (Huisinga *et al.*, 2006, Tamaru, 2010).

A conserved feature at the ends of most eukaryotic chromosomes is a series of tandem arrays of G-rich sequences known as telomeres. These have been extensively studied in recent years and are prevalent in most model organisms (Dehé and Cooper, 2010, Jain and Cooper, 2010). There are, however, several exceptions to this, such as the fruit fly, *Drosophilla melanogaster*, which caps chromosomes with arrays of retrotransposons (Biessmann *et al.*, 1990). The structure and maintenance of these may differ from other eukaryotes, but the function remains the same (Mason *et al.*, 2008). The structural features of telomeres, as well as the proteins that associate with them, have a significant impact on genome stability. Though the repeat sequence, the length of the arrays and the specific proteins that associate with telomeres can vary considerably between organisms, the core functions are retained. These are to provide a solution to the end-replication problem and to protect the chromosome ends from the action of DNA repair mechanisms, the breakdown of both functions being implicated in various disease states (Jain and Cooper, 2010, Lu *et al.*, 2013).

Telomeres are also considered fragile sites, that is, they are prone to secondary structures that may cause replication stress and collapse. However, the proteins associated with telomeres, as explained in a following section, can manage these structures and restart collapsed forks to ensure replication is completed (Ishikawa, 2013).

1.4.1 The end-replication problem

The fact that, other than in certain circumstances, eukaryotic chromosomes tend to be linear structures presents a problem for the replication complex. Although the leading strand can be replicated to the very end of the chromosome, on the lagging strand, the removal of the RNA primer results in a small 3' single-stranded overhang which cannot be filled-in by the conventional replication process. Without a corrective system in place, over multiple cell cycles this would eventually result in the loss of crucial genetic information. This is known as the end-replication problem [Fig 1.1] (Jain and Cooper, 2010, Palm and de Lange, 2008).

Telomeres, being composed of many tandem repeats of DNA, provide a solution to this problem, protecting the chromosome from the loss of essential genetic information by acting as a buffering system. In human somatic cells this results in an ability to undergo multiple cell divisions over a lifetime before the telomeres reach a critical minimum length and the cells are directed towards senescence or apoptosis. Germ-line cells, on the other hand, can have unlimited replicative potential through rejuvenation of the telomeres using the enzyme Telomerase. This enzyme, which is not as active in most somatic cells compared to germ-line cells, can maintain the length of telomeres within a safe range when under proper regulation (Chan and Blackburn, 2004, de Lange, 2009, Harley *et al.*, 1990, Hug and Lingner, 2006).

In certain disease states, such as the majority of cancers, telomerase activity becomes up-regulated. This provides the cells with the possibility of bypassing the limitations on cell proliferation and gain unlimited replication potential (Shay *et al.*, 2001). On the other hand, in some cancers, rather than up-regulating telomerase, the protective ability of telomeres is compromised. However, rather than resulting in genome instability, a telomerase-independent recombination-dependent mechanism, known as Alternative Lengthening of Telomeres (ALT), works to maintain the telomeres (Henson *et al.*, 2002). These mechanisms are key factors that allow cancerous cells to proliferate and, as such, make telomerase and its regulatory processes

the targets in therapeutic strategies in combating cancers and aging-related disease states

(Blasco, 2005).

Figure 1.1: **Schematic demonstrating the End-Replication Problem, based on (Jain and Cooper, 2010) (following page).**

(A) Replication through to a telomere containing an overhang. **(i)** Replication fork progressing through telomere towards the chromosome terminus that ends with a 3' G-rich overhang. Leading strand replication is indicated by dark blue arrows. Lagging strand replication is indicated by red arrows. RNA primers used in lagging strand replication are indicated in light blue. **(ii)** Leading strand replication is able to progress to the end of the chromosome. Lagging strand replication results in Okazaki fragments (short sections of DNA replicated from and RNA primer). **(iii)** Removal of terminal RNA primer from lagging strand results in a small 3' overhang. Leading strand replication has resulted in a blunt end and a slightly shorter overall sequence. **(B) (i)** Complete blunt ended telomere ready for replication. **(ii)** Replication fork approaching blunt ended telomere. **(iii)** Completion of replication to the end of the chromosome results in the leading strand generating a blunt end. The RNA primer on the lagging strand is still present. **(iv)** The removal of the RNA primer from the lagging strand generates a 3' overhang while the leading strand replication did not. There is an overall loss of telomeric sequence in this second round of replication.
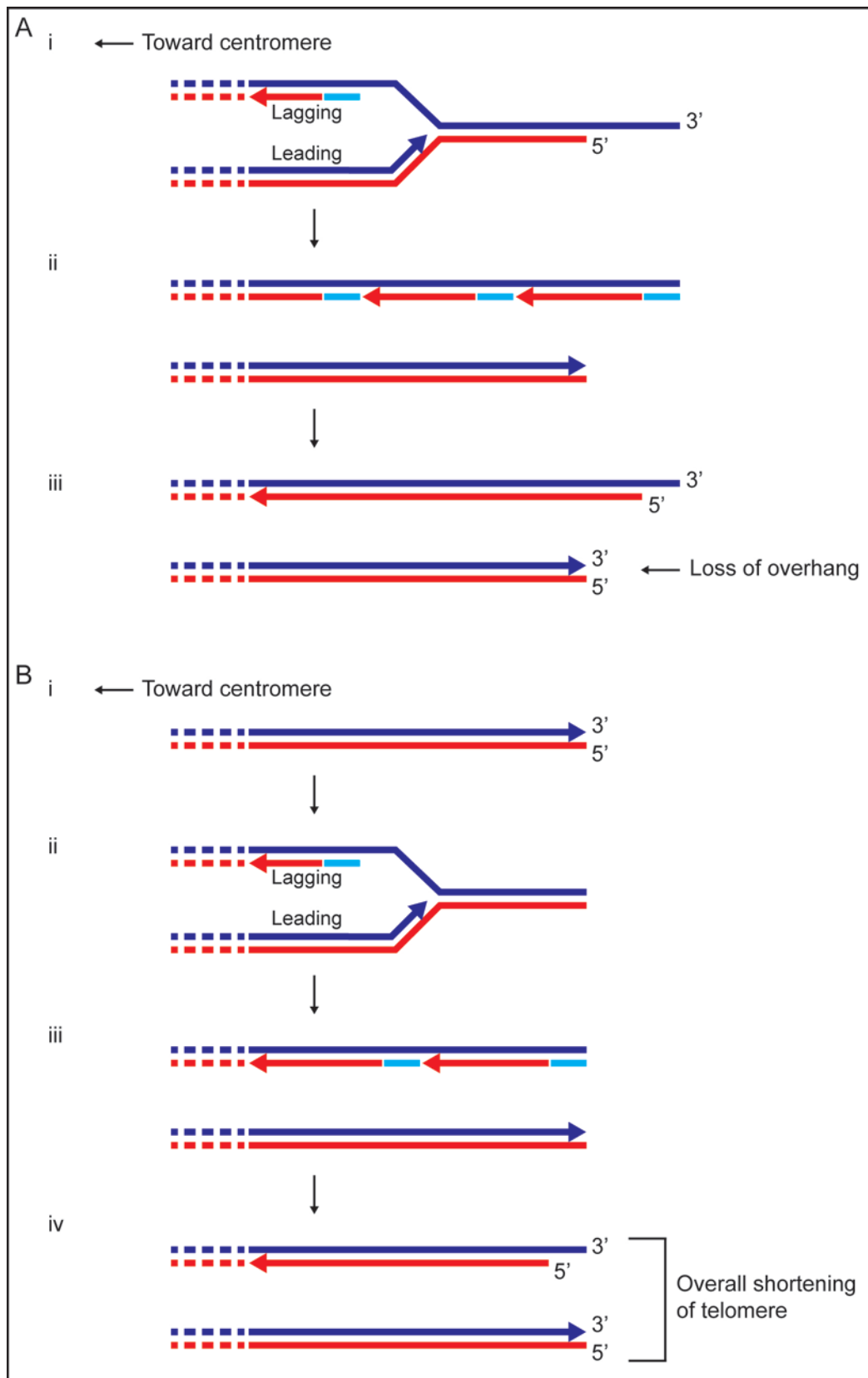
1.4.2 The chromosomal end-protection problem

The double-strand break repair pathways are of particular relevance to telomeres. As eukaryotic chromosomes are linear structures, the ends can mimic a double-strand break (Jain and Cooper, 2010). Indeed, the 3' overhang generated from incomplete replication of the lagging strand makes it an ideal target for the double-strand break repair pathways. Without a mechanism in place to shield the chromosome ends from the repair actions of NHEJ and HR, end-to-end chromosome fusions would occur. This would generate dicentric chromosomes that could be pulled in opposite directions during segregation in anaphase, leading to chromosome breakage and mis-segregation of the DNA between daughter cells, resulting in genetic instability (Capper *et al.*, 2007). This is the chromosomal end-protection problem to which the telomeres provide a solution.

The unique t-loop structural feature, maintenance of correct telomere length (telomere homeostasis), as well as the actions of various telomere-associated proteins provide the protection required to maintain genome integrity (Palm and de Lange, 2008). This protective function is well conserved in yeast, especially so in the fission yeast, *S. pombe*. In addition, and perhaps counterintuitively, several components of the DNA damage response mechanisms also contribute to maintenance of telomeres, as explained in a following section. A breakdown of these mechanisms maintaining the chromosome ends has been implicated in various disease states, including cancer development and, as such, is a focus of much study (Chan and Blackburn, 2004, Lu *et al.*, 2013).

1.4.3 Telomere structure

As already stated, telomeres consist of G-rich tandem repeats that, with the associated proteins, function to provide a solution to the end-replication problem and the chromosome end-protection problem. Eukaryotic telomeric repeat sequence and length varies from species

to species. In humans, the telomere repeat sequence, 5'-TTAGGG-3' and can vary from 5kb to 15kb in length. Yeast telomeres tend to be much shorter and heterogeneous, with fission yeast, *S. pombe*, containing 5'-TTACAG$_{2-5}$-3' repeats and budding yeast, *S. cerevisiae*, containing 5'-TG$_{2-3}$(TG)$_{1-6}$-3' repeats, both between 250 and 400bp in length (Kanoh and Ishikawa, 2003). A variation in telomere length is foundnot just between individual cells but also between each chromosome end within each cell (Lansdorp *et al.*, 1996).

In addition to these terminal repeats, human chromosome ends consist of associated subtelomeric regions. These regions, which contain highly repetitive sequences that are similar to the terminal telomeric repeats, are found within the 500kb region proximal to the telomeric repeats and tend to have increasingly divergent sequence with increasing distance from the telomere (Riethman *et al.*, 2005). Subtelomeric regions are, similarly, found in *S. pombe*, and can be separated into Sub-Telomeric Elements, STE1-3, which make up the 19kb region proximal to the telomeric repeats on chromosomes I and II. The third chromosome, Chromosome III, contains large blocks of rDNA, which are located proximal to the telomeric repeats, rather than the STE1-3 sequences (Dehé and Cooper, 2010).

1.4.3.1 The t-loop structure at telomeres

The telomeres, be they human, yeast or otherwise, have a double-stranded region followed by a single-stranded 3' overhang, composed of the G-rich strand. The majority is double-stranded with a short overhang, 150-300bp in humans and approximately 30 nucleotides in fission yeast, though it may actually be less than this (Tomita *et al.*, 2003, Wright *et al.*, 1997). Due to the nature of the DNA replication machinery, the leading strand is synthesised to the very end of the telomere, leaving no overhang. The nucleases, Exo1 and Apollo, have been implicated in resecting the end of telomeres, both with and without overhangs, to increase and maintain 3' overhang length at both telomeres on each chromosome (Tomita *et al.*, 2004, Wu *et al.*, 2012).

Mammalian telomeres have been shown to form a telomeric loop (t-loop) structure both *in vitro* and *in vivo* [Fig 1.2A]. These are thought to result from the 3' overhang being able to fold back on itself (t-loop) and invade the double-stranded region of the telomere, displacing the G-rich strand (Griffith *et al.*, 1999, Stansel *et al.*, 2001). These t-loops have since been observed in other species (Cesare *et al.*, 2003, Muñoz-Jordán *et al.*, 2001, Murti and Prescott, 1999). This includes fission yeast, which was at first thought to contain telomeres and overhangs that were too short to form t-loops. However, though they were found, the t-loop structures were only obtained *in vitro* using artificial telomeres and only formed in up to 13% of samples (Tomaska *et al.*, 2004). The ability to form t-loops was shown to depend on the presence of the telomere-specific dsDNA-binding proteins, TRF1 and TRF2 in humans and Taz1 in fission yeast (Bianchi *et al.*, 1997, Griffith *et al.*, 1999, Tomaska *et al.*, 2004). These t-loops, by masking the exposed end of the telomere, are thought to contribute to telomere capping by inhibiting access for DNA repair proteins, such as nucleases and ligases but can be disassembled for replication, as required (de Lange, 2004, Luke-Glaser *et al.*, 2012).

1.4.3.2 The G-quadruplex structure at telomeres

Another structure that has been observed in telomeric regions is the G-quadruplex (also known as G-quartet or G4-DNA) [Fig 1.2B]. This is a highly stable structure that can be found in G-rich regions, such as telomeres, where the minimum requirement for formation is a series of four G-rich regions, as would be found in tandem 5'-TTAGGG-3' repeats in human telomeres. They can be formed from a single G-rich strand by Hoogsteen base pairing, where each base acts as both a donor and acceptor for hydrogen bond formation. Alternatively two or four G-rich strands can form intermolecular G-quadruplex structures, as opposed to the intramolecular G-quadruplex from a single strand. Each planar structure resulting from the alternative base-pairing can form one layer of a stacked structure that may be composed of several layers (Lipps and Rhodes, 2009, Lu *et al.*, 2013).

These structures have been observed extensively in vitro and their presence in vivo has been indicated in human cells using anti-G-quadruplex antibodies (Biffi *et al.*, 2013, Lipps and Rhodes, 2009). This would indicate that they may have some biological significance. They would also present a significant obstacle to telomerase action on telomeric 3' overhangs as well as to the replication complex (Lu *et al.*, 2013, Zahler *et al.*, 1991). Specific helicases, such as RTEL1, a mouse helicase essential for telomere maintenance, and Dna2, a fission yeast helicase/nuclease, and those in the RecQ helicase family in humans have been implicated in resolving telomeric structures such as t-loops and G-quadruplex structures (Ding *et al.*, 2004, Huber *et al.*, 2006, Masuda-Sasa *et al.*, 2008, Vannier *et al.*, 2012). This could indicate that these structures have some role in telomerase and telomere length regulation, possibly by acting as an alternative capping structure to t-loops that are specifically unwound for replication.

G-quadruplex structures are also implicated to form at regions other than telomeres. G-rich sequences that meet the requirement are found in promoter and 5'-UTR regions of some genes which, when transcribed, affect the translation efficiency of the resulting mRNA (Kumari *et al.*, 2007, Lipps and Rhodes, 2009). Regions affording formation of these structures are also found in G-rich satellite sequences, rDNA sequences and in proximity to meiotic double-strand break sites (Ishikawa, 2013). These all indicate that G-quadruplex structures have biological functions not just at telomeres but also other regions of the genome.
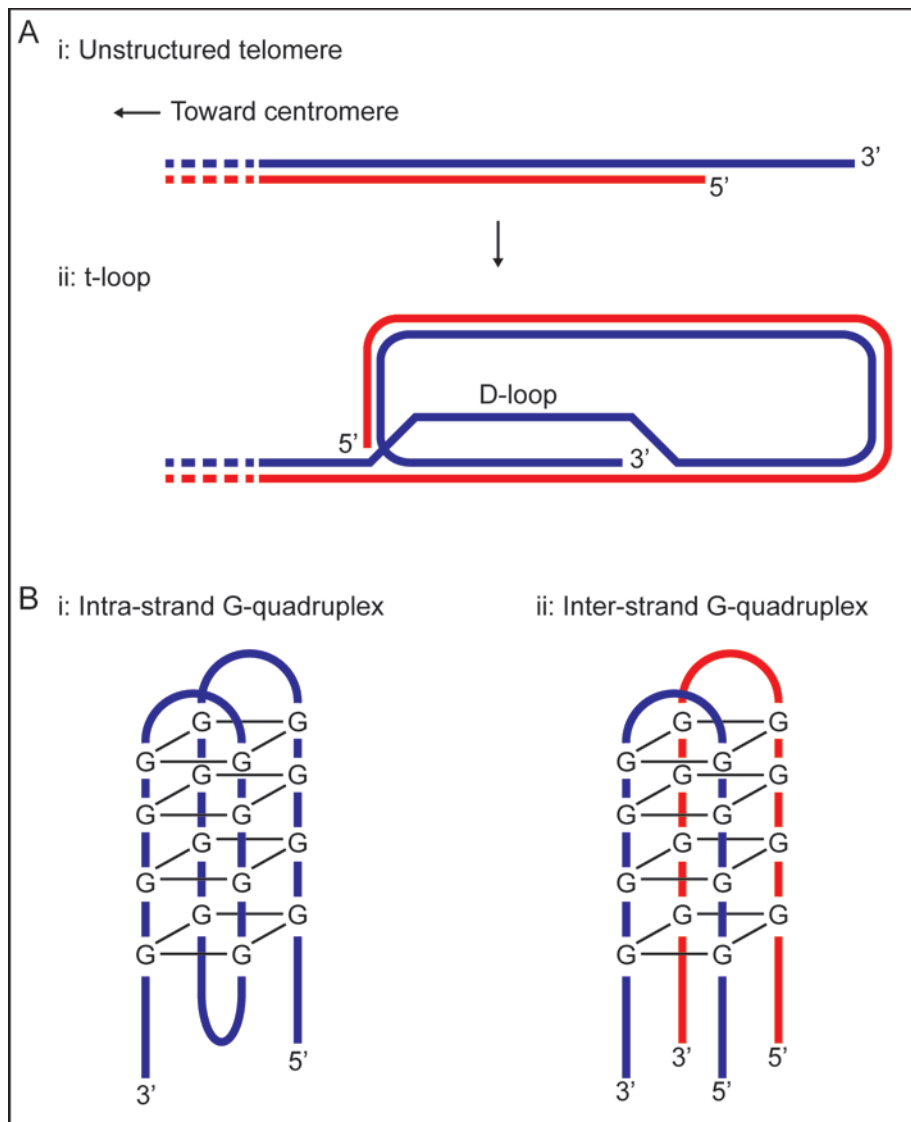
Figure 1.2: Schematic showing t-loop and G-quadruplex structures that can form at telomeres, based on (Nandakumar and Cech, 2013) and (Ishikawa, 2013).

(A) (i) An unstructured telomere consists of a DNA duplex region followed by a 3' overhang. The G-rich strand is indicated in dark blue and the C-rich strand is indicated in red. **(ii)** Formation of a t-loop involved strand invasion of the 3' overhang back into the telomere duplex region. The G-rich strand is displaced, forming a D-loop as indicated, while the 3' overhang is protected from exonuclease activity. **(B)** G-quadruplexes are high stable structures that form from Hoogsteen base pairing, where each base acts as both a donor and acceptor of hydrogen bond formation. **(i)** Intra-strand G-quadruplex structures can form where there are at least 4 stretches of G-rich sequence, as would be found in the telomere. Each planar structure can form one layer of a stacked structure. **(ii)** Inter-strand G-quadruplex structures can result from two (as shown) or four separate G-rich strands. The structure is similar to an intra-strand G-quadruplex. The two separate G-rich strands are indicated in dark blue and red.

1.4.4 The Telomerase ribonucleoprotein

As previously mentioned, to solve the end-replication problem, eukaryotic cells employ the services of the enzyme Telomerase to extend the length of the telomeres, typically 50-60 nucleotides to the G-rich overhang of each telomere during S phase. The C-rich strand is then filled in by the lagging-strand replication machinery (Zhao *et al.*, 2009). The functional form of the Telomerase ribonucleoprotein is composed of multiple components (Greider and Blackburn, 1989). First is the telomerase reverse transcriptase, known as TERT in humans and Trt1 in fission yeast (Nakamura *et al.*, 1997). This contains a catalytic domain that is able to synthesise a new G-rich sequence in the 5'-3' direction. This domain is highly conserved between different species and shares multiple motifs with known reverse transcriptase proteins from viruses (Nakamura and Cech, 1998). In addition, this catalytic subunit contains telomerase-specific regions, the T- and CP-motifs, which are also conserved in telomerase proteins in many eukaryotic organisms and provides points of interaction with the second component of the telomerase holoenzyme (Bosoy *et al.*, 2003, Bryan *et al.*, 2000, Nakamura *et al.*, 1997).

The second component is a non-coding RNA moiety, known as TR or TERC in humans and Ter1 in fission yeast. The RNA component provides a template sequence, which varies between species, for the telomeric repeats that are to be synthesised as well as binding sites for accessory proteins. The template region binds to the terminal G-rich 3' overhang nucleotides allowing the catalytic component to reverse transcribe the template (Feng *et al.*, 1995).

This RNA component has been found to be very variable in length and complex in structure, some of the smallest being found in ciliates and some of the largest in yeast (Chen and Greider, 2004). However, despite the variations in size, some common structural features appear to be conserved. Human TR is 451 nucleotides in length and forms a multi-domain secondary structure composed of a conserved single-stranded RNA template region that forms

a pseudoknot and multiple other stem-loop structures (Chen and Greider, 2004, Feng *et al.*, 1995). Fission yeast Ter1 is much larger, 1213 nucleotides, but contains a similar RNA template pseudoknot that is different in sequence to match the fission yeast telomere repeats, and also forms multiple other stem-loop structures (Webb and Zakian, 2008). With a specific RNA template, it would be expected that the telomeric repeat sequence be specific and identical in every repeat in fission yeast, as is found in humans and other vertebrates. However, the repeat sequences in *S. pombe* are quite heterogeneous. The majority of repeats, approximately 73%, contain the sequence 5'-GGTTACAGG-3' while a minority contain additional guanine, adenine or cytosine nucleotides. This was proposed to be due to variable alignment of the primer to the terminus of the 3' overhang and template primer slippage during reverse transcription that does not appear to occur with human telomerase (Leonardi *et al.*, 2008).

In addition to the template function, the RNA component also provides a scaffold structure onto which the telomerase catalytic component as well as accessory factors can bind to provide telomerase assembly, localisation and regulation roles. These could be considered additional components of the telomerase complex, but most are only transiently associated. In human TR, a 3' domain of the secondary structure, known as an H/ACA box, provides binding sites for a variety of proteins, one of the most interesting of which is Dyskerin (Mitchell *et al.*, 1999a). This provides a stabilising function to TR and is found to be mutated in the X-linked form of Dyskeratosis congenital, a disease linked to proliferative deficiencies in certain proliferative tissues, such as those in the skin and gut (Cong *et al.*, 2002, Mitchell *et al.*, 1999b). Another accessory factor, Est1, is conserved between humans (known as EST1A), fission yeast and budding yeast (Beernink *et al.*, 2003, Reichenbach *et al.*, 2003). Other human Est1 homologues have also been identified but only EST1A was shown to be associated with active telomerase complexes. Est1 in yeast has been shown to be required for telomerase recruitment to telomeres (Beernink *et al.*, 2003). It contains a Ter1-binding site that it shares

with the *S. pombe* telomere-associated protein Ccq1. Recruitment of the telomerase complex is thought to be in response to phosphorylation of a residue in Ccq1 leading to Ccq1-Est1 interaction (Moser *et al.*, 2011, Webb and Zakian, 2012).

1.4.4.1 Biogenesis of the telomerase holoenzyme

Biogenesis of human telomerase occurs in Cajal bodies, which are nuclear organelles used in the assembly of small nuclear ribonucleoproteins. TERT is accumulated in nucleoli while TR undergoes maturation in Cajal bodies, which are then moved to the nucleolar periphery for final assembly (Egan and Collins, 2012). In addition to the Dyskerin binding site, the human TR contains a Cajal box motif (CAB) which directs the RNA to localise to the Cajal bodies thorough binding of an accessory protein, TCAB1 (Richard *et al.*, 2003, Venteicher *et al.*, 2009). During assembly, various accessory proteins transiently associate with the TERT and TR including NOP10, NHP2 and GAR1. After assembly, several accessory proteins, in addition to Dyskerin, remain associated with telomerase. These are thought to process the TR RNA component from a precursor to a mature form, enhance stability of the complex and aid in regulation or recruitment of telomerase (Venteicher and Artandi, 2009). Indeed, this is demonstrated by depletion of Dyskerin or TCAB1 by shRNA which leads to a dramatic reduction of TERT and TR recruitment to telomeres (Zhong *et al.*, 2012).

Similarly, in fission yeast, multiple accessory factors are required for the assembly of the complete telomerase complex. The Ter1 RNA component is processed from a precursor RNA to the mature form by spliceosomal activity. The 3' end of the precursor Ter1 contains an intron and an Sm protein binding site. Sm proteins bind specific U-rich sequences on small nuclear RNA molecules to facilitate import of a ribonucleoprotein to the nucleus. In this case, the Sm proteins facilitate spliceosomal cleavage of the Ter1 RNA in order to separate the 3' exon from the 5' exon. However, unlike standard splicing, the two exons are then not then ligated together, but rather the 3' exon is separated and 5' exon, with intron attached, is retained for

further processing (Box *et al.*, 2008). To generate the mature form, the protein Tgs1 hyper-methylates the 5' cap. The Sm proteins are then replaced by similar Lsm (Like Sm) proteins, Lsm2-8, which promote association with Trt1 and protect the 3' end of the mature Ter1 RNA from nuclease degradation (Tang *et al.*, 2012). Interestingly, Sm proteins are found to be associated with human TR, but, unlike in fission yeast, appear to be dispensable for telomerase function (Fu and Collins, 2007).

1.4.4.2 Alternative solutions to the end-replication/protection problem

Although the majority of eukaryotic species solve the end-protection problem through the use of the telomerase reverse-transcriptase and RNA template, some have alternative methods to maintain the telomere termini (Fulcher *et al.*, 2013). The chromosome ends of prokaryotes, viruses and also mitochondria are structurally different to eukaryotic nuclear chromosomes. In order to provide the same protection, various solutions have developed.

1.4.4.2a Covalently closed hairpins

The *Vaccinia virus*, as well as several bacteriophage species, contains DNA that is capped by covalently closed single-stranded hairpins. These provide protection against exonuclease activity and DNA repair proteins (Baroudy *et al.*, 1982, Beaud, 1995). Similar structures are also seen in *Borrelia burgdorferi*, which contains multiple linear and circular plasmids, as well as one linear chromosome. The linear structures are capped by hairpins which allow the replication machinery to pass through the hairpin loop and continue back down the structure (Chaconas and Kobryn, 2010).

1.4.4.2b Covalently bound terminal protein

Some adenoviruses contain DNA structures capped by inverted terminal repeats and a covalently attached protein (Rekosh *et al.*, 1977). The repeats contain origin sequences while the covalently attached protein provides both protection from exonuclease activity and priming of DNA replication (de Jong and van der Vliet, 1999).

1.4.4.2c Telomeric arrays with 5', rather than 3', overhangs

Telomere-like repeats are present on the termini of *Candida parapsilosis* mitochondrial chromosomes. However, unlike the telomeres of the nuclear chromosomes, they terminate with a 5' overhang (Nosek *et al.*, 1995). This overhang is bound and protected by the mitochondrial Telomere-Binding Protein, mtTBP. In addition, the 5' overhang has been observed to form a t-loop structure, similar to mammalian telomeres (Tomaska *et al.*, 2002).

1.4.4.2d Retrotransposons and the Terminin complex in *Drosophila*

As mentioned in a previous section, the chromosome termini of *Drosophila melanogaster* do not consist of canonical telomeric repeats. Instead, they consist of three tandem retrotransposons, HeT-A, TART and TAHRE (Abad *et al.*, 2004a, Abad *et al.*, 2004b). It is thought that the transcripts of these elements are exported to the cell cytoplasm where translation takes place to produce GAG-like and RT proteins. The GAG-like proteins then associate with the RNA transcript, localising it back to the chromosome termini (Rashkova *et al.*, 2003). The RT proteins are then able to use these RNA transcripts as templates for synthesis of new nucleotides, thereby extending the terminal retrotransposon sequence. This provides the solution to the end-replication problem (Pardue and DeBaryshe, 2003).

To cap the chromosome termini and provide a solution to the end-protection problem, *Drosophila* uses the capping complex, Terminin. This consists of several proteins, HP1, HOAP, HipHop, Modigliani and Verrocchio. Additional proteins are also known to associate with the chromosome termini, but it is these five core proteins of the Terminin complex that specifically cap the chromosome termini, providing protection from DNA repair proteins (Gao *et al.*, 2010, Raffa *et al.*, 2010, Raffa *et al.*, 2009).

1.4.5 The eukaryotic telomeric complexes, Shelterin and CST

The telomerase holoenzyme and cofactors extend the telomeres in eukaryotic genomes to provide a solution to the end-replication problem. Control of the recruitment of telomerase, as well as the capping of telomeres, however, is provided by additional proteins that are associated with telomeres either consistently or transiently. The primary human telomere capping complex, made up of six individual proteins, is known as Shelterin. The proteins that make up this core complex can be roughly separated into double-stranded DNA-binding and single-stranded DNA-binding sub-complexes. The double-stranded DNA-binding proteins include TRF1, TRF2 and associated proteins, RAP1 and TIN2. The single-stranded DNA-binding proteins are POT1 and the associated protein TPP1 (Palm and de Lange, 2008). A separate telomere-associated complex, CST, which also contributes to telomere capping and telomerase regulation, contains proteins that bind to the single-stranded overhang. Originally thought to be unique to budding yeast, *S. cerevisiae*, components of CST; CTC1/Cdc13, STN1 and TEN1, have now been identified in many eukaryotic species, including humans and fission yeast (Wellinger, 2009). Additional proteins, including some of those involved in replication and the DNA damage response, have also been implicated in telomere maintenance roles.

The Shelterin and CST complex from humans have been found to have counterparts in many other species including the fission yeast, *S. pombe* and budding yeast, *S. cerevisiae* [Fig 1.3]. In some cases, however, the sequences of these proteins have diverged beyond recognition, while others have been lost altogether. The fission yeast telomeric complex, however, is very similar to Shelterin, further establishing its usefulness as a model organism.
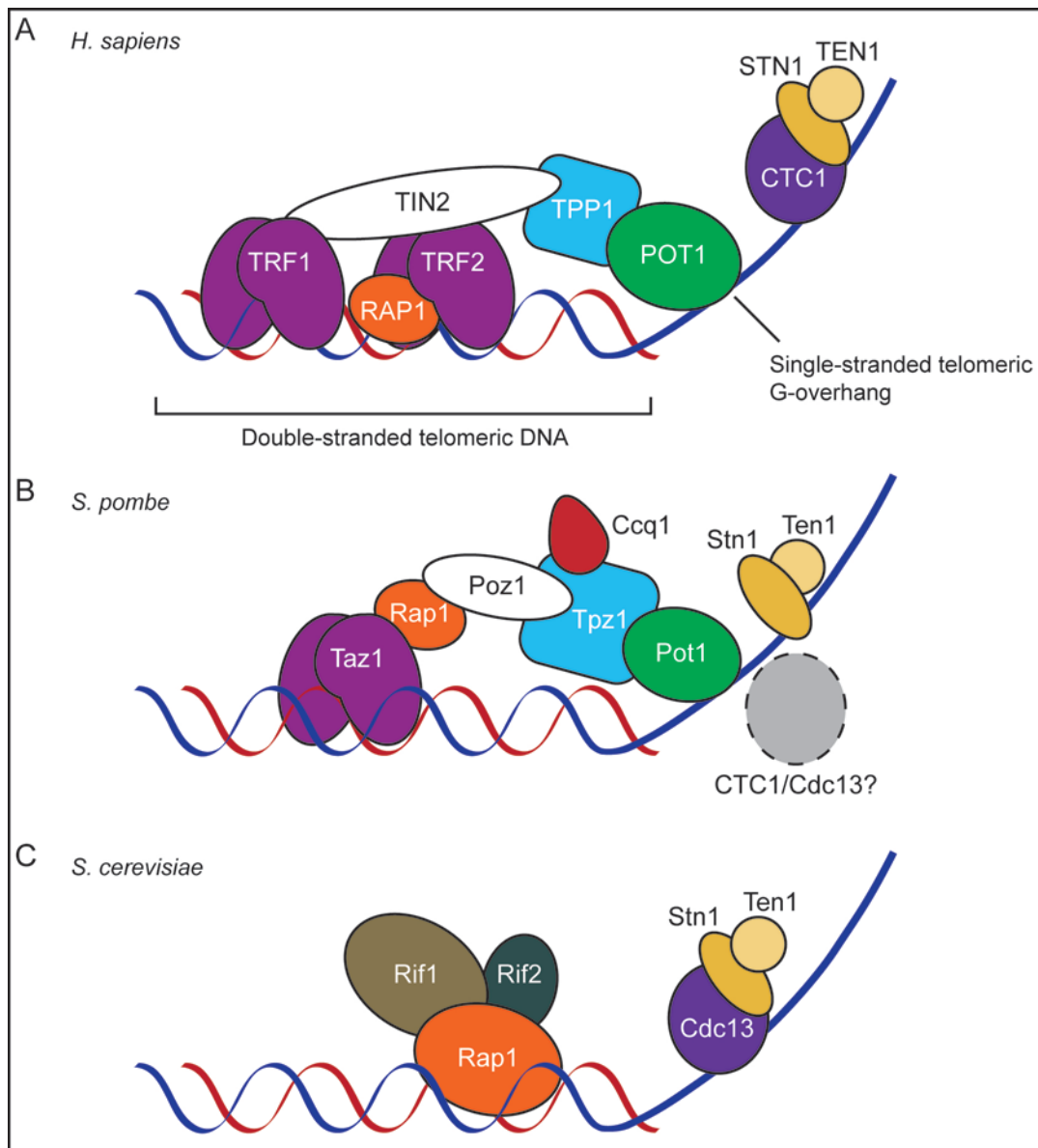
Figure 1.3: Comparison of the currently known proteins in the Shelterin and CST complexes in humans, fission yeast and budding yeast, drawn as cartoon representations.

(A) The human Shelterin complex consists of dsDNA-binding and ssDNA-binding sub-complexes. The dsDNA-binding sub-complex can be thought of as negative regulator of telomerase while the ssDNA-binding complex can be thought of as a positive regulator of telomerase. TRF1 and TRF2 homodimers bind the duplex DNA directly. The dark blue strand of the DNA helix represents the G-rich strand. The red strand of the DNA helix represents the C-rich strand. Associated with TRF2 is RAP1, which supports the function of TRF2. The TIN2 protein bridges these dsDNA-binding proteins and links them to the ssDNA-binding sub-complex which consists of TPP1 and POT1. POT1 is the only component of the complex to bind ssDNA. TPP1 is required in the recruitment of telomerase. The single-stranded G-rich overhang is also bound by the CST complex, consisting of CTC1, STN1 and TEN1. These provide an end-protection function and are implicated in C-rich strand fill-in by Pol-α/primase recruitment. **(B)** The *S. pombe* telomeric complex is structurally similar to the human Shelterin complex. Homologous proteins are found for most components of Shelterin and CST. The colours of the cartoon representations of the proteins reflect the homology between species. For example, Taz1 is the counterpart to TRF1 and TRF2 in humans. Two out of three components of the CST complex are present. No homologue of human CTC1 or budding yeast Cdc13 has been identified, as indicated by the grey oval. **(C)** *S. cerevisiae* telomeric complex contains fewer proteins than humans or fission yeast. Rap1 is the only dsDNA-binding protein and associates with Rif1 and Rif2 at the telomeres. The CST complex is present, however, Cdc13 is not referred to as a homologue of CTC1 due to the lack of sequence homology.

1.4.5.1 The double-stranded DNA-binding proteins of Shelterin

1.4.5.1a TRF1

The TRF1 and TRF2 proteins of human Shelterin contact the double-stranded region of telomeric DNA. TRF1 was originally identified in HeLa cell nuclear extracts and was found to specifically interact with the 5'-TTAGGG-3' telomeric repeats (Zhong *et al.*, 1992). It contains an acidic N-terminal domain, a dimerization domain termed TRFH, and a Myb-domain-like DNA-binding domain. As a result, it is found bound to DNA in the homodimer form and acts as a negative regulator of telomerase as well as providing a capping function (Chong *et al.*, 1995). TRF1 has been shown to be able to bend duplex DNA, thought to contribute to t-loop formation (Bianchi *et al.*, 1997). It is also able to bind TIN2, a bridging molecule, through the TRFH domain (Kim *et al.*, 1999).

1.4.5.1b TRF2

TRF2, the second double-stranded DNA-binding protein was identified through sequence similarity to the Myb-domain-like DNA-binding domain of TRF1 (Bilaud *et al.*, 1997, Broccoli *et al.*, 1997). Though there is substantial similarity, TRF1 and TRF2 are not able to form a heterodimer but TRF2 does form a homodimer like TRF1 (Fairall *et al.*, 2001). In addition to the TRFH domain, it also contains a basic N-terminal domain and is capable of binding both TIN2 and RAP1. The interaction with TIN2 bridges TRF1 and TRF2. Although TRF1 and TRF2 are very similar, different domains on the TRF proteins are used for this interaction, while the interaction with RAP1 occurs on a separate domain and works to suppress NHEJ at the telomere (Arat and Griffith, 2012, Bae and Baumann, 2007, Chen *et al.*, 2008, Houghtaling *et al.*, 2004, Kim *et al.*, 2004, van Steensel *et al.*, 1998). Like TRF1, TRF2 is capable of bending DNA and is also thought to contribute to t-loop formation (Amiard *et al.*, 2007, Poulet *et al.*, 2009, Stansel *et al.*, 2001). Both TRF1 and TRF2 interact with multiple other proteins that are involved in DNA replication and repair. These include the Ku heterodimer, BLM helicase and

ATM for TRF1 and the Ku heterodimer, Apollo, MRN, WRN, FEN1 helicases and nucleases as well as ORC1 and PARP1/2 for TRF2 (Arat and Griffith, 2012, Hsu *et al.*, 2000, Kishi *et al.*, 2001, Lillard-Wetherell *et al.*, 2004, Opresko *et al.*, 2004). A homologous protein, Taz1, is found in *S. pombe* with a similar Myb-like DNA-binding domain and is also a negative regulator of telomerase and repressor of NHEJ (Cooper *et al.*, 1997, Ferreira and Cooper, 2001).

1.4.5.1c RAP1

The RAP1 protein that binds to TRF2 was originally identified in a yeast 2-hybrid screen (Li *et al.*, 2000). It was thought to not contact telomeric DNA directly due to the presence of only one Myb-like domain, compared to two Myb-like domains in the *S. cerevisiae* homologue, Rap1, which does contact DNA directly. However, recent evidence indicates it is capable of independent binding to double-stranded DNA (Arat and Griffith, 2012). In addition to the Rap1 carboxy-terminal (RCT) domain used to bind TRF2, RAP1 contains a BRCT domain which may be used to interact with other proteins but, like the *S. pombe* homologue, is not known to have a specific telomeric function (Fujita *et al.*, 2012, Li and de Lange, 2003). It also does not appear to interact directly with the bridging molecule, TIN2, in humans, unlike the fission yeast counterparts, Rap1 and Poz1 (Miyoshi *et al.*, 2008). Instead, RAP1 only indirectly associates with TIN2 through TRF2 (Li *et al.*, 2000).

1.4.5.1d TIN2

The TIN2 protein that bridges TRF1 and TRF2 was identified by yeast 2-hybrid as a TRF1-interacting protein (Kim *et al.*, 1999). It also interacts with a third telomeric protein, TPP1. This interaction stabilises the first two interactions with TRF1 and TRF2 and is important in the regulation of telomerase recruitment (O'Connor *et al.*, 2006). This is seen by a decrease in TPP1 and TERT at telomeres when TIN2 is depleted (Abreu *et al.*, 2010). The homologous protein in *S. pombe*, Poz1, is also required in regulation of the recruitment of telomerase;

however, it appears to have the opposite effect. Without Poz1, telomeres in *S. pombe* dramatically elongate in a telomerase-dependent manner (Miyoshi *et al.*, 2008).

The binding activity between TRF1-TRF2-RAP1-TIN2 can be thought of as the double-stranded DNA binding sub-complex of Shelterin. As a whole, this sub-complex can be considered a telomerase negative regulator. This is fairly well conserved in fission yeast in the form of the analogous Taz1-Rap1-Poz1 sub-complex (Miyoshi *et al.*, 2008).

1.4.5.2 The single-stranded DNA-binding proteins of Shelterin

1.4.5.2a TPP1

In what can be considered as the single-stranded DNA-binding sub-complex, TPP1 binds TIN2, the bridging molecule, and POT1, which contacts the single-stranded telomeric overhang directly. TPP1 was originally identified through mass spectrometry of TRF1/TIN2-associated proteins and also yeast 2-hybrid screens using TIN2 as bait (Houghtaling *et al.*, 2004, Liu *et al.*, 2004, Ye *et al.*, 2004). TPP1 is capable of recruiting POT1 to telomeres, even when POT1-ssDNA-binding is disrupted (Liu *et al.*, 2004). It is also capable of recruiting telomerase, as seen by telomerase recruitment to TPP1 tethered at a non-telomeric LacO array (Zhong *et al.*, 2012). Indeed, in conjunction with POT1, it is essential for the recruitment and processivity of telomerase (Wang *et al.*, 2007). This appears to be through a patch of amino acids on the surface of the protein in what has been termed the TEL patch (Nandakumar *et al.*, 2012). Indeed, phosphorylation of Serine 111 in close proximity to the TEL patch is required for efficient telomerase recruitment (Zhang *et al.*, 2013). The increased processivity may be due to direct, or indirect, interaction with TERT-TR, stabilisation of the RNA primer association and improvement of translocation efficiency (Abreu *et al.*, 2010, Latrick and Cech, 2010). An *S. pombe* counterpart to TPP1 is found as the protein Tpz1, which similarly binds Poz1 and Pot1 proteins. In addition to these interactions, however, a third protein, Ccq1, is found to interact with Tpz1 (Flory *et al.*, 2004, Miyoshi *et al.*, 2008). This Ccq1 protein is essential for telomerase

recruitment, as well as maintenance of linear chromosomes in the absence of telomerase (Jain *et al.*, 2010, Nakamura *et al.*, 1998). If modelled on the fission yeast system, the interaction of TPP1 with Telomerase may be mediated by a Ccq1-like protein which has yet to be identified in humans. Evidence for this comes from data that indicate TPP1 is not solely responsible for telomerase recruitment. For example, TIN2 knock downs, using siRNA, result in reduced telomerase recruitment. This may be due to the role of TIN2 in recruiting TPP1, however mutations in TIN2 which cause Dyskeratosis Congenita result in reduced TR association in immunoprecipitation studies, whereas TPP1 association is unaffected (Yang *et al.*, 2011). This would indicate a combined function for the recruitment of telomerase by the TIN2-TPP1-POT1 ssDNA-binding complex.

1.4.5.2b POT1

The only single-stranded DNA binding protein in Shelterin, POT1, was first identified by its homology to the DNA-binding domain of the ciliate telomere terminus factor, TEBPα (Baumann and Cech, 2001). The *S. pombe* homologue, Pot1, was also identified in this way. Crystal structure analysis revealed that POT1 contained two oligonucleotide/oligosaccharide-binding (OB) folds that allow it to bind specifically to the single-stranded 3' telomeric overhang, similar to the *S. pombe* homologue (Lei *et al.*, 2004, Loayza *et al.*, 2004, Wang *et al.*, 2007). It is involved in telomerase processivity with TPP1, as already stated, and control of 5' end resection at the telomere termini. It also contributes to end protection by protecting against the ATR-mediated DNA damage response, possibly through displacement of RPA at the single-stranded overhang (He *et al.*, 2006, Hockemeyer *et al.*, 2007, Wu *et al.*, 2006) (Palm *et al.*, 2009).

The TPP1-POT1 binding activity can be thought of as the single-stranded DNA-binding sub-complex that can be considered a positive regulator of telomerase. It is fairly well conserved in

fission yeast in the form of Pot1-Tpz1-Ccq1 (Miyoshi *et al.*, 2008). Certainly, the whole *S. pombe* telomeric complex and Shelterin bear striking similarities in interactions and function.

1.4.5.3 The single-stranded DNA-binding proteins of the CST complex

In the recent past, the CST complex was thought to be unique to budding yeast. Indeed, a decade passed between identification of budding yeast Stn1 and fission yeast Stn1 (Grandin *et al.*, 1997, Martín *et al.*, 2007). In the intervening time, the fission yeast single-stranded DNA-binding protein Pot1 was thought to be a functionally equivalent component, along with human POT1. At the time no part of the CST complex had been identified in humans (Baumann and Cech, 2001). This, however, is not surprising, given the poor sequence conservation between CST components in different species (Price *et al.*, 2010). Since then, components of CST have been identified in a number of species, indicating that it may be more universal than originally thought. Structurally, the CST complex resembles RPA, with similar oligonucleotide/oligosaccharide-binding (OB) folds and winged-Helix-Turn-Helix (wHTH) motifs. These allow it to bind single-stranded DNA and interact with other proteins. In humans, due to a lack of sequence specificity, it is also implicated in competing with RPA for single-stranded DNA both at telomeres and elsewhere (Chen and Lingner, 2013).

1.4.5.3a CTC1/Cdc13

The first identification of a CST component, Cdc13 in *S. cerevisiae*, was in a screen for temperature-sensitive alleles that caused cells to arrest at specific stages of the cell cycle, in this case, during S phase (Pringle and Hartwell, 1981). It was not until 1995 that a telomeric effect of the *cdc13-1* temperature-sensitive allele was identified (Garvik *et al.*, 1995). Cdc13 was shown to bind single-stranded telomeric DNA, the catalytic subunit of DNA polymerase-α and also the telomerase cofactor, Est1 (Lin and Zakian, 1996, Nugent *et al.*, 1996, Qi and Zakian, 2000). Structural studies of this protein later determined that it contained a telomerase recruitment domain for interacting with Est1 and four

oligonucleotide/oligosaccharide-binding (OB) folds which are used to form a homodimer, bind single-stranded DNA at telomeres, bind the CST protein Stn1, and also the Pol1 subunit of DNA polymerase-α (Lewis and Wuttke, 2012, Mitchell *et al.*, 2010, Sun *et al.*, 2011). The *S. cerevisiae* Cdc13 protein was, therefore, determined to provide a capping function and regulation of telomerase (Chandra *et al.*, 2001, Giraud-Panis *et al.*, 2010).

The human counterpart, CTC1, was not identified as a CST component until 2009. It had previously been identified as a subunit of alpha-accessory factor, AAF-132 (Casteel *et al.*, 2009). However, sequence and secondary structure homology searches determined it to be an orthologue of *A. thaliana* CTC1, which itself was identified unexpectedly while searching for *A. thaliana* POT1 mutants (Surovtseva *et al.*, 2009). CTC1 and *S. cerevisiae* Cdc13 sequences, however, are not well conserved. CTC1 was also identified in a parallel study as a STN1 interacting protein by Co-IP (Miyake *et al.*, 2009). Secondary structure prediction of CTC1 indicated that it should contain multiple OB folds, similar to *S. cerevisiae* Cdc13, with homology to the OB folds of the RPA subunit, RPA70 (Casteel *et al.*, 2009). In conjunction with its binding partners, STN1 and TEN1, it is implicated in telomere capping and telomerase regulation and also, by being AAF-132, recruitment of the Pol-α/primase complex to telomeres (Chen *et al.*, 2012, Gu *et al.*, 2012, Wang *et al.*, 2012). Unlike the budding yeast counterpart, however, it does not bind telomeric ssDNA with any sequence specificity as part of CST or separately (Miyake *et al.*, 2009).

In addition to the function at the telomere termini, CTC1, in conjunction with its binding partners, is also suggested to function in another capacity. Specifically, it may use the ability to bind ssDNA and recruit the Pol-α/primase complex to enhance the processivity of the replication fork at telomeres, which are otherwise considered fragile sites prone to fork stalling, and in replication fork restart across the genome (Ishikawa, 2013, Stewart *et al.*, 2012, Wang *et al.*, 2012).

No *S. pombe* homologue of Cdc13 or CTC1 has yet been found. The limited sequence similarity

with *A. thaliana* CTC1 (14% identity, 26% similarity), and the lack of sequence similarity with *S. cerevisiae* Cdc13 makes this unsurprising. It also indicates that the CTC1/Cdc13 component of

CST identified so far may have highly diverged or, perhaps, be the result of convergent

evolution. There is, however, high similarity of the known CST subunits to RPA subunits in

humans, budding yeast and fission yeast which has been suggested to indicate that CST

probably evolved from RPA ancestors (Gao *et al.*, 2007, Gelinas *et al.*, 2009, Giraud-Panis *et al.*,

2010, Sun *et al.*, 2009). In addition, during a domain swap experiment, where the OB fold of

budding yeast Rpa2 was swapped with an OB fold from Stn1, the lethality of an *rpa2* deletion

mutant was rescued by the modified Rpa2-OB^{Stn1} protein, further indicating the close

relationship between these complexes (Gao *et al.*, 2007). The possibility, therefore, exists that

there may be a CTC1/Cdc13 homologue yet to be identified in *S. pombe*, but also the

equivalent subunit in *S. pombe* RPA, Ssb1 (also known as Rad11), could form a CST complex

with the previously identified components, Stn1 and Ten1.

1.4.5.3b STN1

The first Stn1 component of CST was identified in budding yeast, *S. cerevisiae*, in screen for

cdc13-1 temperature-sensitivity suppressors. The *S. cerevisiae* Stn1 protein was found to

suppress the temperature-sensitivity of the *cdc13-1* allele up to 30°C as well as physically

interact with Cdc13 by yeast 2-hybrid analysis (Grandin *et al.*, 1997). Identification in other

species, however, required multiple bioinformatics approaches. Stn1 was identified as an OB

fold-containing protein in *S. pombe* through a screen for sequence similarity to the *S. cerevisiae* Stn1. In the same screen a potential human STN1 was also identified as the

previously annotated OBFC1 (OB Fold Containing 1). The OB folds of these proteins were

determined to be similar to the OB fold in human RPA32 (Martín *et al.*, 2007). In addition, the

human STN1 protein was identified as a subunit of Alpha-Accessory Factor, AAF-44, in the

same screen that identified AAF-132/CTC1 (Casteel *et al.*, 2009). Similar to CTC1, the identity of

OBFC1/AAF-44 was finally confirmed as STN1 by its similarity to *A. thaliana* STN1 and, in parallel, once again, by the similarity of the OB fold sequence with *S. cerevisiae* Stn1 (Miyake *et al.*, 2009, Surovtseva *et al.*, 2009).

As already stated, STN1 found in plants, humans, budding yeast and fission yeast contains an N-terminal OB fold that is highly conserved, not just between CST complexes in different species, but also in the RPA complex (Casteel *et al.*, 2009, Martín *et al.*, 2007, Miyake *et al.*, 2009). Structural data confirmed the similarities of the OB folds but also revealed the presence of C-terminal winged-Helix-Turn-Helix (wHTH) motifs. Whereas the counterpart in RPA, RPA32, contains just one of these wHTH motifs, STN1 contains two in tandem. These wHTH motifs are usually considered DNA-binding motifs, however, in these cases they also provide large surface areas which may be used for protein-protein interactions. Indeed, it has been suggested that the additional wHTH motif may play a telomere-specific role that is not present in RPA (Brennan, 1993, Bryan *et al.*, 2013, Gelinas *et al.*, 2009, Sun *et al.*, 2009, Wintjens and Rooman, 1996).

Human STN1, like CTC1 and Cdc13, has been implicated in telomerase regulation, telomere capping and, by also, by being AAF-44, recruitment of the Pol-α/primase complex to telomeres and stalled forks to aid replication restart (Chen *et al.*, 2012, Stewart *et al.*, 2012, Wang *et al.*, 2012).

1.4.5.3c TEN1

Ten1, like Stn1, was first identified in *S. cerevisiae* in another temperature-sensitivity suppressor screen, this time for suppressors of the *stn1-13* and *stn1-154* alleles. Ten1 was also shown to physically interact with Stn1 by Co-IP and with Cdc13 by yeast 2-hybrid (Grandin *et al.*, 2001). The *S. pombe* homologue was identified by sequence similarity to *S. cerevisiae* Ten1 in the same study as Stn1 identification. It was found to be weakly similar to the budding yeast Ten1 and identified as a member of an uncharacterised family of distantly related proteins in

several other fungal species. However, unlike Stn1, no homology to non-fungal species was found, presumably due to sequence divergence (Martín *et al.*, 2007). The human TEN1, similarly to CTC1, was identified by Co-IP with STN1. Sequence comparisons showed it to have 15.6% and 17.2% sequence identity to the *S. cerevisiae* and *S. pombe* Ten1 proteins respectively. Given that it is composed of only 122 amino acids, it is not surprising that it was not identified by sequence similarity. With the three components of CST identified in humans, yeast 2-hybrid analysis indicated that the TEN1 protein interacted only with STN1 and not CTC1, while the STN1 protein interacted with both CTC1 and TEN1 (Miyake *et al.*, 2009).

Like STN1, TEN1 is implicated in telomerase regulation, telomere capping and recruitment of the Pol-α/primase complex to telomeres and stalled forks to aid replication restart as part of the CST complex (Chen *et al.*, 2012, Stewart *et al.*, 2012, Wang *et al.*, 2012).

1.4.5.4 Non-telomeric proteins involved in telomere maintenance

In order to protect telomeres from the DNA damage response (DDR), it would make sense to completely exclude DDR proteins from the telomere. However, perhaps counterintuitively, a number of proteins involved in replication and the DNA damage response have been found to localise to and function at telomeres in various species including humans, fission yeast and budding yeast (Maser and DePinho, 2004, Slijepcevic and Al-Wahiby, 2005, Verdun and Karlseder, 2007). For example, the removal of the RNA primer during replication on the lagging-strand at the telomere terminus leaves a small 3' overhang. However, the leading strand replication process would leave a blunt end. In order to form a t-loop structure to aid capping of the telomere, a 3' overhang would need to be generated at this end. Evidence of nuclease action on the C-rich strand from the 5' end has been found in multiple species. At human telomeres, the exonuclease action, mediated by MRN, XPF-ERCC1, Exo1 and Apollo, has been implicated in generating the 3' overhang at not only the blunt ended telomere, but the extend the overhang at both telomeres (Chai *et al.*, 2006, Wu *et al.*, 2008). Similarly, in

fission yeast, the MRN and Dna2 have been implicated in generating the 3' overhang (Budd and Campbell, 2013, Tomita *et al.*, 2004).

In addition to these, MRN and ATM have been found to be required in promoting telomerase-depended extension of the telomere. Phosphorylation of TRF1 by ATM, facilitated by MRN, in human cells has been shown to destabilise TRF1-dsDNA binding, thereby reducing the ability of TRF1 to inhibit telomerase recruitment (Wu *et al.*, 2007). Kinase action on TPP1 Serine 111 is also shown to be required for telomerase recruitment (Zhang *et al.*, 2013). In fission yeast, it is the Ccq1 protein that is phosphorylated at Threonine 93 to produce the same effect. The kinases in these two cases, however, may differ. It is thought that CDKs may be responsible for TPP1 phosphorylation while Tel1[ATM] and Rad3[ATR] phosphorylate Ccq1 (Yamazaki *et al.*, 2012). These actions contribute to kinase-dependent protection of telomeres from NHEJ (Chan and Blackburn, 2003).

Ku is also implicated in telomere protection in humans, fission yeast and budding yeast (Baumann and Cech, 2000, Fisher and Zakian, 2005, Hsu *et al.*, 2000, Ribes-Zamora *et al.*, 2013). This has been extensively studied in yeast where Ku is thought to bind at the dsDNA-ssDNA junction and not only protect against HR factors, such as nucleases, but is also required for telomerase recruitment (Bonetti *et al.*, 2010, Maringele and Lydall, 2002, Stellwagen *et al.*, 2003).

Helicases, such as the RecQ-type BLM and WRN also contribute to telomere protection. TRF2 has been shown to bind and stimulate these helicases (Opresko *et al.*, 2002). They are thought to be required for clearing G-quadruplex structures that may impede replication, as well as at the 3' overhang, where they may impede telomerase-binding and lagging-strand synthesis (Crabbe *et al.*, 2004, Laud *et al.*, 2005)}(Huber *et al.*, 2006).

Clearly the situation at the telomere termini is more complex and intricate than at first glance. A multitude of interactions between components of the core Shelterin and CST complexes, the

telomerase holoenzyme as well as a multitude of other factors combine to maintain and protect the chromosome termini. Indeed, ongoing study of the various telomeric and non-telomeric proteins is sure to continue to reveal a more complete picture of telomere maintenance and new targets for therapeutic strategies for associated disease states.

Chapter 2

Materials and Methods

2.1 Common reagents

2.1.1   5xTE

50mM (final)   Tris-HCl

5mM (final)   EDTA

pH 8.0

2.1.2   MP1 (Resuspension buffer)

100mM (final)   Tris-HCl (pH 7.5)

10mM (final)   EDTA

0.2mg/ml (final)   RNAse (Sigma R6513)

2.1.3   MP2 (Lysis buffer)

0.2M (final)   NaOH

1% (w/v)   SDS

2.1.4   MP3 (Neutralisation buffer)

3M (final)   Potassium Acetate

11.5% (v/v)   Glacial Acetic Acid

2.1.5   10x TBE

108g/L   Tris-base

55g/L   Boric acid

5.84g/L   EDTA

Working solution: 0.5x TBE

2.1.6   5x LiAc/TE

0.5M (final)   Lithium Acetate

| 50mM (final) | Tris-HCl (pH 4.9) |
| 5mM (final) | EDTA |

2.1.7 SP1

1.2M (final)	Sorbitol
50mM (final)	Citrate Phosphate
40mM (final)	EDTA

pH 5.6

2.1.8 4x TCA Sample Buffer

250mM (final)	Tris-HCl (pH 6.8)
8% (w/v)	SDS
20% (v/v)	Glycerol
0.4% (w/v)	BromoPhenol Blue (Fisher B392-5)

2.1.9 2x Laemmli buffer

125mM (final)	Tris-HCl (pH 6.8)
4% (w/v)	SDS
20% (v/v)	Glycerol
10% (v/v)	β-mercaptoethanol
0.004% (w/v)	BromoPhenol Blue (Fisher B392-5)

2.1.10 Breaking buffer

10mM (final)	Tris (pH 8.0)
1mM (final)	EDTA
100mM (final)	NaCl
1% (w/v)	SDS
2% (v/v)	Triton x-100

2.1.11 Z-buffer

11.2g/L	Disodium hydrogen phosphate anhydrate (Na_2HPO_4)
5.5g/L	Sodium dihydrogen phosphate (NaH_2PO_4)
0.75g/L	KCl
0.246g/L	Magnesium sulphate heptahydrate ($MgSO_4.7H_2O$)

2.1.12 10x SDS-PAGE Running Buffer

30.3g/L	Tris-base
144g/L	Glycine
10g/L	SDS

2.1.13 10x Transfer buffer for western blotting

58g/L	Tris-base
28g/L	Glycine
3.7g/L	SDS

Working solution: 1x Transfer buffer + 200ml/L Methanol (final)

2.1.14 1xTBS(T)

20mM (final)	Tris-HCl
150mM (final)	NaCl
(0.05% (v/v)	Tween20)

2.1.15 Ponceau

2g/L	Ponceau
30g/L	TCA

2.1.16 Church Hybridisation Buffer

0.5M (final)	Sodium phosphate (pH 7.2)
7% (w/v)	SDS

2.1.17 Church Wash Buffer

40mM (final)	Sodium phosphate (pH 7.2)

1% (w/v)   SDS

2.1.18 HBS

50mM (final)   HEPES (pH7.5)

140mM (final)   NaCl

2.1.19 ChIP Lysis Buffer

50mM (final)   HEPES (pH7.5)

140mM (final)   NaCl

1mM   EDTA (pH 8.0)

1% (v/v)   NP40 (IGEPAL CA-630)

0.1% (w/v)   Sodium deoxycholate

1mM (final)   Phenylmethanesulfonyl fluoride (PMSF), just prior to use

1 tablet/7ml (final)   cOmplete, Mini, EDTA-free (Roche 04693159001), just prior to use

2.1.20 AT1

50mM (final)   HEPES (pH7.5)

140mM (final)   NaCl

1mM   EDTA (pH 8.0)

0.03% (w/v)   SDS

2.1.21 AT2

50mM (final)   HEPES (pH7.5)

1M (final)   NaCl

1mM   EDTA (pH 8.0)

2.1.22 AT3

20mM (final)   Tris-HCl (pH7.5)

250mM (final)   Lithium Chloride

1mM   EDTA (pH 8.0)

| 0.5% (v/v) | NP40 (IGEPAL CA-630) |
| 0.5% (w/v) | Sodium deoxycholate |

2.1.23 AT4

| 20mM (final) | Tris-HCl (pH7.5) |
| 0.1mM (final) | EDTA (pH 8.0) |

2.1.24 TES

20mM (final)	Tris-HCl (pH7.5)
1mM (final)	EDTA (pH 8.0)
1% (w/v)	SDS

2.2 Media

2.2.1 YES (rich media)

5g/L, 0.5% (w/v)   Yeast extract

30g/L, 3% (w/v)   D-glucose (anhydrous)

0.6g/L, 0.06% (w/v)   Supplements: 10g each uracil, leucine, arginine, histidine, 20g adenine

20g/L, 2% (w/v)   Difco Bacto Agar (if required)

pH 6.0

2.2.2 YNG (minimal media)

1.71g/L, 0.171% (w/v)   US Biological YNB w/o AA, Ammonium sulphate, Thiamine HCl

20g/L, 2% (w/v)   D-glucose (anhydrous)

5.07g/L, 0.507% (w/v)   Glutamate

5.3g/L, 0.53% (w/v)   US Biological Drop-out Mix, w/o Yeast Nitrogen Base

20g/L, 2% (w/v)   Difco Bacto Agar (if required)

pH 6.0

2.2.3 ELN (Extra Low Nitrogen sporulation media)

27.3g/L, 2.73% (w/v)   EMM broth without nitrogen (Formedium PMD1302)

0.05g/L, 0.005% (w/v)   Ammonium chloride

0.6g/L, 0.06% (w/v)   Supplements: 10g each uracil, leucine, arginine, histidine, 20g adenine

20g/L, 2% (w/v)   Difco Bacto Agar

2.2.4 YPAD

10g/L, 1% (w/v)   Yeast extract

20g/L, 2% (w/v)   Peptone

20g/L, 2% (w/v)   D-glucose (anhydrous)

30mg/L, 0.0003% (w/v) Adenine hemisulphate

20g/L, 2% (w/v)	Difco Bacto Agar (if required)

pH 6.0

2.2.5   Sc (minimal media)

6.7g/L, 0.67% (w/v)	US Biological YNB w/o AA, Carbohydrate and w/Ammonium sulphate
20g/L, 2% (w/v)	D-glucose (anhydrous)
2g/L, 0.2% (w/v)	US Biological Drop-out Mix, w/o Yeast Nitrogen Base
20g/L, 2% (w/v)	Difco Bacto Agar (if required)

pH 6.0

2.2.6   LB (Luria Broth)

10g/L, 1% (w/v)	Bacto-tryptone
5g/L, 0.5% (w/v)	Yeast extract
5g/L, 0.5% (w/v)	NaCl

pH 7.0

2.3 Drugs and Chemicals added to media

Blasticidin (BSD)	Melford Labs B1105	60μg/ml w/v (final)
Hygromycin B (HYG)	Melford Labs H0125	100 μg/ml w/v (final)
G418 sulphate (KAN)	Melford Labs G0175	500 μg/ml w/v (final)
Nourseothricin (NAT)	Werner Bioagents 50100	100 μg/ml w/v (final)
5-FOA	Melford Labs F5001	8mg/ml w/v (final)
3-Amino,1,2,4-Triazole	Fisher Scientific 10456383	2-7mM (final) as required
Methyl Methanesulfonate	Sigma 129925	0.0005-0.0075% v/v (final)
Hydroxyurea	Fisher Scientific 10502164	1-5mM (final) as required
Ampicillin sodium salt	Sigma A9518	100μg/ml w/v (final)
Kanamycin	Melford Labs K0126	50μg/ml w/v (final)
Phloxine B	Sigma P4030	5mg/L w/v (final)

2.3 Drugs and Chemicals added to media

2.4 Molecular Cloning Techniques

2.4.1 Restriction Digests

Plasmids and PCR products were digested with NEB restriction enzymes according to NEB protocol. Diagnostic digests were incubated for 1 hour at 37°C while digests for cloning were incubated between 8 hours and overnight. The digests were then checked by agarose gel electrophoresis using an appropriate percentage gel.

2.4.2 Ligation

Digested and purified vector and insert fragments were incubated at a 1:2 or 1:3 ratio, as required, with NEB T4 Ligase in T4 Ligase buffer diluted to 1x concentration (final) in 10µl using ddH$_2$O. The ligation reactions were incubated at 16°C overnight.

2.4.3 End-blunting (fill-in)

With the fragment to be blunted dissolved in any 1x NEB restriction buffer, dNTPs are added to 100µM concentration (final) and the sample put on ice. One unit of T4 DNA Polymerase (NEB M0203S) was added per microgram of DNA and the sample incubated on at 12°C in a Bio-Rad C1000 thermal cycler for 15 minutes. The addition of dNTPs to the reaction enabled blunting by 5' overhang fill-in. To stop the reaction, the tube was put back on ice, EDTA added to 10mM concentration and incubated at 75°C for 20 minutes to denature the enzyme.

2.4.4 Colony PCR (*E. coli*)

A single *E. coli* colony was picked using a sterile pipette tip and touched to a fresh LB agar plate with antibiotic selection (Ampicillin or Kanamycin). The remaining cells on the tip were resuspended in the PCR reaction mix (detailed below).

Reagent	Volume per 25µl reaction	Final concentration
10x NEB Taq Polymerase Buffer	2.5µl	1x
NEB dNTPs (10mM each)	0.5µl	0.2mM each
Forward primer (100µM)	0.2µl	0.8µM
Reverse primer (100µM)	0.2µl	0.8µM
NEB Taq Polymerase (5U/µl)	0.1µl	0.02U/µl
ddH$_2$O	21.5µl	-

The reactions were run in a Bio-Rad C1000 thermal cycler with the following conditions.

Annealing temperature varied depending on combination of primers used.

Step	Temperature (°C)	Time	Cycles
Denaturation	95	5 min	1
Denaturation	95	30 sec	30
Annealing	55-68	30 sec	
Extension	72	1 min/kb	
Extension	72	7 min	1

PCR product was then analysed by running agarose gel electrophoresis.

2.4.5   Colony PCR (*S.* pombe)

A single *S. pombe* colony was picked from a fresh streak using a sterile pipette and resuspended in 50µl ddH2O. The cells were then lysed in a Bio-Rad C1000 thermal cycler at 95°C for 12 minutes. 10µl of cell lysate was added to the PCR reaction mix (detailed below).

Reagent	Volume per 25µl reaction	Final concentration
10x Takara ExTaq Buffer	2.5µl	1x
10x Takara dNTPs (2.5mM each)	2µl	0.2mM each
Forward primer (100µM)	0.2µl	0.8µM
Reverse primer (100µM)	0.2µl	0.8µM
Takara ExTaq Polymerase (5U/µl)	0.125µl	0.025U/µl
Cells	10µl	-
ddH$_2$O	10µl	-

The reactions were run in a Bio-Rad C1000 thermal cycler with the following conditions.

Annealing temperature varied depending on combination of primers used.

Step	Temperature (°C)	Time	Cycles
Denaturation	98	5 min	1
Denaturation	98	30 sec	30
Annealing	55-68	30 sec	
Extension	72	1 min/kb	
Extension	72	7 min	1

PCR product was then analysed by running agarose gel electrophoresis.

2.4.6   Error-prone PCR (NEB Taq Polymerase)

Purified plasmid template was diluted to 100ng/μl Target DNA (amplicon). 10x dNTPs for

mutagenesis was made as: 2mM dATP, 2mM dGTP, 10mM dCTP, 10mM dTTP. The unequal

concentration of dNTPs, as well as increased $MgCl_2$ and $MnCl_2$, increases error rate (Pritchard

et al., 2005). Error-prone PCR reaction master mix was then made as detailed below for 6x50μl

reactions:

Reagent	Volume per 50μl reaction	Final concentration
10x NEB Taq Polymerase Buffer	5μl	1x
10x dNTPs for mutagenesis	5μl	1x
Forward primer (100μM)	0.15μl	0.3μM
Reverse primer (100μM)	0.15μl	0.3μM
$MgCl_2$ (50mM)	5.5μl	5.5mM +1.5mM fr. buffer
$MnCl_2$ (5mM)	5μl	0.5mM
Target DNA (100ng/μl)	5μl	10ng/μl
NEB Taq Polymerase (5U/μl)	0.5μl	0.05U/μl
ddH_2O	23.7μl	-

The master mix was split into six reactions and run on a Bio-Rad C1000 thermal cycler with the

following conditions.

Step	Temperature (°C)	Time	Cycles
Denaturation	95	1 min	1
Denaturation	95	30 sec	25-30
Annealing	55-68	30 sec	
Extension	72	1 min/kb	
Extension	72	7 min	1

The PCR products were then checked by agarose gel electrophoresis (1µl of each reaction loaded per lane) for correct PCR product size and efficiency. The PCR products were then pooled together and purified using a Qiagen QIAquick PCR purification kit.

2.4.7   *E. coli* transformation (standard DH5α)

Chemically competent DH5α *E. coli* cells (50µl aliquots) were thawed from the -80°C freezer on ice. For each transformation, up to 5µl of DNA (ligation) was added to an aliquot of cells and incubated for 30 minutes on ice before heat-shock at 42°C for 90 seconds. The cells were placed back on ice for 5 minutes to recover. 1ml of LB was then added and the reactions incubated at 37°C with rotation for 60 minutes. 10% and 90% of the cells were then separately plated on LB Agar plates with antibiotic selection and incubated overnight at 37°C.

2.4.8   *E. coli* transformation (commercial high efficiency DH5α, NEB C2987H)

The commercial DH5α cell aliquots were thawed on ice for 5 minutes and transformed following the supplied protocol. For each transformation, up to 5µl of DNA was added and cells incubated on ice for 30 minutes before heat-shock at 42°C for 30 seconds. The cells were placed back on ice for 5 minutes to recover. 950µl of SOC (supplied with cells) was then added and the reactions incubated at 37°C with rotation for 60 minutes. 10% and 90% of the cells were then separately plated on LB Agar plates with antibiotic selection and incubated overnight at 37°C.

2.4.9   Plasmid DNA preparation

2.4.9.1 Miniprep

A single *E. coli* colony was picked from an agar plate using a sterilised wooden dowel and resuspended in 5ml LB liquid media containing the appropriate antibiotic for selection. This was incubated with rotation overnight at 37°C. A total of 3ml of the culture was spun down in eppendorf tubes using a micro centrifuge at 13 000 rpm for 1 minute. The pellet was then fully resuspended in 200µl MP1 buffer. 200µl of MP2 was then added, the tube inverted to mix and

incubated at RT for 5 minutes. 200μl of MP3 was then added, the tube inverted to mix, and incubated on ice for a further 5 minutes. The tube was then spun down in a micro centrifuge at 13 000 rpm for 5 minutes to pellet the cell debris. The supernatant was then removed and pipetted into a new tube. 420μl of isopropanol was added and the sample mixed briefly by vortex before incubating at RT for 10 minutes. The tube was spun at 13 000 rpm for 10 minutes in a micro centrifuge. The supernatant was discarded and the pellet washed with 500μl of 70% (v/v) ethanol and spun again at 13 000 rpm for 5 minutes. The ethanol was then removed, the pellet air dried at room temperature and resuspended in 50μl of ddH$_2$O. The DNA concentration was then assessed by running 1μl of the prep on an agarose gel alongside a ladder (NEB N3232L) and comparing the prep to the ladder standards.

2.4.9.2 Midiprep (Nucleobond Xtra Midi Cat: 740410.10)

A single *E. coli* colony was picked from an agar plate, as described previously, and grown in 5ml LB with antibiotic selection for 8 hours at 37°C. This starter culture was then expanded to 200ml with shaking overnight at 37°C. The plasmid was then prepared using a Machery-Nagel Nucleobond Xtra Midi kit (Cat 740410.10) following the supplied protocol. The plasmid was resuspended in 120μl elution buffer and DNA concentration assessed by running 1μl of the prep on an agarose gel alongside a ladder (NEB N3232L) and comparing the prep to the ladder standards.

2.4.9.3 Gigaprep (Nucleobond PC 10000 Cat: 740593)

For pTN-TH7 cDNA library amplification, 3 million *E. coli* cDNA library transformants were pooled and centrifuged in a Sorvall RC6 Plus centrifuge to pellet cells at RCF 20 000. The cDNA library was then prepared using a Macherey-Nagel Nucleobond PC 10000 Gigaprep kit (Cat 740593) following the supplied protocol. The library was eluted in 20ml elution buffer and DNA concentration assessed by running 1μl of a 1:10 dilution of the prep on an agarose gel alongside a ladder (NEB N3232L) and comparing the prep to the ladder standards.

2.4.10 TA Cloning into pGEM-T Easy vector

PCR products were cloned into pGEM-T Easy vector according to manufacturer instructions. If the polymerase used does not add an 'A-tail', e.g. Phusion Taq Polymerase, then the PCR product was 'A-tailed'. To do this, 7µl of 100ng/µl PCR product was incubated with 1µl 10x NEB Taq Reaction buffer, 1µl 2mM dATP and 1µl NEB Taq DNA Polymerase (5U/µl) at 70°C for 30 minutes in a Bio-Rad C1000 thermal cycler. The concentration of the PCR product was then checked again by running on an agarose gel alongside a ladder (NEB N3232L) and comparing the prep to the ladder standards. The PCR product was then ligated to pGEM-T Easy in a 3:1 ratio, according to the Promega protocol. To maximise ligation efficiency, overnight incubation at 4°C was preferred over 16°C, as recommended by the protocol.

2.4.11 Column purification of PCR products

PCR products were purified using a Qiagen QIAquick PCR purification kit following the supplied protocol. Up to 10µg of PCR product was used per column and eluted in 50µl elution buffer. The concentration of DNA was assessed by running 1µl on an agarose gel alongside a ladder (NEB N3232L) and comparing to the ladder standards.

2.4.12 Gel Extraction of DNA fragments

Restriction digested DNA (plasmids or PCR products) was run on a 1% agarose gel for 1 hour at 10 V/cm. The desired bands were visualised under a UV transilluminator and excised using a sterile scalpel. The DNA was then extracted and purified from these gel slices using a Qiagen QIAquick Gel Extraction Kit (Cat 28704) following the supplied protocol. Before elution, the elution buffer was heated to 70°C and added to the column. After a 4 minute incubation, the DNA was eluted by micro centrifuge at 13 000 rpm for 1 minute. The concentration of DNA was assessed by running 1µ on an agarose gel alongside a ladder (NEB N3232L) and comparing to the ladder standards.

2.4.13 Sequencing of plasmids and PCR products

Sequencing of plasmids and PCR products were completed by GATC-Biotech. 30-100ng/µl of plasmid DNA or 10-50ng/µl of PCR product in a 20µl volume was sent, along with 10pmol/µl primers. PCR products were purified using a Qiagen QIAquick PCR purification kit before preparation for sequencing.

2.4.14 Gene synthesis

Synthesised genes were made and sequenced by Blue Heron Biotech, LLC (Washington, USA) or Eurofins MWG Operon (Ebersberg, Germany) as required. They were designed according to manufacturer requirements.

2.4.15 Virtual cloning, sequence analysis and primer design

All computer-based **cloning design** was completed using SerialBasics Serial Cloner software.

Sequence trace data from GATC-Biotech was initially analysed using ApE, followed by Serial Cloner.

Serial Cloner, 2.6, March 2013, SerialBasics, http://serialbasics.free.fr/Serial_Cloner.html

ApE, 2.0.46, July 2013, M. Wayne Davis, University of Utah, http://biologylabs.utah.edu/jorgensen/wayned/ape/

Primer design primarily completed using Primer3 software (Untergasser *et al.*, 2012).

Schizosaccharomyces pombe gene sequences and data obtained from Pombase (Wood *et al.*, 2012).

Vertebrate and non-vertebrate species gene and peptide sequences for sequence comparisons obtained from the Ensembl Genome database (Flicek *et al.*, 2012, Kersey *et al.*, 2012).

2.4.16 Sequence alignments and protein structure prediction

Sequence alignments between peptide sequences from different species were through use of Clustal Omega (Sievers *et al.*, 2011) and visualised with BoxShade.

BoxShade server, 3.21, September 2013, K. Hofmann and M. Baron, Memorec Biotech GmbH, Germany, http://www.ch.embnet.org/software/BOX_form.html

Secondary structure prediction was conducted using the PredictProtein server (Rost *et al.*, 2004) and PSIPRED (Buchan *et al.*, 2013, Jones, 1999).

Protein crystal structure models were obtained from the Protein Data Bank (Berman *et al.*, 2000) and visualised using ProteinShader (Weber, 2009).

The effect of amino acid substitutions on **protein stability** was analysed using SIFT (Kumar *et al.*, 2009, Ng and Henikoff, 2006), SDM (Worth *et al.*, 2011) and mCSM (Pires *et al.*, 2013) servers.

2.5 Yeast techniques

2.5.1 *S. pombe* crosses and random spore analysis

Strains of opposite mating types (h$^+$ and h$^-$) were crossed on ELN agar plates by picking a single colony of one strain using a sterile tip and patching in an area approximately 1cm^2. The second strain was then patched over the first using the same technique. Crosses were incubated for 3 days at 25°C to generate tetrads.

Random spore analysis was conducted by taking a loop of cells from the cross and resuspended in 500µl ddH$_2$O. The cells were then heated to 50°C on a heat block with intermitted vortexing for 30 minutes to kill vegetative cells. The spores were cooled to room temperature and diluted 1/100, 1/1000 and 1/10 000. 100µl of each dilution was then plated on an appropriate agar plate for selection of specific auxotrophic markers. For selection of antibiotic resistance, the spores were first plated on non-selective plates, either YES agar or appropriate YNG minimal media. Colonies were then replica-plated to YES agar + antibiotic plates. Colony growth on selective plates was scored according to desired genotype to identify correct haploid strain.

2.5.2 *S. pombe* transformation

Base strains were inoculated in 10ml of appropriate media per transformation and grown overnight to mid-log phase (0.5-1.5x10^7 cells/ml). Cells were harvested by centrifugation at 1800 RPM for 4 minutes using an Eppendorf 580 R centrifuge. Cells were then washed by resuspension of pellet in 5ml sterile water and then centrifuged again. Cells were then washed with 5ml 1x LiAc/TE solution, centrifuged again and resuspended in 100µl 1x LiAc/TE. Between 100ng and 1µg of transforming DNA (up to 10µl) was added followed by 10µl 2mg/ml salmon sperm DNA (Sigma D1626) which had been boiled for 5 minutes at 95°C and cooled on ice. The cells were mixed by gentle vortexing followed by the addition of 260µl of freshly made PLATE solution (40% w/v PEG in 1x LiAc/TE). Transformation mix was then incubated for 2-4 hours at

30°C (4 hours at 25°C for temperature-sensitive strains). 43μl of sterile DMSO was then added and the cells heat shocked at 42°C for 10 minutes (5 minutes for temperature-sensitive strains). The cells were then plated out directly on selective plates and incubated at an appropriate temperature for several days until colonies are formed. For antibiotic marker, the cells are plated on YES for 24 hours, then replica plated to the appropriate selection plate. Alternatively, the cells could be cultured in YES liquid media for 2-3 hours before plating on selective plates.

2.5.3 *S. pombe* gene deletion/disruption

Disruption or deletion of a gene required the integration of a plasmid containing a selectable marker at the genomic locus [Fig 2.1A]. Primers were designed with the aid of Primer3 software to target the promoter and terminator regions of the gene in question, making sure not to disrupt upstream or downstream genes. These are identified by the prefix, T1, T2, P3 or P4. The upstream region is targeted by primers P3 and P4 and downstream by T1 and T2. The T1 and P4 primers are designed with restriction sites from the MCS of a suitable vector at the 5' end followed by appropriate homology to the target regions (typically 300-400bp). Primers T2 and P3 were designed with the sequence: GTCGTGACTGGTACAAC and GTTGTACCAGTCACGAC (antiparallel sequences) at the 5' terminus respectively. This sequence is followed by a restriction site (typically BglII) which will be unique on the final vector and then appropriate homology to the target region. PCR reactions were then performed on genomic DNA to amplify the two target regions P (upstream homology) and T (downstream homology) using primers P3/P4 and T1/T2 using a high performance polymerase, such as Takara ExTaq or Phusion polymerase [Fig 2.1B(i)]. The resulting PCR products were then purified and 100ng of each used as template in a second, fusion PCR reaction using primers T1 and P4 only [Fig 2.1B(ii)]. The specific antiparallel sequences inserted into primers T2 and P3 provide a short homologous section which allows the PCR products to overlap and anneal in the fusion PCR reaction. The product of the fusion PCR reaction was then purified and

digested. This digest product was then cloned into the MCS of a vector containing a selectable marker, for example pFY106 for $ura4^+$ selection [Fig 2.1B(iii)]. The vector was sequenced to confirm no mutations had been introduced during the PCR reactions. Finally, the vector was linearised by cutting at the unique site (BglII) and then transformed into the yeast strain for integration at the targeted locus. Integration is confirmed by PCR.
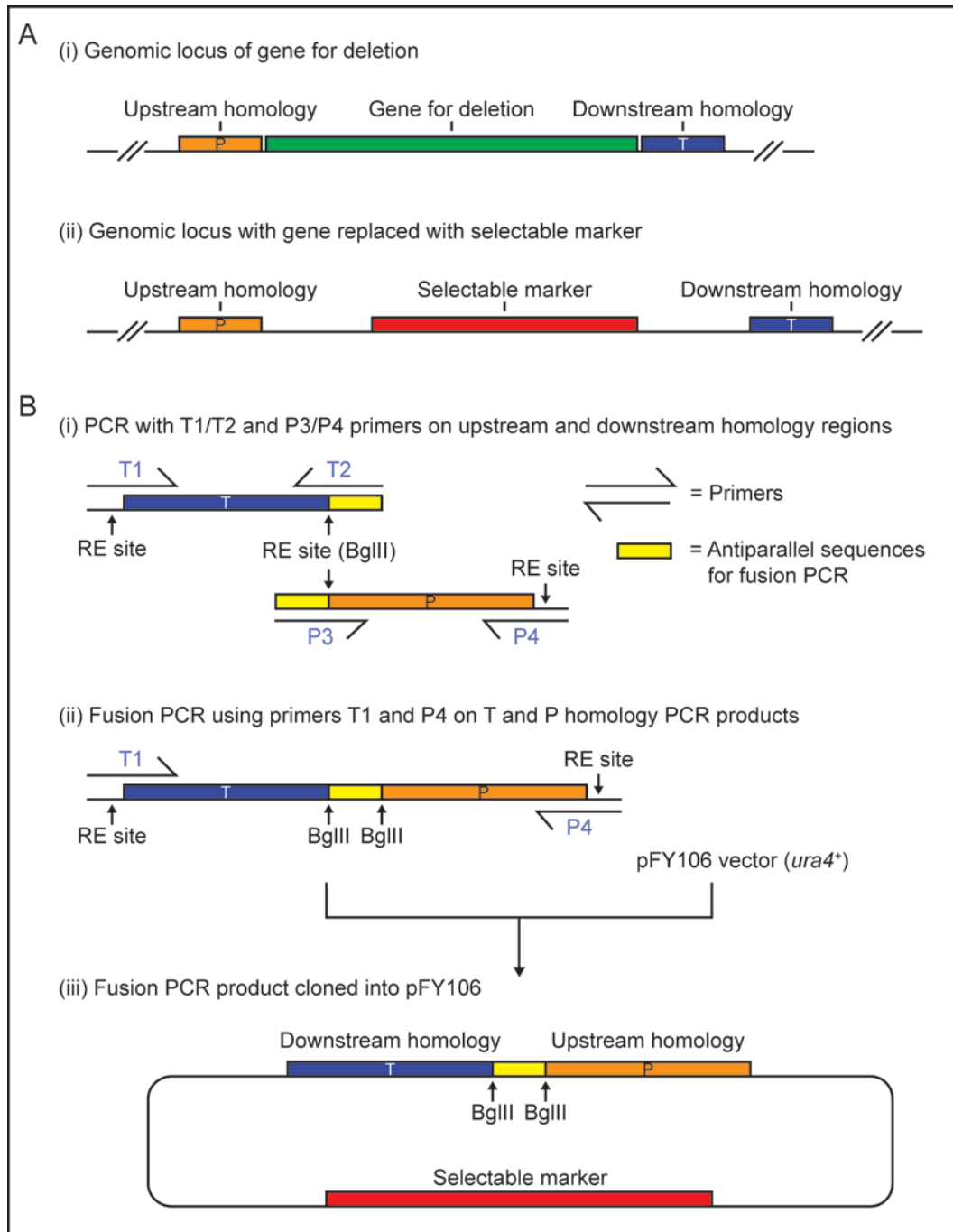
Figure 2.1: Schematic indicating method of deletion/disruption of *S. pombe* genes.

(A) The genomic locus **(i)** of an example gene (green) is flanked by upstream (orange) and downstream (blue) homology regions which relate to the Promoter and Terminator regions. **(ii)** Deletion/disruption of gene by replacement with selectable marker (red) while maintaining upstream (orange) and downstream (blue) homology regions. Method of deletion **(B)** involves PCR **(i)** of downstream region of homology with primers T1 and T2 and upstream region of homology with primers P3 and P4 (see main text for details). Primers T2 and P3 contain specific antiparallel sequences of homology (yellow) which allows annealing in second, fusion PCR. The fusion PCR **(ii)** using the T and P region PCR products with primers T1 and P4 produces a single product containing the central specific antiparallel sequence (yellow) flanked by BglII sites and the T and P regions from the previous PCR. The fusion PCR product is purified and cloned into an appropriate vector, such as pFY106. This vector **(iii)** can be linearised by digest with BglII and integrated at the locus targeted by the P and T homology regions to delete/disrupt the locus.

2.5.4   *S. pombe* Recombination-Mediated Cassette Exchange (RMCE)

RMCE was performed by a method based on Watson *et al* (2008). An appropriate base strain, containing a cassette, typically *ura4⁺*, flanked by loxP and loxM3 sites, was transformed with a vector containing the cassette of interest flanked by the same lox sites. The loxM3 site contains 6 nucleotide changes in the central spacer region when compared to loxP [Fig 2.2A]. This prevents Cre-dependent recombination between loxP and loxM3. (Langer *et al.*, 2002) Activation of Cre-recombinase in a yeast cell containing both lox cassettes allowed recombination between the equivalent lox sites, replacing the genomic cassette with the one contained on the plasmid [Fig 2.2B]. The transformed cells were plated on YNG –Leu (without thiamine) to activate expression of the Cre-recombinase gene and incubated at 30°C (25°C for temperature sensitive strains) for several days to allow colonies to form. These colonies were streaked out onto YES agar plates (contains thiamine) to stop selection of the plasmid and shut off Cre-recombinase expression. Individual transformants were then tested for the loss of the *ura4⁺* marker (by RMCE) from the targeted chromosomal locus by streaking on YNG –Ura, YNG –Leu and YES+5-FOA agar plates. Colonies which were 5-FOA^R and *leu$^-$* were analysed further by PCR for correct integration of the desired cassette.
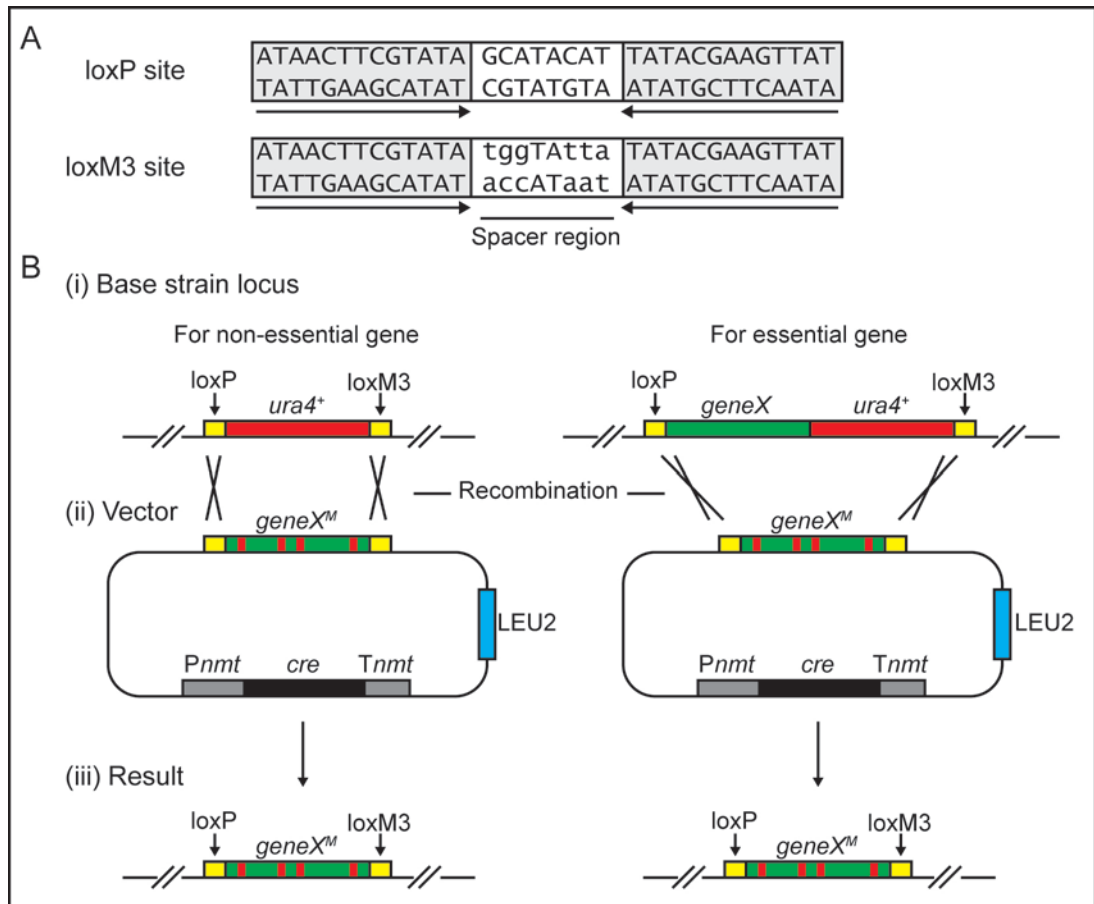
Figure 2.2: Schematic showing use of Recombination Mediated Cassette Exchange (RMCE) in the integration of a gene.

(A) Wild type loxP and mutant loxM3 site sequences (Langer *et al.*, 2002). Both sites consist of identical palindromic arms acting as binding sites for Cre recombinase (grey background). The central spacer region (indicated) deviates from wild type in loxM3, as shown by lower case letters. This prevents Cre-dependent recombination between the two sites. **(B)** Method of RMCE based on Watson *et al.* (2008) for non-essential and essential genes. Base strain contains cassette at locus of interest **(i)** consisting of a marker, ura4+ (red), for non-essential genes or the wild type gene (*geneX* in green) followed by a marker for essential genes. This cassette is flanked by loxP and loxM3 sites (yellow) which can undergo Cre-dependent recombination with equivalent sites, but not each other. A vector is transformed **(ii)**, which contains a modified or mutated gene of interest (*geneX^M* in green with red bars indicating mutations); the *cre* gene (black) under *nmt* control (grey boxes indicating Promoter, P*nmt,* and Terminator, T*nmt*) and a selectable marker, LEU2 (blue). The *cre* gene expression is activated by plating cells on media lacking thiamine which results in recombination between lox sites (indicated). The result **(iii)** is the base strain locus being modified by replacement of the previous cassette (containing *ura4⁺* or *geneX, ura4⁺*) with the modified or mutated form (*geneX^M*).

2.5.5 *S. pombe* Genomic DNA preparation

Strains were cultures in YES liquid media to mid-log phase. A total of 1×10^9 cells were harvested per prep by centrifuging in 50ml centrifuge tubes using an Eppendorf 580 R at 3000 RPM for 5 minutes. Pellets were then resuspended in 1ml SP1 buffer containing 50µl 100T Zymolyase (US Biological Z1004) and incubated at 37°C for 20-30 minutes. After 20 minutes, cells were checked for spheroplasting under a microscope (5µl cells + 5µl 10% SDS). When sphereoplasting reached 80-90% of cells, the samples were centrifuged at 3000 RPM for 5 minutes and resuspended in 450µl 5xTE and transferred to eppendorf tubes. 50µl of 10% (w/v) SDS was then added, the sample inverted several times and incubated for 5 minutes at room temperature. 150µl of cold (4°C) 5M KAc was then added and samples incubated for 10 minutes on ice. The samples were then centrifuged at 13 000 RPM for 10 minutes at 4°C using Thermo Heraeus Fresco 21 refrigerated micro centrifuge. The supernatant was transferred to a fresh tube and 650µl cold isopropanol added. They were then incubated at -20°C for 20 minutes before being centrifuged at 15 000 RPM for 10 minutes at 4°C. The pellets were washed with 500µl 70% (v/v) ethanol and gently resuspended in 500µl of 5xTE. 10µl of RNAse (10mg/ml, Sigma R6513) was added and the samples incubated for 20 minutes at 37°C. 4µl 10% (w/v) SDS and 20µl Proteinase K (10mg/ml, Melford Labs MB2005) was added and samples incubated at 30°C overnight. The next day, 500µl Phenol:Chloroform:Isoamyl alcohol was added and each sample transferred to a peqGOLD PhaseTrap tube (Peqlab 30-0015A-01) and centrifuged for 5 minutes at 13 000 RPM. The supernatant was then transferred to a new PhaseTrap tube and the process repeated. The supernatant was then transferred to a new eppendorf tube where $1/10^{th}$ volume 3M NaAc and 2.5 volumes 90% ethanol was added. The samples were incubated at -20°C for at least 20 minutes before being centrifuged at 15 000 RPM for 15 minutes at 4°C. The pellets were washed with 70% (v/v) ethanol and resuspended in 50µl of 1xTE. 1µl of the genomic preps were then checked for concentration and degradation by agarose gel electrophoresis.

2.5.6 *S. pombe* TCA protein extraction

Strains were grown overnight to mid-log phase. $1x10^8$ cells were harvested by centrifuging at 3000 RPM for 4 minutes using an Eppendorf 580 R centrifuge in 50ml centrifuge tubes. Pellets were resuspended in 1ml sterile water and transferred to skirted screw-cap 2ml tubes. Cells were spun down at 13 000 RPM for 10 seconds and the supernatant removed. Zicornia/silica glass beads (Biospec 11079105z) were added to the 300μl mark followed by 200μl 20% (w/v) TCA. The samples, kept on ice, were lysed immediately by 1 minute shaking in a BioSpec Mini-Beadbeater-16 at 4°C. The sample were transferred into a clean tube by placing a non-skirted tube (with 400μl 5% (w/v) TCA added) inside a 15ml centrifuge tube followed by the skirted sample tube with a hole punctured in the bottom. These were then centrifuged for 1 minute at 4000 RPM. The skirted tube (retaining the beads) was discarded and the non-skirted tube (containing the sample) was centrifuged for 5 minutes at 13 000 RPM. The supernatant was then removed and the pellet resuspended in 400 μl 1x Sample buffer (see below). The samples were vortexed, boiled at 100°C for 5 minutes, vortexed again and centrifuged for 5 minutes at 13 000 RPM to precipitate cell debris. The supernatant could then be used for western blot analysis.

1x TCA Sample Buffer per sample:

90μl 4x TCA sample buffer, 100μl 1M Tris-HCl pH7.5, 200μl ddH$_2$O, 10μl β-Mercaptoethanol

2.5.7 *S. pombe* plasmid recovery

Strains containing plasmid of interest were grown to mid-log phase in 10ml selective media. The cultures were centrifuged at 1900 RPM for 2 minutes and washed with 500μl ddH$_2$O before transfer to eppendorf tubes. The cells were resuspended in 0.5ml SP1 containing 5μl 100T Zymolyase (US Biological Z1004) and incubated at 37°C for 20-30 minutes. The cells were then centrifuged at 13000 RPM for 1 minute and resuspended in 300μl 1xTE. 35μ of SDS was added, the tubes inverted several times and incubated at 65°C for 5 minutes. 100μl of KAc was

then added and the samples incubated on ice for 30 minutes. They were then centrifuged at 13 000 RPM for 10 minutes at 4°C and the supernatant transferred to a new tube. 1 volume of Phenol:chloroform:isoamyl alcohol was added and the tubes centrifuged at 13 000 RPM for 5 minutes. The upper aqueous layer was then transferred to a new tube and 0.7 volumes of isopropanol was added. The samples were centrifuged at 15 000 RPM for 30 minutes and the pellets washed with 70% (v/v) ethanol. The dry pellet was then resuspended in 10µl 1xTE and 5µl used for transformation into NEB DH5α high efficiency competent cells. The transformations were plated on LB agar plates with appropriate antibiotic and incubated overnight at 37°C. The colonies were inoculated the next day in LB liquid media for plasmid prep.

2.5.8 *S.* pombe Chromatin Immunoprecipitation (ChIP)

Strains were grown in 40ml cultures to a density of $1x10^7$ cells/ml and cultures collected in 50ml centrifuge tubes. 1.1ml of 37% v/v formaldehyde was added and the tube rotated at room temperature for 15 minutes. 2ml 2.5M glycine was then added and the samples rated for a further 10 minutes before being transferred to ice. Samples were centrifuged at 4000 RPM at 4°C for 5 minutes and the supernatant removed. The pellets were washed with 30ml ice-cold HBS followed by a 4000 RPM spin at 4°C for 5 minutes. The pellets were washed again with 25ml ice-cold ChIP lysis buffer and centrifuged at 4000 RPM at 4°C for 5 minutes. The pellets were then resuspended in 600µl ChIP lysis buffer plus PMSF plus cOmplete Mini and transferred to 1.7ml Eppendorf tubes which were flash frozen in liquid nitrogen.

The samples were thawed quickly at 37°C and put on ice. Zirconia/silica beads were added to flat-bottomed screw-cap tubes on ice and the samples added. These were then inverted and the tubed topped up with ChIP lysis buffer + PMSF + cOmplete Mini. These were shaken for 2 minutes at 4°C on in a Mini-bead beater. A hole was then punched in the bottom of the tubes with a hot needle and the liquid spun into fresh screw-cap tubes at 3000 RPM, 4°C for 1

minute. These new tubes were then centrifuged at 14 000 RPM at 4°C for 30 minutes. The supernatant was discarded and the pellets resuspended in 600µl ChIP lysis buffer + PMSF + cOmplete Mini and transferred to new tubes on ice. A Bioruptor sonicator was then used at low setting, 5 x 30 second pulses, twice to sonicate the DNA. The samples were then centrifuged at 5000 RPM 4°C for 5 minutes. The supernatant was transferred to new tubes and centrifuged again at 5000 RPM 4°C for 15 minutes. The supernatant was then transferred to a new tube and 10µl removed for the input sample.

To IP, 100µl of anti-myc antibody (from 9E10 hybridoma cell line) was added to the samples and mixed by vortexing. These were then incubated on ice for 1 hour. 40µl of Dynabeads ProteinG (Life Technologies 10003D) per sample were prepared by washing three times in ChIp lysis buffer + PMSF + Complete mini and added to samples followed by 2 hour incubation, rotating at 4°C.

The beads were immobilised on a magnetic rack and the supernatant removed. The beads were then washed with 1.5ml AT1 + 0.003% w/v SDS at room temperature for 5 minutes. This was repeated and followed by washing with AT2 buffer in the same manner, then AT3 and finally AT4, where only a brief mix by inversion was required before removal of supernatant. 140µl of TES was added to beads, vortexed and heated to 65°C for 2 minutes. On a magnetic rack, 120µl of the supernatant was removed and transferred to a fresh tube and incubated at 65°C overnight.

Samples were then purified through Qiagen purification columns and eluted in 50µl

2.5.9 *S. cerevisiae* crosses

Strains with mating type a and α were crossed on rich media (YPAD) by picking a single colony of one strain using a sterile pipette tip and patching in an area approximately 1cm^2. The second strain was then patched over the first using the same technique. Crosses were incubated at 30°C for 24hours before selecting for diploids.

2.5.10 *S. cerevisiae* transformation

Strains were inoculated in YPAD or minimal selective media, as required and grown overnight at 30°C. The cultures were diluted in 50ml liquid media to a density of $5x10^6$ cells/ml and grown for a further 3 hours at 30°C. The cells were harvested by centrifuging at 4000 RPM for 5 minutes in 50ml centrifuge tubes. The pellets were resuspended in 25ml ddH$_2$O and centrifuged again. The pellets were then washed again in 100mM LiAc and transferred to eppendorf tubes. The cells were centrifuged at 13 000 RPM for 15 seconds and the supernatant removed. The cells were then resuspended in 400μl 100mM LiAc and 50μl aliquots made for each transformation. A master mix for each transformation was made, consisting of 240μl 50% (w/v) PEG, 36μl 1M LiAc, 50μl boiled salmon sperm DNA (Sigma D1626), 100ng transforming DNA and ddH$_2$O up to a total volume of 360μl. This was added to the cells, gently mixed and heat shocked at 42°C for 45 minutes. The transformations were then centrifuged at 13 000 RPM for 15 seconds and the cells resuspended in ddH$_2$O. 10% and 90% of the transformations were plated on separate agar plates selective for the transformed DNA. These plates were incubated at 30°C for 2-4 days until colonies were visible.

2.5.11 *S. cerevisiae* Whole Cell TCA Protein Extraction

Strains were grown overnight in appropriate liquid media at 30°C to mid-log phase. $1x10^8$ cells were harvested by centrifugation at 4000 RPM for 5 minutes in 50ml centrifuge tubes. The cells were then washed with 500μl ddH$_2$O and transferred to eppendorf tubes on ice. Zirconia/silica glass beads (Biospec 11079105z) were added to the 300μl mark and the pellets resuspended in 200μl 20% (w/v) TCA. The cells were lysed for 1 minute in a a BioSpec Mini-Beadbeater-16 at 4°C. 400μl of 5% (w/v) TCA was then added and the suspension transferred to new eppendorf tubes. These were then centrifuged at 3000 RPM for 10 minutes and the supernatant discarded. The pellets were then resuspended in 200μl 1x Laemmli buffer which turned yellow due to low pH. 1M Tris pH 10.2 was added until the colour returned to blue. The samples were then boiled for 3 minutes at 100°C and centrifuged at 3000 RPM for 10 minutes.

The supernatant was then transferred to a new eppendorf tube and 5-10μl used for western blotting.

2.5.12 *S. cerevisiae* plasmid recovery

Strains containing the plasmid of interest were grown overnight at 30°C in 3ml minimal media, selective for the plasmid to be recovered, e.g. Sc –LEU for pGADT7 plasmids. 1.5ml of the culture was transferred to a skirted, screw cap 2ml tube and centrifuged at 13 000 RPM for 1 minute. The supernatant was removed and pelleted cells vortexed to resuspend in the residual liquid. 200μl Breaking buffer was added followed by a similar volume of Zirconia/silica beads (Biospec 11079105z). 200μl Phenol:chloroform:isoamyl alcohol was then added. The tubes were capped tightly and vortexed for one minute twice before centrifuging at 13 000 RPM for 5 minutes. 100μl of the aqueous layer was then transferred to a clean eppendorf tube. 1-2μl of this was then transformed into NEB DH5α high efficiency competent cells and plated on LB agar with appropriate antibiotic selection. Plates were incubated overnight at 37°C and colonies inoculated in LB liquid media with appropriate antibiotic selection for plasmid prep.

2.5.13 Replica plating

Agar plates were marked such that the orientation could be tracked between source and destination plates. A sterile piece of velveteen was placed over a cylindrical block and colonies from the source plate gently transferred. The destination plate was then placed on the velveteen in the same orientation as the source plate and the cells gently transferred from the velveteen to the destination plate.

2.6 Molecular assay techniques

2.6.1 Blue-White filter lift assay

Strains to be tested were streaked on agar plates selective for the pGBKT7 and pGADT7 plasmids. Circular pieces of filter paper were placed over the streaks and cells transferred by applying pressure on the reverse side. The filter papers were removed and submerged in liquid nitrogen for ten seconds three times, allowing the filter paper to thaw between each submersion. A second circular piece of filter paper for each plate was placed in an empty petri dish and soaked with 3.5ml fresh Z-buffer/X-Gal (see below). Each filter containing cells was then placed over the Z-buffer/X-Gal soaked filters, cells facing up and allowed to take up the buffer until the filter was soaked. Each dish was then sealed with parafilm and incubated for 5-8 hours at 30°C. When a blue colour became visible on the controls, the filters were removed from the incubator and allowed to dry overnight in a fume hood. Blue-White colouration was then scored.

For 10ml of Z-buffer/X-Gal: 10ml   Z-buffer

                                  27µl   β-mercaptoethanol

                                  167µl   X-Gal (2% stock)

2.6.2 Spot assays

Strains were grown in YES or selective minimal media overnight to mid-log phase at 25°C. The cultures were diluted to the same density and incubated for a further 3 hours at which point an accurate cell count was taken. The cultures were diluted to 1.25×10^7 cells/ml and 1/5 serial dilutions made in a 96-well plate. A pin replicator was then used to transfer 5µl of culture from each well to agar plates. The liquid was allowed to soak into the agar before the plates were incubated at the desired temperatures.

2.6.3 Western Blot

Gels for SDS-PAGE were prepared using ProtoGel (30%, 37.5 to 1 Acrylamide to Bisacrylamide-stabilised solution optimised for SDS-PAGE of proteins, National Diagnostics, ELR-210-010P). The percentage of the running gel was dependent on the expected size of the protein of interest. The table below shows the compositions of the running gels for different percentages of 12ml volume.

Reagent	Volume (ml) for gel percentages indicated				
	7.5%	10%	11%	12%	15%
Protogel (30%)	2.92	4.00	4.24	4.80	6.00
1M Tris pH 8.8	4.50	4.50	4.50	4.50	4.50
H_2O	4.40	3.32	3.08	2.52	1.32
10% (w/v) SDS	0.12	0.12	0.12	0.12	0.12
10% (w/v) APS	0.06	0.06	0.06	0.06	0.06
TEMED	0.02	0.02	0.02	0.02	0.02

The table below shows the composition of the stacking gel (8ml)

Reagent	Volume (ml)
Protogel (30%) (ml)	1.28
1M Tris pH 8.8 (ml)	1.00
H_2O (ml)	5.60
10% (w/v) SDS (ml)	0.08
10% (w/v) APS (ml)	0.04
TEMED (ml)	0.01

Samples were separated by SDS-PAGE using a Bio-Rad Mini-Protean TetraCell. Prestained protein marker (Bio-Rad 161-0374) was loaded as a size reference. The samples were run at 100 volts through both the stacking and running gels in 1x SDS-PAGE running buffer. The gels were then transferred onto Nitrocellulose membrane using a Bio-Rad Mini-Protean Transblot system according to provided protocol in 1x Transfer buffer. The gel was transferred at 240mA for 1 hour 15 minutes at 4°C. The membrane was then stained with Ponceau for 1 minute to check for protein content and loading comparison.

The membrane was blocked with 5% (w/v) milk powder (Marvel dried skimmed milk) in TBST (TBS + 0.05% Tween20) for at least 1 hour at room temperature or overnight at 4°C. The primary antibody was added at a the appropriate dilution factor in 5% (w/v) milk solution and the membrane was incubated for 2 hours at room temperature or overnight at 4°C. The membrane was then washed in TBST for 5 minutes, 5 times. The secondary antibody was then added at the appropriate dilution in 5% (w/v) milk solution and the membrane was incubated for a further 1 hour at room temperature. The membrane was washed in TBST for 5 minutes, 5 times, and the bound antibody was detected by chemiluminescence using ECLPlus reagent (SLS ECLPlus Western Blotting Reagent RPN2132) according to manufacturer provided protocol with final detection using a GE Healthcare ImageQuant LAS 4000 imager.

2.6.4   Southern Blot

Genomic DNA preps were prepared as described. 10-15µl from each of the genomic preps was digested with ApaI or EcoRI restriction enzymes overnight. Samples were loaded onto a 1.5% 150ml agarose gel (for ApaI digests) or 0.8% 150ml agarose gels (for EcoRI digests) and run at 100 volts (constant) for 180 minutes in 0.5xTBE. The ethidium bromide-stained gel was then imaged on a UV transilluminator to assess the loading and running of samples. The gel was then rinsed in water and depurinated by submersion in 0.25M HCl for 15 minutes. The gel was then rinsed again and equilibrated with 0.4M NaOH by submersion for a further 15 minutes. A Perspex tray was filled 1-1.5cm deep with 0.4M NaOH. A glass plate was placed across it and a strip of watmann paper, wide enough to hold the gel, was soaked in 0.4M NaOH and laid out the glass plate, allowing the two ends of the strip to dip into the 0.4M NaOH below. The gel was then placed on the strip of watmann paper with the top surface of the gel facing down, touching the watmann paper. Any air bubbles were eliminated and a piece of positively charged nylon membrane (Roche 11417240001), cut to the size of the gel, was placed over the gel, allowing the buffer to soak through. Wide strips of parafilm were places around the gel and membrane to ensure the buffer could only travel through the gel. Two additional pieces of

watmann paper, cut to 1cm larger than the gel, were then placed on top of the membrane followed by dry paper towels in perpendicular stacks approximately 4cm high. A second glass plate was then placed on the paper towels and a 0.5kg weight placed on the glass plate. This transfer stack was allowed to stand overnight to allow the DNA to be transferred to the membrane by capillary action.

The following day, the stack was dismantled and the membrane removed. The membrane was rinsed with water and then transferred to a hybridisation tube pre-warmed to 65°C in a Stuart S130H hybridisation oven. 30ml of Church hybridisation buffer was then added to the hybridisation tube and the membrane pre-hybridised, rotating in the oven, for one hour. 40ng of telomere probe from the pSpTelo plasmid was diluted in 1xTE up to 45μl. This was then boiled at 95°C for 5 minutes and placed on ice for 2 minutes. The cooled probe was then centrifuged briefly and added to a DNA labelling bead (Amersham Ready-to-go DNA labelling beads (-dCTP) cat: 27-9240-01), resuspending the bead in the solution and placing back on ice. 5μl of radio-labelled dCTP was immediately added (Perkin-Elmer Easytides 5'triphosphate [alpha-32-P] NEG513H) and the tube incubated in a 37°C water bath for 1 hour. Following incubation, the probe was purified through a G-50 micro-column (Illustra ProbeQuant G-50 Micro Columns, Cat 28-9034-08) according to the provided protocol. The purified, labelled probe was then boiled at 95°C for 5 minutes, quickly spun down and added directly to the Church hybridisation buffer incubated with the membrane. The membrane was allowed to hybridise overnight at 65°C.

The following day, the hybridisation buffer was discarded and Church wash buffer, pre-heated to 65°C was added to the hybridisation tube. The membrane was washed at 65°C for 5 minutes, the wash buffer discarded and the membrane washed again for a further 20 minutes. This was repeated once again before the membrane was removed from the hybridisation tube and laid flat on a piece of tissue, DNA side facing up, to allow any remaining buffer to be

removed. The membrane was then wrapped in cling film and exposed to a phosphoimager screen. 2 hour and 16 hour exposures were scanned on Fujifilm FLA-5100 scanner.

2.6.5 Slot Blot

Samples for use in slot blot were prepared using the ChIP protocol. 60% of each ChIP sample was used for blotting in a Hoefer PR 648 slot blot manifold according to the manufacturer supplied protocol.

2.6.6 qPCR

qPCR was performed on ChIP samples (and 1% input) in triplicate. The TAS1 amplicon was targeted using primers TAS1-f6-Sp and TAS1-b5-Sp. A negative control amplicon, Fas2, was targeted using the primers fas2-f1-Sp and fas2-b1-Sp. A Roche LightCycler 480 system was used with SYBR Green Master Mix (Life Technologies) according to manufacturer instructions to generate Ct values. Calculations: $\Delta Ct[TAS1] = Ct[input]-Ct[TAS1]$. $\Delta Ct[Fas2] = Ct[input]-Ct[Fas2]$. Fold Enrichment $= 2^{\wedge}\Delta Ct[TAS1] / 2^{\wedge}\Delta Ct[Fas2]$.

2.6.7 Testing protein-protein interactions by Yeast 2-hybrid

The pGBKT7 Gal4-Binding Domain (GBD) and pGADT7 Gal4-Activating Domain (GAD) plasmids to be tested (as well as positive and negative controls) were transformed into the PJ69-4A yeast 2-hybrid strain using the *S. cerevisiae* transformation protocol shown previously. Transformants were selected on Sc -TRP -LEU agar at 30°C until single colonies formed. Several colonies from each transformation were streaked to single colonies on fresh Sc -TRP -LEU agar at 30°C. Single colonies were then streaked to media selective for the expression of reporter genes (see below) at 30°C. Presence of interaction between the GBD and GAD fusion proteins was determined by observation of growth on this selective media compared to positive and negative controls. The strength of the interaction, relative to controls, could be approximated by comparison of growth on increasingly stringent media.

Selection of HIS3 reporter: Sc -TRP -LEU -HIS (least stringent)

Sc -TRP -LEU -HIS + 2-7mM 3-Amino,1,2,4-Triazole (increasing

stringency with increasing concentration of 3-AT)

Selection for ADE2 reporter: Sc -TRP -LEU -ADE (most stringent)

Selection for HIS3 and ADE2:   Sc –TRP –LEU –ADE –HIS + 2-7mM 3-Amino,1,2,4-Triazole

Table 2.1: List of *S. cerevisiae* strains used in this study.

YAB Strain No.	Strain	Genotype	Source
1517	PJ69-4A	MATa trp1-901 leu2-3,112 ura3-52 his3-200 gal4 gal80 LYS2::GAL1-HIS3 GAL2-ADE2 met2::GAL7-lacZ	Hideo Tsubouchi
1537	Y190	MATa trp1 leu2 ade2 his3 can1 gal4 gal80 URA3::GAL1-LacZ URA3::GAL1-HIS3	Thomas *et al.* (2002)
1609	LY26	MAT-alpha trp1 ura3 leu2 met15 gal4 gal80 ho::KanMX::GAL1-TetR TetO-ADE2 LYS2::LexA-HIS3	Thomas *et al.* (2002)
1629	DY6877	MATa trp1 leu2 ade2 his3 lys2 can1 URA3::LexA-LacZ	Thomas *et al.* (2002)
1930	LY26-Strain 1	MAT-alpha trp1 ura3 leu2 met15 gal4 gal80 ho::KanMX::GAL1-TetR TetO-ADE2 LYS2::LexA-HIS3 TRP1::GBD-SpRap1 URA3::LexA-SpTpz1	This study
1931	LY26-Strain 2	MAT-alpha trp1 ura3 leu2 met15 gal4 gal80 ho::KanMX::GAL1-TetR TetO-ADE2 LYS2::LexA-HIS3 TRP1::GBD-EV URA3::LexA-SpTpz1	This study
1932	LY26-Strain 3	MAT-alpha trp1 ura3 leu2 met15 gal4 gal80 ho::KanMX::GAL1-TetR TetO-ADE2 LYS2::LexA-HIS3 TRP1::GBD-SpTpz1 URA3::LexA-SpRap1	This study
1933	LY26-Strain 4	MAT-alpha trp1 ura3 leu2 met15 gal4 gal80 ho::KanMX::GAL1-TetR TetO-ADE2 LYS2::LexA-HIS3 TRP1::GBD-EV URA3::LexA-SpRap1	This study
1934	LY26-Strain 5	MAT-alpha trp1 ura3 leu2 met15 gal4 gal80 ho::KanMX::GAL1-TetR TetO-ADE2 LYS2::LexA-HIS3 TRP1::GBD-EV URA3::LexA-EV	This study
1935	LY26-Strain 6	MAT-alpha trp1 ura3 leu2 met15 gal4 gal80 ho::KanMX::GAL1-TetR TetO-ADE2 LYS2::LexA-HIS3 TRP1::GBD-SpTpz1 URA3::LexA-EV	This study
1936	LY26-Strain 7	MAT-alpha trp1 ura3 leu2 met15 gal4 gal80 ho::KanMX::GAL1-TetR TetO-ADE2 LYS2::LexA-HIS3 TRP1::GBD-SpRap1 URA3::LexA-EV	This study

Table 2.2: List of *S. pombe* strains used in this study.

BAF Strain No.	Strain	Genotype	Source
3	Wild Type	h- ade6-210 his3-D1 ura4-D18 leu1-32	Bianchi Lab
6	Wild Type	h+ ade6-216 his3-D1 ura4-D18 leu1-32	Bianchi Lab
344	*poz1Δ (ura4$^+$)*	h- poz1::loxP-ura4$^+$-loxM3 ade6-M210 his3-D1 leu-32 ura4-D18	This study
384	loxP-Poz1-FL2	h- poz1::loxP-Poz1-FL2-loxM3 ade6-M210 his3-D1 leu-32 ura4-D18	This study
386	loxP-Poz1-mut20	h- poz1::loxP-Poz1-mut20-loxM3 ade6-M210 his3-D1 leu-32 ura4-D18	This study
387	loxP-Poz1-mut23	h- poz1::loxP-Poz1-mut23-loxM3 ade6-M210 his3-D1 leu-32 ura4-D18	This study
388	Poz1-10Myc	h- poz1::Poz1-10Myc (ura4$^+$) ade6-M210 his3-D1 leu-32 ura4-D18	This study
389	loxP-Poz1-FL2-10Myc	h- poz1::loxP-Poz1-FL2-10Myc (ura4$^+$) ade6-M210 his3-D1 leu-32 ura4-D18	This study
390	loxP-Poz1-mut20-10Myc	h- poz1::loxP-Poz1-mut20-10Myc (ura4$^+$) ade6-M210 his3-D1 leu-32 ura4-D18	This study
391	loxP-Poz1-mut23-10Myc	h- poz1::loxP-Poz1-mut23-10Myc (ura4$^+$) ade6-M210 his3-D1 leu-32 ura4-D18	This study
246	*pot1-1*	h- pot1::pot1-1-GFP-kanR ade6-M210 ura4-D18 leu1-32	Bianchi Lab
247	*pot1$^+$/pot1-1*	h+/h- pot1+/pot1::pot1-1-GFP-kanR ade6-M210/ade6-M216 ura4-D18/ura4-D18 leu1-32/leu1-32	Bianchi Lab
279	*rad16Δ*	h+ rad16::rad16D-L (leu$^+$) ade6-M210 ura4-D18 leu1-32 his3-D1	Bianchi Lab
161	*lig4Δ*	h- lig4::bsdSVEM ade6-M216 ura4-D18 leu1-32 his3-D1	Bianchi Lab
69	*pot1Δ*	h- pot1::bsdSVEM ade6-M216 ura4-D18 leu1-32 his3-D1	Bianchi Lab
382	*rqh1Δ (ura4$^+$)*	h+ rqh1::ura4$^+$ ade6-704 ura4-D18 leu1-32	Johanne Murray
371	*rqh1Δ (his3$^+$)*	h- rqh1::rqh1D-H (his$^+$) ade6-210 his3-D1 ura4-D18 leu1-32	This study
383	*pot1-1 rqh1Δ*	h- pot1::pot1-1-GFP-kanR rqh1::ura4$^+$ ade6-M210 ura4-D18 leu1-32	This study
370	*stn1$^+$-ura4$^+$ (h-)*	h- stn1::loxP-stn1$^+$-ura4$^+$-loxM3 (ura$^+$) ade6-M216 ura4-D18 leu1-32 his3-D1	This study
372	*stn1$^+$-ura4$^+$ rqh1Δ (h-)*	h- stn1::loxP-stn1$^+$-ura4$^+$-loxM3 (ura$^+$) rqh1::rqh1D-H (his$^+$) ade6-M216 ura4-D18 leu1-32 his3-D1	This study
373	*stn1-75 rqh1Δ (h-)*	h- stn1::loxP-stn1-75-loxM3 rqh1::rqh1D-H (his$^+$) ade6-M216 ura4-D18 leu1-32 his3-D1	This study
376	*stn1-75 rqh1Δ (h+)*	h+ stn1::loxP-stn1-75-loxM3 rqh1::rqh1D-H (his$^+$) ade6-M216 ura4-D18 leu1-32 his3-	This study

		D1	
377	*stn1-99 rqh1Δ* (h-)	h- stn1::loxP-stn1-99-loxM3 rqh1::rqh1D-H (his$^+$) ade6-M216 ura4-D18 leu1-32 his3-D1	This study
381	*stn1-99 rqh1Δ* (h+)	h+ stn1::loxP-stn1-99-loxM3 rqh1::rqh1D-H (his$^+$) ade6-M216 ura4-D18 leu1-32 his3-D1	This study
374	*stn1-75* (h-)	h- stn1::loxP-stn1-75-loxM3 ade6-M216 ura4-D18 leu1-32 his3-D1	This study
375	*stn1-75* (h+)	h+ stn1::loxP-stn1-75-loxM3 ade6-M216 ura4-D18 leu1-32 his3-D1	This study
378	*stn1-99* (h+)	h- stn1::loxP-stn1-99-loxM3 ade6-M216 ura4-D18 leu1-32 his3-D1	This study
380	*stn1-99* (h-)	h+ stn1::loxP-stn1-99-loxM3 ade6-M216 ura4-D18 leu1-32 his3-D1	This study
655	*rqh1Δ* (Kan^R)	h+ rqh1::kanR ade6-704 ura4-D18 leu1-32	Johanne Murray
656	*pot1Δ rqh1Δ*	h- pot1::bsdSVEM rqh1::kanR ade6-216 ura4-D18 leu1-32 his3-D1 pBP280 (pot1$^+$)	This study
657	*pot1-1 rad16Δ*	h+ pot1::pot1-1-GFP-kanR rad16::rad16D-L (leu$^+$) ade6-M210 ura4-D18 leu1-32 his3-D1	This study
658	*pot1-1 rad16Δ lig4Δ*	h+ pot1::pot1-1-GFP-kanR rad16::rad16D-L (leu$^+$) lig4::bsdSVEM ade6-M210 ura4-D18 leu1-32 his3-D1	This study
659	*stn1$^+$-ura4$^+$* (h+)	h+ stn1::loxP-stn1$^+$-ura4$^+$-loxM3 (ura$^+$) ade6-M216 ura4-D18 leu1-32 his3-D1	This study
660	*stn1$^+$-ura4$^+$ rqh1Δ* (h+)	h+ stn1::loxP-stn1$^+$-ura4$^+$-loxM3 (ura$^+$) rqh1::rqh1D-H (his$^+$) ade6-M216 ura4-D18 leu1-32 his3-D1	This study
661	*stn1$^+$/stn1$^+$-ura4$^+$ rqh1Δ /rqh1Δ*	h+/h- stn1$^+$/stn1::loxP-stn1$^+$-ura4$^+$-loxM3 (ura$^+$) rqh1::rqh1D-H/rqh1::rqh1D-H (his$^+$) ade6-M210/ade6-M216 ura4-D18/ura4-D18 leu-32/leu-32 his3-D1/his3-D1	This study
662	*stn1$^+$/stn1-75 rqh1Δ /rqh1Δ*	h+/h- stn1$^+$/stn1::loxP-stn1-75-loxM3 rqh1::rqh1D-H/rqh1::rqh1D-H (his$^+$) ade6-M210/ade6-M216 ura4-D18/ura4-D18 leu-32/leu-32 his3-D1/his3-D1	This study
663	*stn1$^+$/stn1-99 rqh1Δ /rqh1Δ*	h+/h- stn1$^+$/stn1::loxP-stn1-99-loxM3 rqh1::rqh1D-H/rqh1::rqh1D-H (his$^+$) ade6-M210/ade6-M216 ura4-D18/ura4-D18 leu-32/leu-32 his3-D1/his3-D1	This study

Table 2.3: List of plasmids used in this study.

pAB Plasmid No.	Plasmid	Description	Source
744	pBP280	Yeast non-integrating, SpPot1, wild type promoter/terminator, ura4+	Bianchi Lab
752	pFY416	Yeast non-integrating, MCS, ura4+	Bianchi Lab
921	pAW8E-noATG	Yeast non-integrating, nmt promoter, Cre recombinase, loxP, loxM3, LEU2	Adam Watson
988	pFY412	Yeast non-integrating, MCS, ade6+	Bianchi Lab
1214	pGBKT7	Yeast non-integrating, Gal4-BD, c-Myc epitope tag, TRP1	Bianchi Lab
1226	pGBKT7SpStn1-C	Yeast non-integrating, Gal4-BD-SpStn1 C-ter, c-Myc epitope tag TRP1	This study
1235	pFY116	Yeast non-integrating, MCS, ura4+	Bianchi Lab
1240	pGBKT7SpStn1-1	Yeast non-integrating, Gal4-BD-SpStn1, c-Myc epitope tag, TRP1	This study
1241	pGBKT7SpTen1-1	Yeast non-integrating, Gal4-BD-SpTen1, c-Myc epitope tag, TRP1	This study
1245	pGADT7	Yeast non-integrating, Gal4-AD, HA epitope tag, LEU2	Bianchi Lab
1246	pGADT7SpStn1-1	Yeast non-integrating, Gal4-AD-SpStn1, HA epitope tag, LEU2	This study
1247	pGADT7SpTen1-1	Yeast non-integrating, Gal4-AD-SpTen1, HA epitope tag, LEU2	This study
1291	pFY106	Yeast integrating, MCS, ura4+	Bianchi Lab
1334	pGEM-T Easy	E. coli vector for TA cloning, AmpR	Promega
1342	pSpTelo	E. coli vector, 306bp S. pombe telomere tract in KpnI-SacI fragment for southern probe, AmpR	Bianchi Lab
1434	pmutSpStn1a	E. coli vector, synthesised Pstn1-loxP-loxM3-Tstn1, AmpR	Eurofins
1435	pGEM-SpTpz1-FL	E. coli vector, SpTpz1 ORF, AmpR	Bianchi Lab
1442	pGBKT7SpPoz1-FL	Yeast non-integrating, Gal4-BD-SpPoz1-FL, c-Myc epitope tag, TRP1	Bianchi Lab
1443	pGEM-SpRap1-FL1	E. coli vector, SpRap1 ORF from fusion PCR (unwanted mutation present), AmpR	This study
1444	pGBKT7SpRap1-FL	Yeast non-integrating, Gal4-BD-SpRap1-FL, c-Myc epitope tag, TRP1	This study
1446	pmutSpStn1-2	E. coli vector, Pstn1-loxP-SpStn1-loxM3-Tstn1, AmpR	This study
1447	pmutSpStn1-3	E. coli vector, Pstn1-loxP-Stn1-Ura4-loxM3-Tstn1, AmpR	This study

1448	pAW8loxless	Yeast non-integrating, nmt41 promoter, Cre recombinase, loxP and loxM3 sites removed, LEU2	Adam Watson
1466	pSpPoz1-G10M106	Yeast integrating, for SpPoz1 10Myc epitope tagging, ura4+	Bianchi Lab
1488	ploxPM3SpStn1-1	Yeast non-integrating, nmt41 promoter, Cre recombinase, loxP-SpStn1-loxM3, for whole plasmid mutagenesis, LEU2	This study
1492	pLexAi-Yip-URA3	Yeast integrating, LexA-BD, URA3	Thomas et al. (2002)
1495	pV5nlsG8mcs	E. coli vector, synthesised V5 epitope, nls and MCS, AmpR	Eurofins
1496	pGal-Yip-TRP1	Yeast integrating, Gal4-BD, TRP1	Thomas et al. (2002)
1497	pLexAi	Yeast integrating, LexA-BD, V5 epitope tag, nls, 8xGlycine codons, modified MCS, URA3	This study
1504	pLexAi-Yip-URA3b	Yeast integrating, LexA-BD, NdeI site in URA3 promoter removed, URA3	This study
1513	pSpRap1nter	E. coli vector, synthesised Rap1 N-ter to correct unwanted mutation in pGEM-SpRap1-FL1, AmpR	Blue Heron
1519	pLexAi-SpTpz1-FL	Yeast integrating, LexA-BD-SpTpz1-FL, V5 epitope tag, integrates at ura3 locus, URA3	This study
1520	pGBDi-SpTpz1-FL	Yeast integrating, Gal4-BD-SpTpz1-FL, integrates at trp1 locus, TRP1	This study
1524	pGBDi-SpRap1-FL	Yeast integrating, Gal4-BD-SpRap1-FL, integrates at trp1 locus, TRP1	This study
1525	pLexAi-SpRap1-FL	Yeast integrating, LexA-BD-SpRap1-FL, V5 epitope tag, integrates at ura3 locus, URA3	This study
1527	pGADT7SpPoz1-FL	Yeast non-integrating, Gal4-AD-SpPoz1-FL, HA epitope tag, LEU2	This study
1528	pGBKT7SpTpz1-FL	Yeast non-integrating, Gal4-BD-SpTpz1-FL, c-Myc epitope tag, TRP1	This study
1535	pSpRqh1D-H	Yeast integrating, for deletion of SpRqh1, his3+	Bianchi Lab
1536	pSpRqh1D-L	Yeast integrating, for deletion of SpRqh1, leu1+	Bianchi Lab
1550	pSpPoz1-FL2	E. coli vector, synthesised SpPoz1 ORF with added restriction sites, AmpR	Eurofins
1604	pEXK-mutSpPoz1-1	E. coli vector, synthesised Ppoz1-loxP-Ppoz1-loxM3-Tpoz1, KanR	Eurofins

1605	pEXK-mutSpPoz1-2	E. coli vector, Ppoz1-loxP-Ppoz1-Ura4-loxM3-Tpoz1, for yeast integration, KanR	This study
1606	ploxPM3SpPoz1-3	Yeast non-integrating, nmt41 promoter, Cre recombinase, loxP-Ppoz1-Ura4-loxM3, LEU2	This study
1607	pGADT7SpPoz1-FL2	Yeast non-integrating, Gal4-AD-SpPoz1-FL2, HA epitope tag, LEU2	This study
1773	pGADT7SPPoz1-mut1	Yeast non-integrating, SpPoz1 Tpz1-interaction disruption candidate 1, HA epitope tag, LEU2	This study
1774	pGADT7SPPoz1-mut17	Yeast non-integrating, SpPoz1 Rap1-interaction disruption candidate 17, HA epitope tag, LEU2	This study
1775	pGADT7SPPoz1-mut19	Yeast non-integrating, SpPoz1 Rap1-interaction disruption candidate 19, HA epitope tag, LEU2	This study
1776	pGADT7SPPoz1-mut20	Yeast non-integrating, SpPoz1 Rap1-interaction disruption candidate 20, HA epitope tag, LEU2	This study
1777	pGADT7SPPoz1-mut23	Yeast non-integrating, SpPoz1 Tpz1-interaction disruption candidate 23, HA epitope tag, LEU2	This study
1778	pSpPoz1-mut20-Ui	Yeast integrating, SpPoz1-mut20, ura4+	This study
1781	ploxPM3SpPoz1-FL2	Yeast non-integrating, nmt41 promoter, Cre recombinase, loxP-Ppoz1-SpPoz1-FL2-loxM3, for yeast integration by RMCE, LEU2	This study
1783	ploxPM3SpPoz1-mut20	Yeast non-integrating, nmt41 promoter, Cre recombinase, loxP-Ppoz1-SpPoz1-mut20-loxM3, for yeast integration by RMCE, LEU2	This study
1784	ploxPM3SpPoz1-mut23	Yeast non-integrating, nmt41 promoter, Cre recombinase, loxP-Ppoz1-SpPoz1-mut23-loxM3, for yeast integration by RMCE, LEU2	This study
1785	pSpStn1N-Ten1	E. coli vector, Ten1 ORF in reverse orientation, Stn1 N-terminus without introns, START codons from single NdeI site, AmpR	Eurofins
1788	ploxPM3SpStn1-5	Yeast non-integrating, SpStn1 ORF, for mutagenesis by error-prone PCR, LEU2	This study
1791	pGEM-SpStn1-75	E. coli vector, SpStn1-75 allele from PCR amplification of SpStn1 locus, AmpR	This study

1792	pGEM-SpStn1-99	E. coli vector, SpStn1-99 allele from PCR amplification of SpStn1 locus, AmpR	This study
1793	pGEM-SpStn1-174	E. coli vector, SpStn1-174 allele from subcloning SpStn1-75 and SpStn1-99 mutations together, AmpR	This study
1794	pSpStn1-75-U	Yeast integrating, SpStn1-75 allele, ura4+	This study
1795	pSpStn1-99-U	Yeast integrating, SpStn1-99 allele, ura4+	This study
1796	pSpStn1-174-U	Yeast integrating, SpStn1-174 allele, ura4+	This study
1797	pSpStn1-U	Yeast non-integrating, SpStn1+, wild type promoter/terminator, ura4+	This study
1798	pSpStn1D-U	Yeast integrating, for deletion of SpStn1, ura4+	This study

Table 2.4: **List of primers used in this study.**

DO Primer No.	Primer	Sequence	Description
224	MUC-A	CGCCAGGGTTTTCCCAGTCACGAC	M13 sequencing primer
225	MUC-S	AGCGGATAACAATTTCACACAGGA	M13 sequencing primer
822	f1+	CGAACGTGGCGAGAAAGGAA	f1+ origin primer, to check 10Myc tag integration
1164	Poz1-f1-Sp	TGATGTTTGATGTATTCTAGATGGC	To check 10Myc tag integration
1258	fas2-f1-Sp	GCGGTGGTTATGACGACTTT	Fas2 qPCR amplicon primer
1259	fas2-b1-Sp	ACGTCCCCTTTCTGTTTCCT	Fas2 qPCR amplicon primer
1344	TAS1-f6-Sp	TATTTCTTTATTCAACTTACCGCACTTC	TAS1 qPCR amplicon primer
1348	TAS1-b5-Sp	CAGTAGTGCAGTGTATTATGATAATTAAAATGG	TAS1 qPCR amplicon primer
1356	MUC-OA	GGCCTCTTCGCTATTACGC	M13 sequencing primer
1357	MUC-OS	ATTAGGCACCCCAGGCTTTA	M13 sequencing primer
1635	stn1-EcoRI-Sp	GCTgaattcTTATACAAACTGATTATCTCGCAC	Stn1 C-ter PCR (lowercase = EcoRI site)
1636	stn1-NcoI-Sp	GCAccatggATTCGCACACCCAAGAAATC	Stn1 C-ter PCR (lowercase = NcoI site)
1978	Rap1-NdeI-Sp	GCTGTGcatatgTCATTTACATTCACCAAAAGCG	Rap1 fusion PCR primer (lowercase = NdeI site)
1979	Rap1-NdeIb-Sp	TCAGCTGCATAAGCTTTCCTTTC	Rap1 fusion PCR primer
1980	Rap1-NdeIf-Sp	GAAAGGAAAGCGTATGCAGCTGA	Rap1 fusion PCR primer
1981	Rap1-XmaI-Sp	GAGAGCcccgggTTAAGAAGTTTGTTTTGAAAGT	Rap1 fusion PCR primer (lowercase = XmaI site)
2020	T1stn1SacI-Sp	GCAACTgagctcTATCACATTGACGCGGAGAT	To amplify Tstn1 for deletion (lowercase = SacI site)
2021	T2stn1BglII-Sp	GTCGTGACTGGTACAACagatctGCTTAGGCCAGTAAGCGATG	To amplify Tstn1 for deletion (lowercase = BglII site)
2022	P3stn1BglII-Sp	GTTGTACCAGTCACGACagatctAAACAATGCACATTGGTGTGA	To amplify Pstn1 for deletion (lowercase = BglII site)
2023	P4stn1KpnI-Sp	CGATTCggtaccTTCAACCATATGATTTGCAATTTT	To amplify Pstn1 for deletion (lowercase = KpnI site)
2074	Tura4-f1-Sp	AAACATTGGTGTTGGAACAGA	Junction PCR to check poz1-2 integration
2075	Tstn1-b2-Sp	GCTTAGGCCAGTAAGCGATG	SpStn1 ORF PCR
2076	Stn1-b2-Sp	TGATAATGTAGGAAATTGATGCG	To check loxP-Stn1-Ura4-loxM3 integration

2079	Pstn1-f2-Sp	AAGTTGCGTGAAACCAGACT	SpStn1 ORF PCR
2088	Stn1-f2-Sp	GGAAATGGAGGCAAGCAAAG	To check loxP-Stn1-Ura4-loxM3 integration
2093	rap1-f1-Sp	GACGCATTTCGATAGATGTTGA	Rap1 ORF sequencing primer
2137	GAD-f1	GCGTATAACGCGTTTGGAAT	Gal4-AD ORF mutagenesis / sequencing
2138	GADT7-b1	GGTTACATGGCCAAGATTGAA	Gal4-AD ORF mutagenesis / sequencing
2249	Ppoz1-f2-Sp	ATATGGGTGTGTTGCGTGAA	Junction PCR to check poz1-2 integration
2250	Poz1-f2-Sp	TTCAATAGTGTGCTCAGTCGAT	To check Poz1-mutant allele integration
2251	Ppoz1-b1-Sp	TGTTTTTACTACCCAAGCCTCTT	Junction PCR to check poz1-2 integration
2252	Tpoz1-b2-Sp	TGGCCCATAAGCCTGTATCT	Junction PCR to check poz1-2 integration
2272	Poz1-b1-Sp	GGCGTTCACAATGGAAGATT	To check Poz1-mutant allele integration
2547	Pstn1-SacII-Sp	CGTCccgcggGTCAGCAATCGAAACCCCTTT	To amplify Stn1 ORF for covering plasmid (lowercase = SacII site)
2548	Tstn1-KpnI-Sp	CGTCggtaccATGAGATGCGCTACCATTGC	To amplify Stn1 ORF for covering plasmid (lowercase = KpnI site)

Chapter 3

Analysis of the roles of Poz1 protein-protein interactions in relation to switching from a telomerase-inhibitive state to a telomerase-permissive state

3.1 Introduction

The fission yeast telomeric complex bridging molecule Poz1 was originally identified in a screen for Pot1-associated proteins (Miyoshi *et al.*, 2008). Mass spectrometry of Pot1 immunoprecipitation samples identified the known Ccq1 protein as well as two previously unidentified proteins. These proteins were identified as predicted ORFs in the fission yeast genome and given the names Tpz1 (TPP1 homologue in *Schizosaccharomyces pombe*) and Poz1 (Pot1-associated in *Schizosaccharomyces pombe*). The interactions between these proteins and telomeric DNA were characterised using immunoprecipitation, fluorescence colocalisation, ChIP and yeast-2-hybrid assays (Miyoshi *et al.*, 2008). Immunoprecipitation experiments of FLAG-tagged Pot1 indicated Ccq1, Tpz1 and Poz1 were physically associated with Pot1 *in vivo*. Immunofluorescence signals from tagged Tpz1, Ccq1 and Poz1 proteins were also found to colocalise with Pot1-Flag. Specific association with telomeric DNA by all these proteins was confirmed by ChIP. However, yeast-2-hybrid analysis indicated that there was no direct interaction between Pot1 and Poz1 or Pot1 and Ccq1. All the proteins, however, interacted with Tpz1. Deletion analysis by yeast-2-hybrid identified the N terminus of Tpz1 as required for Pot1 interaction while the C terminus provided binding for both Poz1 and Ccq1. Taken together, the interactions of these proteins resemble that of the POT1-TPP1-TIN2 complex in humans. Indeed, the Tpz1 protein contains an OB fold closely resembling those found in TEBP-β and TPP1 (Miyoshi *et al.*, 2008).

Analysis of Poz1 revealed that, in addition to Tpz1, it also specifically interacted with Rap1. This interaction was independent of Taz1; indeed, Poz1-Rap1 binding was seen by immunoprecipitation in a *taz1Δ* background (Miyoshi *et al.*, 2008). Though Poz1 interaction with Rap1, as opposed to Taz1, is a notable difference from the equivalent proteins in the mammalian Shelterin complex, these data indicated that Poz1 appeared to play a similar role to TIN2 in bridging and maintaining the link between the dsDNA-binding and ssDNA-binding complexes. Deletion of Poz1, however, rather than negatively affecting telomere length, increases it up to 2kb, indicating a role in the negative regulation of telomerase (Miyoshi *et al.*, 2008). Dyskeratosis congenita-specific mutations in TIN2 reduce overall telomere length (Yang *et al.*, 2011). Conversely, deletion of Ccq1 results in reduced telomere length (to approximately 100bp), indicating it has a role in the positive regulation of telomerase. The final 100bp of telomeric sequence is maintained in a telomerase-independent pathway involving recombination (Miyoshi *et al.*, 2008, Tomita and Cooper, 2008). It is phosphorylation by Tel1/Rad3 kinases that results in telomerase recruitment by Ccq1, as indicated by a lack of telomerase recruitment in a *ccq1-T93A* phosphorylation-deficient mutant (Yamazaki *et al.*, 2012). In addition, Tel1/Rad3-dependent hyperphosphorylation is seen in the absence of telomerase inhibitors Poz1, Rap1 or Taz1 (Moser *et al.*, 2011).

For Poz1, however a more complicated recruitment is indicated. Pot1 and Poz1 can be recruited to artificially-introduced internal telomeric repeats on a circularised chromosome (Miyoshi *et al.*, 2008). This is shown by a ChIP assay, where no enrichment is seen for Pot1 or Poz1 in either Taz1 or Rap1 deletion background. This suggests the complete complex can be recruited in the absence of ssDNA in a Taz1 and Rap1-dependent manner. However, in *taz1Δ* and *rap1Δ* strains, Poz1 is still recruited to ssDNA at telomeres, which seems likely to be dependent on Pot1-ssDNA binding. The telomere protective ability of Poz1 also appears to be independent of Taz1 and Rap1, given that in contrast to *taz1Δ ccq1Δ* and *rap1Δ ccq1Δ*, where a mildly long telomere phenotype is observed, *poz1Δ ccq1Δ* strains lose all telomeric DNA

(Miyoshi *et al.*, 2008). These data indicate Poz1 recruitment to telomeres can be dependent on presence of dsDNA or ssDNA and therefore interaction with either the dsDNA-binding complex or ssDNA-binding complex. Given the protein counting model of telomerase regulation, it may be a balance between the two.

It has been suggested that the Pot1-Tpz1-Ccq1 complex may act as a switch to either positively regulate telomerase activity or transduce the negative regulation signal from the Taz1-Rap1 complex, similar to the model suggested for the human system (Bianchi and Shore, 2008, Miyoshi *et al.*, 2008). Poz1, as the bridging molecule, may play a key role. Should the protein counting model be applicable, it would predict that, at longer telomeres, sufficient Taz1-Rap1 complexes would be bound to the dsDNA region that it associates with all Pot1-Tpz1-Ccq1 complexes. This would keep the telomeric complex, as a whole, in the closed, inactive conformation in a Poz1-dependent manner. When telomeres shorten, however, insufficient Taz1-Rap1 complexes may be present. The Pot1-Tpz1-Ccq1 complex may then be free to recruit telomerase. Though it may not contribute directly to telomerase recruitment; given that Poz1 can localise to telomeres by binding either the Pot1-Tpz1-Ccq1 complex or Taz1-Rap1, it may continue to associate with both complexes in this open, active conformation. This continued association with Taz1-Rap1 may result in a dual function of Poz1, where negative regulation of telomerase continues to take place to some degree as well as any protective function on the telomere. Indeed, in a recent study where Tpz1-Poz1 interaction was disrupted by a specific Tpz1 mutation, an elongation phenotype was seen. This indicated the importance of Poz1-Tpz1 interaction in the negative regulation of telomerase, possibly through maintaining the closed conformation. However, the elongation observed was not to the same degree as a Poz1 deletion (Jun *et al.*, 2013). This leaves open the possibility that Poz1 has additional roles in negatively regulating telomerase, possibly through its continued ability to bind Rap1 in the open state. These data promote the idea of closed and open complex states which are inhibitory and stimulatory to the recruitment and action of telomerase respectively.

3.1.1 Current study

The aim of this study was to understand the roles and significance of the protein-protein interactions between Poz1 and its binding partners, Rap1 and Tpz1, in relation to the structural transition of the Pot1-Tpz1-Ccq1 complex from a closed, inactive state to an open, active state.

With the high conservation between the human and fission yeast telomeric complexes, understanding the role of Poz1 as a bridging and possibly signal-transducing molecule could give insights on the equivalent proteins and structural transitions in human Shelterin.

It is already established that *poz1Δ* cells, although viable, have elongated telomeres, ranging from 0.7 to more than 2kb (Miyoshi *et al.*, 2008). This elongation in the absence of Poz1 indicates the role in the negative regulation of telomerase. However, specific understanding of the part played by the protein-protein interactions has been lacking thus far. Given that some proteins, such as Poz1 and Tpz1, are recruited to telomeres, without contacting the telomeric DNA directly, it is hypothesised that their interacting partners may play a key role in the recruitment and/or activation of said proteins. Poz1 in this case is of particular interest due to being the central protein, bridging the two sub-complexes. One model proposed for the role of Poz1 in the regulation of telomerase involves both an inhibitory and permissive action on telomerase recruitment. Binding of a Tpz1-Pot1 complex to the Taz1-Rap1 complex via interactions with Poz1, creating a closed complex, may be inhibitory to the recruitment of telomerase [Fig 3.1A]. But if the Tpz1-Pot1 complex no longer binds to the Taz1-Rap1 complex, for example when telomeres are short and fewer dsDNA-binding complexes are present, a telomerase-permissive effect may be produced [Fig 3.1B]. The transition between these two states may be handled by Poz1, indicating a key role for the interactions with Rap1 and Tpz1.
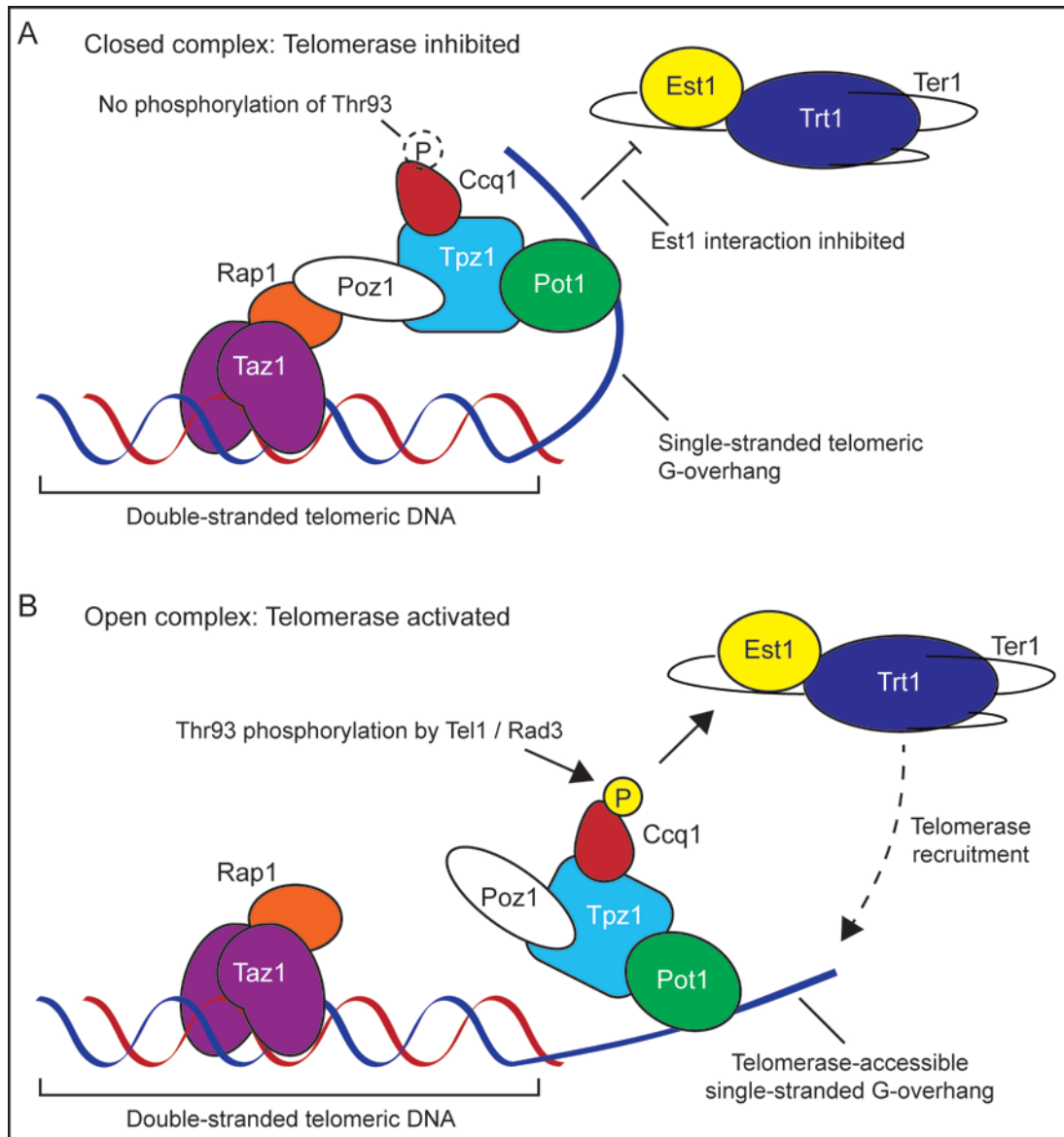
Figure 3.1: Schematic of the two proposed structural states of the fission yeast telomeric complex, permissive and non-permissive to telomerase action.

(A) The closed complex involves the binding of all protein components in a chain, linking the dsDNA- and ssDNA-binding sub-complexes. The Taz1-Rap1 sub-complex (purple and orange) connects to the Pot1-Tpz1-Ccq1 sub-complex (green, blue and red) via the bridging molecule, Poz1 (white). This confirmation is hypothesised to be inhibitory to the recruitment of telomerase, Trt1 (dark blue) and Ter1 (RNA component), through reduced phosphorylation of Ccq1, preventing interaction with Est1 (yellow). Telomerase activity is inhibited through the sequestration of the G-overhang telomerase substrate. **(B)** The open complex is hypothesised to allow recruitment and activation of telomerase. Ccq1 phosphorylation (yellow 'P') by Tel1/Rad3 kinases is permitted, allowing Est1 interaction. The G-overhang is also made available as a substrate for telomerase processing. Sold black arrows indicate activation/interaction. Dashed arrow indicates recruitment to telomere. Shapes and relative sizes of proteins are not representative of actual structures.

3.2 Results

In order to test the structural transition model of telomerase recruitment based on Poz1 interactions, a reverse yeast-2-hybrid system was selected to permit the identification of specific Poz1 mutant alleles. The specific variation of the yeast-2-hybrid system selected was that which was developed and used to identify mutations which disrupt specific protein-protein interactions but leave other interactions unaffected (Thomas *et al.*, 2002). This system, therefore, allows the dual selection of Poz1 mutant alleles lacking, or having greatly reduced, ability to interact with one partner (Rap1 or Tpz1) and maintaining interaction with the other [Fig 3.2].

The principle of the system involves the construction of two bait vectors, in this case Rap1 and Tpz1, and one prey vector (Poz1). One bait vector has the ORF of the protein for which interaction is to be lost subcloned in frame with Gal4 DNA binding domain. The other bait vector has the ORF of the protein for which interaction is to be maintained subcloned in frame with LexA DNA binding domain. The prey vector has the prey gene ORF subcloned in frame with GAL4 activating domain. The bait vectors are then integrated into the *S. cerevisiae* reverse-2-hybrid base strain, LY26, where, upon introduction of mutagenized prey vector, $ADE2^+$ and $HIS3^+$ selection is used to identify alleles with the desired phenotype, as summaried in Fig 3.2. Interaction of the prey with the GAL4-DBD fusion protein (Bait 1) results in TetR (Tetracycline Repressor) transcription activation which, in turn, results in repression of the TetO (Tetracycline Operator); thereby shutting off ADE2 expression. If there is no interaction with the Bait 1, ADE2 continues to be expressed. Interaction of the prey with the LexA-DBD fusion protein (Bait 2) results in activation of HIS3 expression. With no Bait 2 interaction, HIS3 expression is shut off. The desired phenotype (Ade+, His+), therefore, only occurs when the mutagenized prey interacts with Bait 2 and not Bait 1 [Fig 3.2A].
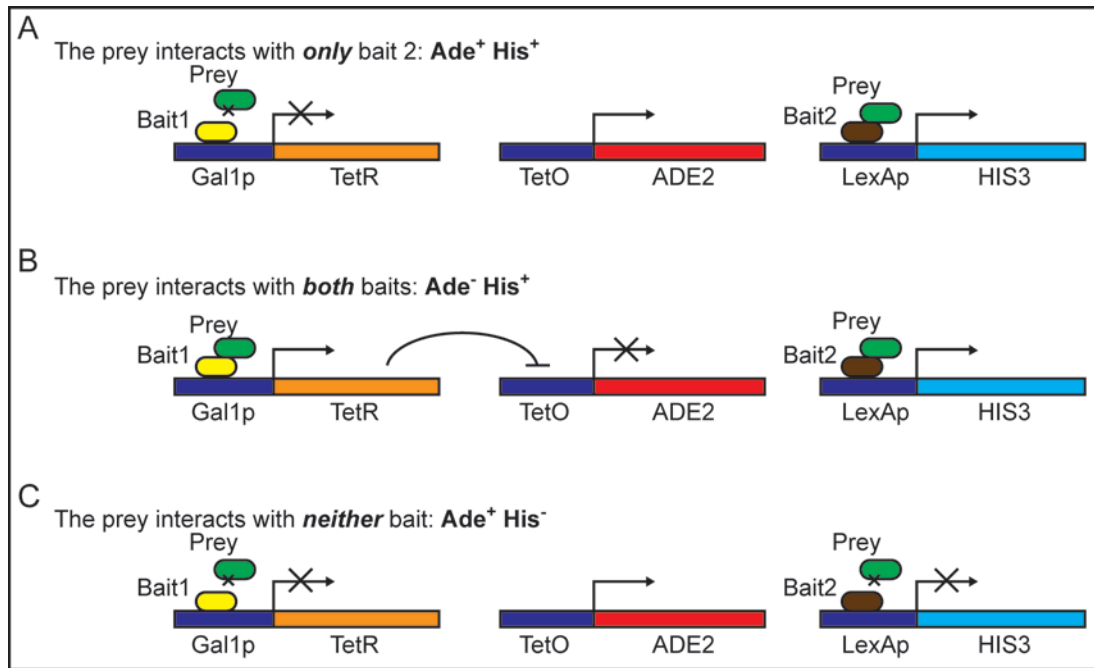
Figure 3.2: Schematic indicating the three possible outcomes from a reverse-2-hybrid screen using mutagenized prey protein in the system developed by Thomas *et al.* (2002).

(A) Desired phenotype. Bait 1 (yellow) binds to Gal1 promoter (Gal1p). Bait 2 (brown) binds LexA promoter (LexAp). Prey protein (green) does not interact with Bait 1, therefore TetR (orange) expression is not activated. As a result, *ADE2* (red) expression continues uninhibited. Prey protein does interact with Bait 2, therefore *HIS3* (light blue) expression is activated. This phenotype can be identified by selection for Ade$^+$ His$^+$. **(B)** Undesired phenotype. Prey protein interacts with both Bait 1 and Bait 2. TetR expression is active and, therefore, TetR protein (transcriptional repressor) binds TetO to deactivate *ADE2* expression. Prey-Bait2 interaction maintains *HIS3* expression. This results in an Ade$^-$ His$^+$ phenotype. **(C)** Undesired phenotype. Prey protein does not interact with either Bait 1 or Bait 2. As a result, *ADE2* expression continues to be active. No Prey-Bait2 interaction results in deactivated expression of *HIS3*. This results in an Ade$^+$ His$^-$ phenotype.

3.2.1 Cloning of reverse yeast 2-hybrid bait and prey constructs

The base plasmids, pGal-YIpTRP1 and pLexA-YIpURA3, were received from the lab of Andrew Thorburn, Department of Cancer Biology and Comprehensive Cancer Centre, Utah, USA [Fig 3.3]. Some modifications of pLexA-YIpURA3 were required to allow subcloning of ORFs from existing Yeast-2-hybrid plasmids. The pLexA-YIpURA3 plasmid was cut with the restriction enzyme NdeI, then blunt filled-in using T4 DNA polymerase supplemented with dNTPs and religated to make pLexA-YIpURA3b. This removed the unwanted NdeI site. However, due to the NdeI site being located within the promoter region of the URA3 marker cassette, the plasmid was transformed into the *S. cerevisiae* LY26 strain to check that URA3 was still functional. Having confirmed this, the plasmid pV5nlsG8mcs was then cut with MfeI-BamHI to

excise a 121bp fragment and subcloned into pLexA-YIpURA3b, cut with EcoRI-BamHI, to make

pLexAi [Fig 3.3B]. This generated a modified multiple cloning site as well as adding a V5

epitope tag, nuclear localisation signal (nls) and the codons for eight glycine residues. These

extra glycines act as a spacer between the LexA-DBD and the bait protein to minimise any

steric hindrance to correct peptide folding. With these modifications it was possible to use

NdeI-XmaI subcloning to transfer ORFs from other, previously cloned, plasmids into pGal-

YIpTRP1 and pLexAi, as required.

Figure 3.3: Vector schematics of base plasmids used to generate Bait and Prey plasmids for reverse 2-hybrid screen (following page).

(A) The pGal-Yip-TRP1 plasmid contains the GAL4-DBD (yellow) and is used for the expression of Bait 1. The ORF of the gene of interest can be cloned into the NdeI-XmaI sites, with the ATG sequence from the NdeI site acting as the START codon. Expression of the Gal4-GBD fusion is controlled by the constituative *ADH1* promoter (Padh1) and terminator (Tadh1). The plasmid is linearised at the BstXI site within *TRP1* (orange) and integrated at the TRP1 locus in the genome. Other features include an ampicillin resistance cassette (pink) and the replication origin sequences, f1(+) and ColE1 (blue). **(B)** The pLexAi plasmid is derived from pLexA-Yip-URA3 and is used for the expression of Bait 2. The pLexAi plasmid has been modified to include a V5 epitope tag and nuclear localisation signal (nls) following in frame of the LexA-DBD (brown). The ORF of the gene of interest can be cloned into the NdeI-XmaI sites where expression is controlled by the *ADH1* promoter (Padh1) and terminator (Tadh1). The plasmid is linearised at the NcoI site within *URA3* (red) and integrated at the URA3 locus in the genome. Other features include an ampicillin resistance cassette (pink) and the replication origin sequences, f1(+) and ColE1 (blue). **(C)** The pGADT7 contains the GAL4-AD (green) followed in frame by a HA epitope tag and is used for the expression of the Prey protein. The ORF of the gene of interest (*poz1*) can be cloned into the NdeI-XmaI sites where expression is controlled by the *ADH1* promoter (Padh1) and terminator (Tadh1). The plasmid is maintained in yeast through the *LEU2* auxotrophic marker (purple). Other features include an ampicillin resistance cassette (pink) and the replication origin sequences, 2μ Ori and pUC Ori (blue).
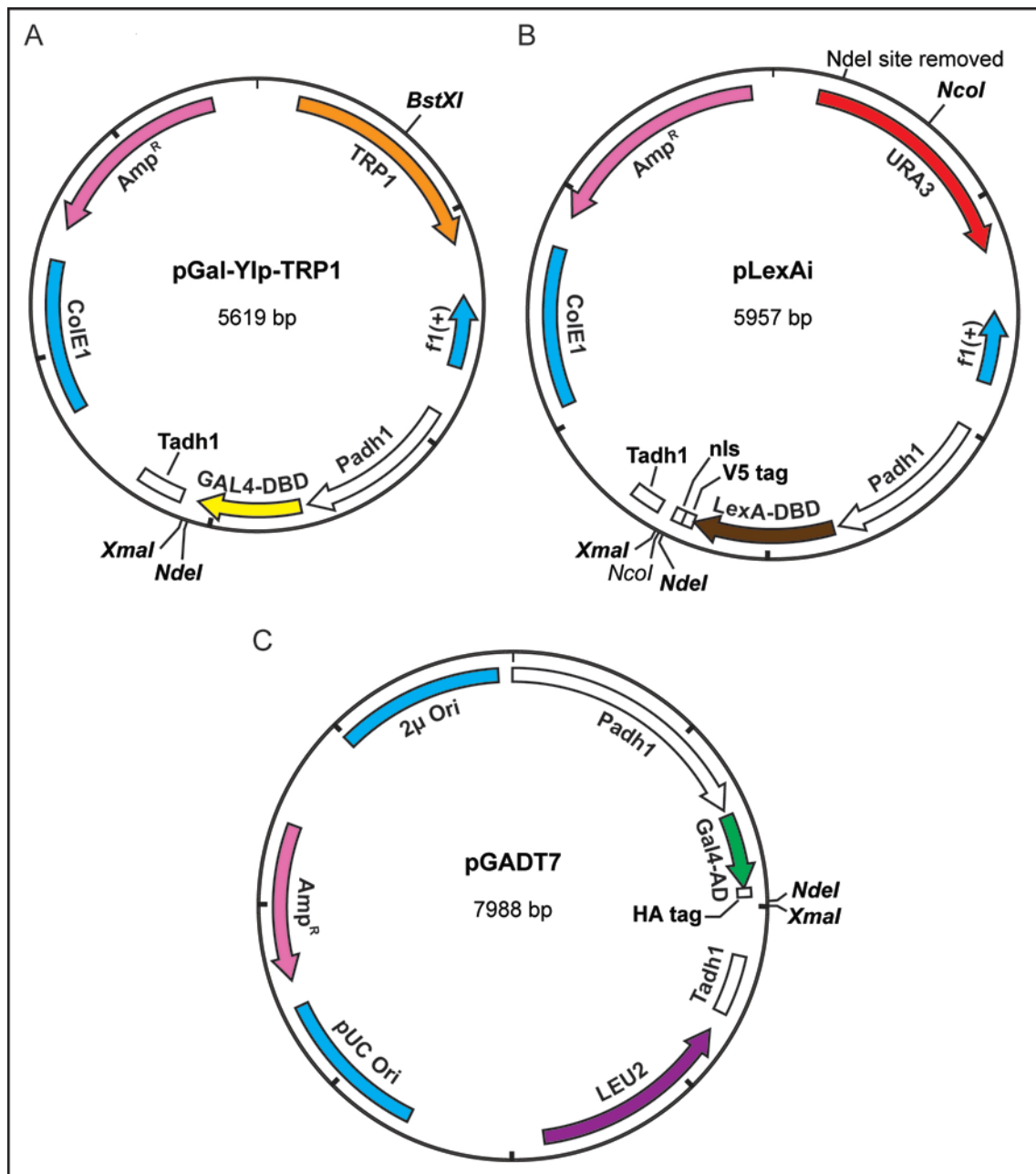
In order to screen for *poz1* mutations which disrupted interaction with Rap1 and those which disrupted the interaction with Tpz1, the ORFs for Rap1 and Tpz1 were subcloned into both the pGal and pLexAi vectors. Due to the presence of an NdeI site at position 1103 within the wild type Rap1 ORF, a modification of the sequence was required. Primers were designed to separately amplify the region proximal and distal to the unwanted NdeI site. The primers at the START and STOP codons (oligonucleotides: Rap1-NdeI-Sp and Rap1-XmaI-Sp) were designed to introduce NdeI and XmaI restriction sites respectively. The central primers (oligonucleotides: Rap1-NdeIb-Sp and Rap1-NdeIf-Sp) contained a long region of overlapping homology and a single base change at the NdeI site location (from CATATG to CTTATG). This allowed disruption of the site without affecting the peptide sequence. The Rap1 ORF was amplified by high-fidelity PCR using Phusion Taq Polymerase in the two sections from a fission yeast cDNA library (Fikes *et al.*, 1990) [Fig 3.4A]. These PCR products were then purified and used as templates in a fusion PCR reaction to generate the complete ORF [Fig 3.4B]. The reaction contained only the "START" and "STOP" codon primers (Rap1-NdeI-Sp and Rap1-XmaI-Sp) and relied on the region of overlapping homology generated from the central primers to anneal the two sections in the first instance. The resulting PCR product, with NdeI site at the start codon, the XmaI site at the stop codon and the unwanted NdeI site disrupted, was A-tailed by incubating with NEB Taq Polymerase in the presence of dATP and cloned into the pGEM-T Easy vector. Sequencing of the ORF indicated an unwanted mutation in the N-terminus [Fig 3.4C]. In the interest of time, the N-terminus was synthesised without the mutation by Blue Heron as pSpRap1nter. The Rap1 N-terminus (NdeI-MfeI fragment), together with the remainder of the ORF (MfeI-XmaI fragment) was then subcloned into the NdeI-XmaI restriction sites in both pGal-YIp-TRP1 and pLexAi to generate pGBDi-SpRap1-FL and pLexAi-SpRap1-FL [Fig 3.4C].

The equivalent vectors for Tpz1 were cloned by NdeI-XmaI restriction digest of the Tpz1 ORF from pGEM-SpTpz1-FL that had been previously generated from a cDNA clone. Similarly, to

generate the prey plasmid, the Poz1 ORF was subcloned by NdeI-XmaI restriction digest from pGBKT7SpPoz1-FL, which had been previously generated, into the pGADT7 vector [Fig 3.3C]. This pGADT7SpPoz1-FL vector contains a unique XbaI site within *poz1⁺* which would aid in the characterisation of mutations by the ability to separate mutations, should positive candidates have multiple changes.

Figure 3.4: Schematic showing molecular cloning process to generate pGBDi-SpRap1-FL and pLexAi-SpRap1-FL bait plasmids (following page).

(A) Rap1 N-terminus PCR (blue, as labelled) using primers Rap1-NdeI-Sp and Rap1-NdeIb-Sp to introduce NdeI site at Rap1 START codon for cloning use and remove NdeI site within Rap1 ORF with single base change (CATATG to CTTATG). Rap1 C-terminus PCR (blue, as labelled) using primers Rap1-NdeIf-Sp and Rap1-XmaI-Sp to remove NdeI site within Rap1 ORF with single base change (CATATG to CTTATG) and introduce XmaI site after STOP codon for cloning use. Vertical red lines represent position of NdeI site within the ORF that has been removed. Sequence change does not affect peptide sequence. **(B)** Fusion PCR using the N-terminus and C-terminus PCR products. Only primers Rap1-NdeI-Sp and Rap1-XmaI-Sp are used. The N- and C-terminus sections anneal through the central overlapping region which containing the removed NdeI site. **(C)** Subcloning of pGBDi-SpRap1-FL and pLexAi-SpRap1-FL plasmids. Rap1 fusion PCR product contains an unwanted mutation toward the N-terminus as determined by sequencing. Rap1 N-terminal section was subcloned as a NdeI-MfeI fragment from pSpRap1nter and ligated with the MfeI-XmaI fragment from the fusion PCR into the pGal-Yip-TRP1 and pLexAi vectors (cut with NdeI-XmaI). The final plasmids contain the Rap1-FL ORF in frame with Gal4-DBD (yellow) or LexA-DBD (brown) with expression controlled by the *ADH1* promoter (Padh1) and terminator (Tadh1). The pLexAi-SpRap1-FL plasmid also contains a V5 epitope tag and nuclear localisation signal (nls) sequence in frame, as indicated. Other features of the plasmids are not shown.
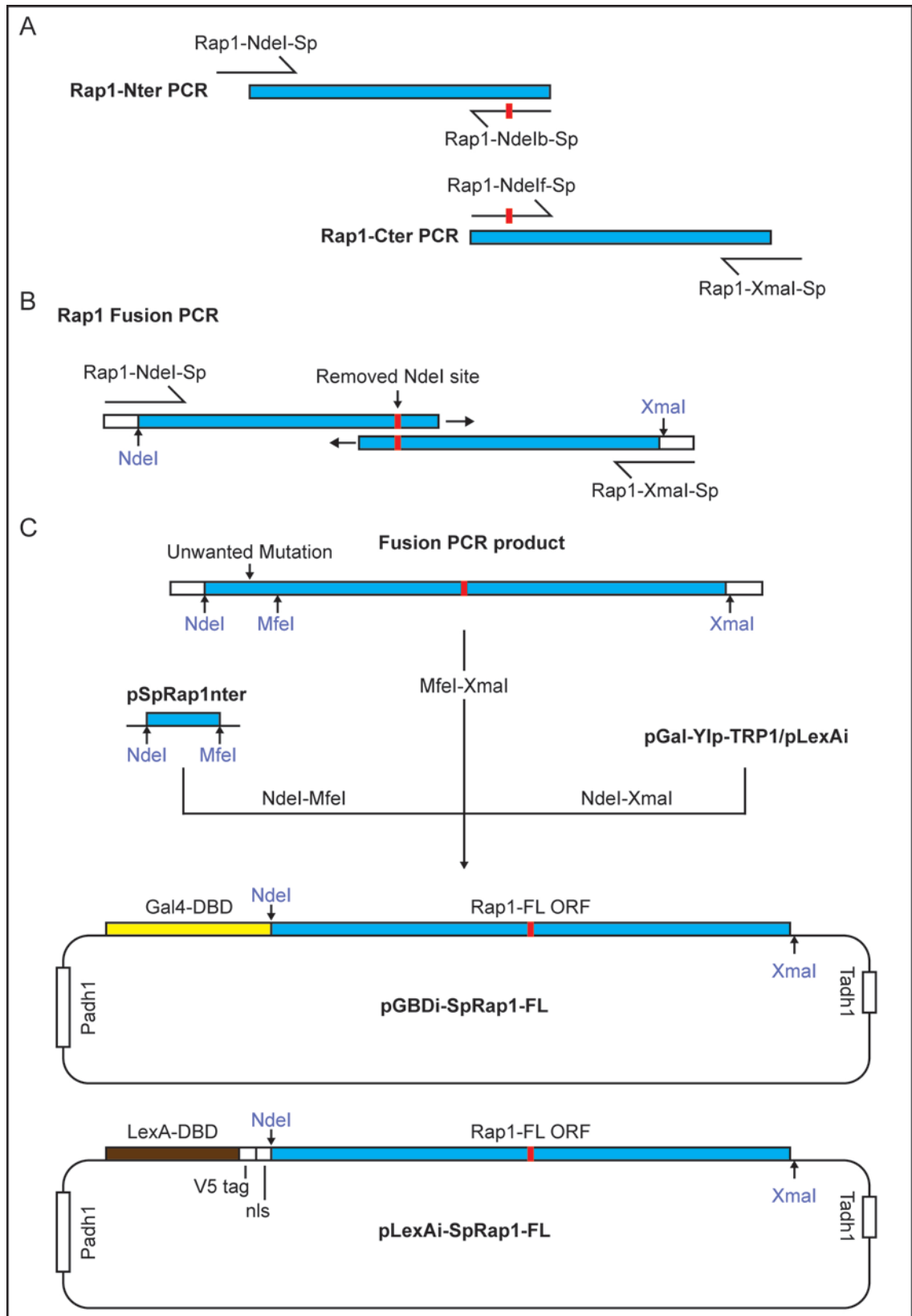
3.2.2 Construction of screening and control strains

The reverse-2-hybrid system being employed requires that the bait vectors be integrated into the genome. As well as generating a stable strain, integration of the vectors allows control of the expression of baits. Overexpression of the baits due to episomal multicopy plasmids is suggested to result in bait-prey protein complexes which are not actually bound to the reporter gene loci (Thomas *et al.*, 2002). This may sequester prey from bait that has localised to the correct reporter, making it more difficult to detect interaction, though this is no different from a standard forward yeast-2-hybrid assay (Fields and Song, 1989). In addition, the variability of copy number may also result in increased background and false positives/negatives due to variability in reporter gene activation, even in the presence of identical prey mutants. Integration of the bait plasmids ensures only one copy of the expression construct is present per cell and expression should be comparable between individual clones.

The pGal-Yip-TRP1 vectors contain a unique BstXI restriction site within the TRP1 ORF while the pLexAi vectors contain a unique NcoI restriction site within the URA3 ORF [Fig 3.3A-B]. These can be used to linearise the vectors and allow them to integrate at the TRP1 and URA3 loci respectively. The pGBDi and pLexAi plasmids for Rap1 and Tpz1 were, therefore, digested with the appropriate enzyme before being co-transformed into the LY26 base strain to generate two screening strains (strains 1 and 3 in Table 3.1). Control strains containing empty vectors integrated at TRP1 and URA3 loci were also generated for use as an additional verification of the functionality of the system (see Table 3.1). Transformants were selected on Sc −TRP −URA. Multiple candidates for each screening strain were restreaked on rich media (YPAD) and then back onto Sc −TRP −URA to verify integration. Growth on rich media removed selection for the transformed plasmid, allowing any that had not integrated to be lost over the several generations required to form colonies. Several of these *URA3* strains were then transformed with pGADT7SpPoz1-FL and separately with pGADT7 EV (Empty Vector) to simulate *poz1*

mutant alleles that retain (Poz1-FL) and lose (EV) interactions. Transformants on Sc –TRP –URA –LEU were tested for reporter gene expression on Sc –TRP –LEU –ADE and Sc –TRP –LEU –HIS + 5mM 3-Amino triazole agar plates [Fig 3.5A]. 3-Amino triazole is a competitive inhibitor of the product of the *HIS3* gene, allowing the modulation of stringency on Sc –HIS selection plates.

Of those screening strains that displayed the expected reporter gene expression (see Table 3.1), one of each type was selected for use in screening for *poz1* mutant alleles, referred to as Strains 1 and 3. The expected phenotypes from wild type and mutant *poz1* alleles with these strains are indicated in Table 3.2.

Streaking the two strains with control plasmids on single and dual selection agar plates indicates that selection on Sc –ADE is stringent. Selection on Sc –HIS, however, appears to be less stringent as some growth with the Empty Vector is observed [Fig 3.5, streaks 2 and 5 on Sc –TRP –LEU –HIS]. Single colonies, however, are not formed and stringency can be modulated by adjusting the concentration of 3-Amino triazole (3-AT). Expression of the GBD and GAD fusion proteins was assessed by western blot [Fig 3.5B-C] from whole cell TCA protein extracts from strains 1 and 3. Both Rap1 and Tpz1 fusion proteins can be detected. GBD-SpRap1 is seen as a 97kDa band from Strain 1 in the first lane of Fig 3.5B. GBD-SpTpz1 is seen as a 75.5kDa band from Strain 3 in the second lane of Fig 3.5B. LexA-SpTpz1 is seen as an 83kDa band from Strain 1 in the first lane of Fig 3.5C. LexA-SpRap1 is seen as 104kDa band from strain 3 in the second lane of Fig 3.5C. The expression of Tpz1 fusion proteins in both strains appears to be less, relative to the Rap1 fusion proteins in the western blot assays (compare intensity of bands in first and second lanes of Fig 3.5B and D). Some variation in expression or correct folding is not unexpected when dealing with fusion proteins, especially those which originate from another yeast species. However, given that the phenotypes were as expected, the strains were deemed acceptable for use in the revers 2-hybrid screen.

Strain	Vectors			Growth	
	GBD	LexA	GAD	Sc –ADE (GBD-GAD)	Sc –HIS (LexA-GAD)
1	Rap1	Tpz1	Poz1	-	+
			EV	+	-
2	EV	Tpz1	Poz1	+	+
			EV	+	-
3	Tpz1	Rap1	Poz1	-	+
			EV	+	-
4	EV	Rap1	Poz1	+	+
			EV	+	-
5	EV	EV	Poz1	+	-
			EV	+	-
6	Tpz1	EV	Poz1	-	-
			EV	+	-
7	Rap1	EV	Poz1	-	-
			EV	+	-

Table 3.1: **Reverse 2-hybrid screening and control strains generated to test reporter system.**

LY26 reverse 2-hybrid strain transformed with GBD and LexA plasmids, Rap1, Tpz1 and Empty vector (EV) in all combinations. Strains 1 and 3 are screening strains which will allow selection of Rap1 and Tpz1 mutants respectively. GAD-SpPoz1 and GAD EV transformed into each strain and reporter activation assessed based on growth on selective plates, Sc –TRP –LEU –ADE and Sc –TRP –LEU –HIS, as indicated (only ADE or HIS indicated). Growth on Sc –ADE indicates no interaction between GBD and GAD fusion proteins. Growth on Sc –HIS indicates interaction between LexA and GAD fusion proteins. The '+' represents growth and '-' represents no growth on specified selection media.

Figure 3.5: Testing stringency and fusion protein expression in screening strains 1 and 3 with control plasmids (following page).

(A) LY26 Strains 1, 2, 3 and 4 transformed with GAD plasmids, as indicated in key, streaked to single colonies on selective media: Sc −TRP −LEU −ADE, Sc −TRP −LEU −HIS (single selection) and Sc −TRP −LEU −ADE −HIS (double selection). Strain 1 (designed to isolate Rap1-interaction disruption alleles) on streaks 1 and 2. Streak 3 phenocopies a real Rap1-interaction disruption strain. Strain 3 (designed to isolate Tpz1-interaction disruption alleles) on streaks 4 and 5. Streak 6 phenocopies a real Tpz1-interaction disruption strain. Growth patterns reflect expected phenotypes from Table 3.1. **(B)** Anti-Gal4 western blot indicating expression of GBD-SpRap1 (97.4kDa) and GBD-SpTpz1 (75.5kDa), as labelled. Black arrows indicate the bands of interest. Ponceau stain of membrane indicates relative loading between lanes on gel. **(C)** Anti-V5 western blot indicating expression of LexA-Tpz1 (83kDa) and LexA-Rap1 (104.8kDa), as labelled. Black arrows indicate the bands of interest. Ponceau strain of membrane indicates relative loading between lanes on gel.

A

Sc -TRP -LEU -ADE   Sc -TRP -LEU -HIS   Sc -TRP -LEU -ADE -HIS

Key: 1: Strain 1 + pGADT7SpPoz1-FL2   4: Strain 3 + pGADT7SpPoz1-FL2
        2: Strain 1 + pGADT7 EV   5: Strain 3 + pGADT7 EV
        3: Strain 2 + pGADT7SpPoz1-FL2   6: Strain 4 + pGADT7SpPoz1-FL2

B

GBD-SpRap1 (Strain 1)
GBD-SpTpz1 (Strain 3)
LY26 Neg
kDa

Anti-Gal4   —100
                 —75

Ponceau   —100
                 —75

C

LexA-SpTpz1 (Strain 1)
LexA-Rap1 (Strain 3)
LY26 Neg
kDa

Anti-V5   —100
                 —75

Ponceau   —100
                 —75

| | Bait 1 | Bait 2 | Poz1 | Growth on | |
				Sc -ADE	Sc -HIS
Strain 1	GBD-Rap1	LexA-Tpz1	wt	-	+
			mutant	+	-
Strain 3	GBD-Tpz1	LexA-Rap1	wt	-	+
			mutant	+	-

Table 3.2: **Reverse 2-hybrid screening strains 1 and 3 with details of bait constructs used and expected phenotype when combined with wild type and mutant prey Poz1.**

Strain 1 allows identification of *poz1* mutant alleles that lose Rap1 interaction but retain Tpz1 interaction. Strain 3 allows identification of *poz1* mutant alleles that lose Tpz1 interaction but retain Rap1 interaction. Correct mutants in either strain will activate both ADE2 and HIS3 expression, as indicated.

In order to allow the phenotypes of *poz1* mutant alleles isolated from the screens to be cross-checked, the yeast-2-hybrid strain PJ69-4A (James *et al.*, 1996) was transformed with pGBKT7SpRap1 and separately pGBKT7SpTpz1 (TRP1 selection) plasmids. The resulting strains were then transformed with pGADT7SpPoz1-FL and pGADT7 Empty Vector to ensure interactions (or lack of interactions) between Poz1 and Rap1 or Tpz1 could be recognised [Fig 3.6]. The PJ69-4A strain contains a *GAL1-HIS3* reporter, similar to the LY26 reverse yeast-2-hybrid strain, the stringency of which can be modulated by addition of 3-Amino triazole. In addition, a more stringent *GAL2-ADE2* and *GAL7-LacZ* reporters are present. Mutant alleles of *poz1* would be transformed into the PJ69-4A + GBD-Rap1/Tpz1 strains to assess and confirm individual interactions. In the test, interaction between GAD-SpPoz1 with GBD-SpRap1 and GBD-SpTpz1 can be identified by growth on the selective plates (Sc –TRP –LEU –ADE and Sc –TRP –LEU –HIS) relative to empty vector controls [Fig 3.6A]. Expression of these fusion proteins is also detectable by western blot on whole cell extracts [Fig 3.6B-C]. Expression of GBD fusion proteins from pGBKT7 can be detected by anti-myc antibodies. Expression of GAD fusion proteins from pGADT7 can be detected by anti-HA antibodies.
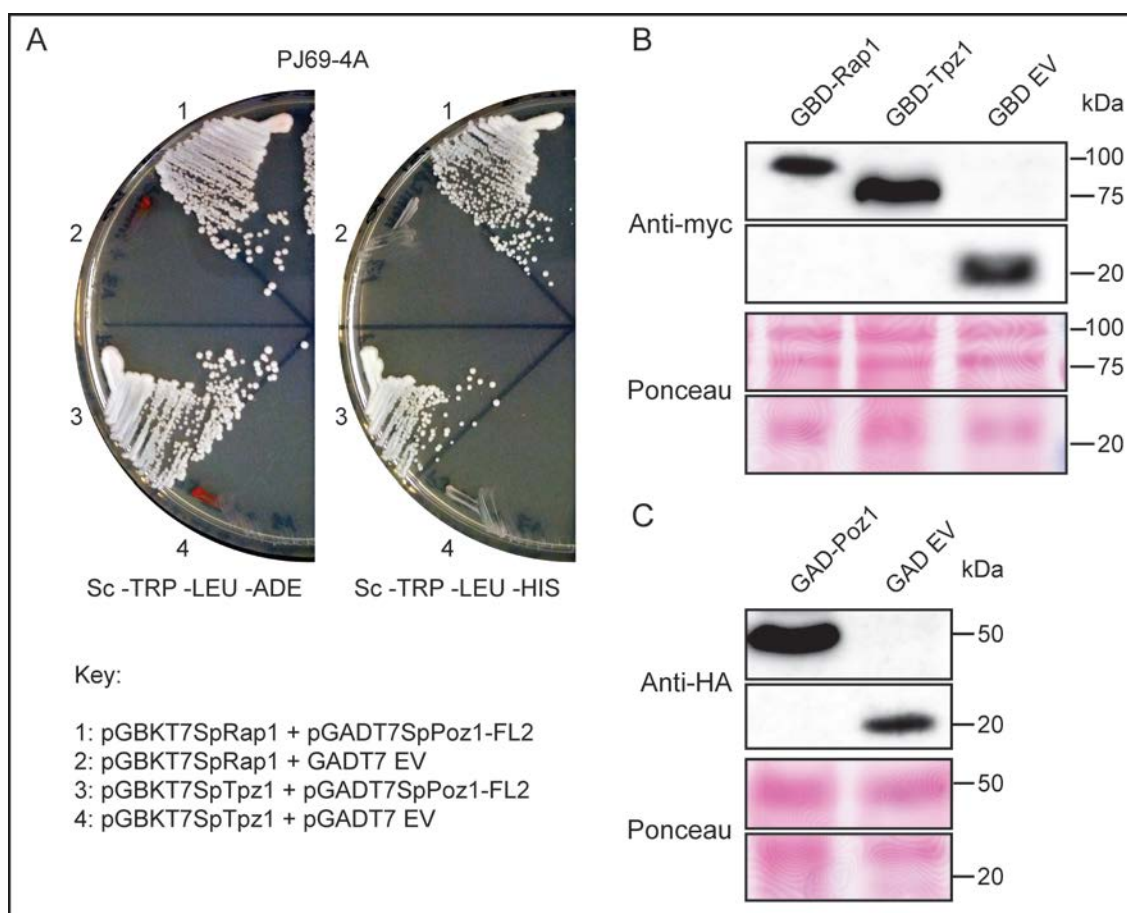
Figure 3.6: Testing phenotype and expression of PJ69-4A yeast 2-hybrid strain with control plasmids.

(A) PJ69-4A yeast 2-hybrid strain transformed with control plasmids: pGBKT7SpRap1, pGBKT7SpTpz1, pGADT7SpPoz1-FL2 and pGADT7 EV (empty vector), as indicated in key. The four combinations of plasmid were streaked on Sc –TRP –LEU –ADE and Sc –TRP –LEU –HIS agar. Growth pattern indicates clear and stringent selection for interaction between Rap1-Poz1-FL2 and Tpz1-Poz1-FL2. **(B)** Expression of GBD-Rap1 (99.4kDa) and GBD-Tpz1 (77.5kDa) fusion proteins checked by anti-myc western blot from PJ69-4A yeast whole cell extracts. GBD EV (21.7kDa) also shown. Ponceau staining of membrane indicates relative loading between lanes. **(C)** Expression of GAD-Poz1-FL2 (47.3kDa) fusion protein checked by anti-HA western blot from PJ69-4A yeast whole cell extracts. GAD EV (20.5kDa) also shown. Ponceau staining of membrane indicates relative loading between lanes.

3.2.3 Mutagenesis of *poz1*

A variety of methods can be used to mutagenize the prey construct. Error-prone PCR mutagenesis was the method adopted in this case. This was due to the degree of control over mutation rates and mutation types through varying template concentration, cycle numbers, buffer composition and dNTP concentrations. Using PCR mutagenesis also allows for targeting of a specific region of a plasmid, as opposed to other methods, such as hydroxylamine-based chemical mutagenesis and use of mutation-prone *E. coli* host cells, where the entire plasmid is mutagenised. In addition, this method has previously been used successfully to introduce mutations for this specific purpose (Thomas *et al.*, 2002).

3.2.3.1 A second prey vector, pGADT7SpPoz1-FL2

Due to the likelihood of needing to separate mutations in positive candidates, a second prey plasmid, in addition to pGADT7SpPoz1-FL, was constructed. It contains two silent base substitutions in the *poz1* ORF; one at base 207 (T to G substitution) and one at base 210 (C to T substitution). This introduced a new, unique BamHI restriction site for additional separation of mutations [Fig 3.7A]. Having two unique restriction sites has the added benefit of redundancy, should one of the sites be disrupted during mutagenesis.

The new *poz1* ORF fragment was wholly synthesised by Eurofins MWG Operon and in addition to the base substitutions, contains several additional restriction sites downstream of the STOP codon, replacing the XmaI site used thus far. The additional restriction sites add redundancy for downstream processing of interesting mutants. Should one site be disrupted during mutagenesis, other sites could be used for subcloning the ORF. The synthesised fragment was subcloned by NdeI-XhoI digestion and ligation into the same sites in the pGADT7 vector to generate pGADT7SpPoz1-FL2 [Fig 3.7B].
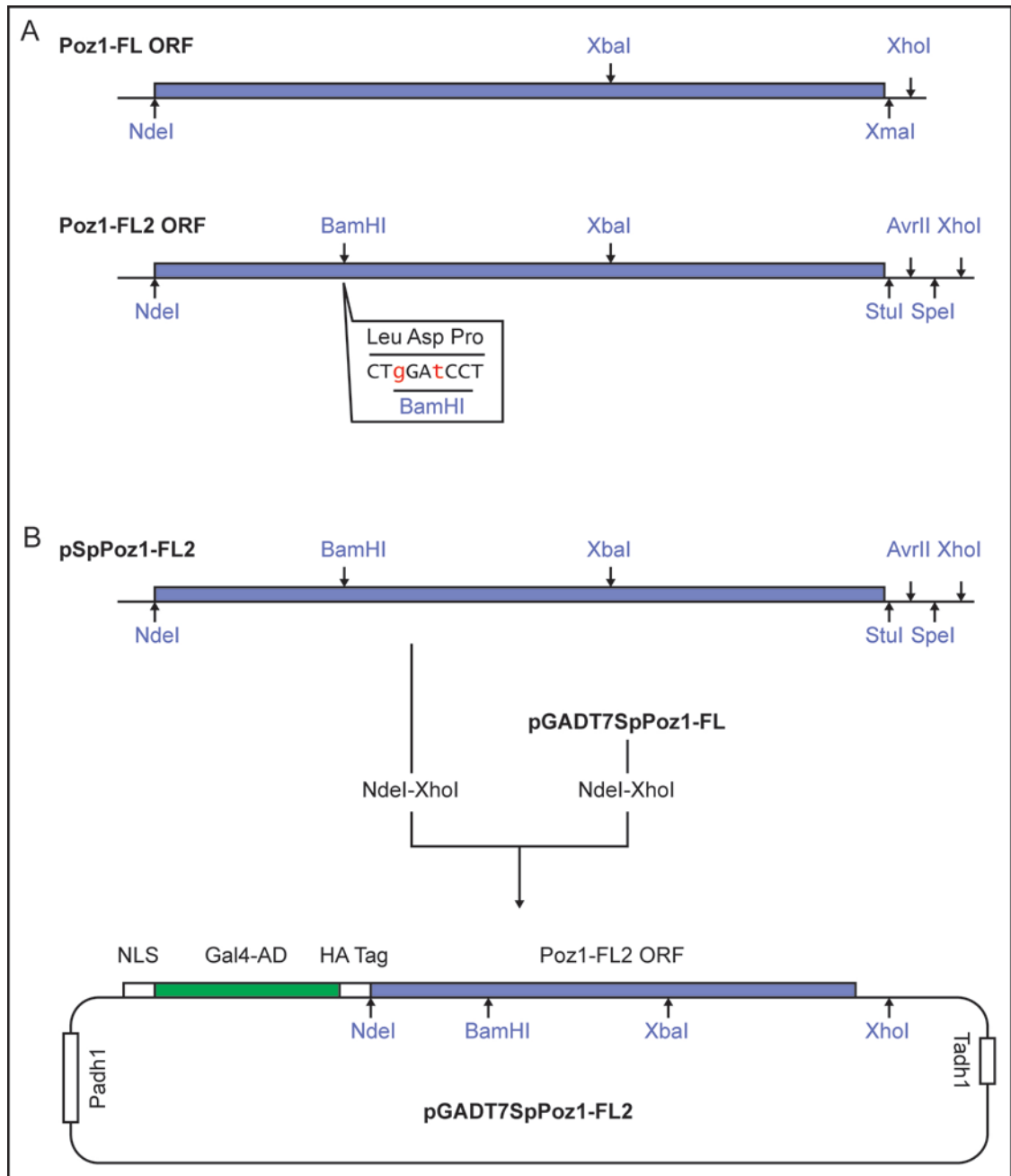
Figure 3.7: Schematic of synthesised Poz1-FL2 ORF subcloning into pGADT7 vector.

(A) Comparison of Poz1-FL and Poz1-FL2 synthesised fragment. Poz1-FL2 contains additional BamHI site within the ORF through a modification of the DNA sequence without affecting the peptide sequence, as indicated (changes in red). Several additional restriction sites downstream of the STOP codon are also added. This results in the loss of the XmaI site, but gain of StuI, AvrII and SpeI site. These additional restriction sites add redundancy for downstream processing of the ORF in interesting mutants. **(B)** Subcloning of the Poz1-FL2 fragment by NdeI-XhoI restriction digest and ligation into same sites in pGADT7. The pGADT7SpPoz1-FL2 plasmid contains the same features as the previous pGADT7SpPoz1-FL plasmid. The *ADH1* promoter, terminator, nuclear localisation signal (NLS) and HA tag are as labelled in white and the Gal4 activating domain in green. Restriction sites are positioned, as indicated.

3.2.3.2 Mutagenesis of pGADT7SpPoz1-FL2 by error-prone PCR

Using this pGADT7SpPoz1-FL2 vector as a template, a series of error-prone PCRs were run using the primers GAD-f1 and GADT7-b1 [Fig 3.8A]. This was done under conditions described in the methods with the aim of generating the minimum number of mutations per kb of target DNA amplified as possible. These conditions, where $MnCl_2$ and dNTP levels have been skewed beyond optimum, and target template levels controlled allow the Taq polymerase to make errors at a predictable frequency. Also, by only allowing sufficient PCR cycles to amplify the target up to 10-fold further minimised excessive numbers of mutations. From six separate reactions, PCR product was verified to be the expected size of 1140bp by agarose gel electrophoresis. The separate reactions were combined and purified by Qiagen QIAquick PCR purification kit. A small portion of the PCR product was cloned into pGEM-T Easy vector by TA cloning and sequenced to verify a low mutation frequency of 3-7 mutations per kb.

The template vector, pGADT7SpPoz1-FL2 was digested with NdeI-XhoI and the vector fragment (7924bp) purified from an agarose gel using a Qiagen Gel Extraction kit. Digesting the vector with these enzymes released the wild type *poz1* ORF, resulting in a large overlap between the vector ends and the mutagenized PCR product, 183bp upstream of the NdeI cut site and 152bp downstream of the XhoI cut site [Fig 3.8B]. The mutagenized PCR product and the vector fragment were co-transformed into the screening strains 1 and 3 where successfully co-transformed cells would generate a complete plasmid by gap repair recombination [Fig 3.8C]. For each strain, three separate control transformations were also performed using No DNA, Empty Vector and pGADT7SpPoz1-FL2 as the transforming DNA. Four screening transformations, containing mutagenized *poz1* were combined into one mix and all transformation mixes plated according to Table 3.3. Each screening transformation consisted of 100ng pGADT7 NdeI-XhoI linear vector and 300ng mutagenized *poz1* PCR product, which is calculated as a 1:20 molar ratio, optimal for gap repair (Pritchard *et al.*, 2005).

Figure 3.8: Schematic demonstrating mutagenesis of Poz1-FL2 using error-prone PCR (following page).

(A) Error-prone PCR using the primers GAD-f1 and GADT7-b1, amplifying from 183bp upstream of *poz1* START codon in the Gal4-AD (green) to 152bp downstream of XhoI site. This introduces random mutations in the Poz1-FL2 target fragment. **(B)** The error-prone mutagenesis PCR product contains mutations, represented by vertical red bars in the Poz1-FL2 ORF. The pGADT7-SpPoz1-FL2 vector is digested with NdeI-XhoI and purified to provide a large overlap to both ends of PCR product. **(C)** Purified vector fragment and mutagenized PCR product transformed into LY26 screening strains 1 and 3. Yeast gap repair (indicated) functions to generate complete pGADT7SpPoz1-FL2 plasmid with mutagenized *poz1* integrated. Mutations represented by vertical bars within Poz1-FL2 ORF. The pGADT7SpPoz1-FL2 plasmid GAD-SpPoz1-FL2 fusion protein is expressed under the control of the *ADH1* promoter (Padh1) and terminator (Tadh1). The fusion protein also contains a nuclear localisation signal (NLS) sequence and a HA epitope tag, as indicated.
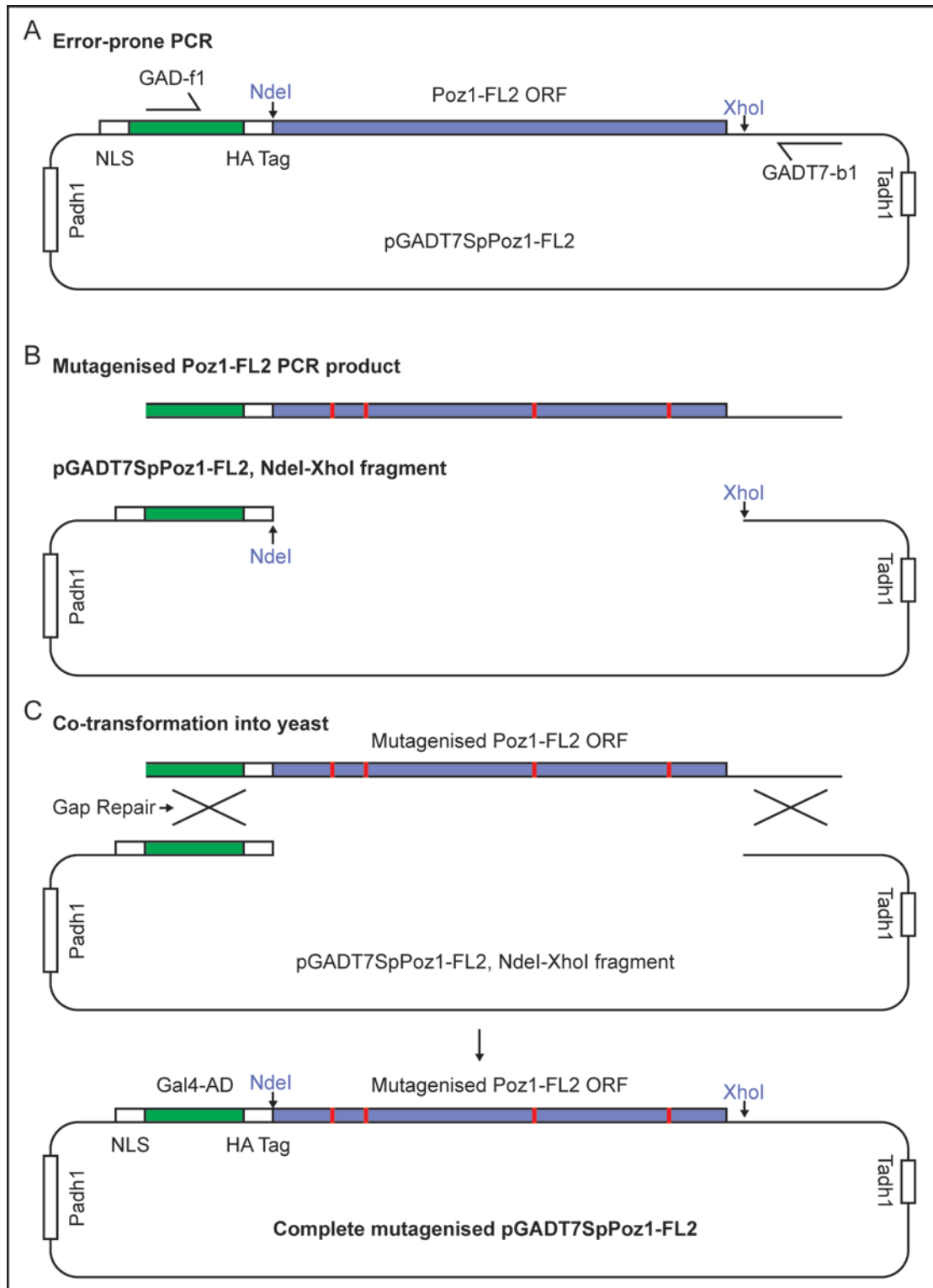
3.2.4 Screening for desired *poz1* mutant alleles

Transformants obtained from screening in Strains 1 and 3 were plated on both media selective to the activation of the reporter genes (Sc –TRP –LEU –ADE –HIS +3-AT) and to just the presence of the complete prey plasmid, as detailed in Table 3.3. Variation in the concentration of 3-Amino,1,2,4-Triazole (3-AT), a competitive inhibitor of HIS3, was required between batches of media, ranging from 4mM to 7mM, however, based on control tests, 6mM was typically found to be optimum for selection in most cases.

Transformation	Media	Expected Phenotype
No DNA	-TRP –LEU	-
pGADT7 EV (100ng)	-TRP –LEU	+
	-TRP –LEU –ADE –HIS +3-AT	-
pGADT7SpPoz1-FL2 (100ng)	-TRP –LEU	+
	-TRP –LEU –ADE –HIS +3-AT	-
pGADT7 (100ng) + mutPoz1 PCR product (300ng)	-TRP –LEU (10µl)	+
	-TRP –LEU –ADE –HIS +3-AT	To be tested

Table 3.3: **Transformations used in screening for *poz1* mutant alleles.**

For empty vector and Poz1-FL2 controls, half of the transformation mixture is plated on each media type (Sc –TRP – LEU and Sc –TRP –LEU –ADE –HIS +3-AT). Growth is only expected on Sc –TRP –LEU plates, due to no selection for reporter gene activation. For screening, the pGADT7 (NdeI-XhoI) EV + mutPoz1 PCR product, 10µl of 1200µl total transformation mix is plated on Sc –TRP –LEU to aid calculation of screening efficiency. Screening efficiency calculated by: no. of cfu/10µl x 1200µl = no. of prey molecules screened. Remaining 1190µl of screening transformation mix is plated on Sc –TRP –LEU –ADE –HIS + 3-AT, split between 12 plates. Colonies that form on these plates are interaction disruption candidates. Expected phenotype: plus symbol (+) = growth expected while minus symbol (-) = growth not expected.

The screening efficiency was determined from the Sc –TRP –LEU plates containing 10µl pGAD-EV + mutPoz1 PCR product for each strain. The Strain 1 plate, which contained 228 colony forming units, indicated that approximately 28 000 mutagenised molecules had been

screened. The Strain 3 plate, which contained 534 colony forming units, indicated that approximately 64 000 mutagenised molecules had been screened, as indicated below:

Strain 1: 228/10*1200= 27 360 molecules screened

Strain 3: 534/10*1200= 64 080 molecules screened

The screening plates for Strain 1 contained several cfu, however, one showed clear, strong growth. This colony grew with a whiter colour, compared to others in the screen, indicative of better ADE2 expression (Zonneveld and van der Zanden, 1995). This colony, containing the mutant allele later designated 'mutant 17', along with several others was streaked onto fresh selective plates. However, it was only the streak containing mutant 17 that subsequently grew well on fresh plates. The Strain 3 screening plates contained several hundred cfu, of which five were selected and streaked onto fresh selective plates. Of these, mutant 1 was the fastest growing. Mutants 2-5 grew less well. These candidates were all taken through to the next stage of plasmid recovery and retesting.

3.2.5 Mutagenised Poz1 plasmid recovery and retesting

Strains containing mutants 1-5 from Strain 3 and mutant 17 from Strain 1 were inoculated in Sc –TRP –LEU liquid media overnight. Plasmid recovery from 3ml of each culture was performed and aqueous solution containing recovered plasmids transformed into commercial, high efficiency, DH5α chemically competent cells (NEB). Of multiple colonies that had formed on the LB agar + Ampicillin plates overnight, 3 were selected for each mutant and inoculated for plasmid miniprep.

The prepped plasmids (3 preps for each mutant) were transformed back into the appropriate strains, Strain 1 for mutant 17 and Strain 3 for mutants 1-5. The activation of reporter genes was assessed by plating on dual selection media (Sc –TRP –LEU –ADE –HIS + 3-AT), as initially

done with the screens. Of these, only mutants 1 and 17 formed colonies on the dual selection [Fig 3.9A-B]. It appeared that mutants 2-5 were false positives in the initial screen. Mutants 1 and 17, therefore, were the only ones taken forward for cross-checking in the PJ69-4A yeast-2-hybrid strain for interactions of the mutant *poz1* alleles with GBD-Rap1 and GBD-Tpz1 fusions.

The yeast-2-hybrid strain PJ69-4A, previously transformed with GBD-Rap1 or GBD-Tpz1 plasmids was now transformed with the pGADSpPoz1-mut1 and mut17 plasmids. The transformants were grown on Sc −TRP −LEU and several cfu streaked to fresh plates. These were then streaked onto plates selective for the reporter genes, *HIS3* and *ADE2* (Sc −TRP −LEU −ADE and Sc −TRP −LEU −HIS) [Fig 3.9C]. Contrary to expectations, although mutant 17 had a clear Rap1 interaction disruption phenotype, mutant 1 no longer appeared to have a Tpz1 interaction disruption phenotype. This was unexpected as growth on dual selective plates when retransformed into Strain 3 appeared to indicate mutant 1 as a true positive.

It is possible that the stringency of the *ADE2* reporter in the LY26 reverse 2-hybrid strain is not sufficient to rule out mutants with weak, and not eliminated, interactions. It is also possible that Strain 3 is susceptible to external mutations, not within the prey protein, which may disrupt the expression of GBD-fusion, the *TetR* gene or, indeed, lead to resistance of the *LacO* promoter to *TetR*. Any of these would lead to leaky expression of *ADE2*, which may be sufficient to score positive in the initial screen where direct selection for Ade[+] His[+] transformants is applied. The high frequency of apparent positive candidates from the initial screen may be indicative of this fact. Indeed, selection of the whitest colonies may have inadvertently resulted in selection of those with unwanted, external mutations.

To test whether external mutations may have been the cause of the mutant 1 false positive phenotype, Strain 3 was transformed again with the same pGADT7SpPoz1-mut1 plasmid prep as before. This time, however, the transformations were plated onto Sc −TRP −LEU, selecting only for the plasmid, rather than the activation of reporter genes. Several cfu were then

streaked onto dual selection media, as used previously [Fig 3.9D]. Of five colonies streaked, none retained the Tpz1 interaction disruption phenotype. This suggested that the false positive phenotype observed previously was likely due to external mutations, selected for by plating directly on dual selection media.

In order to identify a true positive for Tpz1 interaction disruption and eliminate false positives, mutagenized GAD-Poz1 candidates could be assessed for LacZ reporter activity.

Figure 3.9: **Testing interaction of Poz1 mutants 1 and 17 for interaction with Rap1 and Tpz1 (following page).**

(A) LY26 colonies for Poz1 mutants 1 and 5 (from Strain 3 screen). Plasmids were recovered from initial screen and retransformed into the LY26 reverse 2-hybrid strain. These were streaked with controls on Sc –TRP –LEU –ADE –HIS + 6mM 3-AT and show growth for mutant 1 but not mutant 5. **(B)** LY26 colonies for Poz1 mutants 17 (from Strain 1 screen) and 2-4 (from Strain 3 screen). Plasmids were recovered from initial screen and retransformed into the LY26 reverse 2-hybrid strain. These were streaked with controls on Sc –TRP –LEU –ADE –HIS + 6mM 3-AT and show growth for mutant 17 but not mutants 2-4. **(C)** Streaks of yeast 2-hybrid strain PJ69-4A transformed with GBD-SpRap1 or SpTpz1 and plasmids recovered from GAD-SpPoz1 mutants 1 and 17 on Sc –TRP –LEU –ADE. Mutant 17 shows growth with GBD-Tpz1 and no growth with GBD-Rap1, as expected from phenotype displayed in LY26 strain. Mutant 1 shows growth with both GBD-Rap1 and GBD-Tpz1 which is unexpected. **(D)** Streaks of Strain 3 retransformed with pGADT7SpPoz1-mut1 on Sc –TRP –LEU –ADE –HIS + 6mM 3-AT. Of these streaks, Strain 3 + Poz1-mut1 "nr1" to "nr5" are five individual transformants that have been tested. None of these mutant 1 transformants grow on selective media, indicating that mutant 1 was a false positive.

A

Strain: LY26

Key:
1: Strain 3 + Poz1-mut5
2: Strain 3 + Poz1-mut1
3: Strain 3 + Poz1-FL2
4: Strain 3 + GADT7 EV
5: Strain 4 + Poz1-FL2
6: Strain 4 + GADT7 EV

Media: Sc -TRP -LEU -ADE -HIS

B

Strain: LY26

Key:
1: Strain 1 + Poz1-mut17
2: Strain 3 + Poz1-mut4
3: Strain 3 + Poz1-mut3
4: Strain 3 + Poz1-mut2
5: Strain 3 + Poz1-FL2
6: Strain 3 + GADT7 EV
7: Strain 4 + Poz1-FL2

Media: Sc -TRP -LEU -ADE -HIS

C

Strain: PJ69-4A

Key:
1: GBD-Rap1 + GAD-mut17
2: GBD-Rap1 + GAD-mut1
3: GBD-Tpz1 + GAD-mut17
4: GBD-Tpz1 + GAD-mut1
5: GBD-DMC1 + GAD-DMC1
6: GBD-Rif1 + GAD-Taz1
7: GBD EV + GAD EV

Media: Sc -TRP -LEU -ADE

D

Strain: LY26

Key:
1: Strain 3 + Poz1-FL2
2: Strain 3 + GADT7 EV
3: Strain 4 + Poz1-FL2
4: Strain 3 + Poz1-mut1, nr1
5: Strain 3 + Poz1-mut1, nr2
6: Strain 3 + Poz1-mut1, nr3
7: Strain 3 + Poz1-mut1, nr4
8: Strain 3 + Poz1-mut1, nr5

Media: Sc -TRP -LEU -HIS -ADE

3.2.6 Assessment of *LacZ* activity in Tpz1-interaction disruption candidates

To help eliminate false positives, LY26 strain 3 candidates, containing mutagenized GAD-Poz1, were mated, separately, with two additional strains, Y190 and DY6877, provided by the Thorburn lab (Thomas *et al.*, 2002) for use in such cases. The Y190 strain contains a *URA3::GAL1-LacZ* reporter while the DY6877 strain contains a *URA3::LexA-LacZ* reporter. Therefore, mating the candidates with Y190 allows assessment of the interaction with the GBD-fusion protein and mating with DY6877 allows assessment of the interaction with the LexA-fusion protein.

LY26 is a *met15* mutant, but Trp$^+$ Leu$^+$ due to the presence of the GBD bait integration and GAD prey plasmid. Y190 and DY6877 are both Met$^+$ but are both *trp1* and *leu2* mutants. By mating with LY26, diploids can be selected on Sc-TRP –LEU –MET media and *LacZ* activity can be assessed with a blue-white filter lift assay. Control and mutagenized Poz1 candidates are expected to give the phenotypes as shown in Table 3.4.

	LY26(S3)-Y190 (Gal1-LacZ)	LY26(S3)-DY6877 (LexA-LacZ)
GAD-EV	White	White
GAD-Poz1	Blue	Blue
Positive Poz1 mutant	**White**	**Blue**

Table 3.4: **Expected colour phenotypes from Blue-White filter lift assay.**

When LY26 Strain 3 (labelled "S3" in table) Tpz1-interaction disruption candidates are mated to Y190 and to DY6877 strains, *LacZ* activity can be assessed to determine true positives. Y190 contains a *GAL1-LacZ* reporter while DY6877 contains a *LexA-LacZ* reporter. Real positive *poz1* mutant alleles are expected to display white phenotype (loss of interaction) in LY26-Y190 diploid and blue phenotype (retention of interaction) in LY26-DY6877 diploid.

To screen for false positives, 24 candidates from the Strain 3 screen were selected, with a range of growth rate and colour on dual selection. These candidates were mated to both Y190 and DY6877 on YPAD agar plates for 24 hours, after which each was streaked on Sc –TRP –LEU

–MET media to select for LY26-Y190 and LY26-DY6877 diploids. In addition to these candidates, control strains (Strain 3 + pGADT7SpPoz1-FL2 or Empty Vector and Strain 1 + Poz1-mut17-20) were mated with the Y190 and DY6877 strains. [Note: Mutants 19 and 20 were the result of further processing of mutant 17, as detailed in a following section.] A blue-white filter lift assay was then carried out and colour of controls and candidates assessed [Fig 3.10].

Figure 3.10: **Screen for false positives by blue-white filter lift assay on Strain 3, mutagenized Poz1-FL2 candidates (following page).**

(A) Control filters for SpPoz1-FL2 (positive control) and Empty Vector (negative control), as indicated for LY26 Strain 3 crosses with DY6877 (testing Rap1 interaction) and Y190 (testing Tpz1 interaction). Additional tests with SpPoz1-mut17, mut19 and mut20 from LY26 Strain 1, Rap1-interaction disruption screen are also present, as indicated. Blue colour on assay indicates activation of *LacZ* reporter gene and, therefore, positive interaction with *poz1* allele. White colour indicates no detectable activation of *LacZ* and, therefore, no detectable interaction with *poz1* allele. Wild-type interaction can be identified by blue colouration with Poz1-FL2 and no interaction identified by lack of blue colouration with Empty Vector. **(B)** (i) Tpz1-interaction disruption candidate filters from DY6877 show clear blue colouration, as expected. This indicates Poz1-Rap1 interaction is maintained in all candidates. (ii) Y190 filters mostly show white, or non-blue, colouration. This indicates that most candidates are Tpz1 interaction disruption alleles. The exceptions are no.5, 6 and 24, all of which show some blue colour, indicating continued Tpz1 interaction. (iii) Sc –TRP –LEU –ADE –HIS + 3-AT plate images show candidate growth on selective media (LY26, Strain 3).

A

i: LacZ Assay DY6877 Controls

ii: LacZ Assay Y190 Controls

Controls Key:

1: pGADT7SpPoz1-FL2 (Pos)
2: pGADT7 EV (Neg)
3: pGADT7SpPoz1-mut17*
4: pGADT7SpPoz1-mut19*
5: pGADT7SpPoz1-mut20*

*From Strain 1 background

B

i: LacZ Assay DY6877, no. 1-24

ii: LacZ Assay Y190, no. 1-24

iii: Candidates 1-24, Sc -TLAH
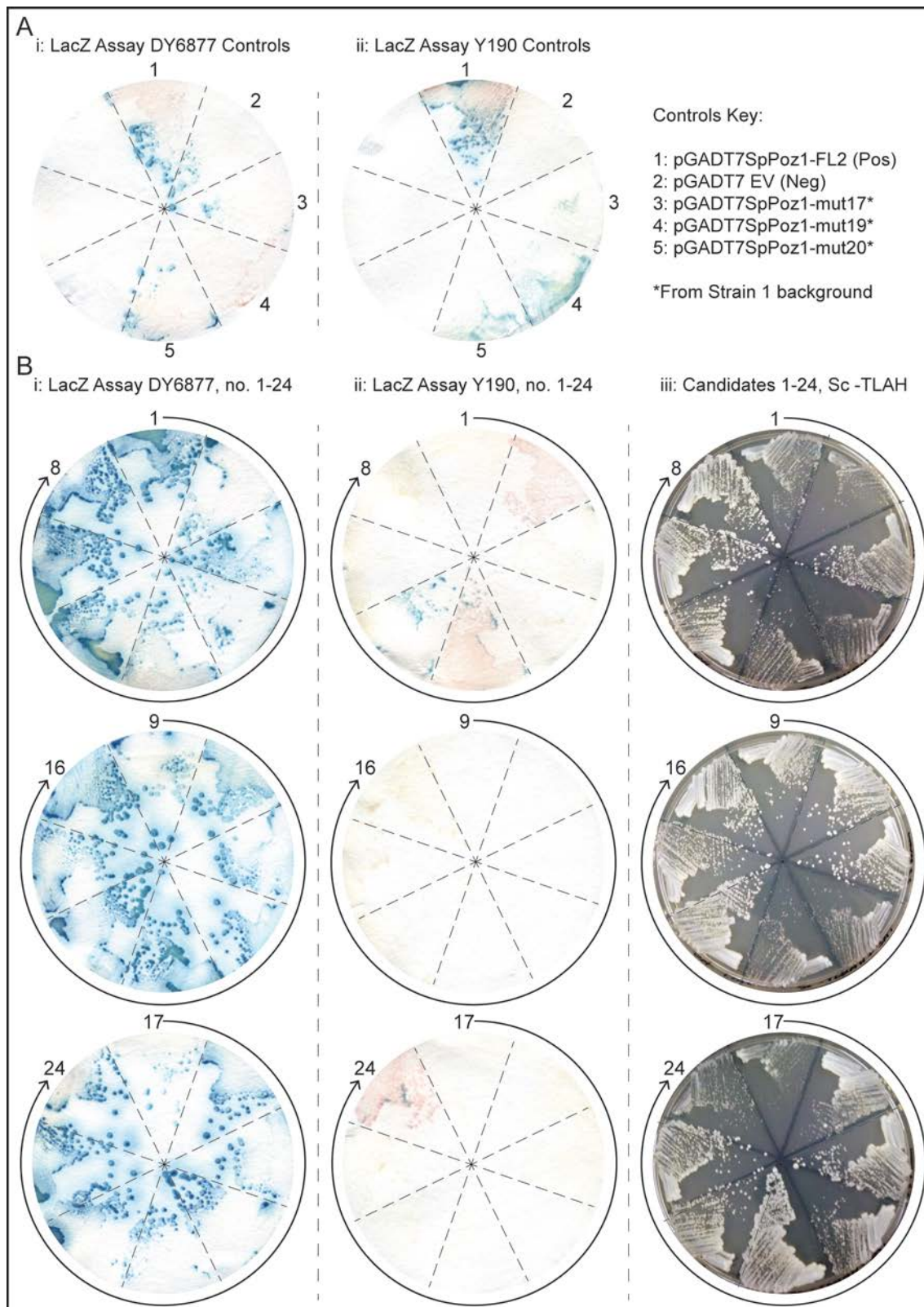
The *LacZ* assay control filters [Fig 3.10A] indicate that the assay is functioning as expected. On the DY6877 filter, the Strain 3 + SpPoz1-FL2 control shows a clear blue colouration and when compared to the Empty Vector, which shows some faint blue colouration that appears to be due to bleed over, indicates this assay is reliable. The equivalent streaks on the Y190 filter also show the same pattern, though in this case there is no blue colouration visible at all on the Empty Vector. The controls from the Strain 1 backgrounds, however, do not have as strong colouration on the DY6877 filter, as compared to the Strain 3 + SpPoz1-FL2 control. This would be of some concern; however, the pattern is as expected. SpPoz1-mut17 and –mut20 show some blue colouration while –mut19 shows none. Further explanation is found in a following section.

The actual Tpz1-interaction disruption candidates tested [Fig 3.10B] show clear differences between the DY6877 and Y190 filters. The majority appear to show the expected colouration (blue with DY6877 and red with Y190), with the exception of some blue colouration on candidate numbers 5, 6 and 24 on the Y190 filter. To some extent, this was surprising, given that all previous candidates had been false positives. However, it may be further indication that the stringency of Strain 3 reporter is not sufficient to remove those clones with weakened, rather than eliminated Tpz1 interaction. As a result of the uniformity of the colouration, despite the different rates of growth on dual selection media, candidates were further processed in batches.

3.2.7 Confirmation of Tpz1-interaction disruption by forward yeast-2-hybrid assay

The pGADT7 plasmids were recovered from the 24 candidates in batches. Due to plasmid recovery not always being successful, the clones were prepped (3 for each clone; A, B and C) and processed in the order that they were successfully recovered. The yeast-2-hybrid strain PJ69-4A, previously transformed with GBD-Rap1 or GBD-Tpz1 plasmids was once again

transformed with the GAD-Poz1 mutants. The transformants were grown on Sc –TRP –LEU, as before, and representative cfu selected from each to be patched onto selective plates [Fig 3.11]. Growth, indicating activation of the reporter genes, *HIS3* and *ADE2*, was then assessed. Patches were used instead of streaks in this case to process a larger number of clones.

The patch tests from the first batch of recovered plasmids indicate that all three preps from clone nr9 (nr9-A, nr9-B and nr9-C) have the expected phenotype, Rap1 interaction, Tpz1 disruption [Fig 3.11B]. One prep from clone nr7 (nr7-B) also shows the correct phenotype [Fig 3.11A]. This would indicate that there may be more than one plasmid clone in candidate nr7. Regardless, out of the initial batch, one candidate containing a clone with the desired phenotype was identified. This was designated pGADT7SpPoz1-mut23 and taken to the next stage of analysis.

Figure 3.11: **Testing Tpz1-interaction disruption candidates by forward yeast-2-hybrid assay.**

(A) Transformants from control plasmids, pGADT7SpPoz1-FL2 and pGADT7, transformed into PJ69-4A strain containing GBD-SpRap1 or SpTpz1 patched on both Ade and His selection plates, as indicated. Clear difference in growth can be seen between wild type and empty vector controls. In addition, Tpz1-interaction disruption candidates nr1 and 7 are transformed into the same strains and patched. Three clones from each candidate were recovered and transformed (A, B and C). Clone nr7-B shows the desired phenotype of Rap1-interaction (growth), Tpz1-disruption (no growth). Location of this clone in the patches is indicated by the shaded boxes in the key. **(B)** Transformants from candidates 8, 9 and 10 in PJ69-4A patched on both Ade and His selection plates, as indicated. Tpz1-interaction disruption candidate patches 9-A, B and C all show the desired phenotype of Rap1-interaction (growth), Tpz1-disruption (no growth). Location of these clones in the patches is indicated by the shaded boxes in the key.

3.2.8 Sequence analysis of Poz1-mut17 ORF

Due to being identified as a clone with the desired Rap1-interaction disruption phenotype before identification of an equivalent Tpz1 interaction disruption clone, processing of Poz1-mut17 had continued. The ORF of Poz1-mut17 was sequenced and base mutations were identified. These nucleotide sequence data were then converted to peptide sequence data using Serial Cloner and the mutant sequence compared to the Poz1-FL2 wild-type sequence using Clustal Omega (Goujon *et al.*, 2010, Sievers *et al.*, 2011). The results of the sequencing and Clustal Omega alignments [Fig 3.12] indicate that six mutations were present in the ORF, leading to five amino acid substitutions: K20N, D25G, C48S, C143R and L157P.
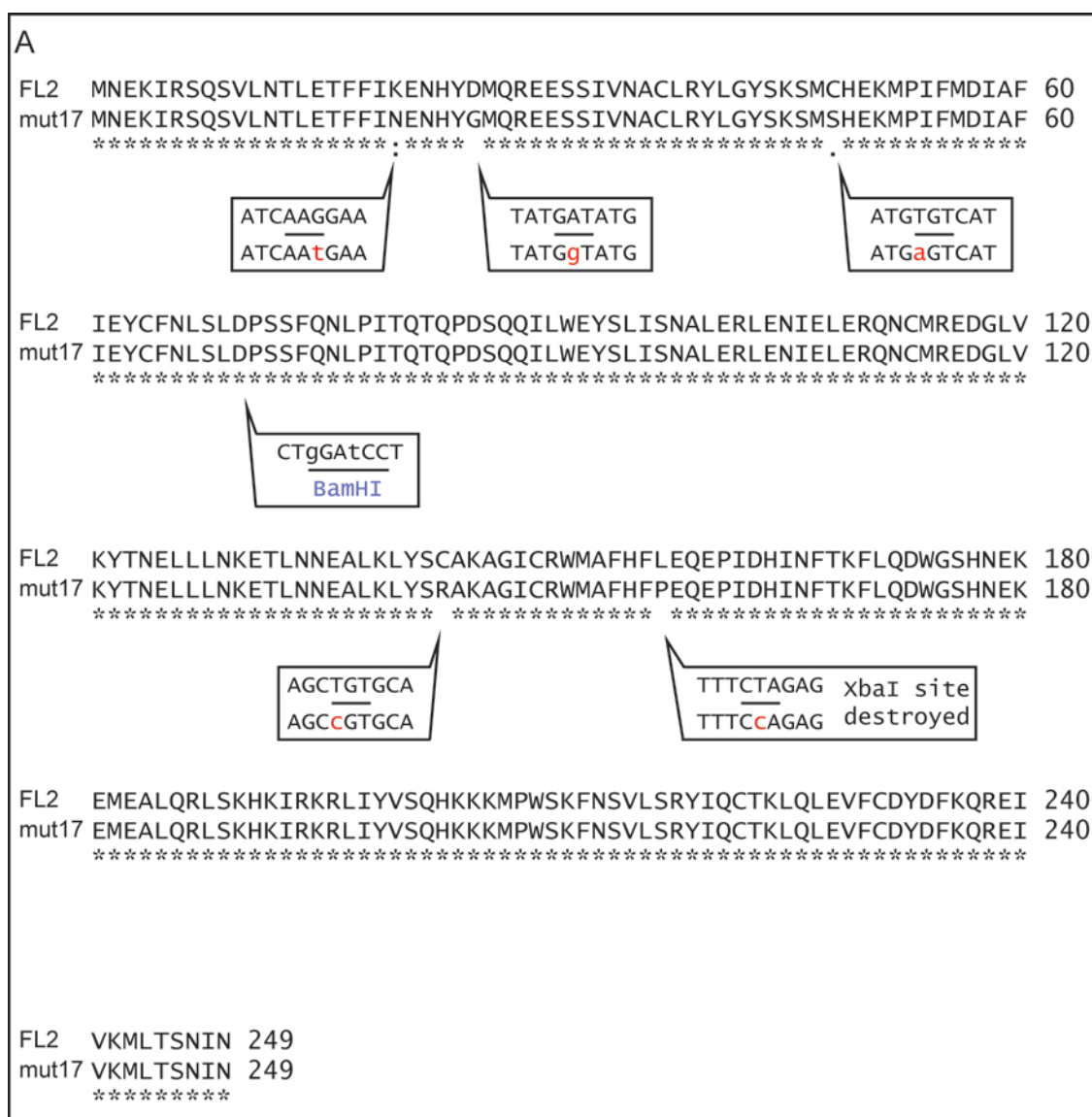
Figure 3.12: Sequence analysis of Rap1-interaction disruption allele Poz1-mut17 ORF and peptide sequence.

(A) Peptide sequence of Poz1-FL2 (wild-type) compared to mutant 17 compared using Clustal Omega. Mutant 17 (mut17) contains five amino acid substitutions: K20N, D25G, C48S, C143R and L157P. Sequence changes at the nucleotide level are highlighted in boxes. The uppercase nucleotide sequence is wild-type and lowercase red sequence indicates the mutation. The horizontal line separating the wild-type sequence (top) and mutant 17 sequence (bottom) indicates the codon affected. The BamHI site location in the ORF is indicated in blue. A mutation leading to the loss of the XbaI site is also indicated in red. An * (asterisk) indicates positions which have a single, fully conserved residue. A : (colon) indicates conservation between strongly similar residues. A . (full stop) indicates positions which have a single, weakly conserved residue. An empty space indicates dissimilar residues.

3.2.9 Separation and testing of mutation clusters in Poz1-mut17 ORF

One mutation, resulting in the L157P amino acid change, destroyed the XbaI site. However, the BamHI site was unaffected. It was, therefore, possible to separate the initial three substitutions, clustered at the N-terminus from the following two in order to identify whether the first or second cluster of mutations was sufficient to retain the Rap1-interaction disruption phenotype. The Poz1-mut17 ORF was separated by subcloning into the wild-type pGADT7SpPoz1-FL2 vector by BamHI-AflII restriction digest and ligation [Fig 3.13A]. This resulted in two new vectors, pGADT7SpPoz1-mut19 and pGADT7SpPoz1-mut20, which each contained one of the two sets of clustered mutations [Fig 3.13B]. Poz1-mut19 retained the K20N, D25G and C48S mutations while Poz1-mut20 retained the C143R and L157P mutations.

To test whether either of these clones retained the combination of mutations sufficient to disrupt Rap1-interaction; they were transformed back into LY26 Strain 1, as well as Strain 3. In addition, they were transformed into the forward 2-hybrid PJ69-4A strains containing pGBKT7SpRap1-FL and pGBKT7SpTpz1 vectors as done previously. Transformants were streaked onto Sc −TRP −LEU −ADE −LEU with control strains and assessed for growth [Fig 3.13C-D].

On the LY26 plate [Fig 3.13C], no growth is observed for Poz1-mut19. However, Poz1-mut20 does show growth when transformed into Strain 1, but not Strain 3, indicating the growth is specific to loss of Rap1 interaction. This trend is also seen on the PJ69-4A plate, where Poz1-mut19 growth is seen with both Rap1 and Tpz1 GBD plasmids, but with Poz1-mut20, growth is only seen with Tpz1 and not with Rap1. These results indicate that the two mutations in Poz1-mut20 allele, C143R and L157P, are sufficient to disrupt interaction with Rap1 while maintaining interaction with Tpz1. Due to both these amino acid substitutions being to dissimilar residues, they are also potentially the most disruptive changes.

Figure 3.13: Separation of mutation clusters in Poz1-mut17 and testing of resulting plasmids (following page).

(A) Mutations in Poz1-mut17 are indicated by red stars on the ORF (blue). These are separable by BamHI-AflII subcloning between pGADT7SpPoz1-mut17 and pGADT7SpPoz1-FL2. The plasmid contains the cassette for the Gal4-AD (green) fusion to the Poz1 ORF. The NLS and HA epitope tag are indicated. Expression is controlled by the *ADH1* promoter (Padh1) and terminator (Tadh1). **(B)** The subcloning results in two new plasmids with clusters of mutations separated, pGADT7SpPoz1-mut19 and pGADT7SpPoz1-mut20, as indicated. Poz1-mut19 contains the mutations resulting in the N-terminal substitutions: K20N, D25G and C48S. Poz1-mut20 contains the mutations resulting in the C-terminal substitutions: C143R and L157P. **(C)** LY26 Strains 1 and 3, Poz1-mut17, Poz1-mut19 and mut20 transformants are streaked on dual selection (Sc –TRP –LEU –ADE –HIS + 6mM 3-AT) media, as indicated. Poz1-mut20 retains the desired phenotype (growth when transformed in Strain 1) indicating Rap1-interaction disruption. **(D)** Forward yeast 2-hybrid PJ69-4A strain, Poz1-mut19 and mut20 transformants are streaked on dual selection (Sc –TRP –LEU –ADE –HIS + 6mM 3-AT) media, as indicated. The Poz1-mut17 and Poz1-mut20 display the same, desired, phenotype. No growth with GBD-SpRap1 and growth with GBD-SpTpz1 indicate that the mutations in Poz1-mut20 are sufficient to disrupt Rap1 interaction and retain Tpz1 interaction.
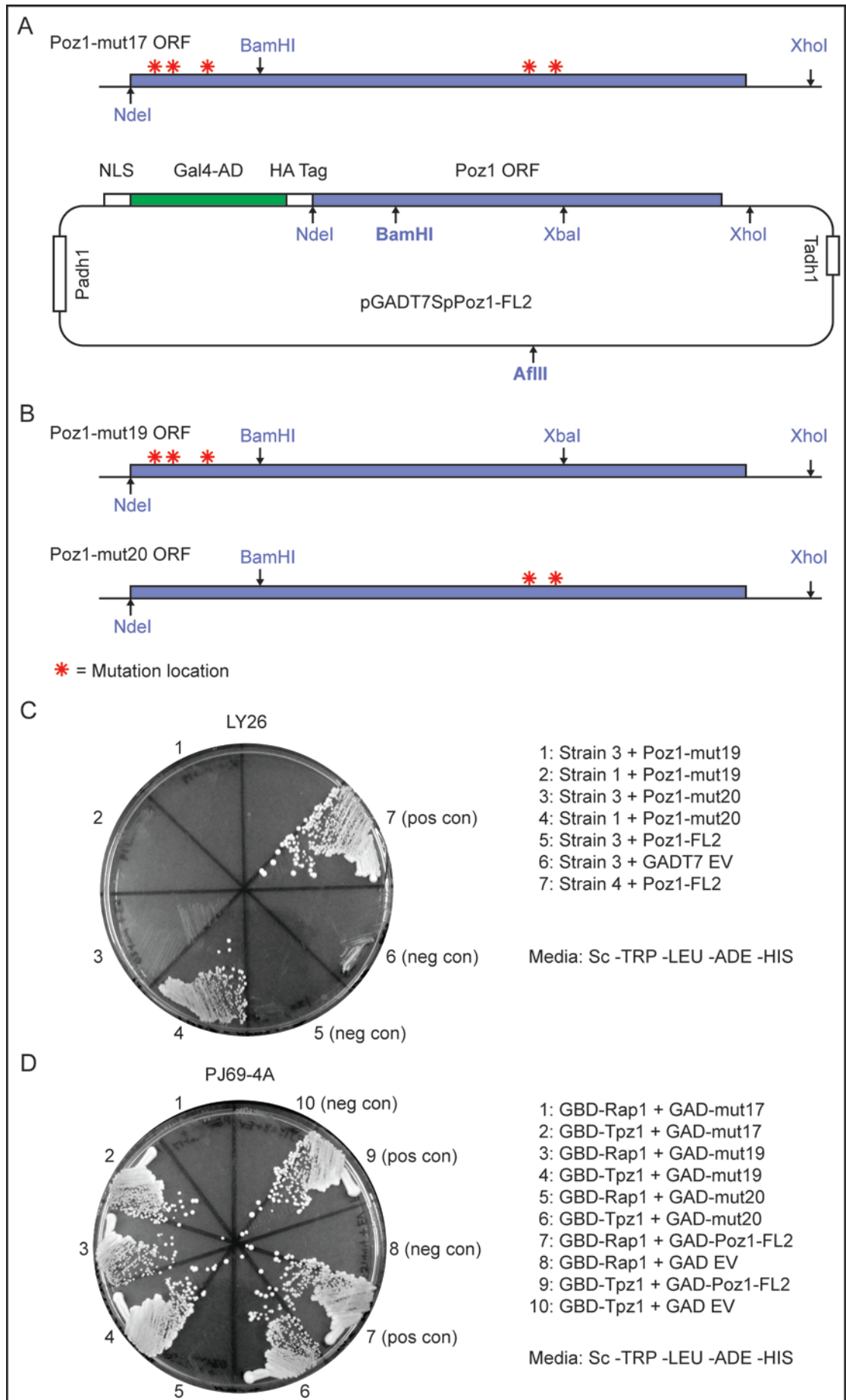
3.2.10 Sequence analysis of Poz1-mut23 ORF

The ORF of Poz1-mut23, from the plasmid pGADT7SPPoz1-mut23, was sequenced and base mutations were identified. These nucleotide sequence data were then converted to peptide sequence data using Serial Cloner and the mutant sequence compared to the Poz1-FL2 wild-type sequence using Clustal Omega, as done with Poz1-mut17. The results of the sequencing and Clustal Omega (Goujon *et al.*, 2010, Sievers *et al.*, 2011) alignments indicate that six mutations were present in the ORF, leading to five amino acid substitutions: F18Y, F65I, I89M, L95H and M243R [Fig 3.14].

As neither BamHI nor XbaI restriction sites were affected by mutagenesis, it was possible to separate the mutations to determine which were sufficient to retain the phenotype. The different clusters could be combined in six combinations. If the three sections of the ORF (NdeI-BamHI, BamHI-XbaI and XbaI-XhoI) are designated A, B and C, as shown in Fig 3.14B, the mutations could be subcloned in the following conbinations:

   I.   A – wt – wt   = Poz1-mut25

  II.   wt – B – wt   = Poz1-mut26

 III.   wt – wt – C   = Poz1-mut27

 IV.   A – B – wt   = Poz1-mut28

  V.   A – wt – C   = Poz1-mut29

 VI.   wt – B – C   = Poz1-mut30
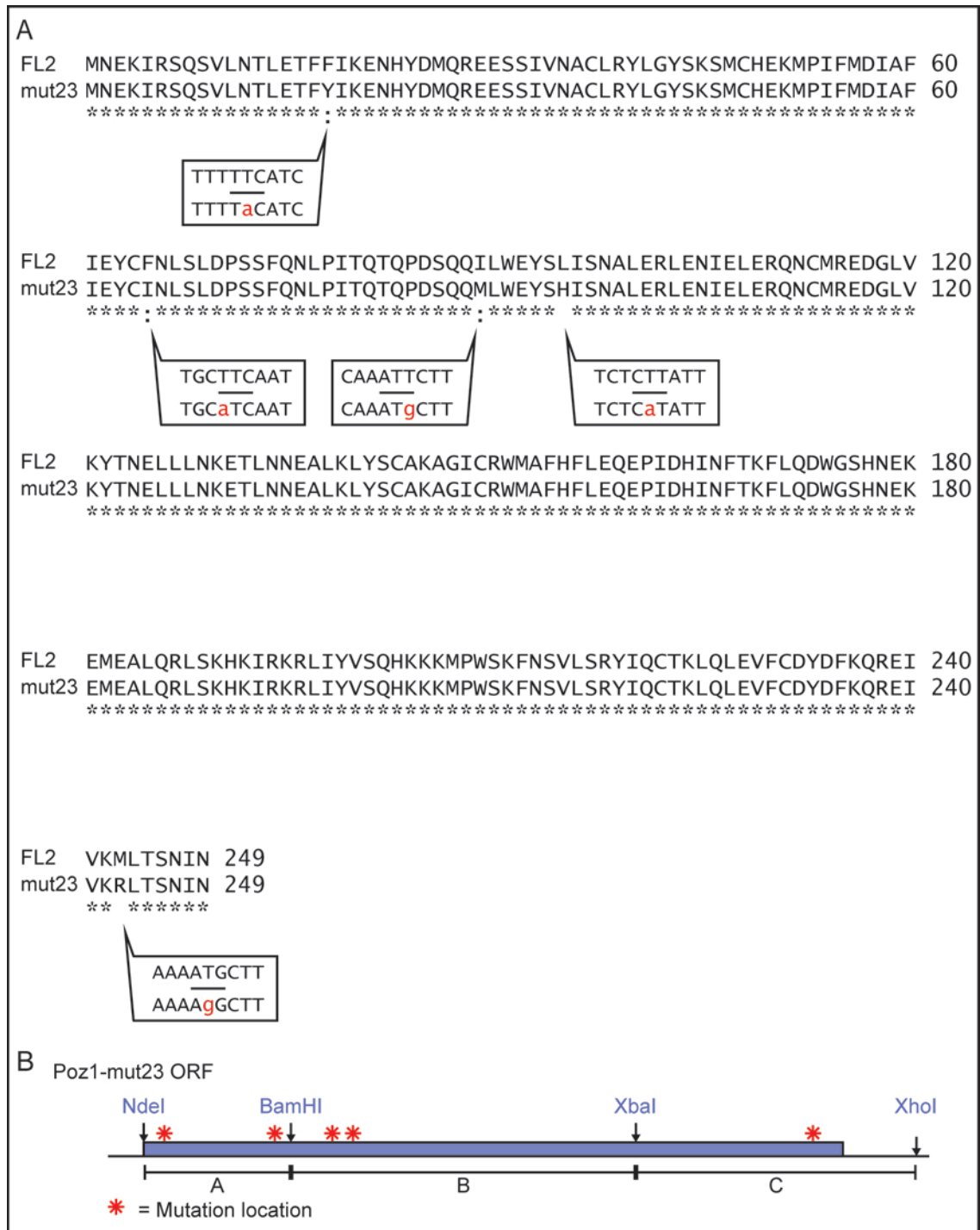
Figure 3.14: Sequence analysis of Tpz1-interaction disruption allele Poz1-mut23 ORF and peptide sequence.

(A) Peptide sequence of Poz1-FL2 (wild-type) compared to mutant 23 compared using Clustal Omega. Mutant 23 (mut23) contains five amino acid substitutions: F18Y, F65I, I89M, L95M and M243R. Sequence changes at the nucleotide level are highlighted in boxes. The uppercase nucleotide sequence is wild-type and lowercase red sequence indicates the mutation. The horizontal line separating the wild-type sequence (top) and mutant 23 sequence (bottom) indicates the codon affected. An * (asterisk) indicates positions which have a single, fully conserved residue. A : (colon) indicates conservation between strongly similar residues. A . (full stop) indicates positions which have a single, weakly conserved residue. An empty space indicates dissimilar residues. **(B)** Schematic of the Poz1-mut23 ORF (blue) with location of mutations indicated by red stars. Mutations can be separated into three clusters (A, B and C) using the restriction sites, as indicated.

3.2.11 Analysis of the conservation of Poz1 residues in the *Schizosaccharomyces* genus

The subcloning to make Poz1-mut26 and Poz1-mut29 would be a two-step process, dependent on first making the others. The central fragment, B [Fig 3.14B], would be problematic to subclone directly, due to the small size. Fragments A and C could be more easily subcloned due to the ability to use restriction sites on the pGADT7 plasmid upstream and downstream of the Poz1 ORF as necessary.

There are five amino acid substitutions in Poz1-mut23, of which L95H and M243R are the most disruptive. L95R results in a change from a small hydrophobic residue side chain in leucine to a positively charged hydrophilic residue in histidine. Similarly, M243R results in in a change from a small hydrophobic residue side chain in methionine to a larger, positively charged hydrophilic residue in arginine. The other three substitutions (F18Y, F65I and I89M) result in changes to residues that are similar to wild-type. Any one or more of these substitutions may be responsible for disruption of Tpz1 interaction, but L95H and M243R may disrupt the protein structure to a greater degree than the others and so could be considered most likely responsible. However, based on the hypothesis that functionally important residues should be evolutionarily conserved a substitution of a highly conserved residue to a similar one may be sufficient to disrupt function.

In order to determine which residues, of those substituted in mutant 23, are likely to be functionally important for Tpz1 interaction, a comparison of the *S. pombe* Poz1 peptide sequence to other yeast in the *Schizosaccharomyces* genus was carried out using Clustal Omega [Fig 3.15]. In addition, due to the unavailability of a crystal structure for *S. pombe* Poz1, a secondary structure prediction was conducted using PSIPRED, based on the Poz1 peptide sequence. This allowed the comparison of the locations of the amino acid substitutions in Poz1-mut20 and Poz1-mut23 to the predicted secondary structure to help determine any likely

effects on Poz1 structural features. Finally, the SIFT webserver was used to predict whether or not the amino acid substitutions in Poz1-mut20 and Poz1-mut23 were likely to be disruptive. Each substitution was given a score by SIFT between 0 and 1, with those ≤0.05 being determined as damaging and those >0.05 determined as tolerable [Table 3.5].

Figure 3.15: **Comparison of Poz1 residue conservation in *Schizosaccharomyces* genus (following page).**

(A) Alignment of Poz1 peptide sequence from *S. pombe* (*S. pom*), *S. octosporus* (*S. oct*), *S. cryophilus* (*S. cry*) and *S. japonicas* (*S. jap*) generated using Clustal Omega and visualised using Boxshade. Ensembl protein ID numbers are as follows: SPAC19G12.13c.1 (*S. pombe*), EPX73809 (*S. octosporus*), EPY51459 (*S. cryophilus*) and EEB06808 (*S. japonicas*). Residues that are fully conserved in at least two of the four species are highlighted in black while similar residues are highlighted in grey. Secondary structure prediction was generated from the peptide sequence of *S. pombe* Poz1 using PSIPRED and displayed above the corresponding peptides. A total of twelve alpha helices (α1-α12) are predicted, as indicated. The location of the amino acid substitutions in *S. pombe* Poz1-mut20 and Poz1-mut23 are shown by blue and red markers respectively. For Poz1-mut20 these substitutions are C143R and L157P. For Poz1-mut23 these substitutions are F18Y, F65I, I89M, L95H and M243R. **(B)** Poz1 peptide sequence identity between each species in *Schizosaccharomyces* genus was calculated by Clustal Omega. Sequence identity for each species indicated on the left is given in percentage. Running left to right the comparison species are in the order: *S. pombe*, *S. octosporus*, *S. cryophilus*, *S. japonicas*, i.e. *S. pombe* Poz1 has 37.77% identity to *S. octosporus* Poz1.

A   Poz1 peptide sequence alignment

α1   α2

S. pom   1 MNEKIR-SQSVLNTLETFFIKENHYDMQREESSIVNACLRYLGYSKSMCH
S. oct   1 MIHHSQ-IAATFKSLEAFFLSENHFQETSENAAIVQACLENLGTCESLEY
S. cry   1 MQHHSQ-VSATLKSLEAFFVSENHFQETKENAPIVQACLENLGTCESLNR
S. jap   1 MHKIEQKAAITMAILEYLLLRSKQEKSAQAHAQGLEAFVEYLGHLPGLET
                              ▲

α3   α5

S. pom   50 EKMPIFMDIAFIEYCFNLSLDPSSFQNLPITQTQPDSQQILWEYSLISNA
S. oct   50 VPVPLFMNMAFLDHCFALKVRTLPD--MNEDLNLTLSQAILWDTDLISRS
S. cry   50 VPIPLFMNIAFIDHCFALGVSTIPS--MNDDSNLTLSQLILWDTHLISRS
S. jap   51 KKPPIFVSLAFLSYCFNIEGEFHGRGESKEDA--SKPIACFWDTDVMSNA
                         ▲   ▲   ▲

α6   α7

S. pom 100 LERLENIELERQNCMREDGLVKY-TNELLLNKETLNNEALKLYSCAKAGI
S. oct   98 LHILACIEEERLECFRSLTSSLNKNDERYARECNLNDEATKLYVVAKTGI
S. cry   98 LQRLSYIENERTECFHLSTSSSNKDDERLAQEINLDAEAKKLYAVAKTGI
S. jap   99 LFQLKNTEHSRKKRILKILR-HDLDEDTTVRLRSLDKEAMRLFAWAKSGI
                                                        ▲

α8   α9   α10

S. pom 149 CRWMAFHFLEQEPIDHINFTKFLQDWGSHNEKEMEALQRLSKHKIRKRLI
S. oct 148 IRWMSFHLLEQRQVDFSALSKFLDEWYMDNPSEKKVLEKIASLYEDKRFQ
S. cry 148 LRWMIFHLLEQRHVDLKSFSDFLDTWYADSSNEKKVLEKITTLDEKKRTQ
S. jap 148 CRWVLFSLTDKERVDEEAVLAFLTMWMIDVPNEIQTFKRLLSYDWDHRRS
                    ▲

α11   α12

S. pom 199 YVSQHKKKMPWSKFNSVLSRYIQCTKLQLEVFCDYDFKQREIVKMLTSNI
S. oct 198 KVQSFQSQMPWVKIHSILGRYLLCTKLELELFHGYNL--------------
S. cry 198 KILHFQSEMPWVRIHSILGRYLLCTKLELEIFHGYNFQQSKILNFF----
S. jap 198 KIKTYKKKIPWSKVYSVIQRYIACTEAQCKLVNQFQFNADTFLQAVVEAI
                                                        ▲

S. pom 249 N---------------
S. oct   ---------------   ▲ = Substitution locations in Poz1-mut20
S. cry   ---------------
S. jap 248 EQNQRVLSIFSGNGI   ▲ = Substitution locations in Poz1-mut23

B   Poz1 peptide sequence identity (%)

	S. pom	S. oct	S. cry	S. jap
S. pom	100.00	37.77	37.60	26.02
S. oct	37.77	100.00	73.08	29.44
S. cry	37.60	73.08	100.00	25.83
S. jap	26.02	29.44	25.83	100.00

Interaction disruption	Substitution	Conserved residue	SIFT score	Disruptive
Rap1-Poz1	C143R	No	0.28	No
	L157P	Yes	0.07	No
Tpz1-Poz1	F18Y	Yes	0.17	No
	F65I	Yes	0.00	Yes
	I89M	Yes	0.09	No
	L95H	Yes	0.01	Yes
	M243R	No	0.23	No

Table 3.5: Predicted characteristics of amino acid substitutions in Poz1-mut20 and Poz1-mut23 using SIFT.

Residue conservation was determined through alignment of Poz1 peptide sequences from *S. pombe*, *S. octosporus*, *S. cryophilus* and *S. japonicas* using Clustal Omega. The F65I and L95H substitutions are predicted to be the most destructive. The remaining substitutions are not predicted to be disruptive individually. SIFT score is a prediction of whether the substitution is likely to be damaging (≤ 0.05) or tolerable (> 0.05) on a scale of 0.00 to 1.00, taking into account the sequence alignment.

The sequence alignment [Fig 3.15] indicates that there is substantial similarity between the Poz1 peptide sequences in *S. octosporus* and *S. cryophilus* (73.08% sequence identity) [Fig 3.15B]. The sequence identity between *S. pombe* Poz1 and that of *S. octosporus* and *S. cryophilus* is 37.77% and 37.60% respectively, though there are many similar residues, indicating that the sequence is slightly less conserved. The *S. japonicus* Poz1 is the least conserved with the most sequence identity (29.44%) with *S. octosporus* Poz1. The secondary structure prediction indicates the possible presence of twelve alpha helices (α1 to α12). These are distributed throughout the protein, with no predicted beta sheets, implying that the regions in between helices may be disordered or looping structures. The potential characteristics of the substitutions in Poz1-mut20 and Poz1-mut23, as determined by SIFT are summarised in Table 3.5.

The amino acid substitutions in Poz1-mut20 (C143R and L157P) are located within the central portion of the protein. Cysteine 143 is located within the predicted α7 helix. This cysteine is

not, however, well conserved. Valine is present at this position in both *S. octosporus* and *S. cryophilus*. Although the cysteine side chain contains a thiol group, unlike the alphatic side chain of valine, it is similar in size and is hydrophobic which may mean that the structure of the α7 helix is similar to that of Poz1 in *S. octosporus* and *S. cryophilus*. The arginine substitution at this location from Poz1-mut20 may affect the structure of α7 given that it is a large, hydrophilic amino acid, however, with a SIFT score of 0.28 it is predicted to be a tolerable substitution. Leucine 157 is located immediately following the predicted α8 helix. It is more conserved than cysteine 143, being present in *S. pombe*, *S. octosporus* and *S. cryophilus*. The L157P substitution may also be a disruptive change, with proline being a cyclic amino acid, which could disrupt the local secondary structure. A SIFT score of 0.07 places it just outside the threshold for a damaging substitution. Given that C143R and L157P are both potentially disruptive substitutions but neither is determined to be damaging by SIFT, both could be required for Rap1-interaction disruption.

The amino acid substitutions in Poz1-mut23 (F18Y, F65I, I89M, L95H and M243R) are distributed throughout the Poz1 sequence. Phenylalanine 18 and 65, as well as isoleucine 89 and Leucine 95, are well conserved, with phenylalanine 65 being present in all four species. Methionine 243, on the other hand, is not conserved. Indeed, it is located at the very C-terminus of Poz1 which is not well conserved as a whole. Given that the remaining four substitutions are all well conserved, any one or more could be responsible for Tpz1-interaction disruption. For example, L95H is a disruptive substitution, located within the predicted α5 helix, with a change from a small, hydrophobic amino acid to a larger, hydrophilic one. SIFT gives this substitution a score of 0.01, determining it as damaging. However, Phenylalanine 65 is a fully conserved hydrophobic and aromatic residue. Therefore, a change to a still hydrophobic, but aliphatic isoleucine may be sufficient to disrupt Tpz1-interaction. The SIFT data agrees with this, with a score of 0.00 it is determined to be damaging. It is, therefore, difficult to determine whether a single substitution is sufficient to display the Tpz1-interaction

disruption phenotype from a sequence comparison. The mutations in the Poz1 ORF would still need to be separated and experimentally tested.

Given that any one or more substitutions in Poz1-mut20 and Poz1-mut23 could be responsible for the respective phenotypes, it was decided that continuing to the next step of yeast integration would be the best course of action. Subcloning to separate mutations in Poz1-mut23 continued while the existing Poz1-mut20 and Poz1-mut23 ORFs were integrated into fission yeast.

3.2.12 Construction of *S. pombe* base strains for integration of mutagenised *poz1*

In order to integrate the Poz1 interaction disruption alleles into fission yeast, a base strain compatible with integration was constructed. This base strain also acts as a *poz1Δ* strain due to the *poz1* ORF being replaced with a *ura4⁺* marker. To construct this strain, a vector (pEXK-mutSpPoz1-1) containing parts of the *poz1* promoter and terminator regions were synthesised by Eurofins MWG Operon to enable integration of any desired sequence at the *poz1* locus in fission yeast. Having the fragment synthesised enabled the immediate incorporation of specific restriction sites for downstream cloning steps, which otherwise would have been substantially more complicated and inefficient. This synthesised fragment [Fig 3.16A] contains loxP and loxM3 recombination sites in the Promoter (P*poz1*) and Terminator (T*poz1*) regions respectively. The loxP site was placed 600bp upstream of the NdeI site (containing the ATG START codon) with the expectation of minimising any disruption to expression. These palindromic sites are able to recombine with equivalent sites on a vector or in the genome, but not with each other due to specific mutations in the loxM3 site spacer region (Watson *et al.*, 2008).

To integrate the synthesised fragment into a fission yeast wild-type strain, the *ura4⁺* marker, containing the wild type promoter and terminator regions were subcloned into pEXK-

mutSpPoz1-1. This was achieved by NdeI digest of the *ura4+* marker from pFY416, blunting the restriction fragment ends with T4 DNA polymerase and subcloning into the EcoRV (Blunt) site within pEXK-mutSpPoz1-1 to produce pEXK-mutSpPoz1-2 [Fig 3.16A]. From this new vector, the KpnI-SacI fragment was transformed into the wild type fission yeast strain, BAF3, by the lithium acetate transformation method. Here, it integrated by homologous recombination at the *poz1* locus, replacing the endogenous *poz1* ORF and promoter with the *ura4*[+] marker and modified promoter [Fig 3.16B]. This integration was confirmed by PCR and the new strain designated BAF344 (SpPoz1::loxP-Ura4-loxM3).
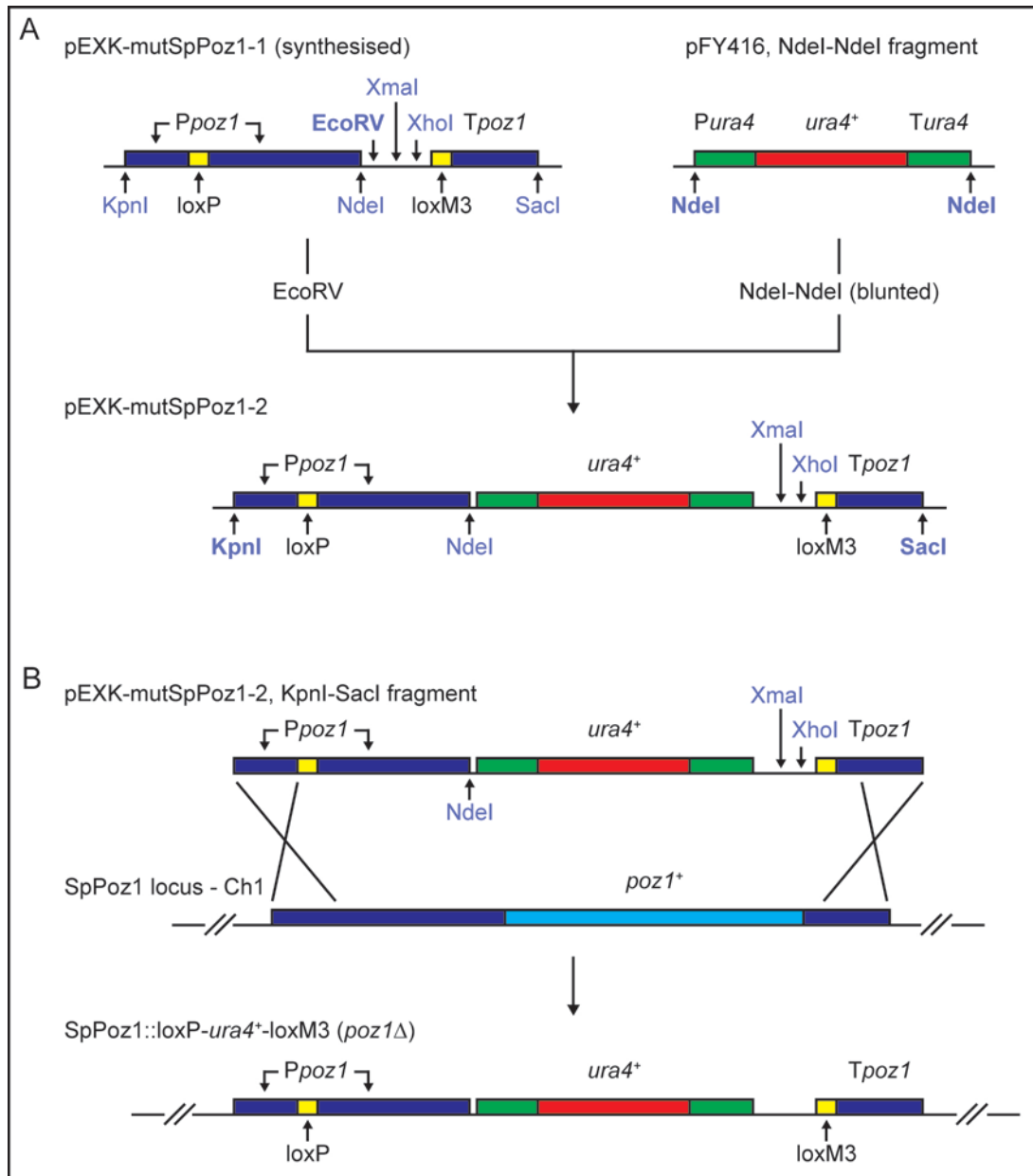
Figure 3.16: Schematic showing process of SpPoz1::loxP-*ura4⁺*-loxM3 (*poz1Δ*) base strain construction.

(A) Construction of pEXK-mutSpPoz1-2 from synthesised pEXK-mutSpPoz1-1 and Ura4 ORF from pFY416. The pEXK-mutSpPoz1-1 plasmid contains a synthesised fragment consisting of parts of the Poz1 promoter (P*poz1*) and terminator (T*poz1*) shown in dark blue. In addition, loxP and loxM3 sites (yellow) are present within the Poz1 promoter (600bp upstream of NdeI site) and upstream of the terminator, respectively. Restriction sites were also included in the synthesised fragment, as indicated. The *ura4⁺* gene (red), including the wild-type promoter and terminator (green) is present as an NdeI-NdeI restriction fragment in pFY416. This fragment is cut out, blunted and ligated to pEXK-mutSpPoz1-1 (EcoRV digest) to make pEXK-mutSpPoz1-2 as shown. **(B)** The KpnI-SacI fragment from pEXK-mutSpPoz1-2 is integrated at the endogenous Poz1 locus of a wild-type strain by homologous recombination. This integration results in a *poz1Δ* strain containing the loxP-*ura4⁺*-loxM3 cassette that allows integration of *poz1* alleles by cre-recombinase dependent RMCE.

3.2.13 Transfer of *poz1* mutant alleles to integration vectors and integration into S. pombe base strain

In order to integrate the *poz1* mutant alleles into the base strain, a vector containing the lox sites and appropriate region of the *poz1* promoter was required to allow recombinase-mediated cassette exchange (RMCE). The HpaI-EcoRI fragment from pEXK-mutSPPoz1-2 was, therefore, subcloned into pAW8E-noATG to make ploxPM3SpPoz1-3 [Fig 3.17A]. This vector, provided by Adam Watson from the Carr lab, contains the Cre recombinase gene and an appropriate marker (*LEU2*) for integration of the 'loxable' fragment and selection of the vector in fission yeast. The fragment that was subcloned included *ura4*[+] due to the large size of the *ura4*[+] fragment, relative to the size of the *poz1* ORF. This aided the identification of correct clones by restriction fragment size when the *poz1* mutant alleles were subsequently subcloned.

Using the NdeI-XhoI sites, the *poz1* ORFs from pGADT7SpPoz1-FL2, pGADT7SpPoz1-mut20 and pGADT7SpPoz1-mut23 were all subcloned to make ploxPM3SpPoz1-FL2, ploxPM3SpPoz1-mut20 and ploxPM3SpPoz1-mut23 vectors and transformed into the base strain, BAF344 [Fig 3.17B]. The *cre* gene on the plasmid is controlled by an *nmt41* promoter and therefore the strain was plated for selection and integration on YNG –Leu –Thyamine agar. Colonies from this transformation were streaked on fresh minimal media as well as rich media (YES). Colonies on YES were then checked for loss of the *ura4*[+] marker from the modified *poz1* locus by streaking on YNG –Ura. Any ura[-] candidates were then checked for correct integration by PCR.

As a result, strains containing the Poz1-FL2 wild-type variation, Poz1-mut20 and Poz1-mut23 ORFs were generated and analysed.

Figure 3.17: Schematic of ploxPM3SpPoz1-3 construction and Poz1 mutant ORF integration in SpPoz1::loxP-*ura4⁺*-loxM3 (*poz1Δ*) base strain (following page).

(A) The ploxPM3SpPoz1-3 vector is cloned by transferring the HpaI-EcoRI fragment from pEXK-mutSpPoz1-2 into the same sites in pAW8E-noATG. This fragment consists of loxP and loxM3 sites (yellow), the *poz1* promoter and terminator (dark blue) and the *ura4⁺* marker (red) flanked by the wild-type *ura4* promoter and terminator sequences (green). The pAW8E-noATG vector consists of the *cre* gene (grey) under *nmt* promoter and terminator control (white). These are indicated in the final ploxPM3SpPoz1-3 vector, in addition to a *LEU2* marker (purple) and ARS1 origin (light blue). This vector allows subcloning of the *poz1* ORF from pGADT7 vectors by using the NdeI-XhoI restriction sites. **(B)** Integration of the *poz1* ORF cassette in ploxPM3SpPoz1-mut^X into the *poz1Δ* base strain to generate a strain containing SpPoz1::loxP-*poz1-mut^X*-loxM3. This cassette, where the *ura4⁺* gene in ploxPM3SpPoz1-3 has been replaced by a hypothetical, mutagenised *poz1* ORF, *poz1-mut^X*, is integrated by RMCE using the loxP and loxM3 sites (yellow) as indicated. The result is a mutagenized *poz1* gene at the endogenous locus, under the control of the wild-type promoter (barring any effect of a loxP site 600bp upstream of the START codon).
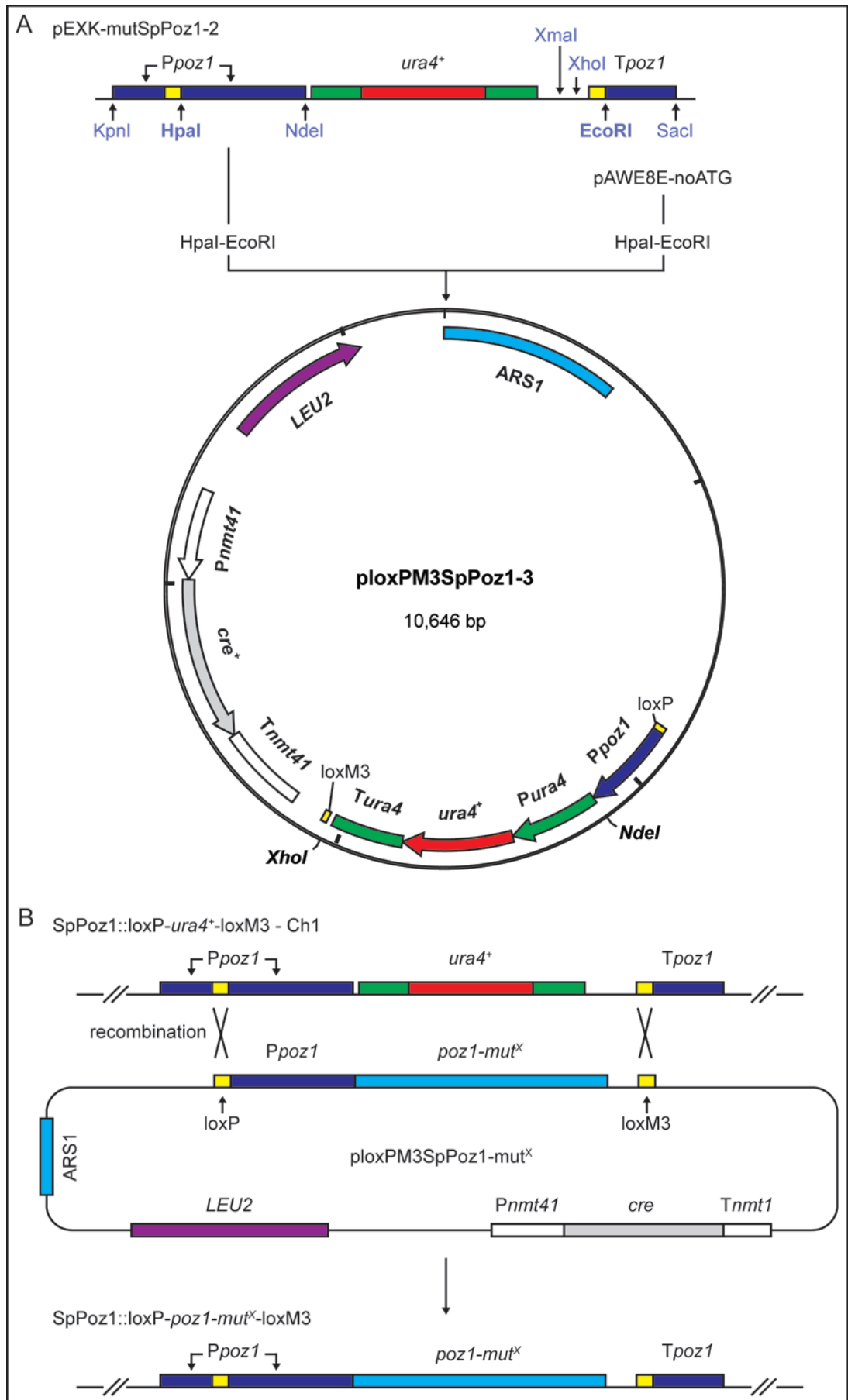
3.2.14 Analysis of telomere lengths in Poz1 strains

Initial analysis of the effect of interaction disruptions of the *poz1* mutant alleles involved analysis of the telomere length. This was to determine whether the key functionality of Poz1, in transducing the signal for repression of telomerase was affected.

The new strains containing Poz1-FL2, Poz1-mut20, Poz1-mut23 constructs and BAF344 (*poz1Δ*, loxP-*ura4⁺*-loxM3) were streaked on rich media (YES) to single colonies 8 times in order to equilibrate telomere length. Based on previous work (Miyoshi *et al.*, 2008), it was expected that the telomere length for BAF344 (*poz1Δ*, loxP-*ura4⁺*-loxM3) would be much higher than wild type. Also, the telomere length of the wild-type variation, Poz1-FL2 in the context of the modified promoter may have a telomere length phenotype, relative to a full wild type strain.

The telomere lengths of these Poz1 strains, as well as the BAF3 wild type parent strain, were assessed by southern blot analysis of EcoRI-digested genomic DNA using a telomere sequence-specific probe, a 300bp ApaI-SacI fragment from pSpTelo [Fig 3.18B]. The apparent size of a wild-type telomere from an EcoRI genomic digest is approximately 1.1kb. This includes the TAS1 region, adding approximately 0.8kb to the actual length of the telomere [Fig 3.18A]. ApaI digests could be used to more accurately reflect telomere length, but digestion efficiency, and therefore success rate, is typically much reduced when using ApaI as opposed to EcoRI.

The southern blot indicates that, at approximately 1.4kb, the telomeres of the Poz1-FL2 modified wild type strain are 300 to 400bp longer than wild type. BAF344, the *poz1Δ* strain (*poz1*::loxP-Ura4-loxM3) has much longer telomeres, approximately 4kb, as one might expect from loss of telomerase inhibition. Interestingly, both Rap1 and Tpz1 interaction disruption mutant allele strains, have telomeres of similar length to the *poz1Δ*. This would suggest that removing the ability to interact with either Rap1 or Tpz1 may either result in reduced Poz1 recruitment to telomeres or affect the telomerase inhibition functionality of Poz1 at telomeres perhaps due to permanently leaving the telomeric complex in the "open" state.
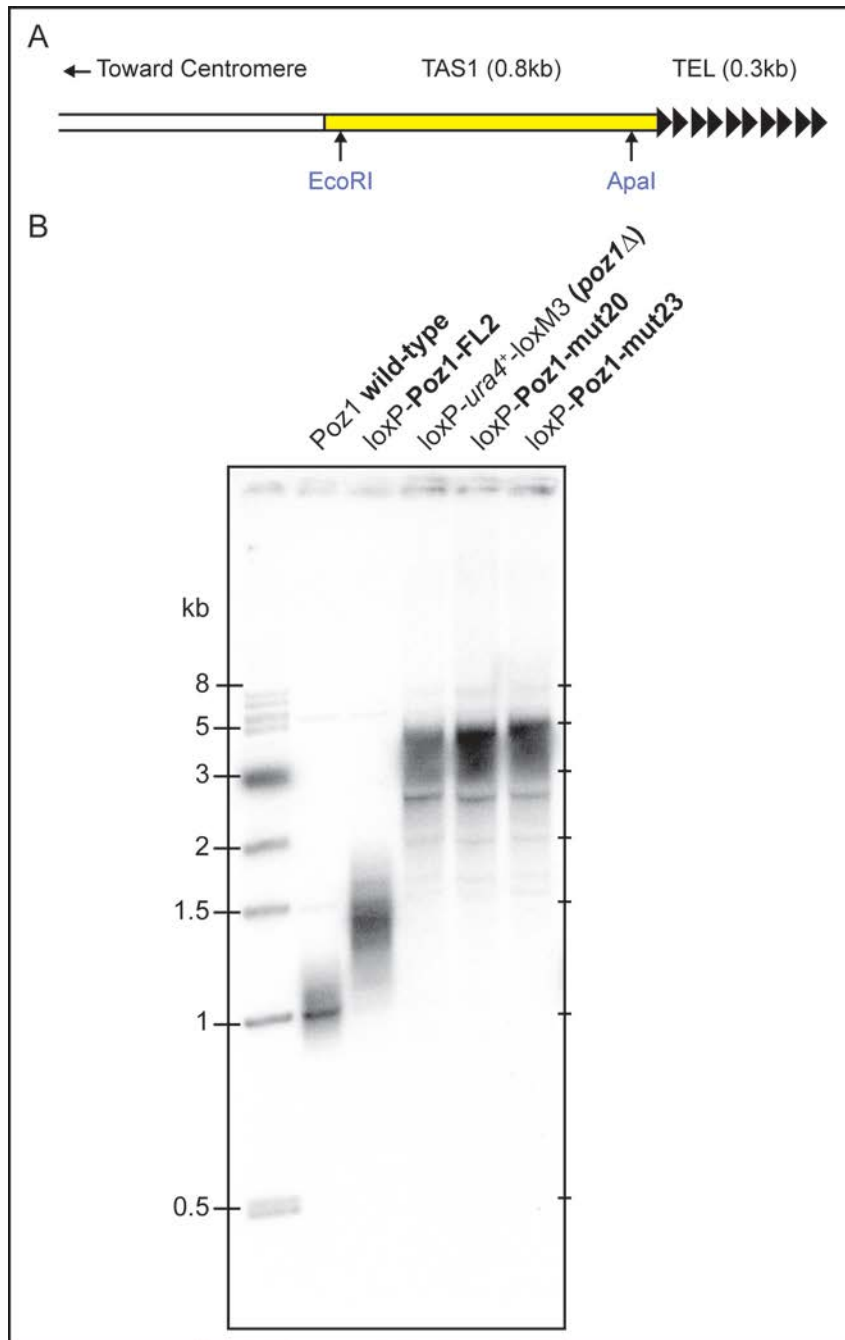
Figure 3.18: Telomere length analysis of modified and interaction-disruption *S. pombe* Poz1 strains.

(A) Schematic of *S. pombe* telomere showing locations of EcoRI and ApaI sites relative to telomere (TEL) and TAS1 region (yellow). Telomere sequence-specific probe from pSpTelo binds to TEL region (approximately 0.3kb in wild-type strains). **(B)** Southern blot analysis of telomere lengths of wild-type, Poz1-FL2 (wild type with modified promoter containing loxP site), *poz1Δ* (loxP-*ura4*[+]-loxM3), Poz1-mut20 and Poz1-mut23 integration strains. Genomic DNA was prepared after strains were streaked to single colonies 8 times to equilibrate telomere lengths. These were digested with EcoRI, run on a 0.8% agarose gel and probed with the telomere sequence-specific probe from pSpTelo. An increase in telomere length of 300-400bp with modified promoter can be seen in the Poz1-FL2 strain. Very extended telomeres (≥ 3kb) can be seen in *poz1Δ*, mut20 and mut23 strains.

3.2.15 Myc epitope tagging and analysis of expression of *poz1* alleles

In order to establish whether recruitment is affected by loss of Rap1 or Tpz1 interaction, the

poz1 alleles were Myc epitope tagged at the C-terminus, as described in the methods, using

the pSpPoz1-G10M106 vector. This contains the C-terminal region of the *poz1* ORF with the

codons for 8 Glycine residues and 10 Myc epitope sequences. When linearised, this allows

integration at the C-terminal end of Poz1, in frame with the ORF, facilitating antibody

recognition of the expressed protein [Fig 3.19A].

Expression, relative to the Myc-tagged wild-type Poz1 was assessed by anti-myc western

blotting on protein samples derived from equal numbers of log phase cells in liquid culture for

each strain. Several positive transformants for each allele (determined by PCR) were compared

to a Myc-tagged wild type, derived from the BAF3 otherwise-unmodified parent [Fig 3.19B].

A doublet is seen in each lane of the blot, except for the negative controls, however, the upper

band appears to be indicative of Poz1-10Myc by size (43kDa) and intensity in the wild-type

strain (first lane in each blot). The lower band may be an artefact of the 10Myc epitope tag,

given that the untagged control and *poz1Δ* lanes do not show these bands. It may also be due

to specific protease activity on the protein as a result of the addition of a tag. The transfer of

the second (lower) blot, from the SDS-PAGE gel, appears to have been less efficient when

comparing the Poz1-10Myc lanes. The Ponceau staining is also indicative of this. Nevertheless,

some conclusions can still be made.

The expression of Poz1 in all strains containing the modified promoter (loxP and NdeI site

upstream of *poz1* ORF) appears noticeably reduced when compared to the wild type (lane 1 on

both upper and lower blots). In the upper membrane, expression of the 43kDa wild type Poz1-

10Myc is several fold higher than that of the wild type with modified promoter (loxP-*poz1*-

10Myc, n1/2/3) in lanes 3 to 5 of the upper blot. Expression in all remaining strains, containing

either the Poz1-mut20 or Poz1-mut23 allele, in both blots appears to be similar to that of the

wild type with modified promoter. These results indicate that the slightly increased telomere

length of the loxP-*poz1*-FL2 strain may well be due to reduced expression.
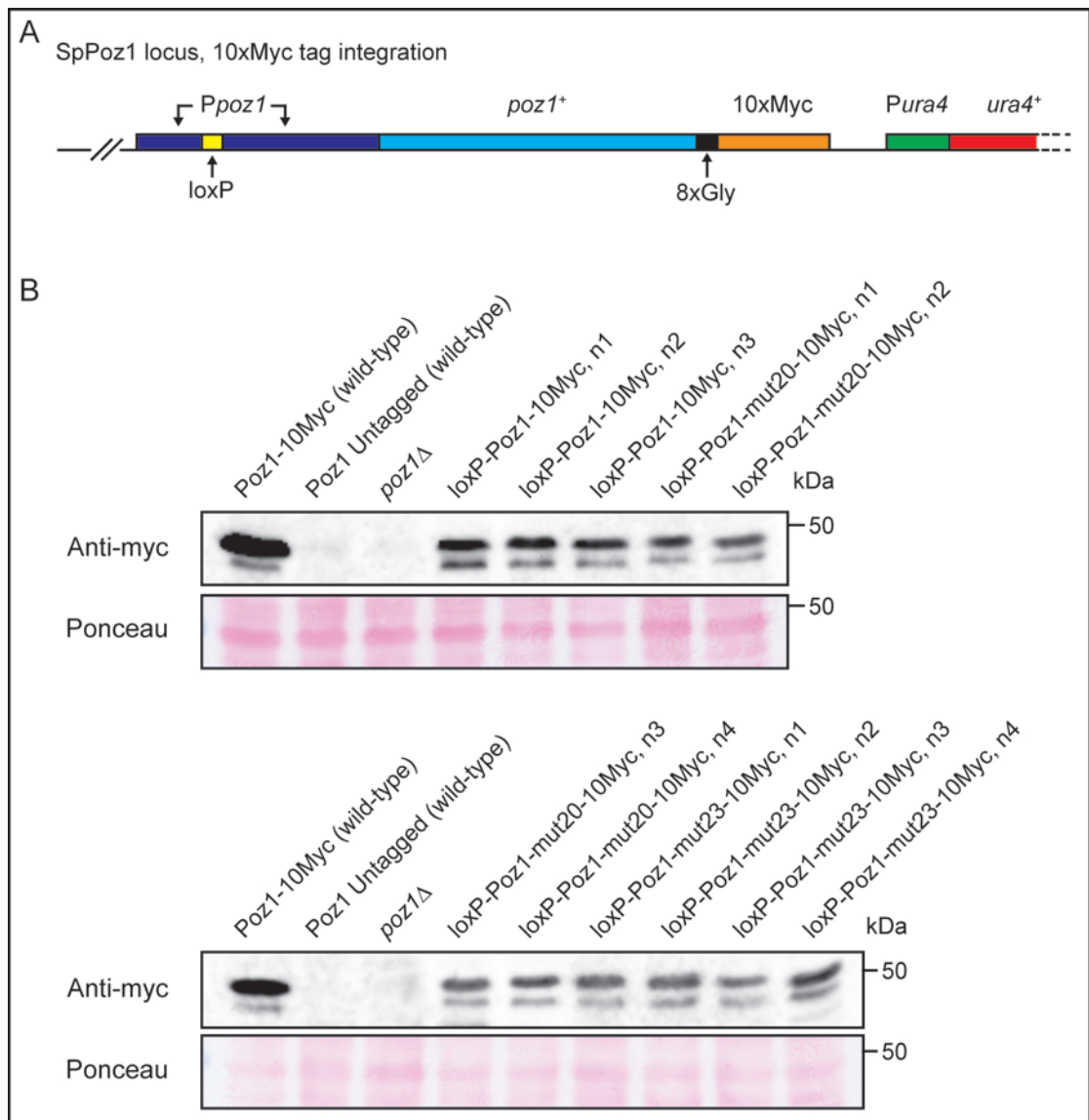
Figure 3.19: Myc-tagged Poz1 expression in modified and mutant allele strains relative to wild-type.

(A) Schematic of Poz1 10xMyc epitope tag integrated at the modified *poz1* locus. Poz1 promoter (dark blue) contains loxP site (yellow). Poz1 ORF (light blue) includes codons for 8xGlycine (black) and 10xMyc repeats (orange) in frame. Downstream of ORF is remainder of integration vector with beginning of selectable *ura4*[+] marker (red) shown with wild-type promoter, P*ura4* (green). The remaining sequence of the plasmid is integrated downstream (indicated by dashed lines). **(B)** Expression of 10xMyc-tagged Poz1 strains comparing mutant alleles and modified strains to epitope tagged wild type by anti-myc western blots on whole cell extracts. Three separate PCR-positive loxP-Poz1-10Myc strains (n1-3), four separate PCR-positive loxP-Poz1-mut20-10Myc strains (n1-4) and four separate PCR-positive loxP-Poz1-mut23-10Myc strains (n1-4) compared to tagged and untagged wild-type strains, as indicated. A doublet is seen for all tagged strains with a larger (43kDa) and more intense upper band likely representative of full length tagged protein. Smaller, less intense band may be indicative of specific protease activity on Poz1-10Myc. Ponceau staining of membranes indicates less efficient transfer on lower blot compared to the upper blot.

3.2.16 Telomere length analysis of 10xMyc-tagged strains

As the addition of epitope tags has the possibility of affecting protein folding or steric hindrance of protein function, the telomere length analysis by southern blot was repeated using the same conditions used previously [Fig 3.20]. This would provide evidence of any further effect on Poz1 function, in addition to the reduced expression that appears to be caused by the modified promoter. Both the tagged and parent untagged strains were streaked to single colonies a further 8 times to equilibrate telomere length and compared by southern blot using EcoRI digest of genomic DNA and telomere-specific probe.

The blot indicates that, after an additional 8 streaks to single colonies, the untagged Poz1-FL2 strain (lane 2) has telomeres very close in length to untagged wild type (lane 1). This suggests that the initial 8 streaks were insufficient for telomeres to fully equilibrate after the parent *poz1Δ* strain was transformed with the Poz1-FL2 ORF. The telomere lengths of the two untagged interaction mutant allele strains, however, do not appear to have been affected. Both Poz1-mut20 and Poz1-mut23 still have telomeres up to approximately 4kb, when corrected for the additional TAS1 sequence. At these lengths, however, it would be difficult to see small changes.

When comparing the telomere lengths of equivalent tagged and untagged strains, for example, the Poz1 wild type tagged (lane 6) against untagged (lane 1), a slight telomere phenotype is evident. This 200-300bp increase in length indicates that the 10xMyc epitope tag does have some effect on Poz1 functionality. This effect appears to be exacerbated in the Poz1-FL2 strain with the modified promoter. The length has increased to approximately 1kb, when corrected for the 0.8kb TAS1 sequence. Therefore, it would appear that the epitope tag, when combined with the reduced expression from the modified promoter, results in a greater reduction in Poz1 functionality than when compared to the epitope tag alone. There is no difference in telomere length observable when comparing the tagged and untagged Poz1-mut20 and Poz1-

mut23 strains. This may be due to limitations in the method, where differentiating small

changes in telomere length would be difficult when they are already so large.
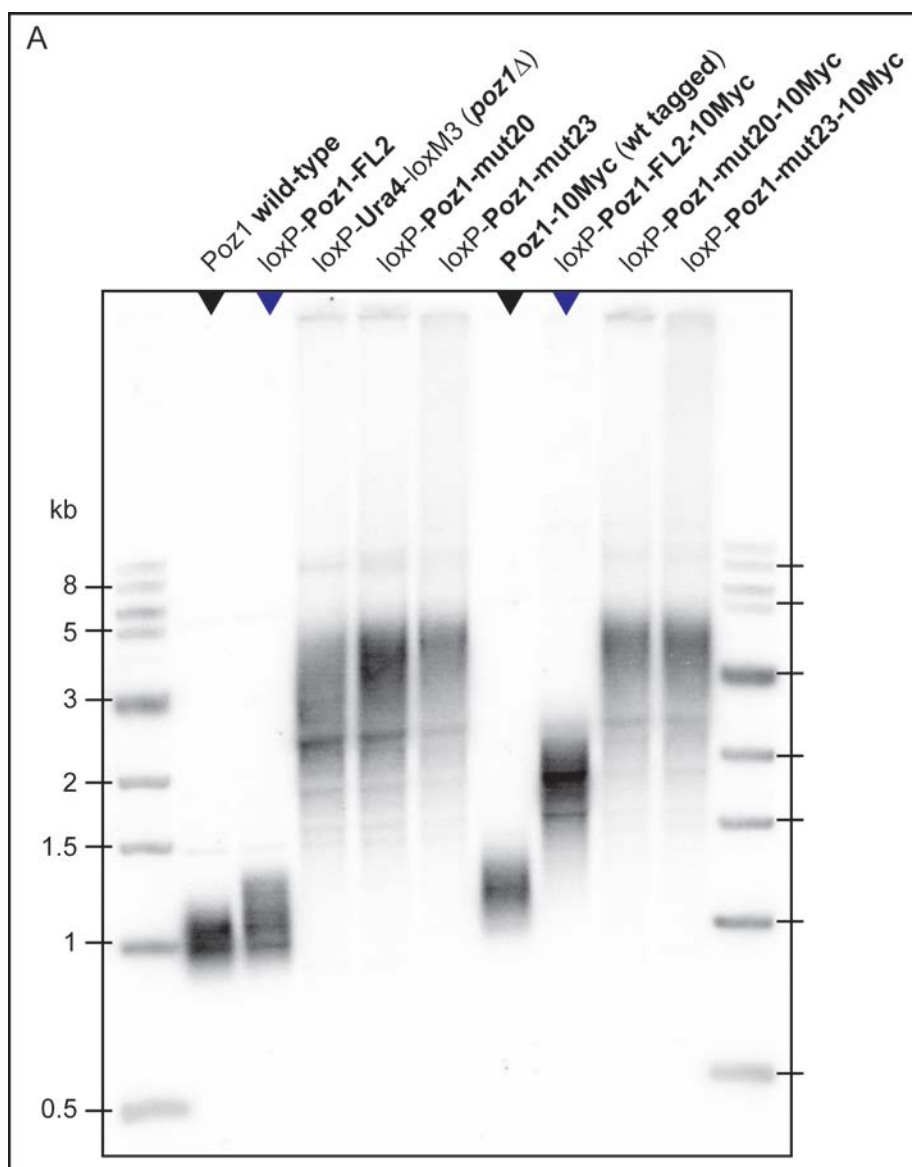
Figure 3.20: Telomere length analysis of *S. pombe* Poz1 strains with and without epitope tags.

(A) Southern blot analysis of telomere lengths of wild-type, Poz1-FL2 (wild type with modified promoter containing loxP site), *poz1Δ* (loxP-Ura4-loxM3), Poz1-mut20 and Poz1-mut23 integration strains with and without 10xMyc epitope tag. Genomic DNA was prepared after strains were streaked to single colonies 8 times to equilibrate telomere lengths. These were digested with EcoRI, run on a 0.8% agarose gel and probed with the telomere sequence-specific probe from pSpTelo. A reduction in telomere length of the untagged loxP-Poz1-FL2 modified wild type strain (lane 2) is seen, compared to previous blot. This is likely due to the additional streaks to equilibrate telomere length. A slight increase in telomere length (approximately 200bp) is seen in the tagged wild-type strain compared to the untagged (compare lanes 1 and 6, black arrows) due to addition of the 10xMyc epitope tag. A more dramatic increase in telomere length is seen in the tagged loxP-Poz1-FL2 (modified promoter) strain relative to untagged (compare lanes 2 and 7, blue arrows). This is likely due to the combination of the modified promoter affecting expression and the tag affecting folding/function. Very extended telomeres (> 3kb) are seen in *poz1Δ*, mut20 and mut23, both tagged and untagged. Any differences cannot be distinguished at these lengths.

These data indicate that a wild type promoter background would be better suited for the analysis of the Poz1 interaction disruption alleles, as opposed to the modified promoter containing loxP and NdeI sites. Nevertheless, a clear phenotype was observed in these two alleles, when compared with the Poz1-FL2. A question that could still be investigated using these strains before transfer of the alleles into a wild type promoter background is whether recruitment of Poz1 to telomeres is affected by the disruptions of interactions with Rap1 and Tpz1. It was already expected that reduced recruitment would be observed due reduced expression from the modified promoter, relative to wild type, but it would still be interesting to determine whether there was any additional effect from the interaction disruptions using these existing strains.

3.2.17 Analysis of Poz1 recruitment to telomeres by ChIP/Slot Blot

In order to assess recruitment of Poz1 to telomeres in the Myc-tagged strains, it was decided that the best approach would be to use ChIP against the Myc epitope tag, followed by a slot blot using the same telomere-specific probe used previously for telomere length analysis. The main advantage of using a slot blot, as opposed to qPCR, is that the telomere probe would bind directly to the telomeres as opposed to having an upstream amplicon for qPCR. In a slot blot, the probe would bind to the telomeric DNA regardless of length. For qPCR, the large size of some of the Poz1 strain telomeres could be problematic as the chromosomal amplicon is located upstream of the telomere in the TAS1 region. Typical sonication settings are set to generate fragments that are 0.5-1.0kb in length. Therefore, with telomeres of ≥3kb, even reducing sonication to a low setting may not be sufficient to shear the DNA such that the amplicon and the whole telomere remain part of a single DNA molecule. The qPCR could then fail to amplify from the ChIP samples as the many of the amplicons could have been lost. This is especially likely in the strain containing the Rap1 interaction disruption allele, as Poz1 is not likely to be found along the double-stranded telomeric sequence and instead, only found in the single-stranded overhang, where Tpz1 is present. In the wild-type and Tpz1 interaction disruption strains, Poz1 may still be found along the double-stranded region of the telomere, bound to Rap1.

The Myc-tagged strains, as well as the untagged wild type control, were grown in rich media to log phase. 2×10^8 cells from each culture were used for cell extracts, of which 2% was kept aside as input. ChIP was performed on the remainder of the samples using anti-myc antibody. 60% of each ChIP sample was then denatured and applied to the slot blot membrane along with 30% of the input samples (equivalent to 1% final). The membrane was then probed with the telomere-specific probe in the same manner as a standard southern blot [Fig 3.21A].

The signal achieved through using the slot blot technique is much lower than expected based on the signal achieved in telomere length blots using the same telomere-specific probe. It is likely that the ChIP/Slot Blot protocol requires optimisation for these strains to reduce background and increase signal intensity. However, the slot blot does indicate that recruitment of the tagged Poz1-mut20 and Poz1-mut23 proteins to the telomere is reduced. Input bands for these strains are equal or greater in intensity compared to those of Poz1-FL2 or wild-type. Given that bands can be seen for both Poz1-FL2 ChIP and wild-type ChIP, it would be expected that if there were recruitment to telomeres, ChIP bands in Poz1-mut20 and mut23 would be visible. Visually, however, this is difficult to determine and the high background makes a quantitative analysis of band intensity unfeasible. Due to these background issues, which have not been an issue in previous southern blots for telomere length, qPCR was used to analyse the remainder of the ChIP and input samples.

3.2.18 Analysis of Poz1 recruitment to telomeres by ChIP/qPCR

Bearing in mind the caveats of using qPCR with samples from strains with extremely long telomeres, qPCR was performed from the same ChIP samples used for the slot blot on a Roche LightCycler 480 system. The primers TAS1-f6-Sp and TAS1-b5-Sp were used to target the TAS1 amplicon, upstream of the telomere. A second, non-telomeric, amplicon in the SpFas2 locus was targeted using the oligos fas2-f1-Sp and fas2-b1-Sp. Fold enrichment over background was then calculated based on Ct values for these amplicons obtained from the LightCycler software, as shown in Table 3.6 and the chart in Fig 3.21B.

Strain	Mean Fold Enrichment (n=3)	Standard Deviation (n=3)
Poz1 Untagged (wild-type)	1.37	0.21
Poz1-10Myc (wild-type)	70.73	28.40
loxP-Poz1-FL2-10Myc	29.77	6.96
loxP-Poz1-mut20-10Myc	1.57	0.65
loxP-Poz1-mut23-10Myc	1.60	0.36

Table 3.6: **Fold enrichment data for Poz1 10Myc ChIP/qPCR analysis.**

ChIP was performed on Poz1 strains, as described in text. Quantitative PCR was performed in triplicate for each ChIP sample, with three ChIP samples per strain, i.e. a total of 9 wells were used per strain. The target amplicon was TAS1 and negative control amplicon was Fas2. Average fold enrichment for the TAS1 amplicon was calculated for each ChIP sample, relative to the Fas2 amplicon. A mean average fold enrichment and standard deviation was then calculated for each strain. See methods for calculation. Data is visualised in a chart in Fig 3.21B.

The qPCR data appears to agree with the analysis of the slot blot, as well as what would be predicted if the mutant alleles were deficient in recruitment to telomeres. The largest fold enrichment is observed in the wild-type strain, where, other than epitope tagging, the *poz1* locus has not been modified in any way. Approximately half the fold enrichment, relative to wild-type is observed for the Poz1-FL2 strain, where the promoter has been modified by addition of loxP and NdeI restriction site. This reduced enrichment for an otherwise wild type

Poz1 protein implies that the expression and, therefore, recruitment to telomeres is reduced, relative to wild type, in agreement with the slot blot [Fig 3.21A], telomere length analysis [Fig 3.18 and 3.20] and the expression analysis by western blot [Fig 3.19]. Fold enrichment for the two mutant alleles, however, appears to be no better than the untagged control. On the surface, this implies that the Poz1 proteins from these strains are not being recruited to telomeres at all. This would be in agreement with the slot blot and telomere length analysis. However, considering that, due to the excessive telomere length, assessing the recruitment of these alleles to telomeres by qPCR may be unreliable; little can be concluded for certain.

In order to generate more reliable data with regard to recruitment to telomeres, the mutant *poz1* alleles would need to be transferred to a fully wild-type locus so that no disruption to wild-type expression skews the results. Improving expression to wild-type levels may also reveal any small differences in telomerase inhibition, currently masked by phenotypes that appear identical to *poz1Δ*.

Figure 3.21: **Analysis of Poz1 recruitment to telomeres by ChIP/Slot blot and ChIP/qPCR (following page).**

(A) ChIP samples (with 1% input) from 10xMyc tagged Poz1 strains analysed by slot blot in triplicate (I, ii and iii). Anti-myc antibodywas used to ChIP $2x10^8$ log phase cells per sample. The samples were then applied to a slot blot manifold and the membrane probed with the telomere sequence specific probe from pSpTelo, as used for southern blots previously. High background prevents quantitative analysis of the blot, but visually appears to show that both wild-type tagged Poz1 and the Poz1-FL2 are recruited to the telomere. Neither Poz1-mut20 (Rap1-interaction disruption) nor Poz1-mut23 (Tpz1-interaction disruption) appears to be recruited. **(B)** Fold enrichment of same ChIP samples based on qPCR Ct values (TAS1 amplicon relative to negative control Fas2 amplicon) and standard deviation of fold enrichment (red bars), see table 3.6. Enrichment is seen for wild-type and Poz1-FL2 variant. Lack of enrichment is seen for Poz1-mut20 (Rap1-disruption) and Poz1-mut23 (Tpz1-disruption) which implies that there is no recruitment to telomeres, agreeing with visual analysis of slot blot and telomere length data.
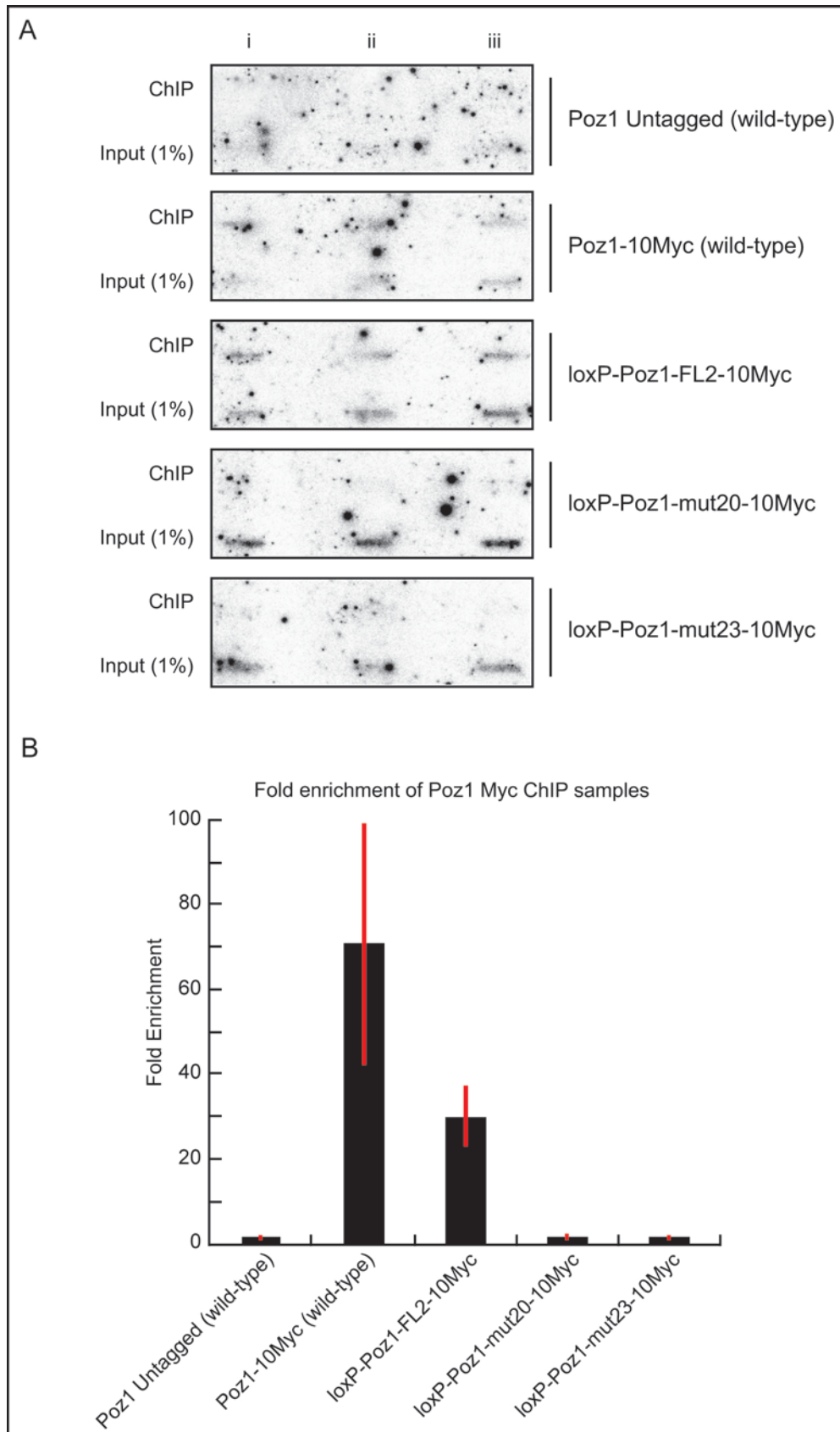
3.2.19 Transfer of *poz1* alleles to wild type (no lox) background

In order to transfer the *poz1* mutant alleles into a wild-type background, the ORFs required subcloning into integration vectors with an appropriate marker. For Poz1-mut20, this was straightforward. The NdeI-StuI fragment from pGADT7SpPoz1-mut20 was subcloned into pFY106, a vector containing a *ura4⁺* marker to make pSpPoz1-mut20-U [Fig 3.22A]. The BamHI site introduced into the ORF in pGADT7SpPoz1-FL2 remains unique in this vector and can be used to linearise the plasmid for integration at the wild-type *poz1* locus. Alternatively, an NcoI site towards the end of the ORF also becomes available in this vector. The integration process results in a duplication of the *poz1* ORF in the genome, though only one is under *poz1* promoter control. Once integrated, the marker can be removed by selecting for rare recombination events between the two copies of the *poz1* ORF using 5-FOA media [Fig 3.22B]. The result is a single; complete *poz1* ORF under control of the wild-type promoter. Some recombination events would result in loss of the mutations. Indeed, though *poz1Δ* mutants are completely viable, it is important to avoid any selection against the retention of the mutations. Starting from a wild-type diploid strain is preferable. Integration would generate a heterozygous strain which should display a wild-type phenotype and allow analysis of telomere length phenotypes by comparing haploids after sporulation.

For Poz1-mut20, this is possible due to both remaining mutations in the ORF being 169bp downstream of the BamHI site or 153bp upstream of the NcoI site. In the case of Poz1-mut23, however, the distribution of mutations along the ORF would not make it possible to integrate in this method without loss of some of the mutations during recombination. It is, therefore, essential to first identify which mutations are sufficient to maintain the Tpz1-interaction disruption phenotype. If the distribution of mutations required does not afford use of this integration method, for example if mutations both upstream and downstream of each restriction site are required, an alternative strategy would need to be devised.
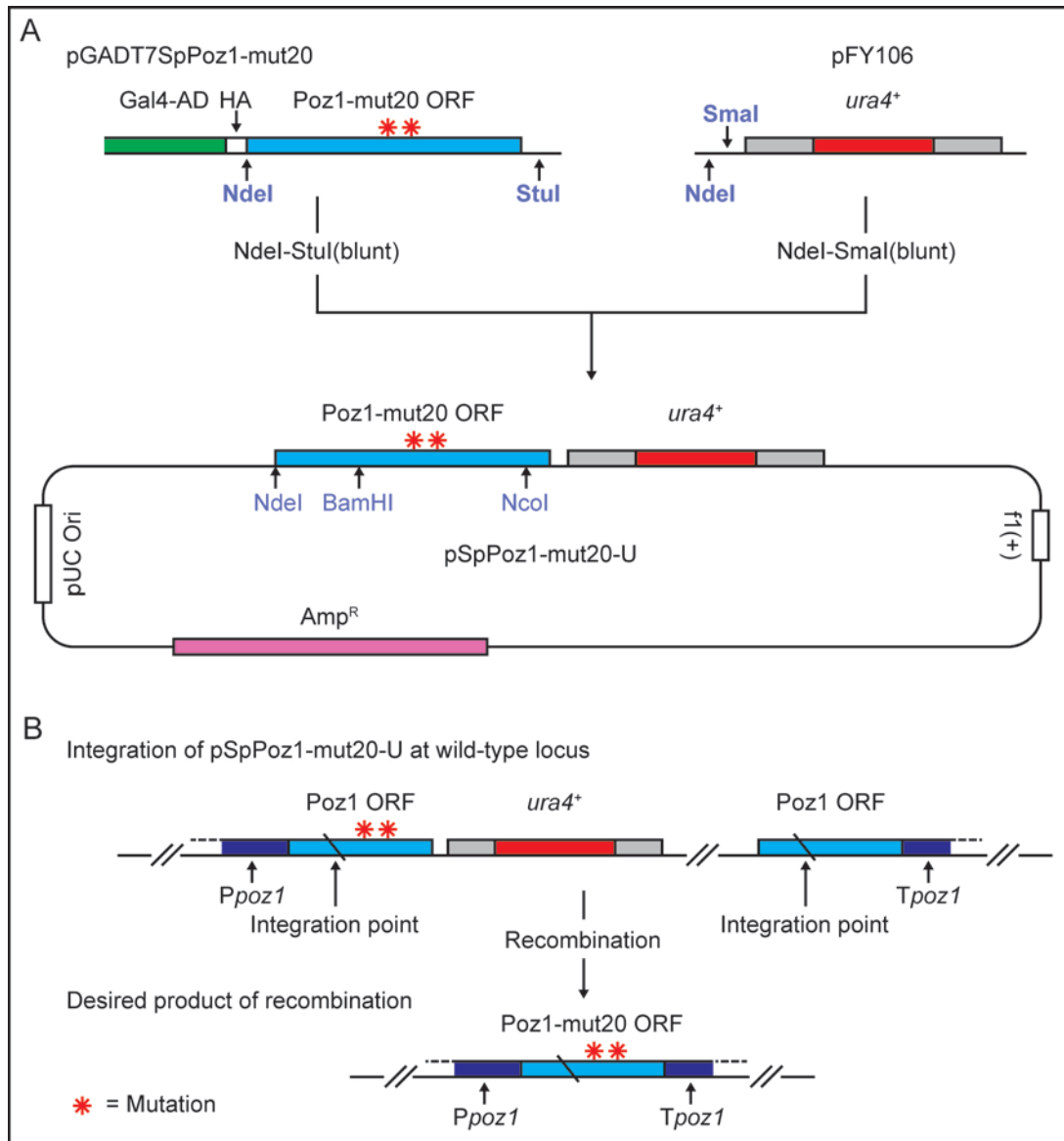
Figure 3.22: Schematic of subcloning and integration process for *poz1* mutant allele integration plasmid to leave a wild-type promoter.

(A) The pSpPoz1-mut20-U integration plasmid was cloned by taking the NdeI-StuI fragment from pGADT7SpPoz1-mut20 and subcloning into the NdeI-SmaI sites of pFY106. The NdeI-StuI fragment from pGADT7SPPoz1-mut20 contains the *poz1-mut20* ORF (light blue). The final vector contains this ORf followed by a *ura4+* marker (red) under the control of the wild-type promoter and terminator (grey), pUC origin, f1(+) origin and ampicillin resistance cassette (Amp^R), as indicated. The Poz1-mut20 ORF contains two internal restriction sites which can be used to linearise the vector for integration, BamHI and NcoI, upstream and downstream of the two mutations (red stars). **(B)** Linearisation of pSpPoz1-mut20-U at the BamHI or NcoI site allows integration into the wild type *poz1* locus. In this case, integration using the BamHI site is shown (integration points indicated). This results in two copies of the Poz1 ORF, a wild-type copy and one containing the mutations. A rare recombination event between the resultant duplicate *poz1* ORFs can create a single ORF integrated in the *poz1* locus, controlled by the wild type promoter, P*poz1*, and terminator, T*poz1*, (dark blue). These events can be isolated by counter-selection of the *ura4+* marker with 5-FOA. Some products of the recombination will retain one or both mutations and some will return to wild-type. This is dependent on the position at which recombination occurs, relative to the position of the mutations. The desired product retains both mutations from Poz1-mut20.

3.3 Summary

The aim of this study was to investigate the roles and significance of the protein-protein interactions between Poz1 and its binding partners, Rap1 and Tpz1. It was hypothesised that these interactions may be responsible for keeping the telomeric complex in the proposed closed, telomerase-inhibitive state. Disruption of these interactions could, therefore, result in modified telomerase recruitment/activation.

Poz1 alleles were, therefore, generated which lacked one interaction but maintained the other. The method used to generate and screen for these alleles was a combination of error-prone PCR mutagenesis of the Poz1 ORF and a reverse 2-hybrid screen in *S. cerevisiae*. The screen produced two alleles, each presenting one of the desired phenotypes, Poz1-Rap1 disruption and Poz1-Tpz1 disruption. These were designated Poz1-mut17 and Poz1-mut23 respectively. Sequence analysis revealed that the first, Poz1-mut17, contained five amino acid substitutions which were separated and retested. A forward 2-hybrid assay determined that the C143R and L157P mutations were sufficient to disrupt Rap1 interaction, while maintaining Tpz1 interaction. Due to limitations in the system, however, it could not be determined whether just one of these substitutions was sufficient. Analysis of the second mutant, Poz1-mut23, revealed five amino acid substitutions which were spread throughout the protein. Sequence analysis and comparison to homologous proteins in other organisms in the *Schizosaccharomyces* genus did not identify any specific substitution which may be responsible for the phenotype. Given that separation and testing of these individual substitutions is problematic, it is a subject of ongoing work.

The RMCE method selected for the transfer of the two alleles to *S. pombe* required a modification to the wild-type locus. An NdeI site was used as an ORF cloning site and doubled as the START codon. A loxP site was integrated 600bp upstream of this NdeI site in an attempt to minimise any impact on expression and a loxM3 site was integrated downstream in the

terminator region. After integrating both mutant alleles and the parent wild-type Poz1-FL2 ORF through RMCE, telomere length analysis revealed phenotypes for all three integrations. The wild-type Poz1-FL2 in the context of the modified promoter resulted in a slight increase in telomere length, indicating an effect on Poz1 expression or function. Both of the mutant alleles resulted in very long telomeres, similar to *poz1Δ* indicating that the disruption of either Rap1 or Tpz1 interaction was sufficient to disrupt Poz1 functionality.

A 10xMyc-epitope tag was added to these alleles, as well as fully wild-type Poz1 in order to assess and compare expression by western blot. This indicated that there may be reduced expression of Poz1 in the context of the modified promoter. Telomere length analysis of these tagged strains revealed a lengthening of the telomeres due to the 10xMyc tag in addition to that which was due to the modified promoter. Testing the recruitment of the tagged Poz1 proteins to the telomere by ChIP/Slot blot and ChIP/qPCR indicated that the modified promoter was resulting in a reduced recruitment of Poz1 to the telomere, relative to a wild-type promoter.

Given these data, it was prudent to design a way to transfer the Poz1 ORFs to a wild-type promoter background. The immediate future of this study, therefore, involves identifying the substitutions sufficient for Tpz1-interaction disruption in Poz1-mut23, and integration of all the ORFs, wild-type, Rap1-disruption and Tpz1-disruption, into a wild-type diploid strain, as described previously. The Poz1 interactions in these strains would then be checked by Co-IP assays to ensure the desired phenotypes are still present in *S. pombe*. These new strains would be a better basis for further investigations.

Chapter 4

A yeast 2-hybrid cDNA library screen for *S. pombe* Stn1 interacting proteins

4.1 Introduction

The full CST complex in budding yeast, as it is known today was identified over many years. Cdc13 was originally identified in a screen for *cdc* mutants. The temperature-sensitive *cdc13-1* allele was later used in a screen for suppressors, of which one was identified as Stn1. This new protein displayed direct interaction with Cdc13 through yeast 2-hybrid analysis and was found to be an essential component at telomeres. Mutations in the *STN1* gene conferred an elongated telomere phenotype and a role in telomere capping in cooperation with Cdc13 was proposed due to activation of the G2/M checkpoint in loss of function mutants (Grandin *et al.*, 1997). Several years later, the third component, Ten1 was identified as a third factor in this telomere capping complex (Grandin *et al.*, 2001).

More recently, Stn1 and Ten1 were identified in *S. pombe* (Martín *et al.*, 2007). Stn1 was found through bioinformatics searches for OB-fold containing sequences in the fission yeast genome. Ten1 was identified in a similar manner. Both of these proteins were found to co-localise but not interact with Pot1, which, up to that point had been the only known ssDNA-binding protein at fission yeast telomeres. These Stn1 and Ten1 proteins were implicated in telomere capping, similar to the budding yeast counterparts.

Up to this point, it had been surmised that Pot1 played an analogous role in fission yeast telomeres to Cdc13 at budding yeast telomeres and that the CST complex was a unique, species-specific component. However, with the identification of Stn1 and Ten1 in fission yeast

as well as all components of CST in both mammals and plants soon after, this RPA-like trimeric complex had begun to be thought of more as the rule rather than the exception (Miyake *et al.*, 2009, Song *et al.*, 2008, Wellinger, 2009). A Cdc13 homologue in *S. pombe*, however, has not been found. It is possible that it is still yet to be identified or perhaps even doesn't exist. This is due to the possibility of the equivalent protein from RPA, Ssb1 (formerly known as Rad11), taking this role.

There is very little sequence conservation between CST components between species; indeed, the human CTC1 is still not identified as a true homologue, but rather a protein with similar interactions and functions (Miyake *et al.*, 2009). This may be one of the reasons for a Cdc13 homologue in *S. pombe* not yet being identified. Regardless, this complex has since been implicated, not only in inhibition of telomerase RNA-binding to telomeres and capping of telomeres to prevent access to DNA damage sensors in higher eukaryotes, but also involvement in recruiting the Pol-α primase complex to telomeres for synthesis of the lagging C-strand, similar to the budding yeast complex (Casteel *et al.*, 2009, Chandra *et al.*, 2001). This function could even extend to assisting stalled and collapsed replication forks or replication through structured DNA, such as G-quadruplexes (Price *et al.*, 2010).

3.1.1 Current study

The aim of this current study, therefore, is to search for a yet unidentified *S. pombe* Cdc13/CTC1 homologue. It is clear that the CST complex has some interesting and varied functions at telomeres and possibly elsewhere. It is no surprise that it is a target of much work in the telomere biology field. And yet, a Cdc13/CTC1 homologue in *S. pombe* has yet to be identified. It remains to be determined whether this is due to poor sequence conservation, no homologue existing and/or Ssb1 being the third component in this complex instead.

4.2 Results

In order to screen for Stn1-interacting proteins, a forward yeast 2-hybrid screen was devised. Interactions between various components of the fission yeast telomeric proteins, including Stn1 and Ten1, have previously been tested and confirmed using yeast 2-hybrid assays (Martín *et al.*, 2007). The sensitivity of a yeast 2-hybrid assay can also be adjusted to suit the requirements and by using a strain, such as PJ69-4A (James *et al.*, 1996), that contains more than one reporter gene; false positives ought to be kept to a minimum.

Similar to the reverse yeast 2-hybrid, the principle of the system involves constructing a Gal4 DNA binding domain fusion vector as bait and a Gal4 activating domain library as prey to screen for interactors. In this case, the *S. pombe* proteins Stn1 and Ten1 were selected for use as baits. The ORFs for these proteins would be cloned in frame with the Gal4 DNA binding domain (GBD) and an appropriate Gal4 Activating Domain (GAD) library obtained for screening. Positive interactions could be identified by combing the bait and prey library in the PJ69-4A strain and selecting for activation of the *HIS3* and *ADE2* reporter genes [Fig 4.1].
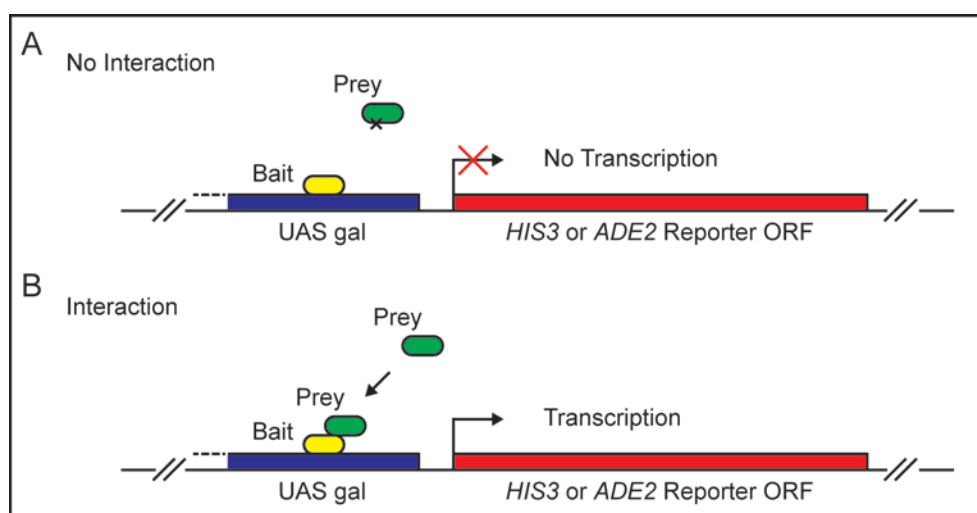
Figure 4.1: **Schematic representing principle of the forward yeast 2-hybrid system in strain PJ69-4A.**

(A) With bait fusion protein (yellow) bound to UAS gal (dark blue), if no interaction takes place with prey protein (green), transcription of reporter genes (*HIS3* and *ADE2*) will not be activated. **(B)** If prey protein (green) does interact with bait (yellow), transcription of reporter genes (red) does get activated and can be selected for by appropriate media.

4.2.1 Cloning of forward yeast 2-hybrid vectors

The plasmid pGBKT7 was used as the base for cloning the bait plasmids pGBKT7SpStn1-1 and pGBKT7SpTen1-1 [Fig 4.2A]. Once these GBD plasmids were made, the *stn1⁺* and *ten1⁺* ORFs were transferred into the pGADT7 vector [Fig 4.2B] by NdeI-XmaI subcloning for use as positive controls in the screen.

Cloning the initial GBD plasmids required several steps. This was to allow *stn1⁺* to be integrated without the introns found in the genomic copy of the gene. The C-terminus of *stn1⁺* was amplified in a high fidelity PCR reaction from *S. pombe* genomic DNA using the primers stn1-NcoI-Sp and stn1-EcoRI-Sp [Fig 4.3Ai]. The 511bp product was purified, checked by sequencing, then digested with NcoI-EcoRI and subcloned into the same sites in pGBKT7 to make pGBKT7SpStn1-C [Fig 4.3Aii]. The N-terminus was synthesised without introns by Eurofins MWG Operon as the plasmid pSpStn1NTen1. An NdeI site (CATATG) acts as the START codon in this vector allowing the N-terminus to be precisely subcloned by NdeI-AflII digest in frame into the same sites in pGBKT7SpStn1-C to make pGBKT7SpStn1-1 [Fig 4.3Aiii]. The *ten1⁺* ORF was also synthesised as part of pSpStn1NTen1 as it was relatively small. It is synthesised such that the ORF runs in the opposite direction to *stn1⁺* on the antiparallel strand, sharing the NdeI site as a START codon. This allowed it to be subcloned in frame directly into pGBKT7 using the NdeI-EcoRI restriction sites [Fig 4.3B].

The ORFs were then subcloned into pGADT7 using the NdeI-XmaI restriction sites to construct pGADT7SpStn1-1 and pGADT7SpTen1-1 vectors.

[172]
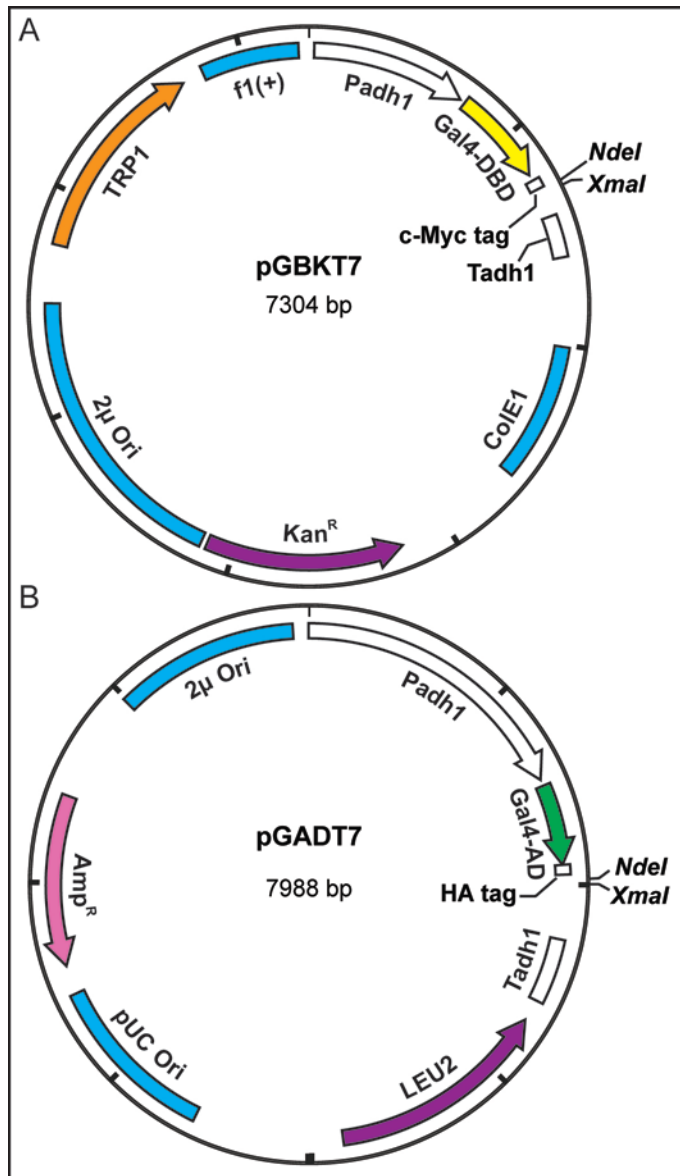
Figure 4.2: Vector schematics of base plasmids used to generate bait and prey plasmids for forward 2-hybrid screen.

(A) The pGBKT7 vector contains the GAL4-DBD (yellow) followed in frame by a c-Myc epitope tag and is used for the expression of the Bait protein. The ORF of the gene of interest can be cloned into the NdeI-XmaI sites where expression is controlled by the *ADH1* promoter (Padh1) and terminator (Tadh1). The plasmid is maintained in yeast through the *TRP1* auxotrophic marker (orange). Other features include a kanamycin resistance cassette (purple) and the replication origin sequences 2μ, f1(+) and ColE1 (blue). **(B)** The pGADT7 contains the GAL4-AD (green) followed in frame by a HA epitope tag and is used for the expression of the Prey protein. The ORF of the gene of interest can be cloned into the NdeI-XmaI sites where expression is controlled by the *ADH1* promoter (Padh1) and terminator (Tadh1). The plasmid is maintained in yeast through the *LEU2* auxotrophic marker (purple). Other features include an ampicillin resistance cassette (pink) and the replication origin sequences, 2μ Ori and pUC Ori (blue). Both pGBKT7 and pGADT7 vectors contain unique NdeI and XmaI restriction sites, suitable for subcloning of ORFs.

Figure 4.3: Schematics showing cloning steps to make pGBKT7SpStn1-1 and pGBKT7SpTen1-1 yeast 2-hybrid bait plasmids (following page).

(A) Construction of pGBKT7SpStn1-1. **(i)** The C-terminus (purple) of $stn1^+$ was amplified from genomic DNA using the primers stn1-NcoI-Sp and stn1-EcoRI-Sp, as indicated. This PCR product was then cloned into the NcoI-EcoRI sites of pGBKT7 to make pGBKT7SpStn1-C. **(ii)** The pGBKT7SpStn1-C plasmid contains the Gal4-DBD (yellow) in frame with a c-Myc epitope tag sequence (white). The pSpStn1NTen1 plasmid contains the N-terminus of $stn1^+$, synthesised by Eurofins MWG Operon. This plasmid also contains the $ten1^+$ ORF (red) with codons in the reverse direction on the antiparallel strand, as indicated by the left-pointing red arrow compared to the right-pointing purple arrow for Stn1-Nter. Both Stn1-Nter and $ten1^+$ share the NdeI site (CATATG) as a START codon. The $stn1^+$ ORF was subcloned from pSpStn1NTen1 into the NdeI-AflII sites to make pGBKT7SpStn1-1. **(iii)** The pGBKT7SpStn1-1 plasmid contains the Gal4-DBD (yellow), c-Myc epitope tag (white) and the complete $stn1^+$ ORF (purple) in frame. The GBD-SpStn1 fusion protein is under the control of the *ADH1* promoter and terminator (not shown). **(B)** The pGBKT7SpTen1-1 plasmid was constructed by subcloning $ten1^+$ (red) from pSpStn1NTen1 into the NdeI-EcoRI sites of pGBKT7. This contains the Gal4-DBD (yellow), c-Myc epitope tag (white) in frame upstream of $ten1^+$ under the control of the *ADH1* promoter and terminator (not shown).
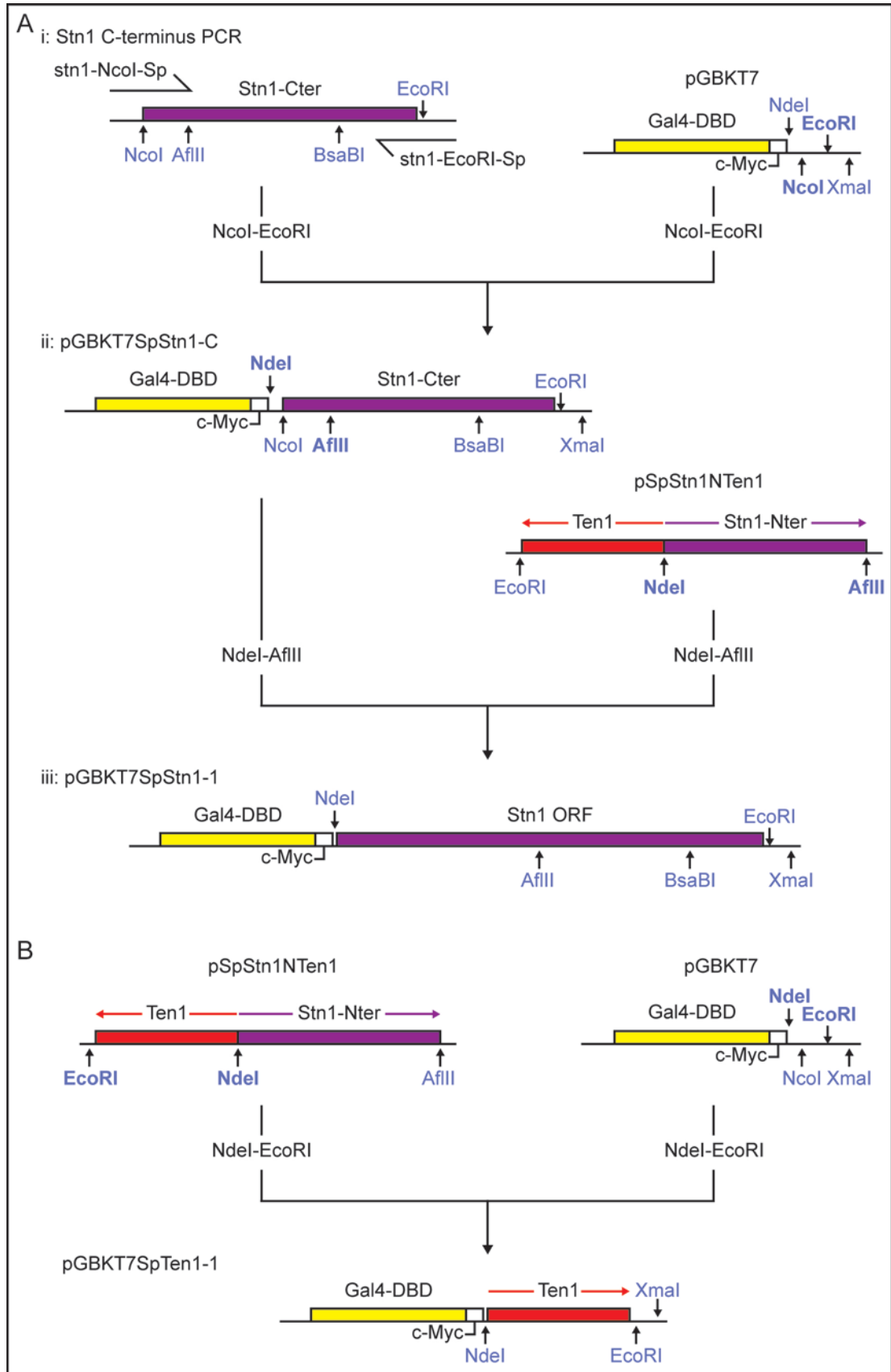
4.2.2 Expression and interaction of Stn1 and Ten1 fusion proteins in PJ69-4A yeast 2-hybrid strain

The bait and prey plasmids, with empty vector controls were co-transformed into the PJ69-4A strain in the appropriate combinations; GBD-Stn1 + GAD-Ten1 and GBD-Ten1 + GAD-Stn1 and plated on Sc –TRP –LEU agar. Expression by western blot was checked on whole cell TCA protein extracts from liquid cultures grown from these transformants. GBD-Stn1/Ten1 and GAD-Stn1/Ten1 fusion proteins could be detected using anti-myc (for GBD fusion proteins) and anti-HA (for GAD fusion proteins) primary antibodies respectively and appeared to be of the expected sizes [Fig 4.4A-B].

Additional control plasmids were also transformed into PJ69-4A. GBD-DMC1 and GAD-DMC1 plasmids were provided by Hideo Tsubouchi as positive controls. The *S. cerevisiae* DMC1 protein is known to form a homodimer and demonstrate a clear activation of reporter gene in a yeast 2-hybrid assay (Bishop *et al.*, 1992). The empty pGBKT7 and pGADT7 vectors were also co-transformed with each other as well as with the Stn1 and Ten1 plasmids. Transformants were streaked out on reporter gene-selective media: Sc –TRP –LEU –ADE and Sc –TRP –LEU –HIS. Several concentrations of 3-Amino triazole (3-AT) were tested. A concentration of 3mM was found to be optimal for Stn1-Ten1 fusion protein interaction detection. Representative images from selective streaks are shown in Figure 4.4C.

The DMC1 dimerisation is easily detected on both –ADE and –HIS selection plates. The Stn1-Ten1 interaction is also detectable on both, however, growth on Sc –TRP –LEU –ADE results in a pink colour to the colonies. This is typical of a reduced level of *ADE2* expression indicative of a weak interaction. This is not unexpected as Stn1-Ten1 interaction has been shown as fairly weak by yeast 2-hybrid assay previously (Martín *et al.*, 2007). This may be a result of steric hindrance due to being translated as fusion proteins with this particular pair of genes or an indication of a weak or transient interaction. Within the yeast 2-hybrid setup, it is not possible

to differentiate between these possibilities. Nevertheless, interaction can be detected and empty vector controls do not produce any growth on either selection media. Using the yeast 2-hybrid method to screen for possible Cdc13 or CTC1 homologues, therefore, is still viable.

Figure 4.4: Expression of Stn1 and Ten1 fusion proteins and ability to detect interaction in PJ69-4A yeast 2-hybrid strain (following page).

(A) Whole cell TCA protein extracts from PJ69-4A strain transformed with GBD-Stn1/Ten1/EV and GAD-Stn1/Ten1/EV plasmids were tested for expression by western blot. GBD fusions required anti-myc antibody. Bands of expected size can be seen for GBD-SpStn1-1 (57.88 kDa), GBD-SpTen1-1 (31.45 kDa) and GBD Empty Vector (21.72 kDa). GAD fusions required anti-HA antibody. Bands of expected size can be seen for GAD-SpStn1-1 (55.57 kDa), GAD-SpTen1-1 (29.14 kDa) and GAD Empty Vector (20.5 kDa). **(B)** Positive (DMC1) and negative (EV) control plasmids as well as GBD-Stn1/Ten1 and GAD-Stn1/Ten1 transformants in PJ69-4A yeast 2-hybrid strain were streaked on Sc −TRP −LEU, Sc −TRP −LEU −ADE and Sc −TRP −LEU −HIS + 3mM 3-AT agar plates. Ade$^+$ and His$^+$ phenotype is observed for positive controls as well as Stn1-Ten1 combinations. Reduced growth is observed for Stn1-Ten1 compared with DMC1. A pink colour is also observable in the Stn1-Ten1 streaks, typical of reduced *ADE2* expression. This is indicative of a weak interaction, consistent with previous studies (Martin *et al.* 2007). No growth is observed for negative controls, as expected.
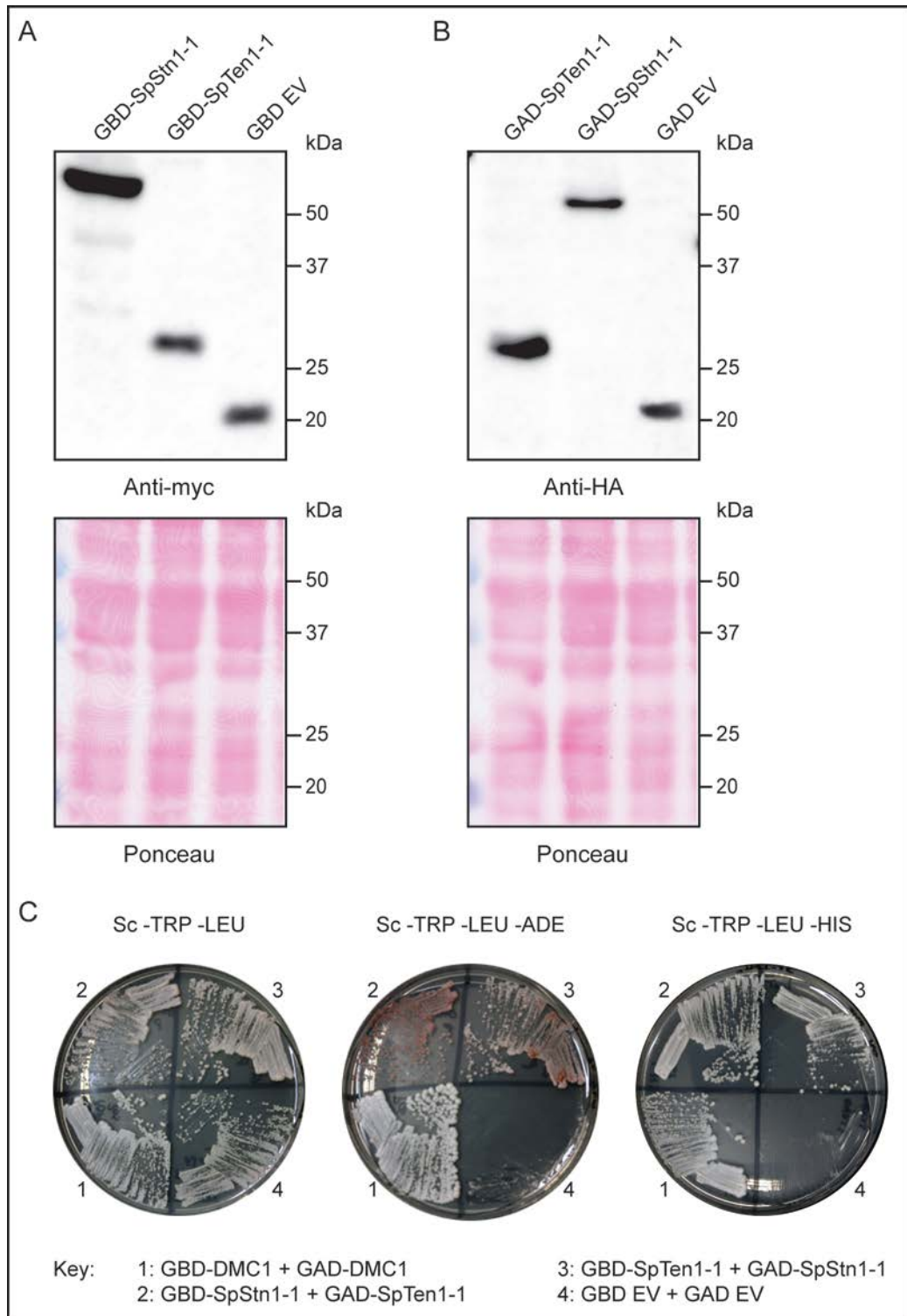
4.2.3 Amplification of an *S. pombe* cDNA library

The *S. pombe* cDNA library pTN-TH7, which contains 1 million independent clones in the pGAD424 yeast 2-hybrid vector, was provided by the NBRP of the MEXT Ministry of Education, Japan. With only approximately 5100 protein coding genes in the *S. pombe* genome (Wood *et al.*, 2012), this library was expected to provide sufficient coverage of protein coding genes. The pGAD424 vector used in this library may be different from the pGADT7 vector used in the control prey plasmids, but the cDNA inserts are under control of an identical *ADH1* promoter and so is unlikely to cause any issues due to difference in expression.

The titre of the library was calculated by transforming 0, 1, 2 and 5µl of the library into NEB DH5α high efficiency *E. coli* cells. Dilutions of each transformation were plated on LB agar plates with ampicillin selection and incubated overnight at 37°C. The number of colony forming units were counted and an approximate figure of 20 000 cfu/µl of library was calculated as the titre.

It was decided that at least 3 million cfu should be prepped in the amplification of the library to ensure every clone is represented at least once. Therefore, a total of 150µl of the library was transformed into NEB DH5α high efficiency cells in 30 separate transformations. These were pooled in LB liquid media and plated across 300 LB agar plates with ampicillin selection and incubated overnight at 37°C. Each plate was then washed with LB liquid media, without any antibiotic, and the colonies scraped off using a sterile plastic spreader into three 500ml screw capped centrifuge bottles. The cells were pelleted in the centrifuge bottles using a Sorvall RC6 Plus centrifuge at RCF of 20 000. The pellets were then weighed and the library was prepped using a Macherey-Nagel Nucleobond PC 10000 Gigaprep kit which yielded 20mg of cDNA library, diluted to a concentration of 1µg/µl.

4.2.4 Testing screen protocol using control plasmids and cDNA library

To check the library was suitable for screening and that the screening method was sound, a series of control transformations were completed. The PJ69-4A strain was transformed with the bait plasmid, pGBKT7SpStn1-1, and plated onto Sc –TRP agar. Transformants were then checked for auto-activation of the reporter genes on Sc –TRP –ADE and Sc –TRP –HIS agar, of which there was none. One transformant was inoculated in 10ml Sc –TRP liquid media overnight at 30°C. This was then transformed with control plasmids and the cDNA library as detailed in Table 4.1.

Transformation	Media	Expected Phenotype	CFU obtained
No DNA	-TRP –LEU	-	0
pGADT7 EV (100ng)	-TRP –LEU (10%)	+	877
	-TRP –LEU –ADE (45%)	-	0
	-TRP –LEU –HIS + 3-AT (45%)	-	0
pGADT7SpTen1-1 **(100ng)**	-TRP –LEU (10%)	+	903
	-TRP –LEU –ADE (45%)	+	566
	-TRP –LEU –HIS + 3-AT (45%)	+	640
pTH-TN7 cDNA library **(100ng)**	-TRP –LEU (10%)	+	1101
	-TRP –LEU –ADE (45%)	To be tested	0
	-TRP –LEU –HIS +3-AT (45%)	To be tested	0

Table 4.1: PJ69-4A yeast 2-hybrid transformations used in a Stn1 interactor screen test.

The PJ69-4A strain was transformed with pGBKT7SpStn1-1. One transformant was then inoculated and transformed with control vectors and cDNA library, as indicated. For No DNA control, the full transformation mixture was plated onto an Sc –TRP –LEU plate. For Empty Vector (negative) and pGADT7SpTen1-1 (positive) controls, 10% was plated on Sc –TRP –LEU with the remaining 90% split between Sc –TRP –LEU –ADE and Sc –TRP –LEU –HIS + 3-AT agar plates. The cDNA library transformation was plated in the same manner. The expected phenotype, growth or not growth, is indicated by + or – for each transformation on each type of media. The number of colony forming units obtained is also indicated. Colonies numbers obtained for the positive control pGADT7SpTen1-1 transformation with –ADE and –HIS media are 566 and 640 cfu respectively. This is approximately 1/8th of the expected number, given that 903 cfu were obtained from 10% of the transformation mix on non-selective Sc –TRP –LEU media, indicating a low screening efficiency.

The control transformations using pGADT7 EV resulted in 877 cfu on the Sc −TRP −LEU plate and no cfu on either Sc −TRP −LEU −ADE nor Sc −TRP −LEU −HIS + 3-AT plates. This would indicate that there were approximately 9000 transformants from 100ng of pGADT7 EV. Similarly, the pGADT7SpTen1-1 positive control transformation resulted in 903 cfu on the Sc −TRP −LEU plate. Based on this number, in theory all transformants should score positive on the selective plates, and a total of approximately 9000 cfu would be present. In reality fewer cfu would be expected as 100% of all interacting transformants wouldn't necessarily be expected to grow on the selective plates. However, even taking this into account, the number of cfu obtained on the two types of selection plates (Sc −TRP −LEU −ADE and Sc −TRP −LEU −HIS +3-AT) was quite low. With 566 cfu as a result of selecting for the *ADE2* reporter and 640 cfu as a result of selecting for the *HIS3* reporter, only 10-15% of the total number of expected cfu was obtained. This indicated that the screening efficiency using this method was quite low. This may be a result of directly selecting for activation of the reporter genes; however, as typical 2-hybrid screening would require this, it may be more likely an unexpected consequence of the weak Stn1-Ten1 fusion protein interaction.

Nevertheless, several of the cfu from the pGADT7SpTen1-1 test transformation were put through plasmid recovery. The preps were then checked by diagnostic digest for the correct size of insert for the *ten1*[+] ORF. These showed the expected band sizes for pGADT7SpTen1-1 and, therefore, it was decided that the screen could operate well enough to pull out interactors and should proceed.

4.2.5 Screening an *S. pombe* cDNA library for Stn1 interacting proteins

The PJ69-4A screening strain was prepared by transformation with the pGBKT7SPTen1-1 vector as previously done with the pGBKT7SpStn1-1 vector. This resulted in two strains for screening, one to screen for Stn1-interacting proteins and the other to screen for Ten1-

interacting proteins. As an initial, small scale screen, these were then both transformed with 1µg of the cDNA library, pGADT7 EV and No DNA control. The cDNA library transformation mixtures were plated, split between Sc –TRP –LEU, Sc –TRP –LEU –ADE and Sc –TRP –LEU –HIS + 3-AT agar plates (1% on the Sc –TRP –LEU and 10% on each of the other plates). For the controls, 1/3rd of the transformation mixtures were plates on one of each type of plate.

Multiple colonies were found to be growing on both the Sc –TRP –LEU –ADE and Sc –TRP – LEU –HIS +3-AT plates from both sets of cDNA library transformations while none grew for the empty vector. These cfu were streaked to fresh plates and then put through plasmid recovery. Given that plasmid recovery is not always successful, as each was successfully recovered and prepped, they were sequenced with GAD-f1 primer, which allowed sequencing through the cDNA insert in the vector. Many of these candidates, however, were false positives that were identified by nucleotide BLAST search to contain *S. pombe ade6^{+}* and *his5^{+}* genes, depending on which reporter was selected in the screen. Several different clones of these were identified. Surprisingly, one in particular also contained a portion of the 5' UTR of *tpz1^{+}* in addition to the *his5^{+}*.

Given that *S. pombe ade6^{+}* and *his5^{+}*appear to complement *S. cerevisiae HIS3 and ADE2*, the screening method was modified for subsequent screens [Fig 4.5]. This involved plating on Sc –TRP –LEU initially to allow clones which may have weak interactions, and therefore slower growth, to reach a reasonable colony size. These colonies would then be replica plated onto the primary screen plates, Sc –TRP –LEU –ADE and Sc –TRP, -LEU –HIS +3-AT. Growing colonies would then be put through a secondary screen on either Sc –TRP –LEU –ADE or Sc –TRP –LEU –HIS + 3-AT, depending on which reporter was initially selected. An AluI digest was also introduced to help differentiate known *ade6^{+}* and *his5^{+}* clones from potentially interesting clones. By using a 4 base cutter like AluI, specific clones containing *ade6^{+}* and *his5^{+}* could be

identified fairly reliably based on comparison of the restriction pattern obtained from agarose gel electrophoresis of the digested vector.

Approximately 450 000 clones were screened for Stn1 interacting proteins and 380 000 clones for Ten1 interacting proteins using this method [Table 4.2]. Representative images of patches on dual selection plates [Fig4.6A] show the variation in growth and colour of candidates. The gel electrophoresis image of a set of the recovered plasmids from these candidates digested with AluI [Fig 4.6B] show the typical variation of restriction patterns observed. Although many clones passed the secondary screen and AluI restriction fragment comparisons, none retained the reporter gene activation when retransformed [Fig 4.6C]. It was expected that, with the initial plating on Sc –TRP –LEU agar, at least *stn1⁺* and *ten1⁺* clones would have been identified, however, this has not been the case.

Bait	Clones screened (approx.)	Primary screen positives	Secondary screen positives	Retransformed positives
GBD-SpStn1-1	450 000	97	48	0
GBD-SpTen1-1	380 000	34	3	0

Table 4.2: **Details of clone numbers taken through each stage of the yeast 2-hybrid screening protocol as per Fig 4.5.**

PJ69-4A was transformed with GBD-SpStn1-1 and GBD-SpTen1-1 for use as baits. Based on cfu number on Sc –TRP – LEU plates, 450 000 and 380 000 clones were screened for Stn1-interacting and Ten1-interacting candidates respectively. The numbers of positives, as judged by growth on selective plates for the primary and secondary screen stages, are as indicated. No candidates that were retransformed into PJ69-4A after the secondary screen, followed by AluI digest, scored positive.

A

Transformation of library into PJ69-4A + pGBKT7SpStn1-1 onto Sc -TRP -LEU

↓

1° Screen: Replica to selective plates

Sc -TRP -LEU -HIS

Sc -TRP -LEU -ADE

↓

2° Screen: Patch to new selective plates

Sc -TRP -LEU -ADE

Sc -TRP -LEU -HIS

Sc -TRP -LEU -ADE -HIS + 3-AT

↓

Plasmid Recovery

↓

AluI digest (to check for clonality and His5/Ade6)

↓

Retransformation to PJ69-4A on Sc -TRP -LEU

↓

Patch transformants to Sc -TRP LEU -ADE -HIS +3-AT

↓

Sequence and Analyse Positives

Figure 4.5: Flow chart of yeast 2-hybrid screening method.

The PJ69-4A strain was transformed with pGBKT7SpStn1-1, or pGBKT7SpTen1-1 (not shown). The strain was then transformed with the cDNA library and plated on Sc –TRP –LEU agar, followed by replica of cfu to primary screen plates: Sc –TRP –LEU –ADE and Sc –TRP –LEU –HIS + 3-AT agar. The growing cfu were then patched onto secondary screen plates, followed by dual selection on Sc –TRP –LEU –ADE –HIS + 3-AT agar, as indicated. Plasmids were then recovered and a sample digested with AluI restriction enzyme to compare the restriction pattern between individual clones and with known *ade6*[+] and *his5*[+] clones. Candidate clones were then retransformed into PJ69-4A + appropriate bait to confirm interaction phenotype. Positives were to be sequenced and further analysed.

Figure 4.6: Representative images of growth of yeast 2-hybrid screen candidates on selective media and AluI digested restriction fragments (following page).

(A) (i-ii) Candidates passing the secondary screen (with GBD-Stn1 and GBD-Ten1 as baits) with Ade[+] His[+] phenotypes were patched on Sc –TRP –LEU –ADE –HIS + 3mM 3-AT dual selection media. DMC1 controls grow with a clear white colour indicating strong *ADE2* expression. Stn1-Ten1 control grows with red colour indicating lower *ADE2* expression due to weaker interaction in 2-hybrid strain. No growth is seen with the empty vector control. **(B)** Image of AluI-digested restriction fragments from agarose gel electrophoresis shows a set of candidates compared against typical false positive *ade*[+] and *his*[+] clones. An NEB 100bp DNA ladder is shown, as indicated. The pattern of restriction fragments can be used to identify likely identical *ade*[+] and *his*[+] clones. **(C)** Images of 2-hybrid strain patches. **(i-iii)** PJ69-4A retransformed with recovered plasmids from secondary screen was patched on Sc –TRP –LEU –ADE –HIS + 3mM 3-AT dual selection media. Controls grow as expected. DMC1 positive control patches grow with a clear white colour, indicating strong *ADE2* expression. Stn1-Ten1 control patches grow with a red colour, indicating lower *ADE2* expression due to weaker interaction in 2-hybrid strain. No growth is seen with the empty vector control patches. Strains containing GAD-SpAde6 and GAD-SpHis3 controls do not grow on dual selection, as expected. None of the candidates which passed the secondary screen stage and were retransformed grow on Sc –TRP –LEU ADE –HIS + 3mM 3-AT.

Sc -TRP -LEU -ADE -HIS + 3-AT

Sc -TRP -LEU -ADE -HIS + 3-AT

Key: 1: GBD-DMC1 + GAD-DMC1
        2: GBD-SpStn1 + GAD-SpTen1
        3: GBD EV + GAD EV
        4: GBD-SpStn1 / GAD-SpAde6
        5: GBD-SpStn1 / GAD-SpHis5
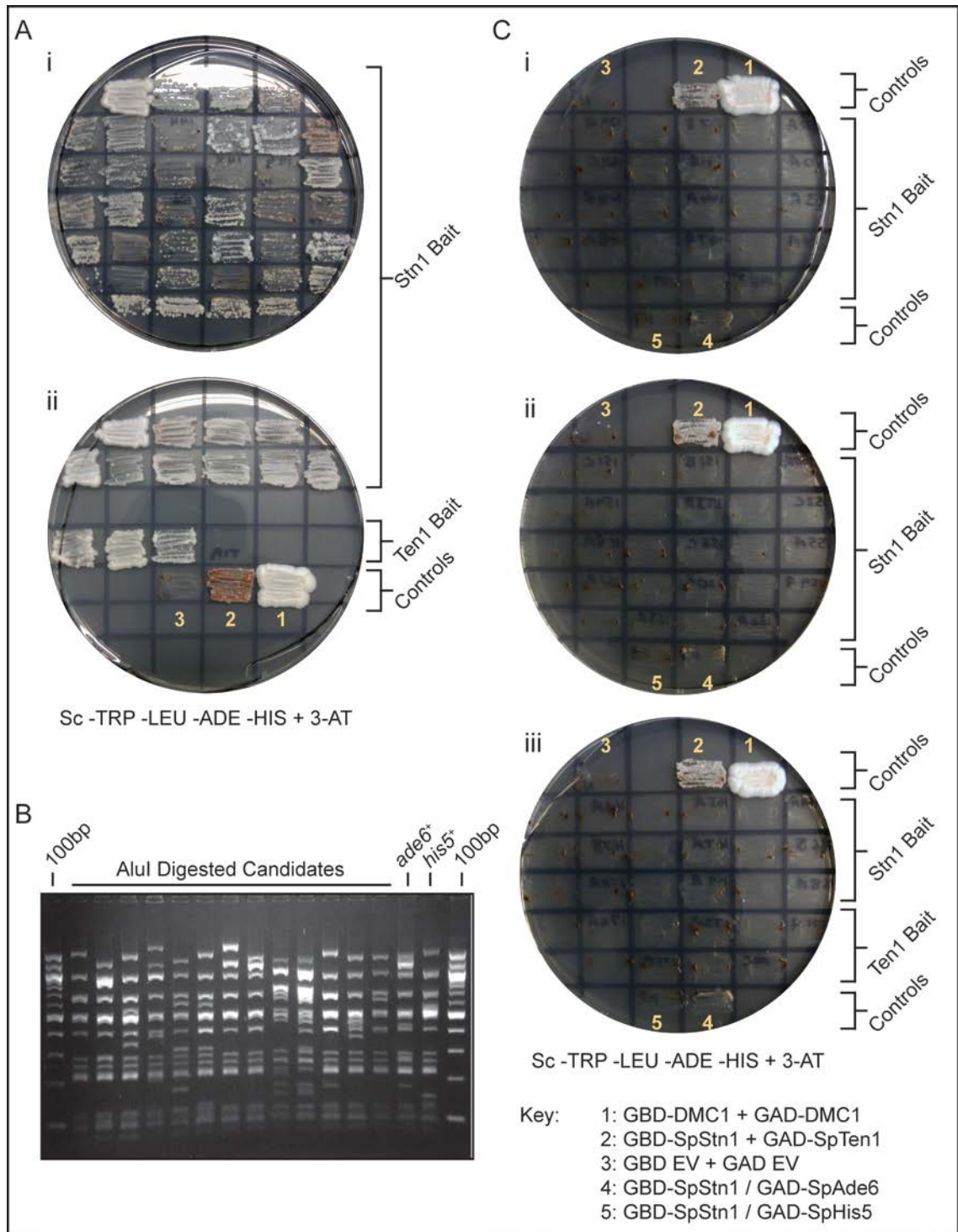
Neither *ten1⁺* nor *stn1⁺* clones were pulled out of this screen despite filtering out the high frequency of false positive clones (*ade6⁺* and *his5⁺*) as well many unknown clones which did not retransform positive after passing all stages of the initial screen. This implied that the interaction between Stn1 and Ten1 through a 2-hybrid screen may be too weak or transient to detect, despite being overexpressed by a constitutive promoter. Although less than half of the library had been screened, given that the number of *S. pombe* protein coding genes is quite small relative to the size of the library, it was likely that most, if not all, proteins would have already passed through the screen at least once. Therefore, it was decided that this method of screening was not a reliable technique for identifying novel Stn1 and Ten1 interacting proteins and pursuing it would require further modifications and testing of the method.

4.3 Summary

The aim of this study was to use a forward yeast 2-hybrid system to screen an *S. pombe* cDNA library for Stn1 and Ten1 interactors. Given that Stn1 and Ten1 have been identified to form parts of a heterotrimeric complex in other species, it was thought that a yet unidentified Cdc13 or CTC1 homologue might be pulled from the screen.

Bait plasmids based on the pGBKT7 and pGADT7 vectors were generated. These expressed *S. pombe* Stn1 and Ten1 tethered to Gal4-DBD and Gal4-GAD as fusion proteins. These were transformed into the PJ69-4A yeast 2-hybrid strain to confirm that a Stn1-Ten1 interaction could be detected using the 2-hybrid assay. After confirming interaction and determining optimal selection method through small scale tests, a larger scale screen was conducted. A cDNA library, based in the pGAD424 vector, was transformed into the PJ69-4A strains containing GBD-SpStn1 and GBD-SpTen1. A total of 450 000 clones were screened for Stn1 interacting proteins and 380 000 clones for Ten1 interacting proteins using this method. Of these clones, 48 and 3 passed the secondary screen stage for Stn1-interactors and Ten-interactors respectively. However, upon retransformation, these were determined to be false positives.

The interaction between Stn1 and Ten1 has previously been shown to be relatively weak (Martín *et al.*, 2007) and this has been confirmed in this study [Fig 4.4]. As a result, only 10-15% of positive control transformants were pulled out of a test in the study. This indicated that Stn1-Ten1 interaction is only just within the detection threshold of the system. In addition, background in the form of *S. pombe ade6$^+$* and *his3$^+$* clones complicated the screening method. These, and likely a combination of other factors such a low level of reporter auto-activation, may have resulted in the accumulation of these false positives. In order to improve the chances of finding Stn1 and Ten1 interactors, a modified or alternative method would need to be employed.

Chapter 5

Generation and characterisation of *S. pombe stn1* temperature-sensitive alleles

5.1 Introduction

In many organisms, deletion, deactivation or depletion of a protein implicated in telomere end-capping can result in chromosome end-to-end fusions, resulting in genome instability and lead to eventual replicative senescence or cell death (O'Sullivan and Karlseder, 2010, Palm and de Lange, 2008). In *S. pombe*, however, due to the genome being split into just three chromosomes, the result of telomere deprotection can be chromosome circularisation (Nakamura *et al.*, 1998). In one relevant example, when the ssDNA-binding protein Pot1 is lost, intra-chromosomal fusions can result in circularisation. Through the single-strand annealing pathway, dependent on homology found in the sub-telomeric regions of chromosome I and II, somewhat unhealthy but otherwise very viable cells can be generated (Wang and Baumann, 2008). The regions of homology involved in circularisation are located at least 10kb from the telomeres. During circularisation, repair of the exposed chromosome ends occurs via annealing of the homologous sequences and deletion of the intervening sequences. At least 7kb of terminal sequence is lost through this mechanism [Fig 5.1B]. Other mutants such as *trt1Δ, taz1Δ*, *stn1Δ*, *ten1Δ* and *tel1Δ rad3-136* double mutants can circularise chromosomes, though not necessarily using the same pathway, under the same conditions or with a similar level of viability (Ferreira and Cooper, 2001, Martín *et al.*, 2007, Naito *et al.*, 1998, Nakamura *et al.*, 1998). For example, *taz1Δ* only form intra-chromosomal fusions through the NHEJ pathway during G1 arrest and would otherwise continue through the cell cycle with elongated telomeres (Ferreira and Cooper, 2001). Fusions that do occur in this manner, however, do not

generate the same robust survivors found when the fusions occur through an HR-related pathway. Without end protection, a small proportion of cells are still able to maintain linear chromosomes through continual amplification and shuffling of heterochromatic sequences (Jain *et al.*, 2010). Known as HAATI cells, the ability to maintain linear chromosomes comes from two paths. HAATI[rDNA] cells spread rDNA from chromosome III to Chromosomes I and II while HAATI[STE] cells retain rDNA only on chromosome III, but amplify and rearrange sub-telomeric elements exclusively on chromosomes I and II.

5.1.1 Current study

As part of the on-going effort to identify an *S. pombe* homologue of Cdc13 or CTC1, the aim of the current study was to develop an alternative method for screening for proteins which interacted with *S. pombe* Stn1. To this end, it was decided that a Stn1 temperature-sensitive protein suppressor screen could be carried out. This would require generation of a *stn1* temperature-sensitive allele which at the time was not available. Characterisation of such an allele could also provide additional insight into the function of *S. pombe* Stn1 protein. An advantage of using a suppressor screen, rather than a yeast 2-hybrid screen would include the possibility that proteins which may not directly bind Stn1 could be picked up as suppressors. Additionally, the screen could be carried out in fission yeast, as opposed to budding yeast, and without the need for expressing fusion proteins which might otherwise interfere with protein folding or obstruct interactions. Even if a Cdc13-related protein is not identified, other suppressors could be interesting to investigate. The possibilities remain that other components of the existing telomeric complex may interact with Stn1 or even that Ssb1 (also known as Rad11), the equivalent protein to RPA1, may be identified as a suppressor. Having a *stn1* temperature-sensitive allele would also open the possibility to study and further characterise Stn1 itself.

A screen using a temperature-sensitive allele of a telomeric protein to identify suppressors is not unprecedented. Indeed, the *S. cerevisiae* Stn1 and Ten1 proteins were identified through such a screen using the temperature-sensitive alleles *cdc13-1* and *stn1-13* (Grandin *et al.*, 2001, Grandin *et al.*, 1997). It would, therefore, be useful to generate such a *stn1* temperature-sensitive allele in *S. pombe*. However, one issue which is unique to *S. pombe* remains; survival of telomere deprotection through chromosome circularisation. The initial task, therefore, would be to investigate methods to enhance the telomere deprotection phenotype, preferably to lethal levels.
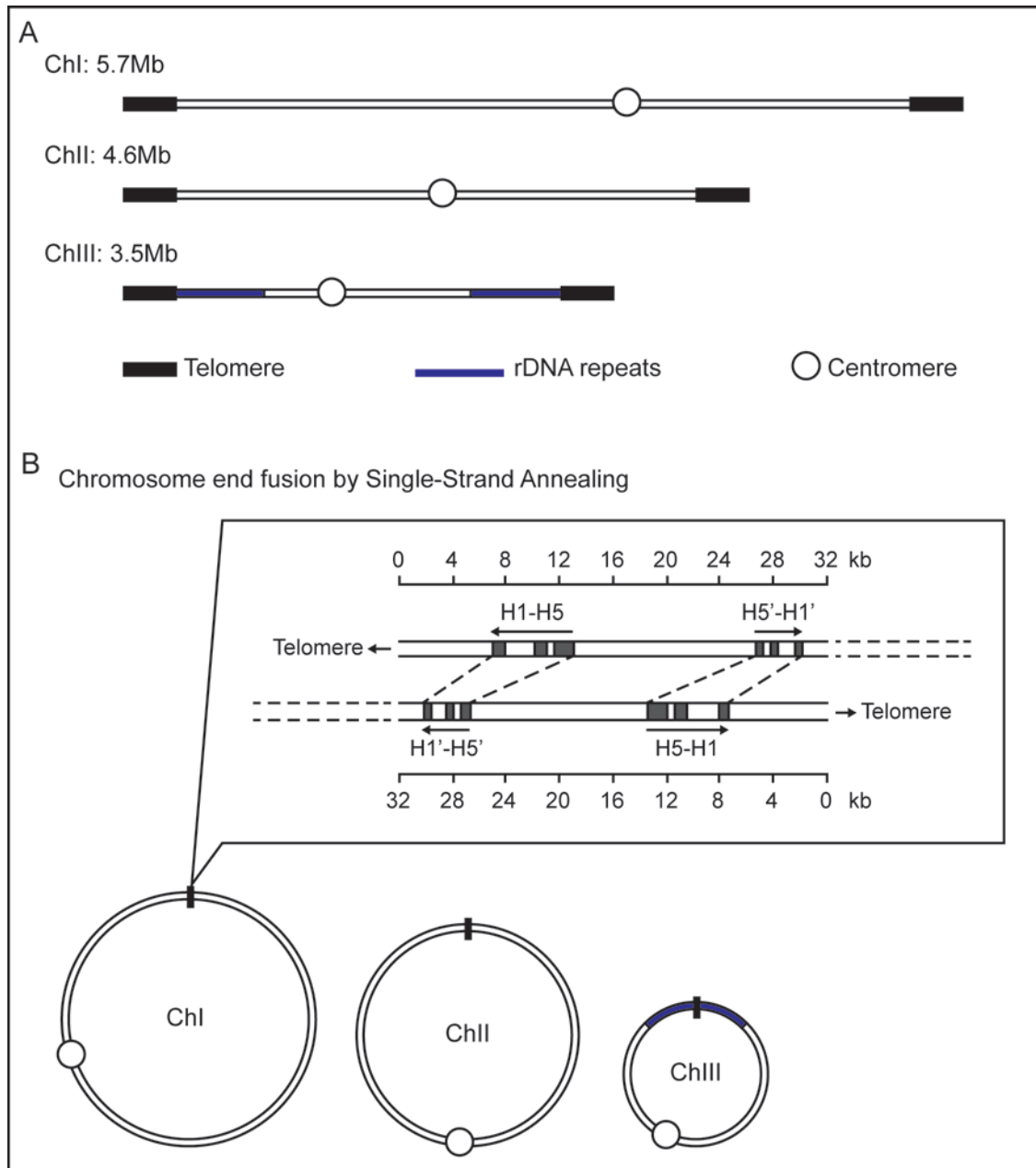
Figure 5.1: Schematic representation of *S. pombe* chromosomes and circularisation through single-strand annealing (SSA).

(A) *S. pombe* contains three linear chromosomes, ChI = 5.7Mb, ChII = 4.6Mb and ChIII = 3.5Mb in size, as indicated. Each chromosome contains telomeric sequences at the terminal ends. Chromosome III also contains rDNA repeats of variable size. **(B)** Under telomere deprotection *S. pombe* is able to circularise it's chromosomes in a manner dependent on the Single-Strand Annealing (SSA) pathway of homologous recombination. A schematic of two chromosome ends in head-to-head orientation is shown with blocks of homology indicated (H1-H5 and H1'-H5'). Approximate distance from telomere for each block is indicated. Fusions occur between a homology block in the telomere-proximal set (H1-H5) and the homologous region (H1'-H5') on the other chromosome arm. The arrows at these homology blocks indicate the matching orientation of repeats for SSA. Between 7 and 13kb of terminal sequence is lost from one arm while more than 27kb can be lost from the other arm to expose the H1'-H5' homologous sequences for SSA.

5.2 Results

5.2.1 Testing lethality of *pot1-1* temperature-sensitive allele in combination with other genetic backgrounds

In order to identify genetic backgrounds which would enhance the phenotype of a temperature-sensitive telomere deprotection mutant allele, the *pot1-1* allele was selected as a stand-in for the investigations. Loss of Pot1 results in chromosome circularisation, much like the loss of the Stn1 protein (Martín *et al.*, 2007). Generated in a screen for temperature-sensitive alleles, the *pot1*-1 allele contains three mutations which result in two amino acid changes. In addition to this, the study determined that a requirement for the temperature-sensitive phenotype is the tethering of GFP to the C-terminus (Pitt and Cooper, 2010). As a key fission yeast telomeric ssDNA-binding protein like Stn1, any genetic backgrounds which prove lethal in combination with this allele could also be lethal with a *stn1* temperature-sensitive allele. Previous investigations in determining the pathway responsible for circularisation in *pot1Δ* strains identified several genetic backgrounds which resulted in loss of viability when a *pot1⁺* covering plasmid was removed (Wang and Baumann, 2008).

Two of the genetic backgrounds which proved to have a viability phenotype with *pot1Δ* were *rad16Δ* and *lig4Δ*, with the former resulting in a complete loss of viability and the latter resulting in a partial loss. These phenotypes were attributed to the inability to form intra-chromosomal fusions through the SSA pathway and NHEJ pathway respectively (Wang and Baumann, 2008). Several strains were, therefore, generated by crossing a *pot1-1* haploid strain with a *rad16Δ* strain. The resulting *pot1-1 rad16Δ* double mutant strain was then crossed with a *lig4Δ* strain to generate a triple mutant, *pot1-1 rad16Δ lig4Δ*. These mutants were tested for viability at the *pot1-1* non-permissive temperature of 36°C by spot assay and compared against the individual single mutants and a *pot1Δ* pre-circularised strain [Fig 5.2A]

The spot assay indicated that the *pot1-1 rad16Δ* double mutant viability was reduced at 36°C as compared to 25°C, but no more so than the *pot1-1* single mutant. The *pot1-1 rad16Δ lig4Δ* triple mutant was, surprisingly, slightly more viable at 36°C than the double mutant. The reason why these strains are able to survive the *pot1-1* non-permissive temperature is unknown. They may still be circularising chromosomes, indicated by a drop in viability to levels similar to the *pot1-1* single mutant. Given that the original experiments were conducted in a *pot1Δ* background, as opposed to the *pot1-1*, it is possible that there is a difference in the way chromosome ends fuse between a mutant which loses Pot1 protein completely and one which retains a dysfunctional one. On the other hand, these may be HAATI survivors. In these cells, though telomeres have been lost, Ccq1 continues to be recruited to the chromosome ends via the SHREC complex. This is a quartet of proteins involved in heterochromatic transcriptional gene silencing (Sugiyama *et al.*, 2007). As a result, Pot1 continues to be recruited to the chromosome ends in the absence of telomeric binding sites. The heterochromatin, rDNA and sub-telomeric elements (STEs) in these cells continually shift between chromosome ends, resulting in a buffering and capping system that allows the maintenance of linear chromosomes (Jain *et al.*, 2010). It is possible that in the case of *pot1-1*, sufficient Pot1 function exists to allow HAATI survivors to emerge. With the previous study using *pot1Δ*, as opposed to *pot1-1*, HAATI survivors could not have emerged.

An alternative genetic background was, therefore, considered. An *rqh1Δ* in combination with *pot1Δ* had also been shown to be lethal. *S. pombe* Rqh1 is a RecQ-type helicase which appeared to be essential in either allowing *pot1Δ* cells to generate circularised chromosomes or to maintain them after the initial fusion (Wang and Baumann, 2008). It was recently proposed that Rqh1 is required to inhibit crossover events between circular chromosomes which would otherwise lead to generation of dimers that are incapable of correct segregation (Nanbu *et al.*, 2013). This is dependent on Rad51, shown by removal of *rad51*[+] resulting in a suppression of the synthetic lethal phenotype. Restoration of *rad51*[+] on a covering plasmid

also restores the synthetic lethal phenotype, albeit not immediately. Lethality was only observed on the 2nd streak after reactivation of *rad51+*. Depletion of Rqh1 in thiamine-rich liquid culture in a *pot1Δ/nmt-rqh1* background (where the endogenous *rqh1+* promoter has been replaced by the *nmt81* promoter) resulted in a reduction in viability of cells with circularised chromosomes. Depletion of Pot1 using an auxin-based degron system was shown to still allow chromosomes to circularise. The auxin-inducible degron (*aid*) tag was added to the C-terminus of Pot1 to generate an *nmt-pot1-aid rqh1Δ* background. Adding both thiamine and auxin to the cells allowed Pot1 to be efficiently depleted and chromosomes to circularise. These results indicated that the presence of Rqh1 was not required for the initial fusion step but rather in the maintenance of circularised chromosomes (Nanbu *et al.*, 2013). Given these data, it was decided that combining *pot1-1* with *rqh1Δ* would be the next best approach in attempting to generate a conditional synthetic lethal mutant, though it didn't rule out the possibility of more HAATI survivors emerging.

A *pot1Δ rqh1Δ* strain was initially generated by crossing the two single mutant strains. A *pot1+* covering plasmid (pPB280) was maintained by *ura4+* selection to prevent circularisation. Separately, the *rqh1+* locus was disrupted in *pot1+/pot1-1* diploid and wild type strains by integrating the pSpRqh1D-H plasmid at the *rqh1+* locus as described in the methods. The diploid was then sporulated and the resulting *pot1-1 rqh1Δ* strain maintained at 25°C to avoid circularisation.

The *pot1Δ* and *pot1Δ rqh1Δ* strains were streaked to single colonies on YES and on YES + 5-FOA (counter-selection of *pot1+* covering plasmid) agar plates [Fig 5.2B]. Growth of the *pot1Δ* on YES is robust, while the *pot1Δ rqh1Δ* double mutant is reduced but single colonies were still formed. On YES + 5-FOA,, however, although the *pot1Δ* showed slightly reduced growth, indicative of some viability loss during circularisation, the *pot1Δ rqh1Δ* double mutant did not

form any colonies at all. This result indicated that the combination of *pot1Δ* and *rqh1Δ* was, indeed, synthetically lethal.

Having established this, the *pot1-1 rqh1Δ* temperature sensitive mutant was tested for synthetic lethality at the non-permissive temperature [Fig 5.2C]. Similar to the previous test, the *pot1-1 rqh1Δ* strain did not produce any colonies at the non-permissive temperature of 36°C while the single mutants both produced colonies, as expected. A spot assay was carried out to confirm the synthetic lethality using two separate *pot1-1 rqh1Δ* haploid strains [Fig 5.2D]. Viability of the double mutant was found to be severely diminished at the non-permissive temperature while the single mutants remained viable, as before. There was also no evidence of potential HAATI survivors emerging. Having established a genetic background in which a *pot1-1* temperature-sensitive allele can become synthetically lethal, the process to generate *stn1* temperature sensitive alleles in this background was begun.

Figure 5.2: Tests establishing synthetic lethality with *pot1-1* temperature-sensitive allele (following page).

(A) Spot assay testing the viability of wild-type, *pot1-1 rad16Δ* and *pot1-1 rad16Δ lig4Δ* strains in 1/5-fold serial dilutions. Single mutants and pre-circularised *pot1Δ* are compared to these double and triple mutants. The *pot1-1 rad16Δ* and *pot1-1 rad16Δ lig4Δ* strains were found to retain some viability, possibly due to HAATI survivors. **(B)** Streaks of *pot1Δ* and *pot1Δ rqh1Δ* strains on YES and YES + 5-FOA, allowing comparison of growth with and without a *pot1⁺* covering plasmid respectively. The streaks show that the double mutant, *pot1Δ rqh1Δ*, is synthetic lethal with no colonies forming when the covering plasmid is lost. **(C)** Streaks of wild-type, *pot1-1*, *rqh1Δ* and *pot1-1 rqh1Δ* strains on YES at 25°C and 36°C comparing the viability of the *pot1-1* temperature-sensitive mutant. The streaks show that *pot1-1 rqh1Δ* is synthetic lethal at the non-permissive temperature (36°C), as indicated by the lack of colony formation. **(D)** Spot assay testing the viability of *pot1-1 rqh1Δ* at permissive (25°C) and non-permissive (36°C) temperatures in 1/5-fold serial dilutions. Two *pot1-1 rqh1Δ* double mutant strains (*nr1* and *nr2*) are found to be synthetic lethal at the non-permissive temperature as shown by lack of colony formation at 36°C.
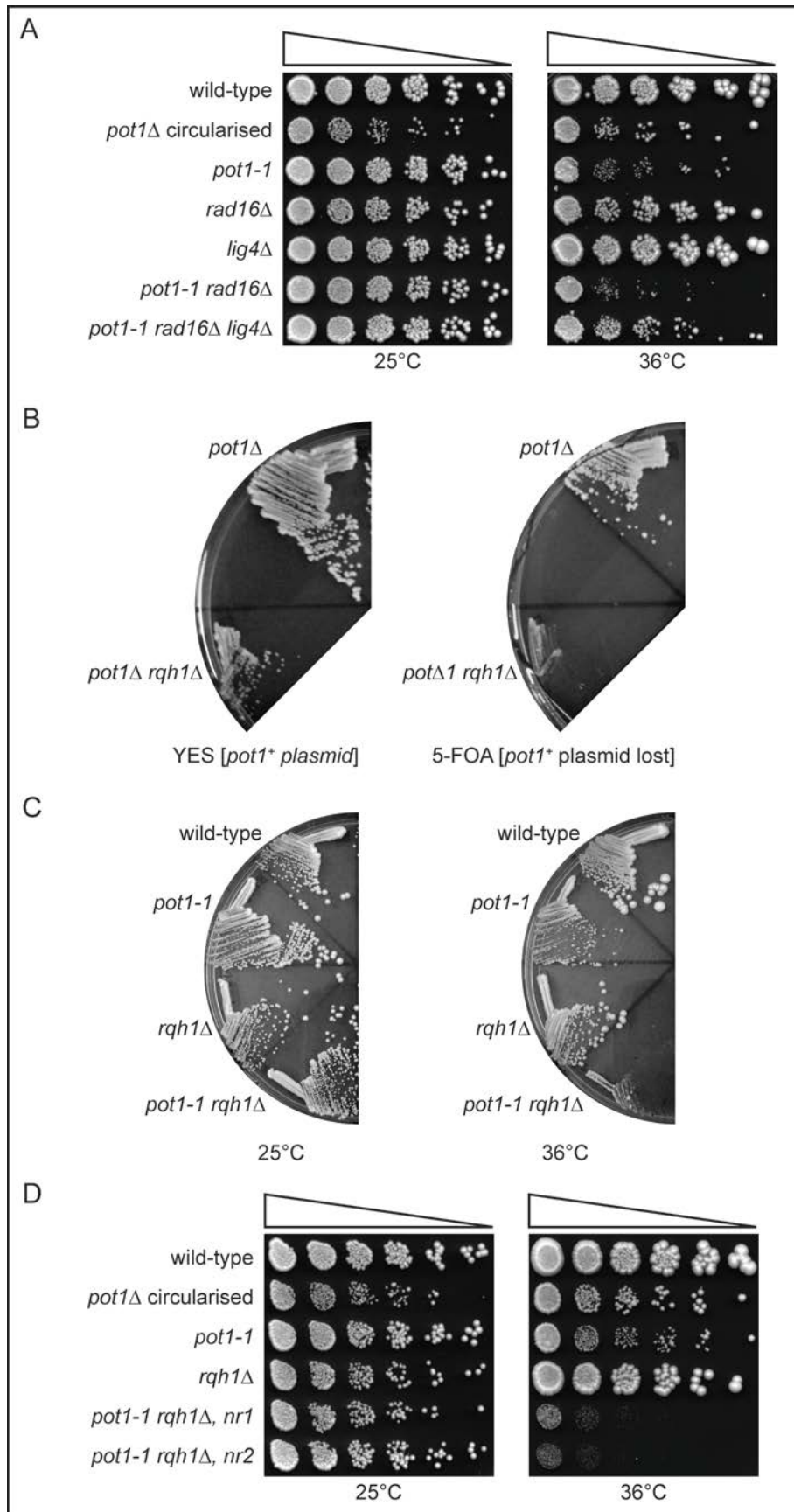
5.2.2 Base strain construction for identification and integration of *stn1* temperature-sensitive alleles

In order to generate a base strain capable of easily integrating mutagenised *stn1*, the plasmid pmutSpStn1a was synthesised by Eurofins MWG Operon. It contained a fragment of the *stn1+* promoter and terminator flanking loxP and loxM3 recombination sites, which in turn flanked several restriction enzyme sites [Fig 5.3Ai]. The *stn1+* ORF was subcloned into pmutSpStn1a by NdeI-EcoRI restriction digest and ligation into the same sites to make pmutSpStn1-2 [Fig 5.3Aii]. The *ura4+* cassette from pFY416 was then excised by NdeI restriction digest, blunted with T4 polymerase and subcloned into the EcoRV site in pmutSpStn1-2 to make pmutSpStn1-3 [Fig 5.3Aiii]. BstBI-HindIII restriction digest of this plasmid released the loxP-*stn1+*-*ura4+*-loxM3 fragment flanked by the *stn1+* promoter and terminator fragments. This excised fragment was purified by gel extraction and transformed into an *S. pombe* wild-type diploid strain for integration at the *stn1+* locus. This diploid strain was sporulated to produce a haploid containing the loxP-*stn1+*-*ura4+*-loxM3 cassette which would allow the integration of *stn1* temperature sensitive alleles by Recombinase-Mediated Cassette Exchange (RMCE) [Fig 5.3B].
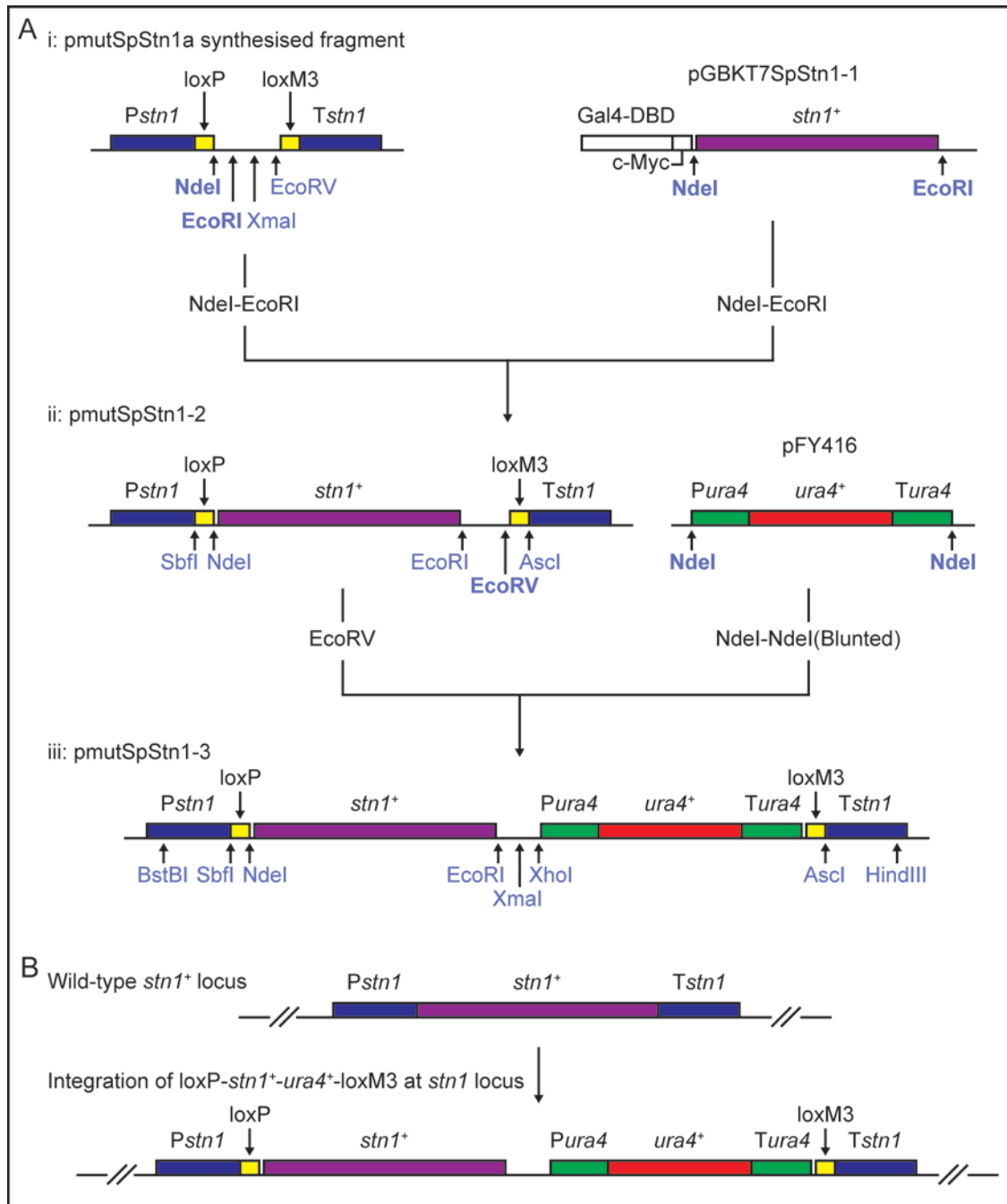
Figure 5.3: Schematic of *S. pombe* stn1::loxP-*stn1⁺-ura4⁺*-loxM3 base strain construction.

(A) (i) The pmutSpStn1a vector was synthesised by Eurofins MWG operon, consisting of *stn1* promoter (P*stn1*) and terminator (T*stn1*) sequences (dark blue) flanking loxP and loxM3 sites (yellow). The wild-type *stn1⁺* ORF (purple) was subcloned by NdeI-EcoRI from pGBKT7SpStn1-1 into the pmutSpStn1a vector to make pmutSpStn1-2. **(ii)** The *ura4⁺* ORF (red) and flanking promoter (P*ura4*) and terminator (T*ura4*) sequences (green) from pFY416 were subcloned into pmutSpStn1-2 by blunted NdeI-NdeI digests into the EcoRV site of pmutSpStn1-2 to make pmutSpStn1-3. **(iii)** The pmutSpStn1-3 vector contains a cassette consisting of *stn1* promoter (P*stn1*) and terminator (T*stn1*) sequences (dark blue) flanking loxP and loxM3 sites (yellow), which in turn flank the wild-type stn1 ORF (purple) and *ura4+* expression cassette (green and red). This cassette can be excised by BstBI-HindIII digest for integration at the wild-type *stn1⁺* locus. **(B)** Schematic indicating the integration of P*stn1*-loxP-*stn1⁺-ura4⁺*-loxM3-T*stn1* cassette into the wild type *stn1⁺* locus by homologous recombination with the BstBI-HindIII fragment of pmutSpStn1-3. Integration can be selected for by *ura4⁺* expression.

5.2.3 Telomere length analysis of loxP-*stn1+-ura4+*-loxM3 base strain

This *stn1+-ura4+* base strain was then transformed with linearised pSpRqh1D-H, as done previously to disrupt *rqh1+* in the *pot1-1* background. These two strains were streaked out to single colonies on YES agar 8 times to equilibrate the telomere lengths. The telomere lengths were then assessed by southern blot on ApaI-digested genomic DNA using a telomere-specific probe [Fig 5.4]. This was to check that the modification of the promoter had not dramatically affected capping or any telomerase inhibition functions.

The southern blot indicated that the wild-type strain had telomeres of the expected 300bp length. The *stn1+-ura4+* strains (nr1 and nr2) as well as *stn1+-ura4+ rqh1Δ* strains (nr1 and nr2) had mildly elongated telomeres at approximately 700-800bp. This elongation may be due to disruption of the endogenous *stn1+* promoter with the loxP site. If the *S. pombe* Stn1-Ten1 complex functions similarly to CST in mammals and budding yeast to inhibit telomerase recruitment to the telomeric ssDNA in addition to the capping function it would be expected that any reduced expression would lead to telomere elongation. Reduced expression of *stn1+*, and therefore fewer Stn1-Ten1 protein complexes bound to the telomeric G-strand overhang may enable better access to the telomere ssDNA telomerase substrate. For the purpose of this study, the slight increase in telomere length was inconsequential and still allowed the strain to be used for identification of temperature-sensitive alleles.
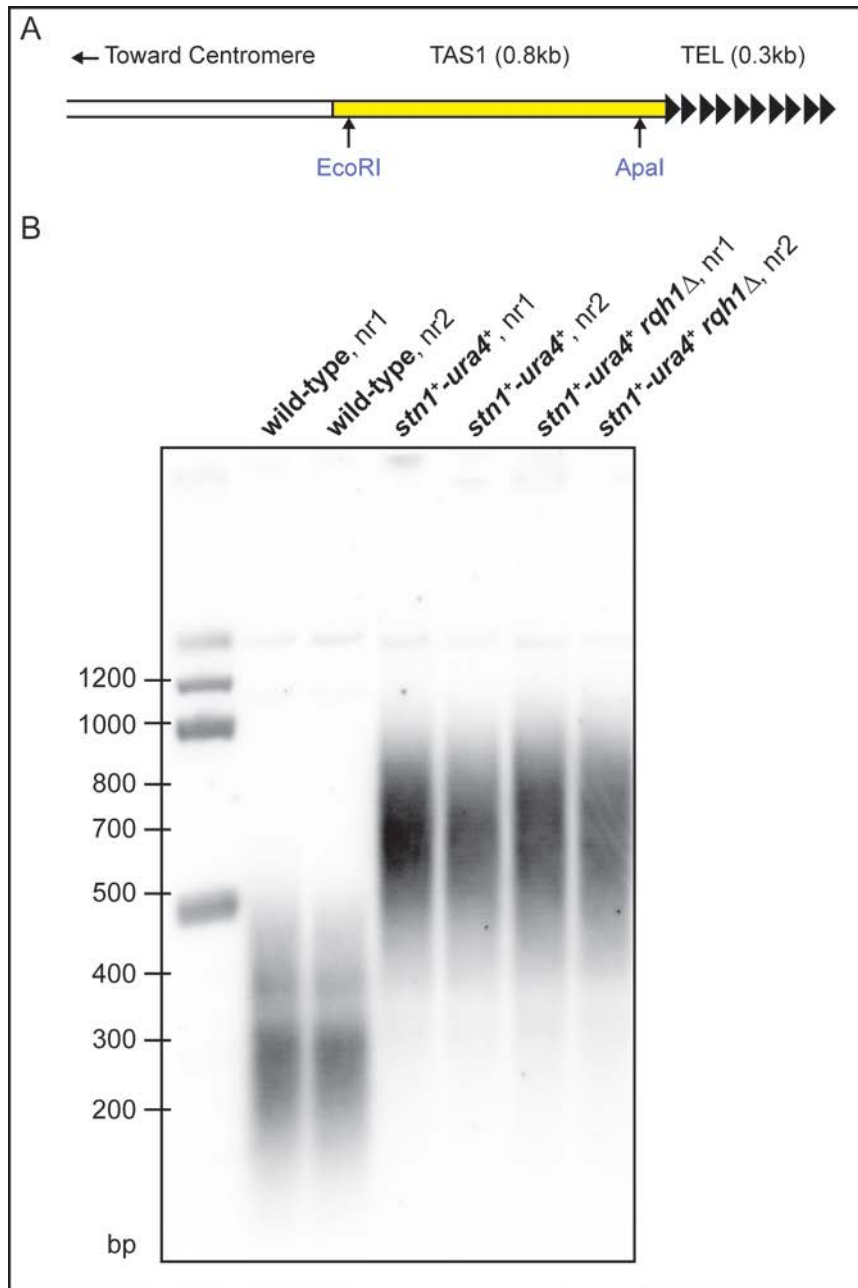
Figure 5.4: Telomere length analysis of *stn1⁺-ura4⁺* and *stn1⁺-ura4⁺ rqh1Δ* strains.

(A) Schematic of *S. pombe* telomere showing locations of EcoRI and ApaI sites relative to telomere (TEL) and TAS1 region (yellow). Telomere sequence-specific probe from pSpTelo binds to TEL region (approximately 0.3kb in wild-type strains). Genomic DNA from wild type strains digested with ApaI are, therefore, expected to be approximately 300bp. Digests with EcoRI result in an additional 800bp of TAS1 sequence. **(B)** Southern blot analysis of the telomere lengths of wild-type, *stn1⁺-ura4⁺* and *stn1⁺-ura4⁺ rqh1Δ* strains from ApaI-digested genomic DNA (samples loaded in duplicate, indicated by 'nr1' and 'nr2'). The wild-type strain has telomeres of the expected length. Test strains, *stn1⁺-ura4⁺* and *stn1⁺-ura4⁺ rqh1Δ*, both have slightly elongated telomeres at approximately 700-800bp This is likely to be a result of modification of the *stn1* promoter region to include loxP and NdeI sites.

5.2.4 Construction of vectors for mutagenesis of *stn1*

The ploxPM3SpStn1-1 and ploxPM3SpStn1-5 vectors were constructed to allow mutagenesis of

stn1⁺ by more than one method, in order to maintain flexibility. The loxP-*stn1*⁺-loxM3 fragment

from pmutSpStn1-2 was subcloned by SbfI-AscI digest into the same sites in pAW8loxless

(provided by Adam Watson, Carr lab) to make ploxPM3SpStn1-1 [Fig 5.5A]. This vector,

containing *LEU2* and the Cre-recombinase gene under control of P*nmt41* was constructed for

use in methods requiring complete vector for mutagenesis, for example, with mutagenic *E. coli*

strains such as Agilent XL-1 Red cells or the Agilent GeneMorph II mutagenesis kit. In this

particular case, however, error-prone PCR became the preferred choice. This required the

construction of ploxPM3SpStn1-5 by subcloning the PstI-AscI loxP-*stn1*⁺-loxM3 fragment from

ploxPM3SpStn1-1 into pFY412 [Fig 5.5B]. This generated a vector with an *ade6*⁺ marker that

could be transformed separately to a vector that expressed Cre-recombinase. Appropriate

primer sites for error-prone PCR are also located flanking the insert.

Error-prone PCR using the primers MUC-OA and MUC-OS could then be used to amplify the

entire loxP-*stn1*⁺-loxM3 cassette. This PCR product could then be transformed into the *stn1*⁺-

ura4⁺ *rqh1Δ* base strain for integration at the *stn1* locus by RMCE [Fig 5.5C].

5.2.5 Mutagenesis of *stn1+* by error-prone PCR

Using the ploxPM3SpStn1-5 vector as a template, a series of error-prone PCRs were run using

the primers MUC-OA and MUC-OS. This was done under the conditions described in the

methods with the aim of generating the minimum number of mutations per kb of target DNA.

From six separate reactions, the PCR product size of 1498bp was verified by agarose gel

electrophoresis. The separate reactions were then combined and purified using the Qiagen

QIAquick PCR purification kit.

Figure 5.5: Schematic of plasmids constructed for *stn1⁺* mutagenesis and integration into *stn1::stn1⁺-ura4⁺* locus by RMCE (following page).

(A) The ploxPM3SpStn1-1 plasmid is designed for whole-plasmid mutagenesis. It was made by subcloning the SbfI-AscI fragment from pmutSpStn1-2 into same sites in pAW8loxless. The ploxPM3SpStn1-1 plasmid contains the wild-type *stn1⁺* ORF (purple) flanked by loxP and loxM3 recombination sites (yellow). The plasmid also contains the Cre-recombinase gene (*cre*) under the control of the *nmt41* promoter (P*nmt41*) and terminator (T*nmt1*), a *LEU2* selection marker and ARS1 origin sequence for maintenance in yeast, as indicated. **(B)** The ploxPM3SpStn1-5 plasmid is designed for mutagenesis of *stn1⁺* by error-prone PCR. It was made by subcloning the PstI-AscI fragment from ploxPM3SpStn1-5 into same sites in pFY412. Primer sites for MUC-OA and MUC-OS (indicated in red) flanking the insert allows the loxP-*stn1⁺-ura4⁺*-loxM3 cassette to be amplified by error-prone PCR. The final ploxPM3SpStn1-5 plasmid also contains an *ade6⁺* marker and ars3002 origin sequence. **(C)** Integration of the mutagenized *stn1* ORF, *stn1^mutX^* (mutations indicated by red bars), into the base strain is achieved by RMCE. The *stn1⁺-ura4⁺* base strain contains the wild-type *stn1⁺* gene (purple) followed by a *ura4⁺* marker (red with promoter and terminator in green), both flanked by loxP and loxM3 sites (yellow) at the *stn1* locus. Integration of *stn1^mutX^* results in loss of the *ura4⁺* cassette leaving the mutagenised *stn1^mutX^* flanked by loxP and loxM3 sites, which are all flanked by the *stn1* promoter (P*stn1*) and terminator (T*stn1*) sequences (dark blue).
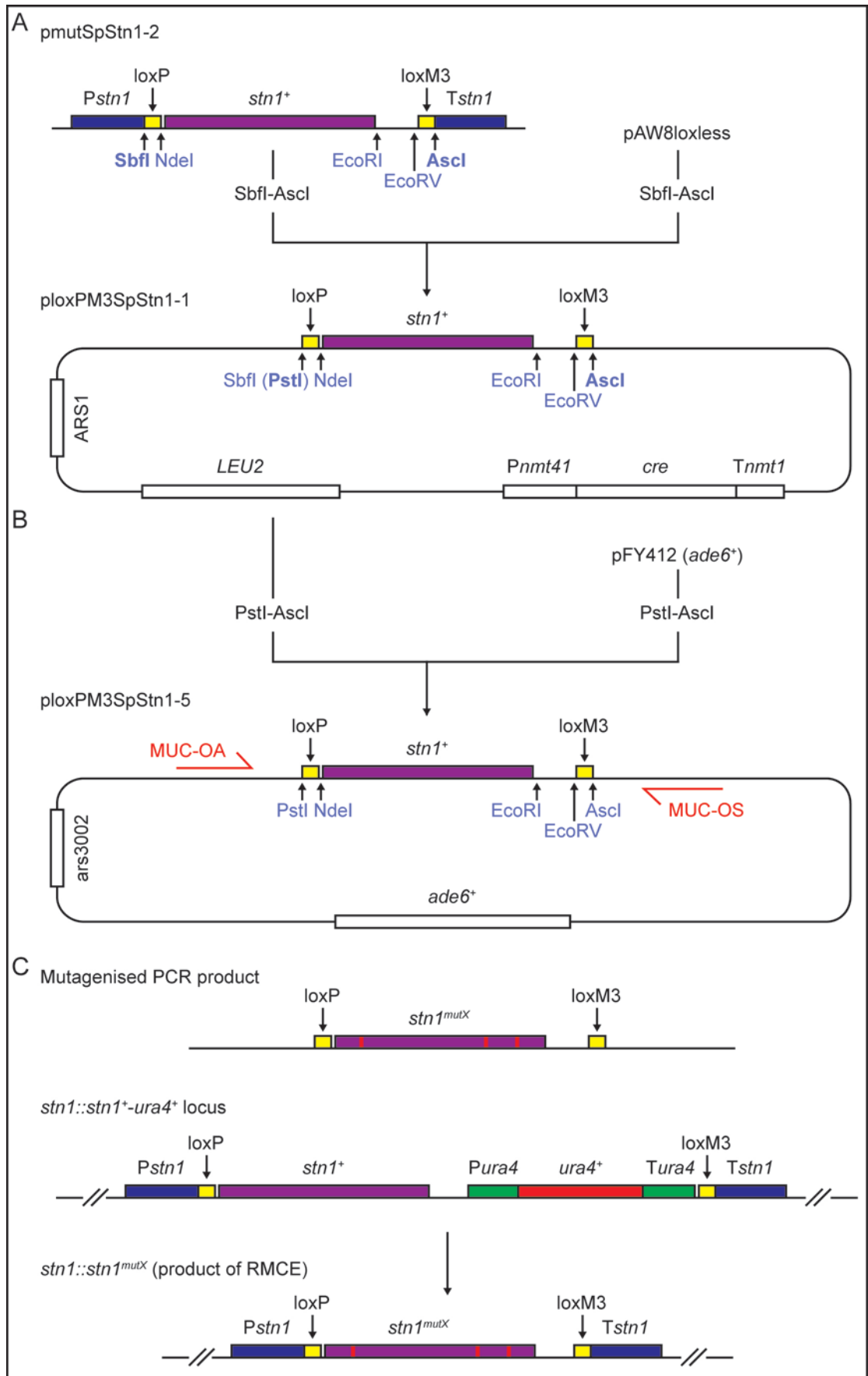
5.2.6 Screening for *stn1* temperature sensitive alleles

The *stn1$^+$-ura4$^+$ rqh1Δ* base strain was initially transformed with pAW8loxless, a plasmid containing Cre-recombinase gene under *nmt81* promoter control but without loxP and loxM3 sites. The transformation was plated on YNG −Leu agar plates with thiamine. The absence of loxP and loxM3 sites in the vector ensures that, no substrates for recombination are available. Only the loxP and loxM3 sites at the *stn1* locus are present, which cannot recombine with each other. Transformants were streaked to fresh YNG −Leu agar with thiamine before one was selected for inoculation in YNG −Leu media (without thiamine, to activate *cre* expression) for transformation with the mutagenised PCR product.

A series of five transformations with the *stn1$^+$-ura4$^+$ rqh1Δ* base strain (pre-transformed with pAW8loxless) were prepared. The purified PCR product from the error-prone PCR mutagenesis was transformed, 1µg per transformation into the base strain and plated on five YNG −Leu agar plates without thiamine. The plates were then incubated at 25°C for two days to allow the Cre-recombinase to act and integrate the mutagenized *stn1* ORF at the modified *stn1* locus. The transformed cells were then replica-plated onto YES + 5-FOA and incubated at 25°C until colonies of at least 2mm in diameter were visible. Switching to *ura4$^+$* counter-selection at this early stage allows only those colonies containing cells which have integrated the mutagenised *stn1* ORF to be further processed.

The colonies were then replica-plated again to two fresh YES + 5-FOA plates per source plate. One was incubated at 25°C and the other at 36°C for a further 2 to 3 days until differences in growth due to loss of viability were apparent. The colonies were scored for adequate growth at 25°C and loss of viability at 36°C. Those matching these desired criteria were streaked to single colonies from the 25°C plate to fresh YES + 5-FOA plates and incubated at 25°C for further processing.

5.2.7 Identification of *stn1* temperature-sensitive alleles integrated at modified *stn1* locus

From the candidates, two temperature-sensitive alleles were identified. Candidates 75 and 99 were able to grow to single colonies at 25°C but unable to form colonies at 36°C [Fig 5.6]. These alleles were designated *stn1-75* and *stn1-99*. Other candidates did have some sensitivity to 36°C, but were able to form single colonies, indicating the sensitivity may not be a result of complete loss of end-capping.

5.2.8 Sequencing analysis of *stn1-75 and stn1-99*

The *stn1* locus of the two strains that exhibited a viability phenotype at 36°C was amplified by high fidelity PCR using the primers Pstn1-f2-Sp and Tstn1-b2-Sp, purified and sent for sequencing using the same primers. The sequencing indicated that the first allele, designated *stn1-75*, contained two mutations which would lead to one amino acid change [Fig 5.7]. The second allele, designated *stn1-99*, contained just one mutation, slightly further downstream than the mutation that causes an amino acid substitution in *stn1-75* [Fig 5.8]. The positions of the substitutions in both alleles were compared against previous Stn1 alignment data (Sun *et al.*, 2009) [Fig 5.9A-B]. This revealed that the amino acid substitution from *stn1-75* is located in the C-terminus towards the beginning of the Stn1 WH1 motif. The amino acid substitution from *stn1-99* is also located in the C-terminus, this time towards the end of the first WH1 motif. Interestingly, though a specific function for the two predicted helix-turn-helix WH motifs hasn't been identified, the equivalent motif in budding yeast Stn1 has been show to interact with Cdc13 (Chen and Lingner, 2013). Given the structural similarities of the Stn1 proteins from each organism, it is possible that these amino acid substitutions are disrupting the interaction with another protein, possibly even an unidentified Cdc13 homologue.
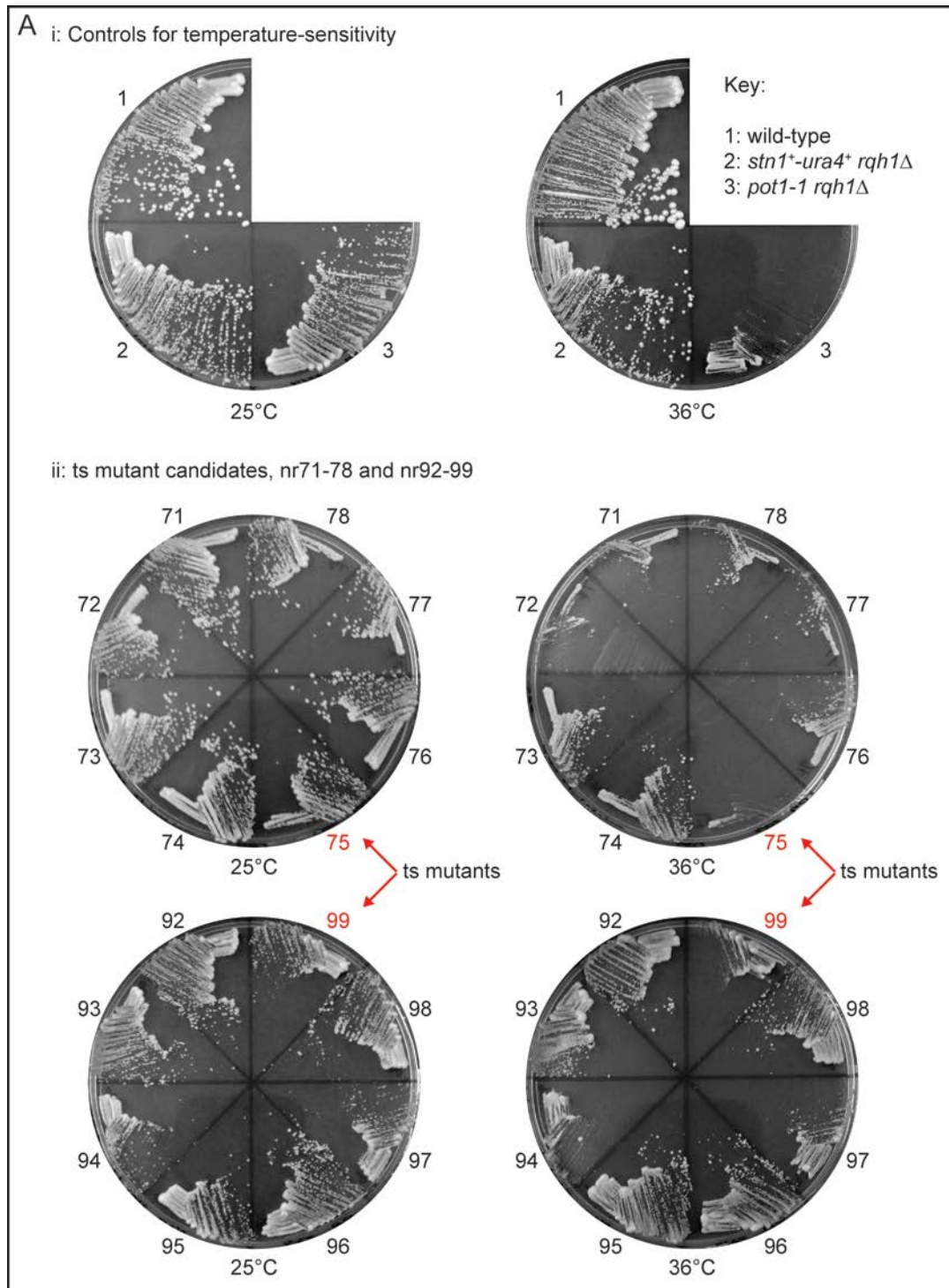
Figure 5.6: Identification of two *stn1* temperature-sensitive alleles, *stn1-75* and *stn1-99*.

(A) (i) Control strains for temperature-sensitivity were streaked on YES agar plates and incubated at 25°C and 36°C. Wild-type and *stn1⁺-ura4⁺ rqh1Δ* strains form colonies at both 25°C and 36°C. The *pot1-1 rqh1Δ* strain forms colonies at 25°C but not at 36°C. **(ii)** Temperature-sensitive candidate strains were streaked on YES at 25°C and 36°C. Two candidates, numbers 75 and 99 out of the 16 shown, displayed viability loss at 36°C as indicated by lack of colony formation (red arrows).
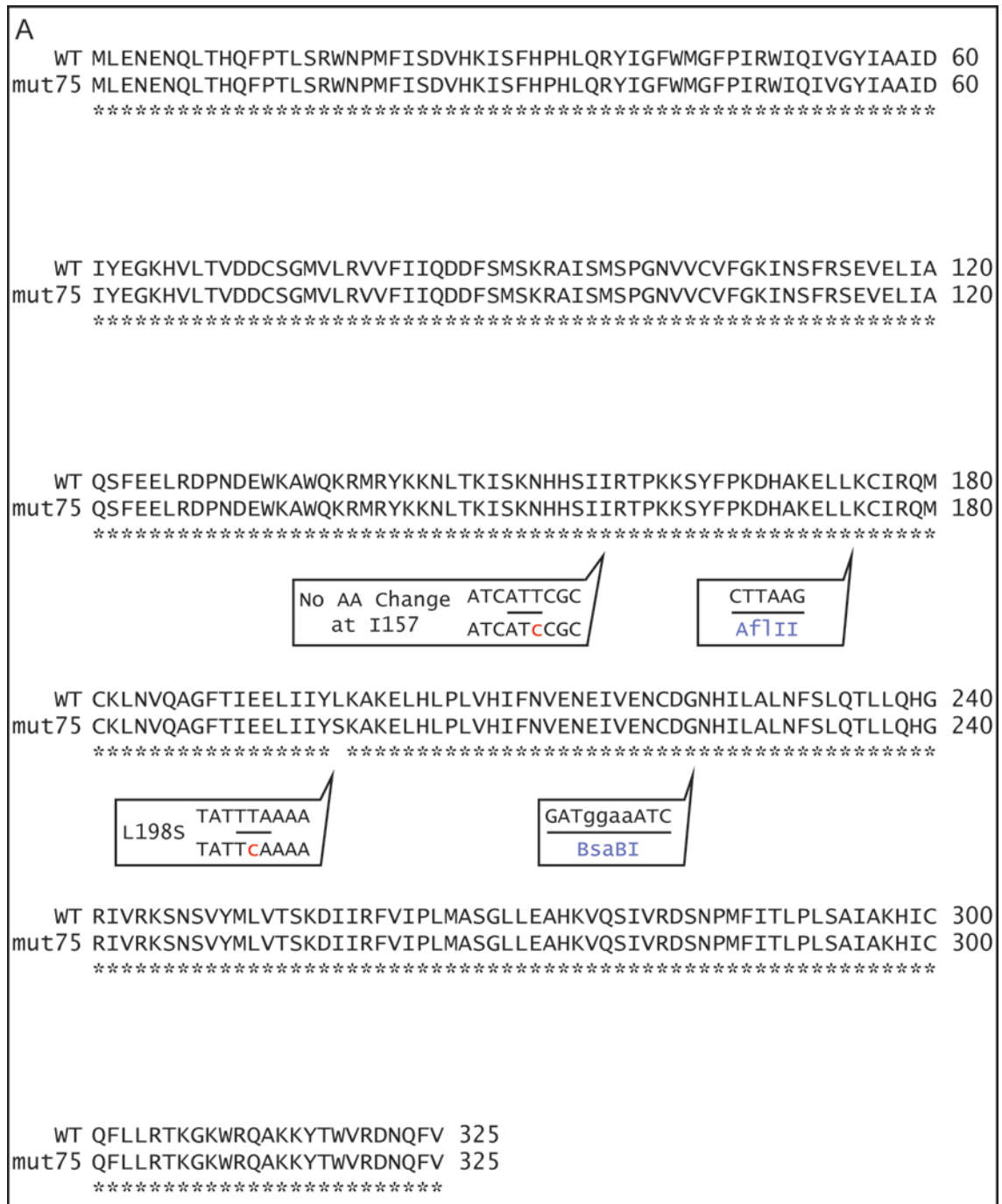
Figure 5.7: Alignment of Stn1 peptide sequence, comparing wild-type to mutant number 75 (*stn1-75*).

(A) Peptide sequence alignment of wild-type Stn1 and mutant 75 (*stn1-75*) from Clustal Omega. Sequence changes at the nucleotide level are highlighted in boxes. The uppercase nucleotide sequence is wild-type and lowercase red sequence indicates the mutation. The horizontal line separating the wild-type sequence (top) and mutant 75 sequence (bottom) indicates the codon affected. The alignment indicates that the amino acid I157 is not affected by a nucleotide change. There is one amino acid substitution towards the C-terminus of the protein: L198S. The AflII and BsaBI restriction sites, indicated in blue, are unaffected. An * (asterisk) indicates positions which have a single, fully conserved residue. A : (colon) indicates conservation between strongly similar residues. A . (full stop) indicates positions which have a single, weakly conserved residue. An empty space indicates dissimilar residues.
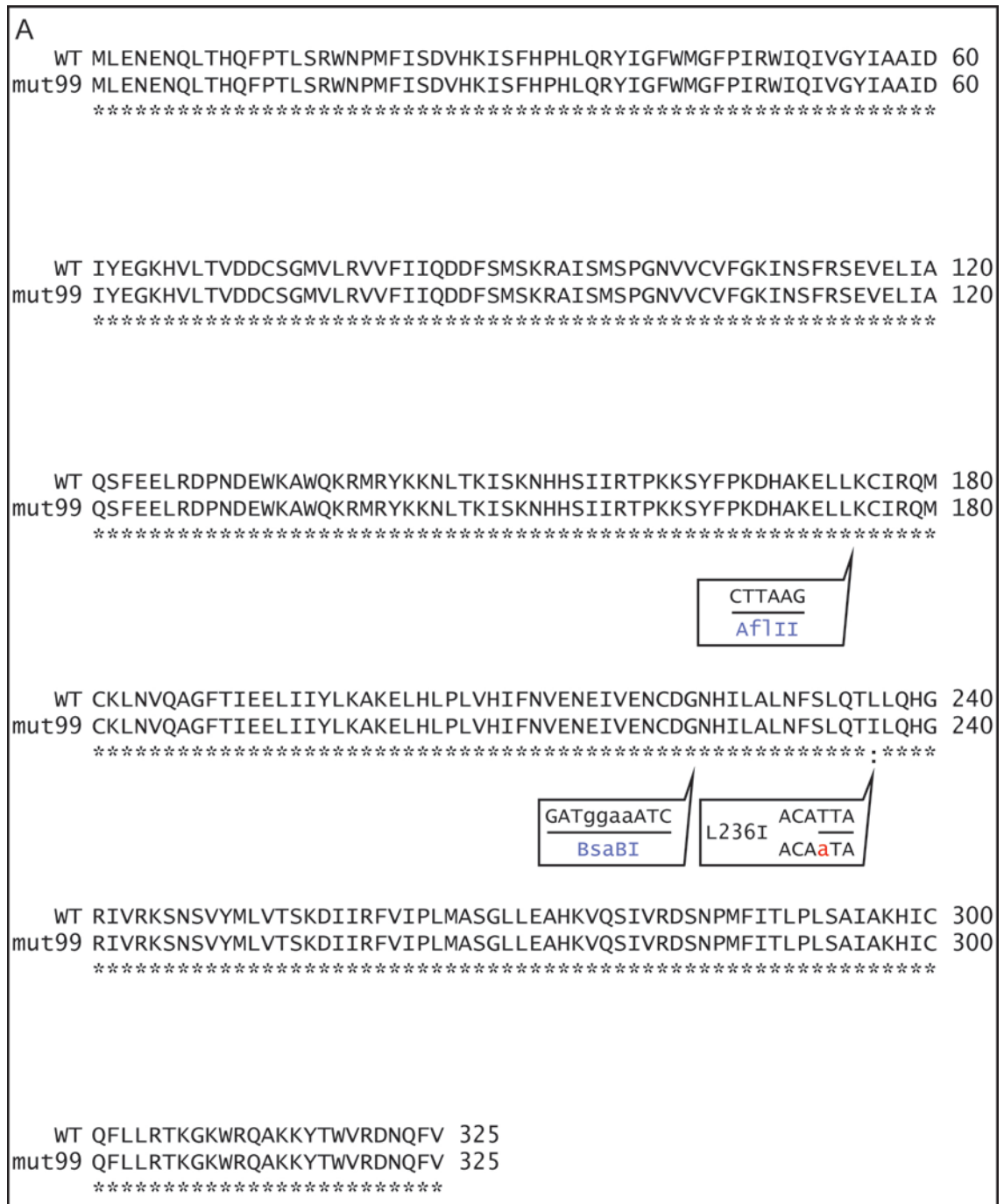
Figure 5.8: Alignment of Stn1 peptide sequence, comparing wild-type to mutant 99 (*stn1-99*).

(A) Peptide sequence alignment of wild-type Stn1 and mutant 99 (*stn1-99*) from Clustal Omega. Sequence changes at the nucleotide level are highlighted in boxes. The uppercase nucleotide sequence is wild-type and lowercase red sequence indicates the mutation. The horizontal line separating the wild-type sequence (top) and mutant 99 sequence (bottom) indicates the codon affected. The alignment indicates that there is one amino acid substitution towards the C-terminus of the protein: L236I. The AflII and BsaBI restriction sites, indicated in blue, are unaffected. An * (asterisk) indicates positions which have a single, fully conserved residue. A : (colon) indicates conservation between strongly similar residues. A . (full stop) indicates positions which have a single, weakly conserved residue. An empty space indicates dissimilar residues.

5.2.9 Analysis of the conservation of residues substituted in *stn1-75* and *stn1-99*

The sequence analysis of the two *stn1* alleles indicated that the amino acid substitutions were located in the C-terminus of the protein. Previous studies of the Stn1 protein identified the domains of *S. cerevisiae* Stn1 based on crystal structure analysis of the N-terminus and C-terminus (Gelinas *et al.*, 2009, Sun *et al.*, 2009). The C-terminus of *S. cerevisiae* Stn1 was determined to contain two winged Helix-Turn-Helix motifs [PDB ID: 3KEY or 3K10], herein referred to as WH motifs. The WH1 motif of *S. cerevisiae* Stn1 was found to be very similar to the WH (winged Helix-Turn-Helix) motif of *H. sapiens* RPA32 [PDB ID: 1Z1D or 1DPU]. An alignment of these motifs with Stn1 from several other species, including *S. pombe*, identified several conserved hydrophobic residues [Fig 5.9A]. By comparing this alignment to the substitutions in *stn1-75* and *stn1-99* it was determined that the affected residues, Leucine 198 and Leucine 236, were not only located within the predicted WH1 motif of *S. pombe* Stn1, but were also two of these conserved residues [Fig 5.9B].

To further study the conservation of these residues, the predicted WH1 motif of *S. pombe* Stn1 was compared to the Stn1 peptide sequence of other yeast in the *Schizosaccharomyces* genus using Clustal Omega. This alignment was merged with the previously established alignment by Sun *et al.* (2009) [Fig 5.9A]. In addition, due to the structure of *S. pombe* Stn1 being unsolved, the secondary structure of *S. cerevisiae* Stn1 WH1 motif was aligned to the peptide sequence to aid identification of structural features that may be affected by substitutions in *stn1-75* and *stn1-99* [Fig 5.9A].

The alignment of Stn1 WH1 between species in the *Schizosaccharomyces* genus indicated that this motif had several well conserved residues. On merging with the alignment by Sun *et al.* (2009), several of the previously identified conserved hydrophobic residues appear to also be well conserved in the *Schizosaccharomyces* genus. These include *S. pombe* Stn1 Leucine 198 and Leucine 236; the affected residues in the *stn1-75* and *stn1-99* alleles. Leucine 198 is fairly

well conserved, with identical or similar (isoleucine and valine) residues present in almost all sequences in the alignment. The exception is *S. cryophilus*, which contains a hydrophobic, but structurally very different (aromatic) phenylalanine. Leucine 236 is very well conserved, with identical residues in almost all sequences. The exception is *S. pombe* Stn1 WH2, which has previously been shown to align better with *S. cerevisiae* Stn1 WH1, but with fewer conserved residues than *S. pombe* WH1. In this case, a hydrophilic and structurally different arginine is present in the place of a leucine. The high conservation of both of these hydrophobic residues, L198 and L236, would imply that they are structurally or functionally important. Based on the secondary structure, the residues equivalent to *S. pombe* Stn1 L198 and L236 were identified to be L323 and L380 of *S. cerevisiae* Stn1 WH1. From this, it was proposed that the α1- and α3-helices of the motif were the structures affected by the amino acid substitutions.

Figure 5.9: Comparison of Stn1 WH motif residue conservation between species in the *Schizosaccharomyces* genus as well as others, as used by Sun *et al.* (2009), and identification of secondary structure elements affected in *stn1-75* and *stn1-99* alleles (following page).

(A) Alignment of winged Helix-Turn-Helix (WH) motif peptide sequences from Stn1 in the species indicated and *H. sapiens* RPA32. The alignment of WH domains from Sun *et al.* (2009) was combined with a new alignment of the Stn1 WH1 sequences from the species in the *Schizosaccharomyces* genus: *S. octosporus*, *S. cryophilus* and *S. japonicas* using Clustal Omega and visualised using Boxshade. The protein accession numbers are as follows: NP_010367 (*S. cerevisiae* Stn1), XP_714522 (*C. albicans* Stn1), CTRG_01841 (*C. tropicalis* Stn1), XP_001713126 (*S. pombe* Stn1), NP_002937 (*H. sapiens* RPA32), EPX74243 (*S. octosporus* Stn1), EPY49365 (*S. cryophilus* Stn1) and EEB07276 (*S. japonicas* Stn1). Residues that are fully conserved in at least half of the sequences compared are highlighted in black while similar residues are highlighted in grey. Dashed lines indicate a gap in the sequence due to the alignment. The secondary structure of *S. cerevisiae* Stn1 WH1 was obtained from Sun *et al.* (2009). This was aligned to the *S. cerevisiae* Stn1 WH1 peptide sequence. The positions of conserved hydrophobic residues identified by Sun *et al.* (2009) are indicated by black triangles. The positions of the residues affected in *S. pombe* *stn1-75* and *stn1-99* are indicated by blue and red triangles respectively. The *S. pombe* L198 residue is conserved as small hydrophobic residues (Leucine, Isoleucine and Valine) in all but *S. cryophilus*. The *S. pombe* L236 residue is conserved in all sequences except *S. pombe* Stn1 WH2. Mapping these residues to the secondary structure from *S. cerevisiae* Stn1 WH1 indicates that the α1- and α3-helices would be affected by the substitutions. Notably, neither the *Schizosaccharomyces* genus species nor *H. sapiens* RPA32 contain the insertion relating to the *S. cerevisiae* Stn1 WH1 α2'-helix. **(B)** Schematic of the full length *S. pombe* Stn1 protein (325 amino acids) showing the locations of the OB fold (green), WH1 (yellow) and WH2 (blue) motifs. Positions of the WH domains are based on the alignment with *S. cerevisiae* Stn1 WH1 by Sun *et al.* (2009). The location of the L198S and L236I substitutions within the WH1 motif are indicated.

A Stn1 wHTH peptide sequence alignment
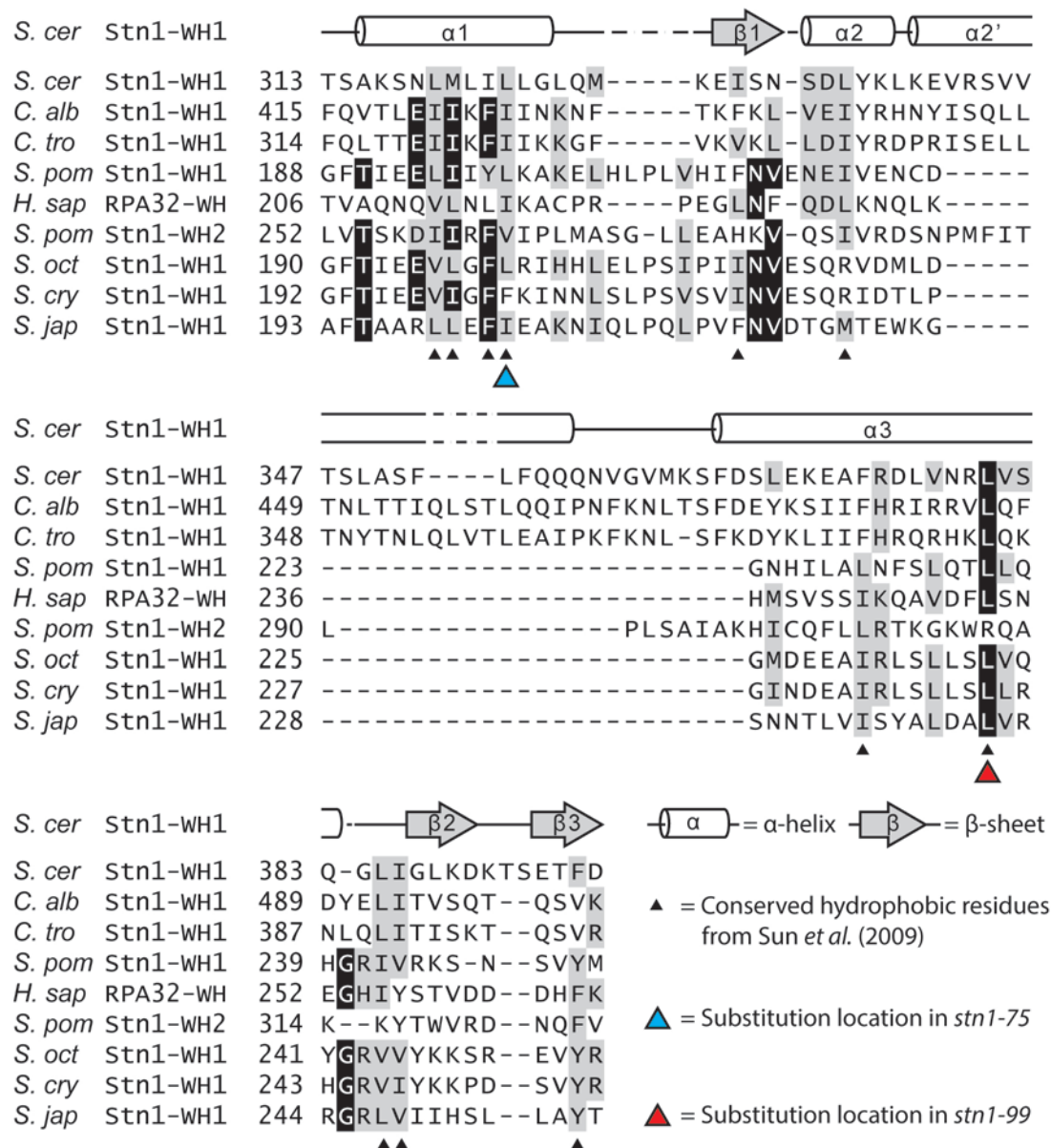
B stn1-75 and stn1-99 allele protein structure
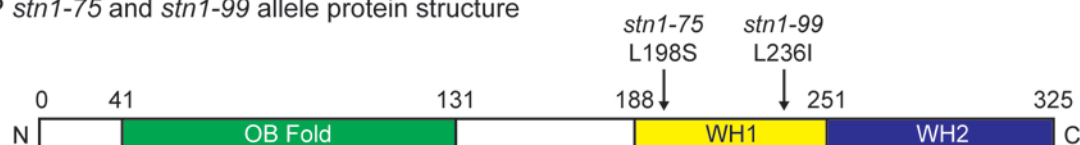
5.2.10 Structural conservation of *S. pombe* WH1 motif

With the conserved residues in *S. cerevisiae* Stn1 WH1 now identified, further analysis of the specific structures affected by the L198S and L236I substitutions in *S. pombe* could be conducted. If the structure of the WH1 motif in *S. pombe* Stn1 could be determined, the data obtained through this analysis would be more trustworthy. Therefore, due to the unavailability of a crystal structure for *S. pombe* Stn1 C-terminus, a secondary structure prediction was run with PSIPRED, using the *S. pombe* Stn1 WH1 peptide sequence as a template. Although the *S. cerevisiae* Stn1 contained the conserved hydrophobic residues L323 and L380 (equivalent to L198 and L236 in *S. pombe* Stn1), the peptide sequence contains an insertion not present in *S. pombe* Stn1 WH1 (the α2'-helix). This additional section is only conserved in *C. albicans* and *C. tropicalis*. Due to this, *H. sapiens* RPA32 was selected as an alternative structure for comparison with *S. pombe* Stn1 WH1. A solved crystal structure for the C-terminal WH motif was available [PDB ID: 1Z1D or 1DPU] and it did not contain the additional sequence relating to the a2'-helix. It also contained conserved residues, Isoleucine 216 and Leucine 249, which were equivalent to the L198 and L236 residues of interest. This was, therefore, predicted to be potentially a better structural template on which to map the amino acid substitutions from *stn1-75* and *stn1-99*.

The predicted secondary structure of *S. pombe* Stn1 WH1 was, therefore, compared to both the secondary structure of *S. cerevisiae* Stn1 WH1 and *H. sapiens* RPA32 WH motif [Fig 5.10]. Also, to aid direct comparison of the structural features, the secondary structures for each protein WH1 motif were aligned to match with the peptide sequences alignment in Fig 5.9A.
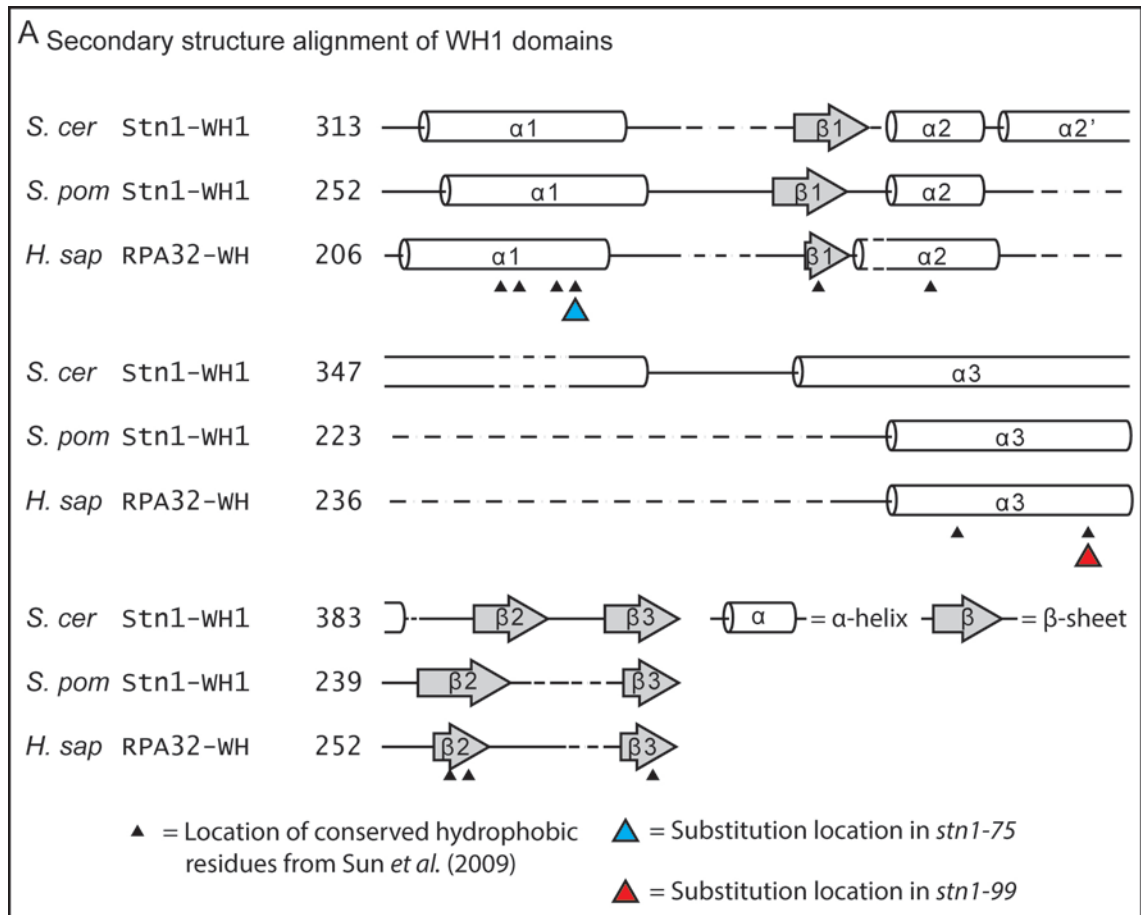
Figure 5.10: Alignment of secondary structures for WH1 motifs in *S. cerevisiae* Stn1, *S. pombe* Stn1 and *H. sapiens* RPA32.

(A) Secondary structure of *S. cerevisiae* Stn1 WH1 motif is displayed as shown in Fig. 5.9, based on the solved crystal structure [PDB ID: 3KEY]. A secondary structure prediction of *S. pombe* Stn1 WH1 was generated using PSIPRED with the peptide sequence as a template. Three α-helices and three β-strands are predicted in the confirmation: α-β-α-α-β-β, as found in *S. cerevisiae* Stn1 WH1 (barring the additional α2'-helix). This structure prediction is shown aligned to the *S. cerevisiae* Stn1 WH1 structure, based on the sequence alignment in Fig. 5.9. The secondary structure of *H. sapiens* RPA32 WH motif was determined using the solved crystal structure [PDB ID: 1Z1D and 1DPU] and aligned to the other structures based on the sequence alignment in Fig. 5.9. The alignment of the structures indicates good structural conservation between *S. pombe* Stn1 WH1 and *H. sapiens* RPA32 WH motifs. The positions of the conserved hydrophobic residues identified by Sun *et al.* (2009), as they relate to the secondary structures, are shown by black triangles. The positions of the residues affected in S. pombe stn1-75 and stn1-99 are indicated by blue and red triangles respectively. The L198 residue substituted in *stn1-75* is located in the predicted α1-helix of *S. pombe* Stn1 WH1. The L236 residue substituted in *stn1-99* is located in the predicted α3-helix of *S. pombe* Stn1 WH1. Dashed lines indicate gaps in the sequence due to the alignment.

The comparison of secondary structures between the previously solved *S. cerevisiae* Stn1 WH1 and *S. pombe* WH1 indicates that there is good structural conservation between these motifs. Taking into account the lack of the additional α2'-helix, the secondary structure *S. pombe* Stn1 WH1 is predicted to consist the α-β-α-α-β-β conformation that is similar to a typical winged helix-turn-helix motif. Therefore, the amino acid substitutions in *stn1-75* and *stn1-99* would indeed affect the α1 and α3-helices respectively, as previously suggested. Taking into account the high conservation of each of the residues, it is possible that L198S and L236I substitutions could disrupt the structure of these helices and, therefore, destabilise the protein enough to generate the temperature-sensitive phenotypes.

The *H. sapiens* RPA32 WH1 structure resembled the predicted structure of *S. pombe* Stn1 WH1 more closely than *S. cerevisiae* Stn1 WH1, as expected. The α-β-α-α-β-β conformation is followed here as well with the positions of the structures aligning better than those of *S. cerevisiae* Stn1 WH1.

5.2.11 *S. pombe* Stn1 residues of interest, L198 and L236, modelled on the solved C-terminal crystal structures of *S. cerevisiae* Stn1 and *H. sapiens* RPA32

In order to study the likelihood and extent of protein structure disruption in *S. pombe*, the L198S and L236I substitutions were mapped to the solved crystal structure of a homologous protein. The C-terminus of *S. cerevisiae* Stn1 [PDB ID: 3KEY] was initially used as the template [Fig 5.11A-C]. The hydrophobic L323 and L280 residues (equivalent to L198 and L236 in *S. pombe* Stn1) were found to be located on the hydrophobic surfaces of the α1- and α3-helix respectively, as would be expected from the secondary structure comparisons. These residues are found to be relatively close on the hydrophobic surfaces of adjacent α-helices [Fig 5.11B]. The C-terminal structure of *H. sapiens* RPA32 [PDB ID: 1Z1D] was also used to identify the relative locations of the conserved residues, I216 and L249 [Fig 5.11D-F]. This structure shows

that the residues in question are again fairly close and the α-helices in the same configuration as *S. cerevisiae* Stn1 WH1. Although there is some difference in positioning, the absence of the α2'-helix in RPA32 does not appear to affect the relative orientation of the α1- and α2-helices to any great degree. Given that this configuration of secondary structure elements is typical of winged Helix-Turn-Helix motifs, it is possible that the orientations of these features are a conserved and functionally important element of the motif.

Figure 5.11: Position of conserved residues in *S. cerevisiae* Stn1 and *H. sapiens* RPA32 that are equivalent to *S. pombe* Stn1 residues of interest, L198 and L236 (following page).

(A) The *S. cerevisiae* Stn1 C-terminal crystal structure [PDB ID: 3KEY] is shown as a cartoon representation oriented with the α1- and α2'-helices of the WH1 motif in the foreground. The WH1 and WH2 motifs each consist of a series of helices and beta strands in the conformation: α-β-α-α-β-β, as labelled. The conserved residues, L323 and L380, are located in the α1- and α3-helices and indicated in blue and red respectively. **(B)** Close-up view of the location of the conserved L323 and L380 residues in the *S. cerevisiae* Stn1 WH1 motif shown in blue and red respectively. The orientation of the structure is the same as in (A). Secondary structure components in proximity of the conserved residues are indicated. **(C)** The *S. cerevisiae* Stn1 C-terminal crystal structure rotated 90° from the cartoon representation in (A), as indicated. The conserved residues, L323 and L380, are shown in blue and red respectively. **(D)** The *H. sapiens* RPA32 C-terminal crystal structure [PDB ID: 1Z1D] is shown as a cartoon representation oriented with the α1- and α2-helices in the foreground. The WH motif consists of a series of helices and beta strands in the conformation: α-β-α-α-β-β, as labelled. The conserved residues, I216 and L249, are located in the α1- and α3-helices and indicated in blue and red respectively. **(E)** Close-up view of the location of the conserved I216 and L249 residues in the *H. sapiens* WH motif shown in blue and red respectively. The orientation of the structure is the same as in (D). Secondary structure components in proximity of the conserved residues are indicated. **(F)** The *H. sapiens* RPA32 C-terminal crystal structure rotated 90° from the cartoon representation in (D), as indicated.

A   *S. cer* Stn1 C-terminus

B

C

D   *H. sap* RPA32 C-terminus

E

F
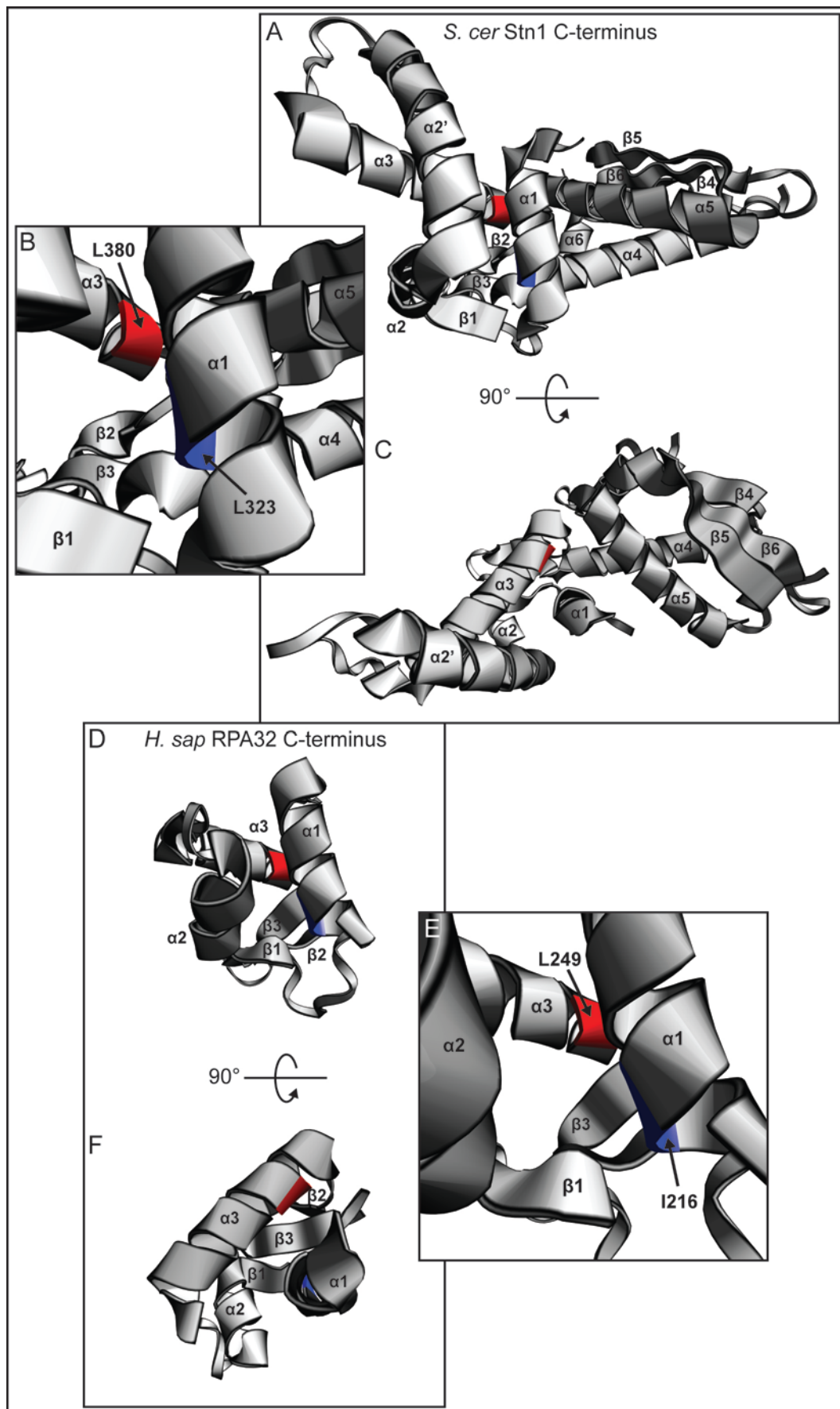
5.2.12 Conservation between *S. pombe* Stn1 and *H. sapiens* STN1 WH motifs

In a comparison of the N-terminal OB-fold of *H. sapiens* and *S. pombe* Stn1, several conserved residues were identified (Miyake *et al.*, 2009). To determine whether this conservation extends to the WH motifs, the *S. pombe* Stn1 WH1 sequence was compared to the *H. sapiens* WH1 and WH2 motifs, as determined from the recently solved C-terminal crystal structure (Bryan *et al.*, 2013), using Clustal Omega. The *H. sapiens* RPA32 WH motif was also aligned. Multiple conserved residues were identified, though conservation did not appear to be as robust as what was found in the Stn1 OB fold [Fig 5.12A]. The initial 19 residues of *H. sapiens* STN1 WH1 did not align to *S. pombe* Stn1 WH1, the *H. sapiens* RPA32 WH or the *H. sapiens* STN1 WH2 motif. In addition, another insertion is present after a further 22 residues is present. The WH2 motif, on the other hand, appeared to align better, though it indicated the presence of several smaller insertions when compared to the *S. pombe* Stn1 WH1 and *H. sapiens* RPA32 WH sequences.

Based on the alignments, the residue equivalent to *S. pombe* Stn1 L198 looked to be F224 in the WH1 motif and Q309 in the WH2 motif. Although F224 is a hydrophobic residue, it has a much larger side chain than a leucine or isoleucine that would be expected in this position based on previous alignments. Although some variation was seen, in the sequences compared previously, one of the small hydrophobic residues (leucine, isoleucine or valine) tended to be present. Q309 is not hydrophobic. Instead, it has a neutrally charged, but polar side chain. This called into question the accuracy of the alignment. Indeed, when examining both of these residues in the crystal structure of *H. sapiens* STN1 C-terminus [PDB ID: 4JQF], they were not found in the positions that would be expected for conserved, properly aligned residues. F224 is found on the β-strand immediately before the α4-helix, rather than within the α3-helix. Q309 is found in the expected α8-helix, but not on the hydrophobic surface [Fig 5.12B-E]. The additional non-conserved residues shown in the alignment equated both additional and slightly longer α-helices in both *H. sapiens* STN1 WH1 and WH2 than found in RPA32 or *S.*

cerevisiae Stn1. Using the *H. sapiens* RPA32 crystal structure as a template, and the position of the conserved I216 residue on this template, a more likely residue equivalent to *S. pombe* Stn1 L198 was identified. L216 in the WH1 motif is located on the hydrophobic surface of the α3-helix, in approximately the same position as I216 in RPA32. Doing the same for the WH2 motif, I308 was identified, located on the hydrophobic surface in a similar position in the α8-helix.

The alignment for the second residue of interest from *S. pombe* Stn1, L236, appears to be accurate. This residue, already found to be conserved in several species including *H. sapiens* RPA32, has equivalent residues in *H. sapiens* STN1 WH1 and WH2. The WH1 residue is identified as L274, found on the hydrophobic surface of the α7-helix, in a very similar position to *H. sapiens* RPA32 L249 [Fig 5.12D]. The equivalent WH2 residue is identified as L351, found in the α11-helix [Fig 5.12E]. If the level of conservation is an indication of importance in the structure of these motifs, it is possible that substitutions at these residues may disrupt STN1 protein stability. To determine whether or not these residues would make good candidates for targeted substitutions in human cells, a prediction on their effect on protein stability was carried out. This composed part of a set of predictions which modelled substitutions analogous to the L198S and L236I in *S. pombe* on the crystal structures used previously.

Figure 5.12: **Alignment of *H. sapiens* STN1 WH1 and WH2 motifs to *S. pombe* Stn1 and *H. sapiens* RPA32 and position of conserved residues the crystal structure that are equivalent to *S. pombe* Stn1 residues of interest, L198 and L236 (following page).**

(A) Alignment of winged Helix-Turn-Helix (WH) motif peptide sequences from *S. pombe* Stn1 and *H. sapiens* RPA32 with *H. sapiens* STN1 WH1 and WH2 using Clustal Omega and visualised using Boxshade. The protein accession numbers are as follows: XP_001713126 (*S. pombe* Stn1), NP_002937 (*H. sapiens* RPA32) and NP_079204 (*H. sapiens* STN1). Residues that are fully conserved in at least half of the sequences compared are highlighted in black while similar residues are highlighted in grey. Dashed lines indicate a gap in the sequence due to the alignment. The positions of the residues affected in *S. pombe* *stn1-75* and *stn1-99* are indicated by blue and red triangles respectively. The alignment indicates that the residues equivalent to *S. pombe* Stn1 L198 and *H. sapiens* RPA32 I216 are F224 and Q309 in the *H. sapiens* STN1 WH1 and WH2 motifs respectively. These specific residues appear not to be well conserved. The residues equivalent to *S. pombe* Stn1 L236 and *H. sapiens* RPA32 L249 are L274 and L351 in the WH1 and WH2 motifs respectively. **(B)** The *H. sapiens* STN1 C-terminal crystal structure [PDB ID: 4JQF] is shown as a cartoon representation oriented to show both the WH1 and WH2 motifs. The motifs each consist of a series of helices and beta strands in the conformation: α-β-α-α-β-β, as labelled. By comparing the locations of conserved residues in *S. cerevisiae* Stn1 and *H. sapiens* RPA32 crystal structures to these WH1 and WH2 motifs, alternative residues equivalent to *S. pombe* Stn1 L198 were identified. These L216 and I308 residues are located in the α3- and α9-helices of WH1 and WH2 respectively and indicated in blue. The conserved L274 and L351 residues are located in α7- and α11-helices of WH1 and WH2 respectively and indicated in red. **(C)** The *H. sapiens* STN1 C-terminal crystal structure rotated 90° from the cartoon representation in (B), as indicated. Residues L216 and I308 are shown in blue and residues L274 and L351 are shown in red. **(D)** Close-up view of the location of the conserved I216 and L274 residues in the *H. sapiens* STN1 WH1 motif shown in blue and red respectively. The location of F224 is also indicated. The orientation of the structure is the same as in (B). **(E)** Close-up view of the location of the conserved I308 and L351 residues in the *H. sapiens* WH2 motif shown in blue and red respectively. The location of Q309 is also indicated. The orientation of the structures in (D) and (E) are the same as in (B).

A wHTH peptide sequence alignment

```
S. pom Stn1-WH1  188 -------------------------GFTIEELIIYLKAKELH
H. sap RPA32-WH  206 -------------------------TVAQNQVLNLIKACPR-
H. sap STN1-WH1  190 EEALSNPGALDLPSLTSLLSEKAKEFLMENRVQSFYQQELE
H. sap STN1-WH2  294 -------------------TREDKDLHRKIHRIIQQDCQK-
```

```
S. pom Stn1-WH1  205 ----------LPLVHIF----NVENEI-VEN-----CDGNH
H. sap RPA32-WH  222 ------------------PEGL----NF-QDL-KNQ-----LKHMS
H. sap STN1-WH1  231 MVESLLSLANQPVIHSA----SSDQVNFKKD-----TTSKA
H. sap STN1-WH2  315 --------------PNHMEKGCHF-LHI-LACARLSIRPGLS
```

```
S. pom Stn1-WH1  226 ILA-LNFSLQTL-------LQHGRIVRKS-NS---VYM-
H. sap RPA32-WH  239 VSS-IKQAVDFL-------SNEGHIYSTVDDD---HFK-
H. sap STN1-WH1  263 IHSIFKNAIQLL-------QEKGLVFQKD-DGFDNLYYV
H. sap STN1-WH2  341 EAV-LQQVLELLEDQSDIVSTMEHYYTAF----------
```

▲ = Substitution location in *stn1-75* ▲ = Substitution location in *stn1-99*

B *H. sap* STN1 C-terminus

C

D

E
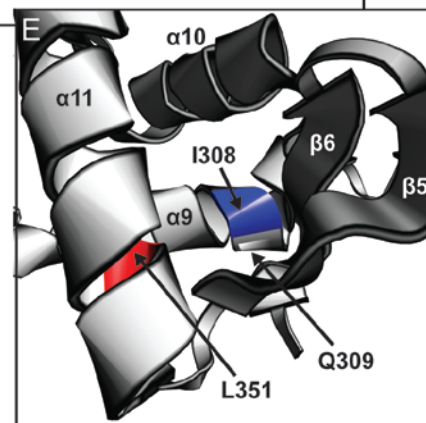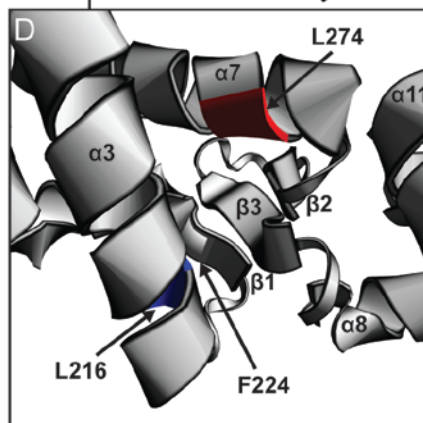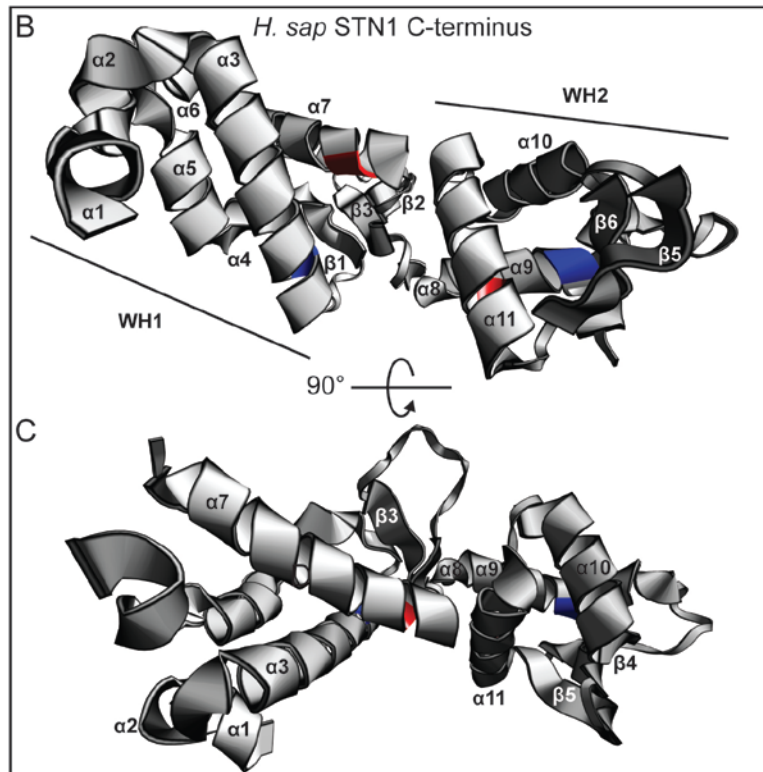
5.2.13 Effects of *S. pombe* Stn1 L198S and L236I substitutions on protein stability

In order to predict the extent to which the *S. pombe* Stn1 L198S and L236I substitutions can be tolerated, the SIFT webserver was used to predict whether or not they were likely to be disruptive. Each substitution was given a score by SIFT between 0 and 1, with those ≤0.05 being determined as disruptive and those >0.05 determined as tolerable [Table 5.1].

stn1 allele	Substitution	Conserved residue	SIFT score	Disruptive
stn1-75	L198S	Yes	0.01	Yes
stn1-99	L236I	Yes	0.12	No*

Table 5.1: **Predicted characteristics of amino acid substitutions in *stn1-75* and *stn1-99* alleles using SIFT.**

Residue conservation was determined through alignment of Stn1 peptide sequences from multiple species and RPA32 from *H. sapiens* using Clustal Omega (see Fig. 5.9). The L198S substitution was determined to not be tolerable (is disruptive). The L236I substitution was determined to be tolerable (not disruptive). SIFT score is a prediction of whether the substitution is likely to be damaging (≤ 0.05) or tolerable (> 0.05) on a scale of 0.00 to 1.00, taking into account the sequence alignment between 9 homologous protein sequences.

* Indicates that SIFT webserver determined that this prediction may be unreliable due to there being not enough variability of this residue between homologous proteins from the 9 species analysed.

The SIFT predictions indicate that the L198S substitution in *S. pombe* Stn1 WH1, with a score of 0.01, would not be tolerable. The webserver compares the sequence of interest with homologous sequences, in this case the sequences previously aligned to *S. pombe* Stn1 WH1 in Fig. 5.9. The prediction would, therefore, indicate that the substitution would affect a residue that is conserved and may be important in the function of the protein. The L236I substitution, on the other hand, with a score of 0.12, was predicted to be tolerable and, therefore, no phenotype is predicted to be displayed. This second prediction, however, was generated with a caveat attached. The webserver was unable to find enough variability at this residue in aligned sequences to generate a reliable prediction. This is unsurprising, given that the residue is conserved as a Leucine in almost all sequences compared in Fig 5.9. Although the substitution results in an amino acid change from leucine to isoleucine, a very similar small hydrophobic residue, it does still result in a temperature-sensitive phenotype. It is possible

that the *stn1-99* allele, containing this substitution, would display a less dramatic phenotype compared to the L198S substitution in *stn1-75*. Further investigation and comparison of the phenotypes in *stn1-75* and *stn1-99* would reveal whether or not this is the case.

To further characterise the effects of *S. pombe* Stn1 L198S and L236I substitutions and predict whether analogous substitutions would affect protein stability, the C-terminal crystal structures of *S. cerevisiae* Stn1 and *H. sapiens* RPA32 and STN1 were once again used as templates. The extent to which analogous substitutions in each protein were likely to affect protein stability was investigated through the use of the SDM and mCSM protein stability prediction webservers (Pires *et al.*, 2013, Worth *et al.*, 2011). The two crystal structures that were available for both *S. cerevisiae* Stn1 [PDB ID: 3KEY and 3K10] and *H. sapiens* RPA32 [PDB ID: 1Z1D and 1DPU] as well as the structure for *H. sapiens* STN1 [PDB ID: 4JQF] were fed into the webservers along with specific substitutions in the residues equivalent to *S. pombe* Stn1 L198 and L236. This produced protein stability scores for each substitution in each structure [Table 5.2].

The stability of a protein is defined as the Gibbs free energy difference (ΔG) in Kcal/mol between the native and denatured states. The SDM webserver gives each substitution a stability score as a predicted change in the Gibbs free energy difference (pseudo $\Delta\Delta G$) to indicate the predicted effect of the substitution on protein stability (Worth *et al.*, 2011). A negative score indicates a destabilising change in the protein while a positive score indicates a stabilising change. The webserver also predicts the change in solvent accessibility of a residue in percentage. An increase in solvent accessibility implies that the hydrophobic residues become less buried within the structure. The mCSM webserver also gives each substitution a stability score as $\Delta\Delta G$, similar to the SDM webserver. A negative score indicates a destabilising change in the protein while a positive score indicates a stabilising change.

S. pombe allele (substitution)	Model protein	PDB ID	Substitution	------------------------SDM Results------------------------			----------mCSM Results----------	
				ΔΔG (Kcal/mol)	Solvent accessibility	Destabilising	ΔΔG (Kcal/mol)	Destabilising
stn1-75 (L198S)	ScStn1 C-ter	3KEY	L323S	-4.56	+2.0%	Yes	-3.34	Yes
		3K10	L323S	-4.56	+5.5%	Yes	-3.06	Yes
	HsRPA32 C-ter	1Z1D	I216S	-5.09	+4.5%	Yes	*No data	-
		1DPU	I216S	-5.09	+3.4%	Yes	*No data	-
	HsSTN1 C-ter	4JQF	L216S	-4.56	+8.0%	Yes	-3.37	Yes
			I308S	-5.09	No change	Yes	-3.27	Yes
stn1-99 (L236I)	ScStn1 C-ter	3KEY	L380I	-0.37	-0.3%	No	-1.23	Yes
		3K10	L380I	-0.37	+1.1%	No	-1.14	Yes
	HsRPA32 C-ter	1Z1D	L249I	-0.37	+0.4%	No	*No data	-
		1DPU	L249I	-0.37	+1.2%	No	*No data	-
	HsSTN1 C-ter	4JQF	L274I	-0.37	+1.3%	No	-1.39	Yes
			L351I	-0.37	-2.8%	No	-1.22	Yes

Table 5.2: Predicted characteristics of amino acid substitutions in conserved residues of ScStn1, HsRPA32 and HsSTN1 using SDM and mCSM webservers.

Substitutions used in model structures obtained from PDB were equivalent to L198S and L236I in *S. pombe stn1-75* and *stn1-99* alleles respectively. The SDM webserver uses the PDB models to predict the change in protein stability as ΔΔG (Kcal/mol), the change in solvent accessibility and whether or not a substitution is likely to be destabilising. The mCSM webserver uses the PDB models to predict the change in protein stability as ΔΔG (Kcal/mol) and whether or not this is likely to be destabilising but not the change in solvent accessibility. A negative ΔΔG indicates a destabilising change in the protein while a positive score indicates a stabilising change. An increase in solvent accessibility (positive percentage) in these hydrophobic residues implies they are predicted to be less buried in the protein structure.

*No data – indicates that mCSM was unable to process the PDB file due to the presence of multiple models.

The SDM and mCSM webservers predicted effects on protein stability are similar to the SIFT webserver predictions for *S. pombe* Stn1 WH1, although there is some variability between analogous substitutions in different model structures. The predictions of whether the substitutions produce a stabilising, neutral or destabilising effect, however, remains constant within the results of each webserver. Specifically, analogous substitutions to *S. pombe* Stn1 L198S in all models are determined to be destabilising by SDM as indicated by a ΔΔG of at least -4.56Kcal/mol in all predictions. In almost all cases this is also predicted to result in an increase in solvent accessibility of between a low of 2.0% in the *S. cerevisiae* Stn1, model 3KEY, WH1 motif and a high of 8.0% in the *H. sapiens* STN1, model 4JQF, WH1 motif. Interestingly, the exception to this is the I308S substitution in the *H. sapiens* STN1 C-terminus WH2 motif where no change is predicted. Although there is a similar change in stability between the WH1 and WH2 motifs (-4.56 versus -5.09Kcal/mol respectively), the difference in the changes in solvent accessibility implies that the structural conformation of the WH1 motif α3-helix is more easily disrupted than the WH2 motif α9-helix. Alternatively this could be an indication that the hydrophobic surface of the α3-helix is less buried than the α9-helix. Similar predictions are generated by the mCSM webserver; however, no solvent accessibility data is produced. The predicted differences in ΔG are also slightly lower than for SDM, likely due to the differences in bioinformatics methods employed. In addition, no data is generated for *H. sapiens* RPA32 (PDB ID: 1Z1D and 1DPU] models. The PDB files contain multiple models and, at present, the mCSM webserver is not capable of processing such files.

A difference is seen in the predictions generated by SDM and mCSM for the second set of substitutions that are analogous to *S. pombe* Stn1 WH1 L236I. The predictions generated by SDM agree with the SIFT predictions. In all models, the analogous substitutions are predicted to result in little change in protein stability, as indicated by the value of -0.37Kcal/mol given to all substitutions in all models. The mCSM predictions, however, disagree with the SDM and SIFT predictions. Although, once again, the *H. sapiens* RPA32 models could not be processed,

the other predictions indicate that analogous substitutions in *S. cerevisiae* Stn1 WH1 and *H. sapiens* STN1 WH1 and WH2 would be destabilising. This is shown by ΔΔG values of at least -1.14Kcal/mol. These are smaller changes in ΔG as compared to the predictions for the substitutions analogous to *S. pombe* L198S. The differences imply that the destabilisation effect due to substitutions analogous to *S. pombe* Stn1 L236I would be less than the effect due to substitutions analogous to *S. pombe* Stn1 L198S. As previously stated, further investigation and comparison of the phenotypes in the *S. pombe stn1-75* and *stn1-99* alleles may reveal whether or not this is the case.

5.2.14 Temperature sensitivity range of *stn1-75 and stn1-99*

The characterisation of the two *S. pombe* temperature-sensitive alleles continued in the form of assessing the temperature-sensitivity range. As the *stn1-75* mutant was identified first, initially the *stn1-75 rqh1Δ* strain alone was streaked to single colonies with control strains on YES agar at a range of temperatures, from 25°C to 36°C [Fig 5.13A]. There was no sign of a viability phenotype with this strain up to 30°C. At 32°C, a reduction in colony size and irregular colony morphology was visible to the naked eye. At 33.5°C, there was little evidence of colony forming units. Small micro colonies could be seen but these did not progress further.

The *stn1-99 rqh1Δ* strain, along with two other candidates, was streaked out onto YES agar at a range of temperatures [Fig 5.13B]. At 25°C and 33.5°C the *stn1-99 rqh1Δ* strain formed colonies similar to the *pot1-1 rqh1Δ* strain. At 36°C, however, the viability reduced and no colonies were visible. It is interesting that the amino acid substitution in the α3-helix of the WH1 motif results in a more acute phenotype than the one within the α3-helix. These phenotypes confirm the predictions made through the previous bioinformatics analysis using the SIFT, SDM and mCSM protein stability prediction webservers.

With regards to the suppressor screen, a loss of viability at a lower temperature would have been preferable. Given that in the *S. cerevisiae* Stn1 protein has been shown to only suppress *cdc13-1* up to a temperature of 30°C, it is possible that some partial suppressors could be missed at the higher temperatures required with these *S. pombe* alleles (Grandin *et al.*, 1997).

In order to better quantify the sensitivity of these strains a colony counting assay was used. The *stn1-75 rqh1Δ* and *stn1-99 rqh1Δ* strains were cultured overnight at the permissive 25°C temperature along with the control strains. The cell density was checked and the cultures were diluted and plated on multiple YES agar at 300 cells per plate. These plates were incubated at 25°C, 33.5°C and 36°C and colony forming units were counted and compared to the initial plating of 300 cells [Fig 5.14]. The mean average cfu per strain at each temperature are shown in Table 5.3.

Figure 5.13: Determination of temperature-sensitivity range of *stn1-75 rqh1Δ* and *stn1-99 rqh1Δ* strains (following page).

(A) Streaks of wild-type, *stn1⁺-ura4⁺ rqh1Δ*, *pot1-1 rqh1Δ* and *stn1-75 rqh1Δ* strains on YES to assess viability at 25°C, 27.5°C, 30°C, 32°C, 33.5°C and 36°C. The wild-type and *stn1⁺-ura4⁺ rqh1Δ* controls retain viability throughout temperature range. The *pot1-1 rqh1Δ* temperature-sensitive control strain has a reduction in viability at 33.5°C and loss of viability (synthetic lethal) at 36°C (no cfu). The *stn1-75 rqh1Δ* strain shows a substantial reduction in viability at 33.5°C and complete loss of viability at 36°C (no cfu). **(B)** Streaks of wild-type, *stn1⁺-ura4⁺ rqh1Δ*, *pot1-1*, *pot1-1 rqh1Δ*, *stn1-88 rqh1Δ*, *stn1-94 rqh1Δ* and *stn1-99 rqh1Δ* strains on YES to assess viability at 25°C, 33.5°C and 36°C. The wild-type and *stn1⁺-ura4⁺ rqh1Δ* controls retain viability throughout temperature range. The *pot1-1* temperature-sensitive control shows a reduction in viability at 36°C, but colonies are still formed. The *pot1-1 rqh1Δ* temperature-sensitive control strain has a reduction in viability at 33.5°C and complete loss of viability (synthetic lethal) at 36°C (no cfu). The *stn1-88 rqh1Δ* and *stn1-94 rqh1Δ* strains show reduced viability, but not complete loss, at 36°C. The *stn1-99 rqh1Δ* strain shows a reduction in viability at 33.5°C and loss of viability (synthetic lethal) at 36°C (no cfu).

A *stn1-75 rqh1Δ* temperature-sensitivity range

25°C   27.5°C   30°C

32°C   33.5°C   36°C

Key: 1: wild-type   3: *pot1-1 rqh1Δ*
        2: *stn1⁺-ura4⁺ rqh1Δ*   4: *stn1-75 rqh1Δ*

B *stn1-99 rqh1Δ* temperature-sensitivity range

25°C   33.5°C   36°C

Key: 1: wild-type   4: *pot1-1 rqh1Δ*   7: *stn1-94 rqh1Δ*
        2: *stn1⁺-ura4⁺ rqh1Δ*   5: *pot1-1 rqh1Δ*   8: *stn1-99 rqh1Δ*
        3: *pot1-1*   6: *stn1-88 rqh1Δ*
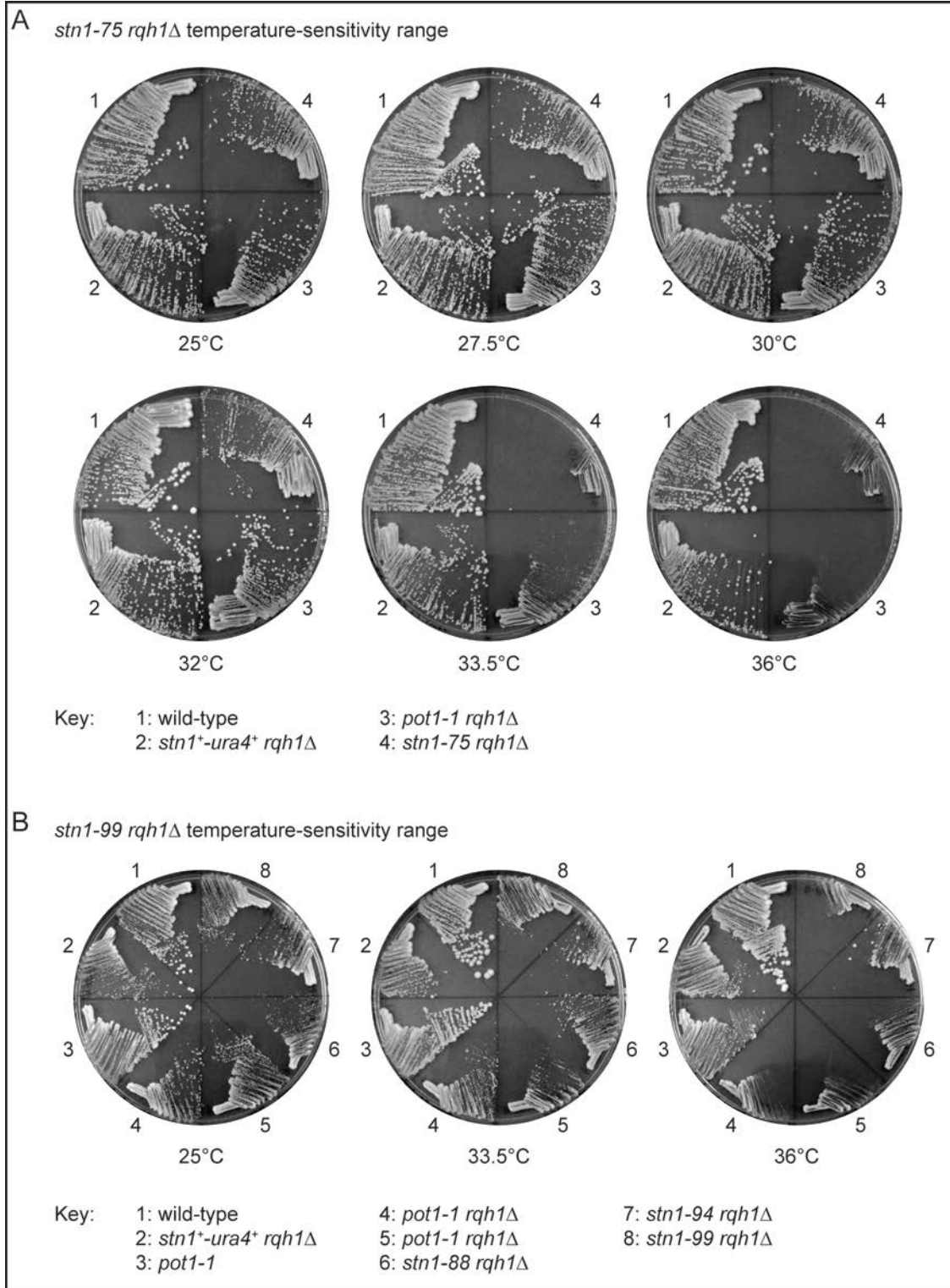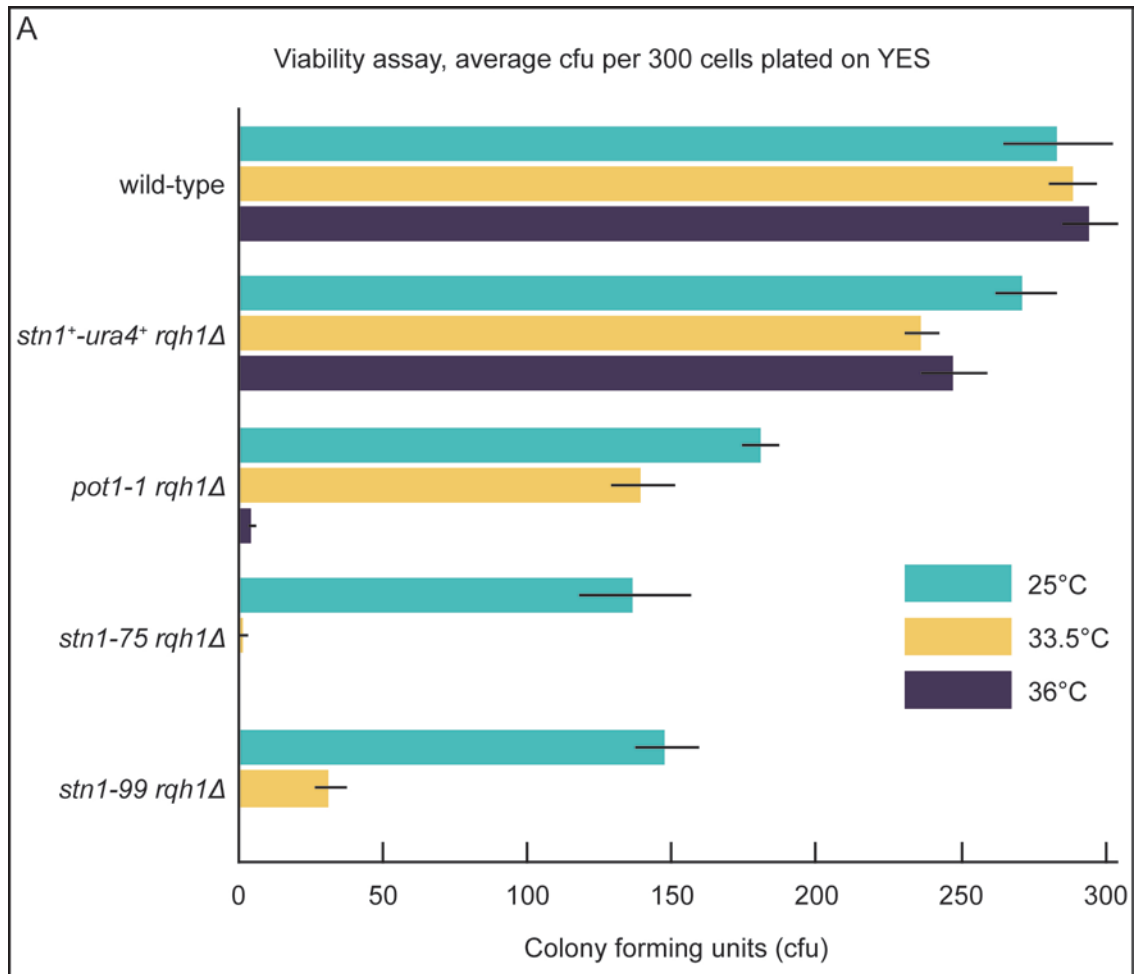
Figure 5.14: Quantification of viability for temperature-sensitive strains at 25°C, 33.5°C and 36°C.

(A) The wild-type, *stn1⁺-ura4⁺ rqh1Δ*, *pot1-1 rqh1Δ*, *stn1-75 rqh1Δ* and *stn1-99 rqh1Δ* strains were plated on YES agar at 300 cells per plate and incubated at 25°C, 33.5°C and 36°C. The mean average number of cfu on the plates, from sets of 3 plates per temperature per strain, is shown in the graph. Coloured bars represent each temperature, as indicated. Black horizontal lines indicate standard deviation for each set of plates at each temperature. The data indicates that the most acute, synthetic lethal, phenotype is achieved in the *stn1-75 rqh1Δ* strain. There is no significant difference in the average number of cfu for the wild-type strain at each temperature. A slight loss of viability is seen in the *stn1⁺-ura4⁺ rqh1Δ* control strain which is expected in *rqh1Δ* strains. The *pot1-1 rqh1Δ* strain shows partial loss of viability, even at 25°C and almost complete loss of viability at 36°C. The *stn1-75 rqh1Δ* and *stn1-99 rqh1Δ* strains both show a partial loss of viability at the permissive 25°C and complete loss of viability at 36°C. The data indicate that the most acute, synthetic lethal, phenotype is achieved in the *stn1-75 rqh1Δ* strain.

Strain	25°C	33.5°C	36°C
wild-type	284	289	295
stn1⁺-ura4⁺ rqh1Δ	272	236	247
pot1-1 rqh1Δ	181	140	5*
stn1-ts75 rqh1Δ	137	2.5*	0
stn1-ts99 rqh1Δ	148	32	0

Table 5.3: Mean average cfu count in temperature-sensitive strain viability assay.

The wild-type, *stn1⁺-ura4⁺ rqh1Δ*, *pot1-1 rqh1Δ*, *stn1-75 rqh1Δ* and *stn1-99 rqh1Δ* strains were plated on YES agar at 300 cells per plate and incubated at 25°C, 33.5°C and 36°C. The mean average number of cfu on the plates, from sets of 3 plates per temperature per strain was calculated.

* - Indicates colonies that were formed unexpectedly, based on previous streaks [Fig. 5.13]. Colony growth was stunted and morphology irregular but still visible to the naked eye.

The viability plating assay essentially confirmed the results from the streaks in Figure 5.13; that the *stn1-75 rqh1Δ* strain displays a more acute phenotype than the *stn1-99 rqh1Δ* strain or even the *pot1-1 rqh1Δ* strain. Surprisingly, a few *pot1-1 rqh1Δ* colonies did form at 36°C, though these were very small compared to colonies at lower temperatures. This may be an indication that some cells occasionally develop internal suppressors or perhaps are HAATI survivors. This, however, does not appear to be the case with the *stn1* mutants, which did not form any colonies at 36°C.

5.2.15 Analysis of morphology and growth rate of *stn1-75* and *stn1-99* strains at permissive and non-permissive temperatures

To observe the morphological phenotype of the temperature-sensitive cells when shifting to non-permissive temperatures, without the synthetic lethality preventing continued proliferation of the cells, single mutants were generated. The double mutant strains were back-crossed with the wild-type in order to separate the *stn1* temperature-sensitive alleles from the *rqh1Δ*. The genotypes of the resulting strains were identified based on colony colour with the vital strain, Phloxine B. Healthy strains export Phloxine B out of the cell; however, strains which circularise are much less efficient. Strains which are *rqh1Δ* are also unable to

export the dye. Therefore, the strains were scored based on the desired criteria of normal colouration at 25°C and a pink colouration at 36°C.

Several strains that displayed this phenotype, as well as additional ones which were synthetic lethal at 36°C, were isolated. The strains were inoculated in YES liquid media at 25°C overnight and cell morphology observed. These cultures were split into two sets, one kept at 25°C and the other shifted to 36°C. Images of the cell morphology over the following 30 hours were taken, as well as cell densities at regular intervals [Fig 5.15].

Figure 5.15: Morphology and growth rate of *stn1-75* and *stn1-99* cells at permissive and non-permissive temperatures (B and C on following page).

(A) The wild-type, *stn1⁺-ura4⁺*, *pot1-1, stn1-75* and *stn1-99* strains were compared at permissive and non-permissive temperatures. Elongated cells can be seen by 6 hours at 36°C in both *stn1-75* and *stn1-99*, similar to *pot1-1*. Reduction in elongation is seen in all cells after 30 hours at 36°C, but many non-viable cells are present. **(B)** The *rqh1Δ*, *pot1-1 rqh1Δ, stn1-75 rqh1Δ* and *stn1-99 rqh1Δ* strains were compared at permissive and non-permissive temperatures. Elongated cells are visible by 6 hours at 36°C with irregular morphology in all four strains. Non-viable cells were observed by 30 hours at 36°C. **(C)** Comparison of growth rates of all strains reveals two populations at 25C (i and ii, as indicated). Those containing *rqh1Δ* have a slower growth rate than *rqh1⁺*. At 36°C, three populations emerge (iii, iv and v, as indicated). Group iii contains the wild-type, *stn1⁺-ura4⁺*, *stn1-75* and *stn1-99* strains. A growth plateau is seen after 18 hours. An earlier plateau at a lower density is seen for *pot1-1, rqh1Δ* and *stn1⁺-ura4⁺* strains in group iv. Group v, containing *pot1-1 rqh1Δ, stn1-75 rqh1Δ* and *stn1-99 rqh1Δ,* shows a decrease in cell density by 18 hours, likely due to cell death. Note: the scale on the x-axis is not linear.
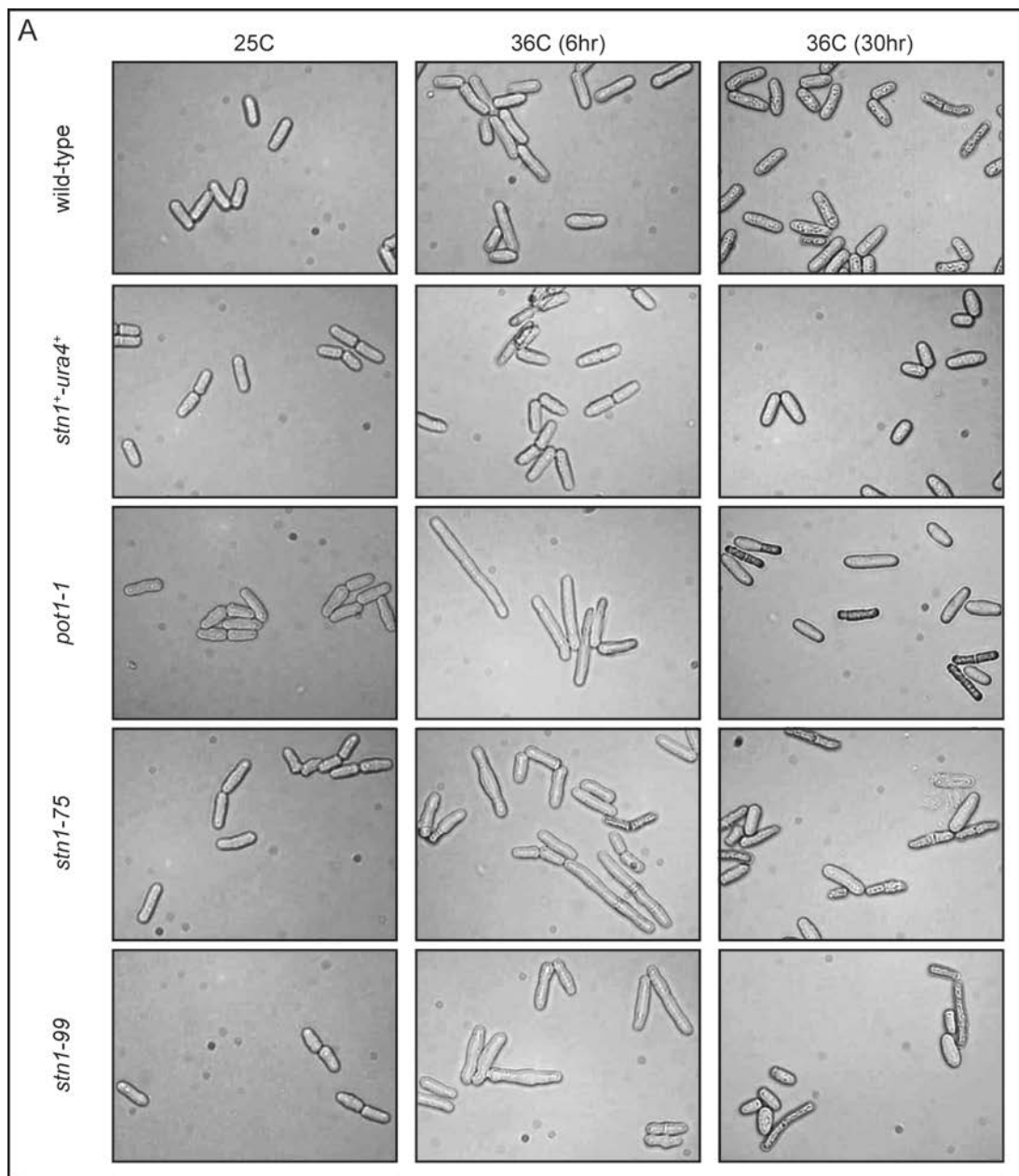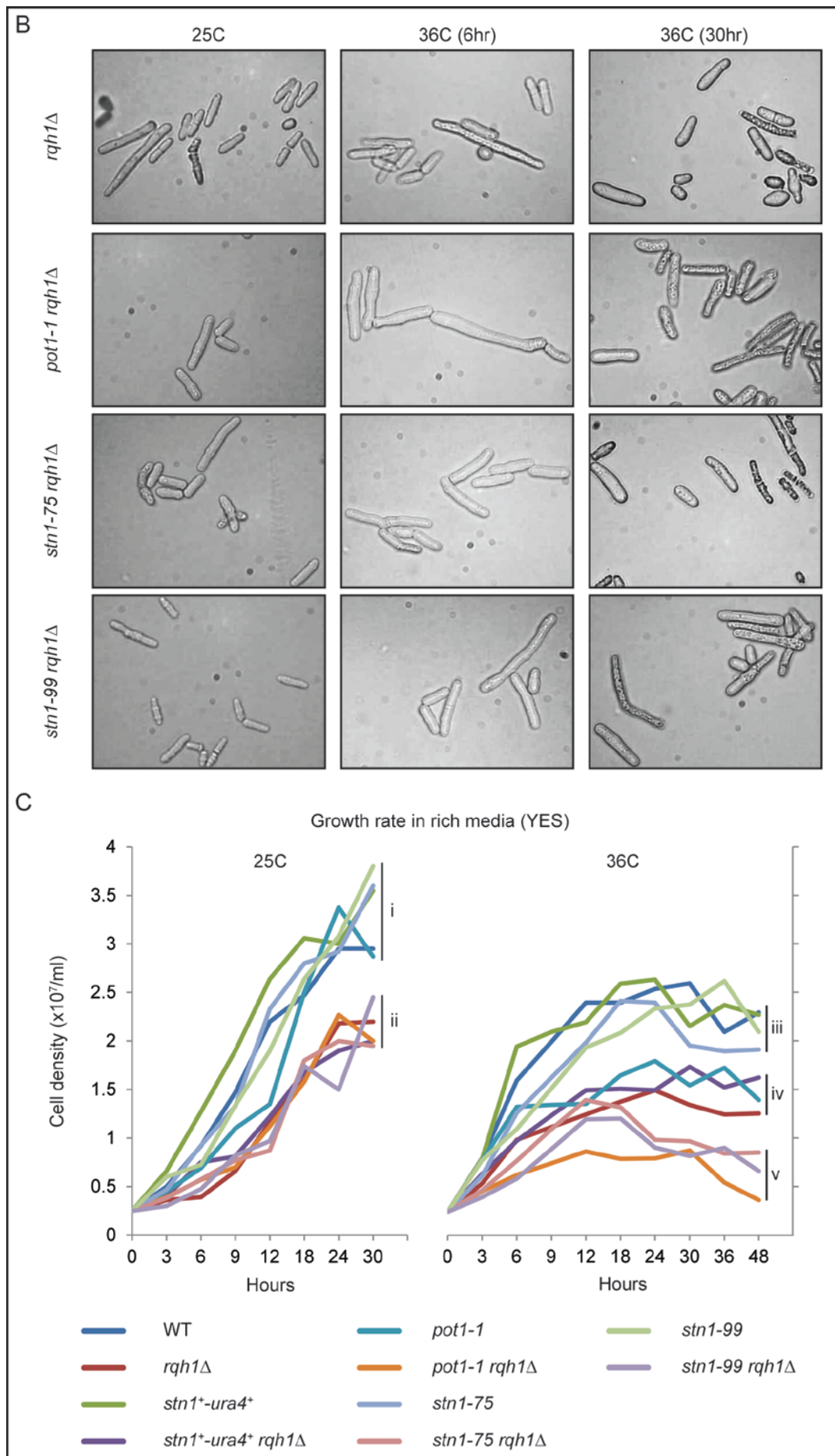
The morphology of the single mutants, *pot1-1, stn1-75* and *stn1-99*, were very similar when compared at both 25°C and 36°C. Cell size and shape at 25°C is very similar to the wild-type and *stn1⁺-ura4⁺* control strains indicating that under permissive conditions, these cells are fairly healthy. Indeed, the growth curve [Fig 5.15C] indicates that the single mutants grow at a similar rate at 25°C to the wild-type and *stn1⁺-ura4⁺* controls. When the cells are shifted to 36°C, however, clear differences are observed. The temperature-sensitive single mutants all elongated by 6 hours, indicating a cell cycle arrest while the wild-type cells continue to grow normally. This is partly reflected in the growth curve, where *pot1-1* is shown to grow at a slower rate and plateau at a lower cell density. The plateau is more likely an indicator of rate of cell death equalling cell division within this time range, rather than complete cell cycle arrest as *pot1-1* cells can remain viable at 36°C at a fairly high frequency (Wang and Baumann, 2008). By 30 hours, although some cells have recovered from the cellular crisis (possibly by chromosome circularisation), many are not viable or very unhealthy, as indicated by the rough texture to the cell surfaces.

The *stn1* single mutants, on the other hand, appear to grow at a similar rate to wild-type cells at 36°C despite being elongated. A reduction in elongation is seen by 30 hours at 36°C, implying that the cells have overcome the crisis, possibly by circularising chromosomes. This may explain the growth rate observed, however, there was another possibility. Although some cells may have been circularising chromosomes and, like *pot1-1*, arresting the cell cycle long enough to recover, however, if the population also contained cells which did not circularise in the first cell cycle, continued proliferation may have occurred. A proportion of cells at the 6 hour time point at 36°C in both *stn1-75* and *stn1-99* do not appear to be displaying an elongation phenotype. Perhaps, unlike *pot1-1*, these cells were not arresting as they did not pass into a state of telomere deprotection.

The rqh1Δ strain contained elongated cells at 25°C and continued to retain both normal and elongated cells throughout the time course. This is not unexpected as these cells are known to have an abnormal DNA damage checkpoint. The double mutant strains, *pot1-1 rqh1Δ, stn1-75 rqh1Δ* and *stn1-99 rqh1Δ*, all displayed very elongated cells at 6 hours at 36°C [Fig 5.15B] and many were no longer viable after 30 hours, as expected. This is reflected well in the growth curve by a noticeable trend of decreasing density of cells after 18 hours [Fig 5.15C].

5.2.16: Gradual telomere loss with no evidence of shortening

Given the discrepancies in cell morphology and growth rates at non-permissive temperatures, a time course was conducted with the intention of identifying whether or not telomeres were lost in the *stn1-75* and *stn1-99* strains, as has been previously shown for *pot1-1* strains (Pitt and Cooper, 2010). The wild-type, *stn1$^+$-ura4$^+$*, *pot1-1, stn1-75* and *stn1-99* strains were cultured at 25°C to log phase, then shifted to 36°C for a period of 48 hours. Samples were taken at time points throughout the experiment for genomic DNA prep and subsequent analysis of telomeres by southern blot [Fig 5.16].

The southern blot indicates that the wild type and *stn1$^+$-ura4$^+$* strains maintain telomeres at 36°C. However, there is a reduction in telomere signal for *stn1$^+$-ura4$^+$* at 36°C. This may be due to the accumulation of dead cells after 48 hours at 36°C resulting in a poorer genomic DNA prep or reduced EcoRI-digestion efficiency. Otherwise it may suggest a telomere phenotype for this strain, possibly as a result of the modified promoter, which was not apparent in telomere assays from cells cultured at 25°C used previously. The *pot1-1* strain displays a dramatic loss of all telomere signal within the 48 hour time course. Indeed, based on previous work, it would be expected to lose telomere signal within 24 hours (Pitt and Cooper, 2010). The *stn1-75* strain appears to retain telomere signal for at least the first 8 hours of the time course. But then appears to gradually lose telomere signal over the remaining hours, with the final time point

appearing to show an almost complete loss. The apparent dramatic loss in the second 24 hours, however, may be misleading due to a slightly reduced loading of DNA in the final two time points, as shown in the ethidium bromide-stained gel image [Fig 5.16B]. A very gradual decrease in telomere signal is also apparent with the *stn1-99* strain. However, the strain does not appear to lose all telomere signal within the 48 hours of being shifted to 36°C. Like *pot1-1*, however, neither *stn1-75* nor *stn1-99* strain have a reduction in length to accompany the reductions in signal. This may imply that similar or related mechanisms may be acting for telomere loss in both *pot1* and *stn1* mutants.

Whether or not this is the case, there does appear to be some loss of telomeric signal, but this is not nearly as acute as with *pot1-1*. Combined with the growth rate data, this would imply that at least some cells are able to maintain telomeres or avoid sudden telomere loss for a number of cell cycles.

Figure 5.16: Gradual loss of telomeres with no evidence of shortening at non-permissive temperature in *stn1-75* and *stn1-99* (following page).

(A) Southern blot analysis of EcoRI-digested genomic DNA from a 48 hour time course of strains cultured at 25°C and 36°C. A telomere-specific probe was used from pSpTelo. Time points for wild-type, *stn1^{+}-ura4^{+}* and *pot1-1* strains were taken at 0hr at 25°C (lanes 1, 3 and 5) and after 48hrs at 36°C (lanes 2, 4 and 6). Time points for *stn1-75* and *stn1-99* strains were taken at 0hr (25°C), 2hrs, 4hrs, 8hrs, 24hrs, 36hrs and 48hrs (36°C) in lanes 7-13 and 14-20 respectively. The triangles over these lanes represent the progression of the time course. A very gradual loss of telomeric signal is observed in both the *stn1-75* and *stn1-99* strains. The *stn1-75* strain appears to retain telomeric signal until at least the 8hr time point. Following this a reduction in signal is observed. The *stn1-99* strain appears to retain telomeric signal throughout the time course, but with a reduction in signal intensity. No change in telomere length is seen in either strain throughout the time course. **(B)** Ethidium bromide stained image of southern gel (colour inverted) shows relative loading between lanes. Reduced loading can be seen in lanes 2, 4 and 6, indicating why reduced signal intensity is seen in the corresponding lanes of the southern blot. Reduced loading of genomic DNA can also be seen in lanes 12, 13 and 20 which would indicate why the telomeric signal intensity in these lanes of the southern blot may appear to be lower than previous lanes.
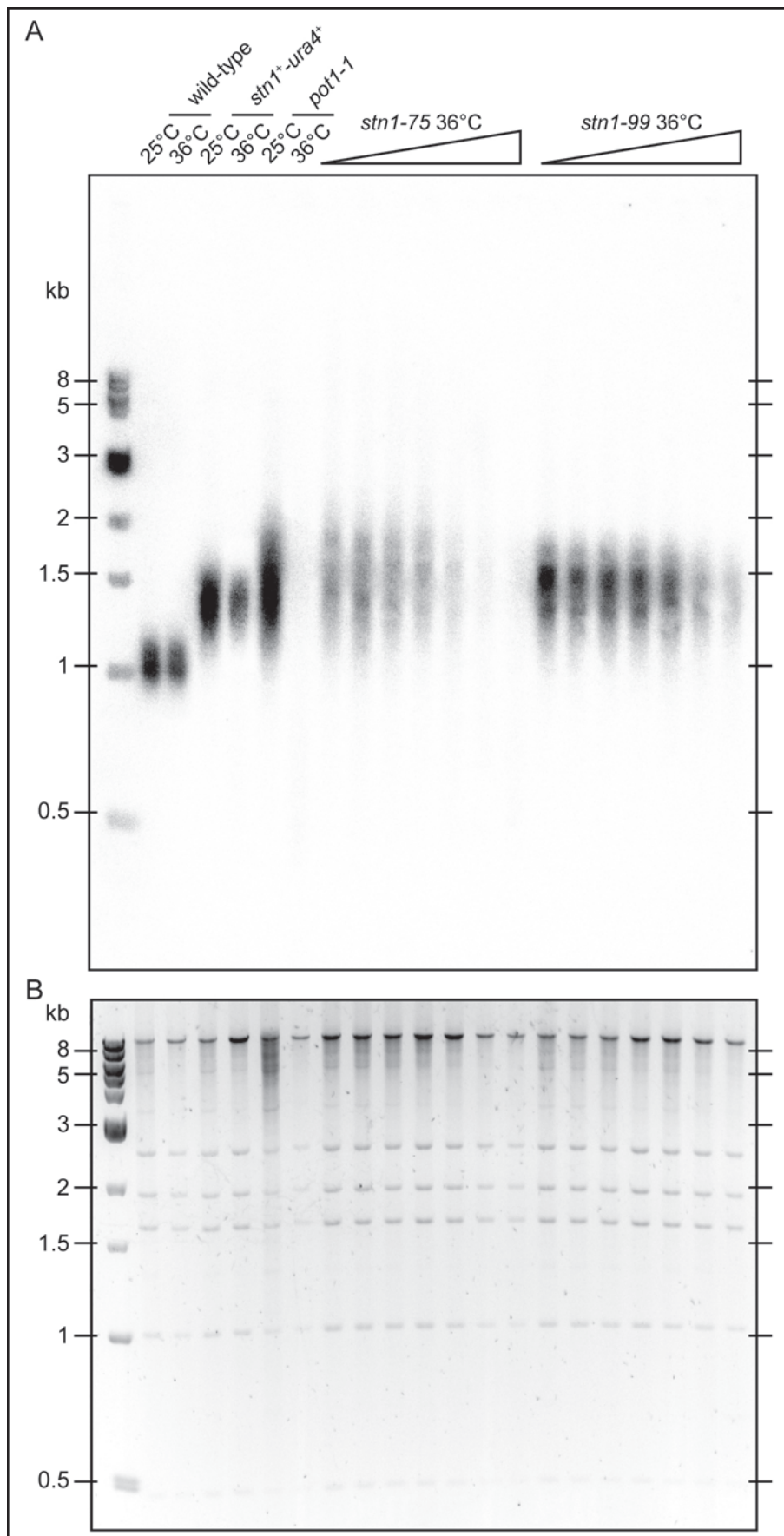
5.2.17 *stn1-75 and stn1-99* sensitivity to MMS at permissive and non-permissive temperatures

Though the *stn1* temperature-sensitive strains appeared to gradually lose telomeres, it is possible that the reason for synthetic lethality with combined with *rqh1Δ* may not be entirely due to chromosome circularisation. It was, therefore, prudent to further investigate the phenotypes of these alleles.

The ability to circularise chromosomes in *S. pombe* provides a means of survival without end protection, but does result in a very acute sensitivity to DNA damaging agents, such as MMS. Only those cells which retain linear chromosomes, despite loss of telomeres, as seen in HAATI survivors, remain resistant to MMS (Jain *et al.*, 2010). Therefore, the use of MMS could be used to determine whether the *stn1-75* and *stn1-99* strains circularise chromosomes. Some resistance to MMS could indicate the ability to retain linear chromosomes despite the loss of end protection.

Spot assays were, therefore, conducted with the temperature-sensitive strains. These were spotted with control strains onto YES, YES + Phloxine B and several concentrations of YES + MMS agar plates. These were then incubated at 25°C, 33.5°C and 36°C and sensitivity observed [Fig 5.17].

Figure 5.17: **Spot assays reveal MMS sensitivity of *stn1* temperature-sensitive alleles (following page).**

(A-B) Spot assay using wild-type, $stn1^+$-$ura4^+$, *pot1-1, stn1-75*, *stn1-99* and a pre-circularised strain *pot1-1 CIR* (retained from a previous test) on YES and YES + Phloxine B in 1/5-fold serial dilutions. The spots indicate a slight loss of viability in *pot1-1*, *stn1-75* and *stn1-99* mutants at 36°C on YES. On YES + Phloxine B, these strains have a further loss of viability and increase in pink colouration at 33.5°C and 36°C compared to the same temperature on YES, with *stn1-75* being the most acutely affected. **(C)** Spot assays using the same strains from same cultures as (A) and (B) on 0.0025%, 0.005 and 0.0075% MMS plates at 25°C, 33.5°C and 36°C in 1/5-fold serial dilutions All strains are sensitive to MMS to some degree with the *stn1-75* strain the most acutely sensitive at 33.5°C and 36°C, more so than *pot1-1*. The *stn1-99* has a similar MMS sensitivity to *pot1-1* while the pre-circularised *pot1-1 CIR* strain is very sensitive, even at 0.0025% MMS.
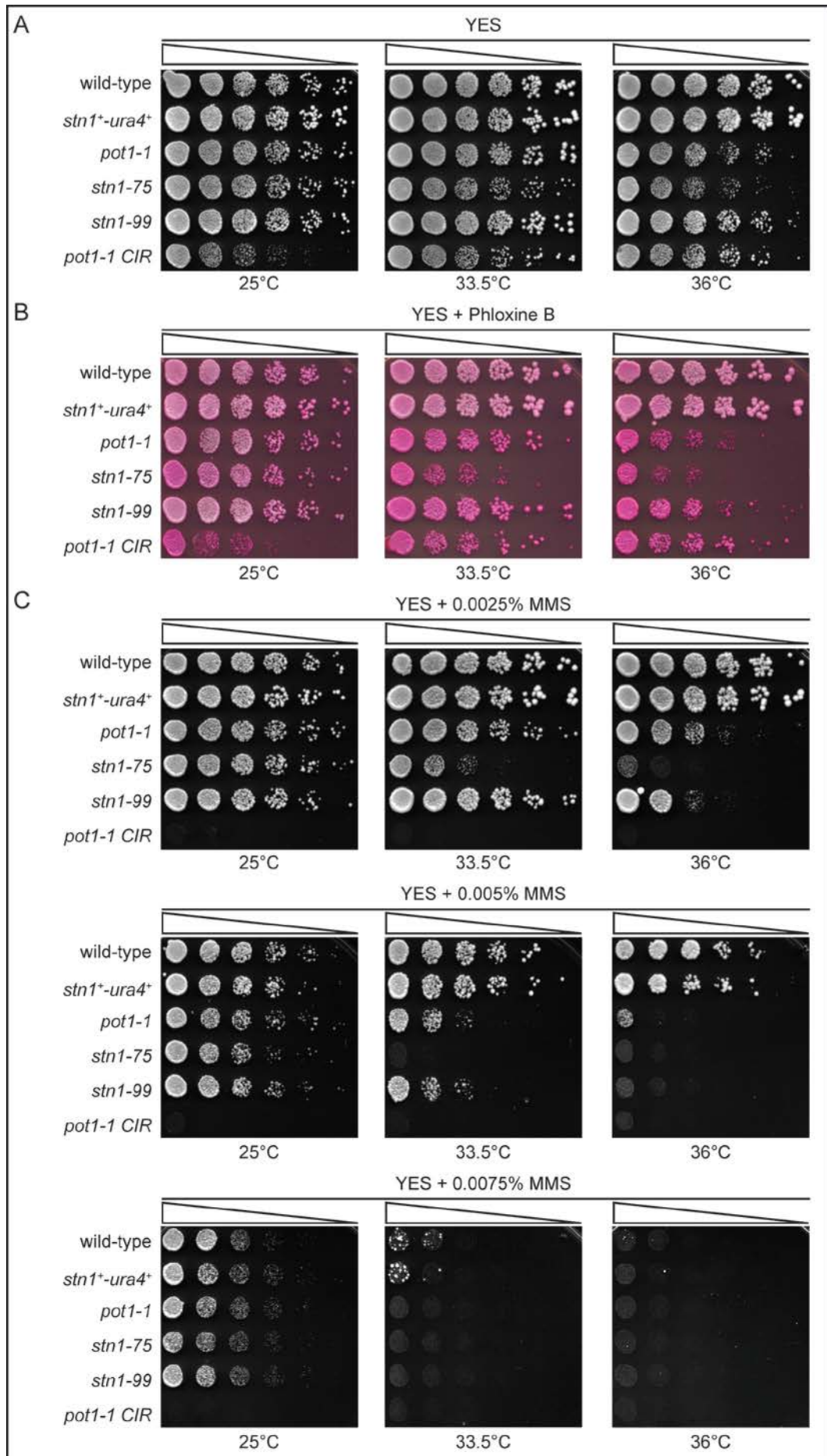
The spot assay on YES plates indicated that the *pot1-1, stn1-75, stn1-99* strains had reduced viability at 33.5°C and 36°C, as expected. The spot assay on YES + Phloxine B plates indicated that the *pot1-1, stn1-75*, and *stn1-99* were unhealthy at non-permissive temperatures, more so than YES alone. The increased pink colouration of these strains, relative to the wild type and *stn1$^+$-ura4$^+$* suggested that they may all have circularised, similar to the *pot1-1 CIR* (circularised *pot1-1* retained from a previous test). However, this individually, is not proof of circularised chromosomes, but just an indicator of cell viability which is reduced in circularised strains.

The MMS sensitivity spot assays indicated that *stn1-75* was acutely sensitive to MMS, more so than *pot1-1* or *stn1-99*. The *pot1-1 CIR* strain is also very sensitive to MMS at all concentrations, as expected for an already circularised strain. This would be a good indicator of circularised chromosomes, and indeed, it may well be the case. However, given that *pot1-1* is known to circularise chromosomes and is less sensitive to MMS, it may be an indication that the *stn1-75* allele is affecting a function other than or in addition to telomere capping. On the other hand, given that *stn1-75* is temperature-sensitive from the lower temperature of 33.5°C, unlike *pot1-1* and *stn1-99* which are sensitive at 36°C, it may simply be an artefact of telomere uncapping and chromosome fusion at the lower temperature. Further characterisation of these alleles is, therefore, required to determine the cause of the differing phenotypes.

5.3 Summary

The aim of this study was to develop an alternative method for screening for proteins which interacted with *S. pombe* Stn1, specifically any Cdc13 or CTC1 homologues that may be present. To that end, a Stn1 temperature-sensitive suppressor screen was selected as an alternative to the yeast 2-hybrid screen used previously. In order to generate appropriate temperature-sensitive alleles, a suitable genetic background was required that prohibited the proliferation of cells containing circularised chromosomes under non-permissive temperatures. By circularising chromosomes, *S. pombe* cells have a unique method of surviving the loss of telomere capping, which is the consequence of a number of null and temperature-sensitive alleles of *S. pombe* telomeric proteins, including Pot1. The ideal temperature-sensitive *stn1* allele would have a clear phenotype, preferably synthetic lethal, in the genetic background selected for the suppressor screen. However, to determine the most appropriate genetic background, a suitable, well characterised, temperature-sensitive allele was required. The *pot1-1* allele was, therefore, selected and several genetic backgrounds were investigated that had previously proved to be synthetic lethal with a *pot1* null mutation.

The investigations identified that an *rqh1Δ* background would be most suitable for the generation of *stn1* temperature-sensitive alleles. This background proved to be synthetic lethal when combined with the *pot1-1* allele under non-permissive conditions. Error-prone PCR-based mutagenesis was used to generate *stn1* alleles that were integrated into an *rqh1Δ* strain by RMCE and screened for temperature-sensitive phenotype. Two alleles were identified, *stn1-75* and *stn1-99*, which were found generate a relatively normal phenotype at the permissive temperature of 25°C but were not viable at the non-permissive temperature of 36°C. Sequence analysis identified one amino acid substitution in each, L198S and L236I, present within the first predicted winged Helix-Turn-Helix motif. These individual substitions appeared to be sufficient for the temperature-sensitivity phenotype. However, due to the method of integration requiring modifications to the *stn1* locus, any changes in expression resulting from

the presence of lox sites may also contribute to the phenotypes. Evidence for this was seen in slightly elongated telomeres for strains containing a wild-type *stn1* gene in the context of the modified locus.

Alignment of the position of the substitutions to the predicted secondary structure of the *S. pombe* Stn1 identified the secondary structural features affected. These were found to be the α1- and α3-helices of the *S. pombe* Stn1 WH1 motif. Sequence alignments identified the positions of equivalent amino acids in homologous structures, *S. cerevisiae* Stn1 C-terminus, *H. sapiens* RPA32 C-terminus and *H. sapiens* STN1 C-terminus. In addition, the protein stability prediction webservers, SDM and mCSM, were used to generate prediction of the possible effects of analogous substitutions in these structures. These were largely in agreement with the predictions made for *S. pombe* Stn1 in that an acute phenotype would be present for the first substitution, L198S, which a much less acute phenotype would be present with the second substitution, L236I.

These predictions were confirmed in further investigations where the first of the *stn1* alleles, stn1-75, was found to have a more acute sensitivity to temperature and the DNA damaging agent MMS. The phenotypes also pointed to these alleles disrupting Stn1 telomere-capping, resulting in chromosome circularisation. However analysis of the telomere signal from samples taken of cultures under non-permissive conditions did not show the same dramatic loss of telomeres seen in *pot1-1* cells. The cell morphology and growth characteristics of both *stn1* alleles under permissive and non-permissive temperatures do fit well with the established characteristics of *pot1-1* cells.

Given the various differences and similarities in phenotype between the two *stn1* alleles and *pot1-1*, currently due to unknown reasons, it would be prudent to continue the analysis. However, it would be beneficial to first transfer these alleles to a background with a wild-type promoter. This would firmly establish whether the amino acid substitutions alone are sufficient

to produce the temperature-sensitivity phenotypes. It would also establish whether the modified promoter region and the subsequent effects on *stn1* expression contribute toward any of the displayed phenotypes, other than the increase in telomere length.

Chapter 6

A *stn1* temperature-sensitive mutant suppressor screen

6.1 Introduction

Given that the *stn1-75* temperature sensitive allele is acutely sensitive to changes in temperature through both a combination with *rqh1Δ* and on MMS agar, it would provide a useful tool for the identification of suppressors of a telomere uncapping phenotype. Indeed, with the more acute sensitivity at the lower temperature of 33.5°C compared to the *stn1-99* or even *pot1-1* alleles, several possible strategies could be and are being devised.

6.2 Results

6.2.1 Testing for a dominant negative phenotype in *stn1-75*

The *stn1-75* allele has several phenotypic features which make it a useful tool for a temperature-sensitivity suppressor screen, however, one potential issue was not addressed during characterisation. Should the allele have a dominant negative phenotype, it would unlikely be successful in identifying suppressors. Even a *stn1*$^+$ clone would not suppress the phenotype.

Therefore, to test this, *stn1*$^+$/*stn1-75 rqh1Δ*/*rqh1Δ* and *stn1*$^+$/*stn1-99 rqh1Δ*/*rqh1Δ* diploid strains were generated by crossing *stn1-75 rqh1Δ* and *stn1-99 rqh1Δ* strains with a *stn1*$^+$ *rqh1Δ* strain of the opposite mating type. The resulting diploids were streaked on YES agar plates along with a *stn1-75 rqh1Δ* haploid control and incubated at 25°C and 36°C until single colonies were visible on both sets of plates [Fig 5.1A].

The streaks show that the *stn1*$^+$/*stn1-75 rqh1Δ*/*rqh1Δ* control strain was able to grow at both 25°C and 36°C, while the haploid *stn1-75 rqh1Δ* did not form colonies at 36°C, as expected. The *stn1*$^+$/*stn1-75 rqh1Δ*/*rqh1Δ* and *stn1*$^+$/*stn1-99 rqh1Δ*/*rqh1Δ* test strains grew similarly to the *stn1*$^+$/*stn1-75 rqh1Δ*/*rqh1Δ* control strain, with no visibly unhealthy colonies at either temperature. This indicated that the *stn1* alleles were recessive and, therefore, suitable for use in a suppressor screen.

6.2.2 Closer analysis of MMS sensitivity in *stn1-75*

Given that the MMS sensitivity of *stn1-75* was also of interest, it was decided that a more quantitative analysis of the sensitivity would be beneficial. To that end, wild-type, *pot1-1* and *stn1-75* strains were cultured at 25°C to mid-log phase and plated at a density of 300 cells per plate on YES + MMS at several concentrations. These were then incubated at 25°C and 36°C. Colony formation was observed and viability on each plate calculated as the percentage of cells forming colonies relative to 0% MMS at 25°C [Fig 5.1B].

These data showed that the *pot1-1* and *stn1-75* strains were very acutely sensitive to MMS; however, some background was found at 0.001% and 0.0025% concentrations of MMS at 36°C for both strains. At a higher, 0.005% MMS, concentration, no colonies were formed at 36°C, however, it appeared that this concentration of MMS combined with the 36°C temperature was more generally cytotoxic to all three strains. This is shown by the high sensitivity of the wild-type strain at this concentration of MMS whereas it was largely viable at all other concentrations and temperatures. This was surprising, given that the same wild-type strain had been shown to be resistant to MMS at this concentration and temperature by spot assay [Fig 5.13]. It was, therefore, proposed that the sensitivity at this concentration and temperature could be a dosage related artefact. With only 300 cells spread across each plate, each individual cell was in receipt of a much higher dosage of MMS from the surrounding area compared with the spot assays, where the cells were spotted at a higher density. It is possible that, during an actual screen, with a much higher density of cells spread across each plate, the dosage effect would be reduced. However, the use of 0.0025% MMS may be preferable over 0.005% in order to maximise the number of candidates that could be checked for temperature-sensitivity suppression, though this would be likely to increase the number of false positives pulled from the screen.

Figure 6.1: **Test for dominant negative phenotype in *stn1-75* and *stn1-99* strains and quantitative assay for MMS sensitivity in *stn1-75* strain.**

(A) Streaks on YES agar at 25°C and 36°C, testing for any indications of a dominant negative trait of *stn1-75* and *stn1-99* alleles through streaking of diploid strains, *stn1+/stn1-75 rqh1Δ/rqh1Δ* and *stn1+/stn1-99 rqh1Δ/rqh1Δ*. These would be synthetic lethal if the alleles were dominant negative. The *stn1+/stn1-75 rqh1Δ/rqh1Δ* control strain is able to grow at both 25°C and 36°C. The *stn1-75 rqh1Δ* haploid is not viable at 36°C, as expected. The test strains, of which there are two isolates of each (nr1 and nr2), grow with no indication of unhealthy morphology at the non-permissive temperature, indicating that the alleles are recessive. **(B)** Percentage survival of wild-type and temperature-sensitive strains, *pot1-1* and *stn1-75* single mutants, on YES + MMS plates at 25°C and 36°C relative to wild-type at 25°C, 0% MMS. Coloured bars represent different concentrations of MMS, as indicated. The data indicates that the *pot1-1* and *stn1-75* strains do have an acute sensitivity to MMS at 36°C but less so at 25°C. Some background is present at concentrations of MMS lower than 0.005%. A dosage-related cytotoxic effect of MMS may be present on 0.005% MMS plates when strains are incubated at 36°C, as indicated by a loss of viability in wild-type strain in these conditions.

A *stn1-75 and stn1-99* test for dominant negative phenotype on rich media (YES)

25°C

36°C
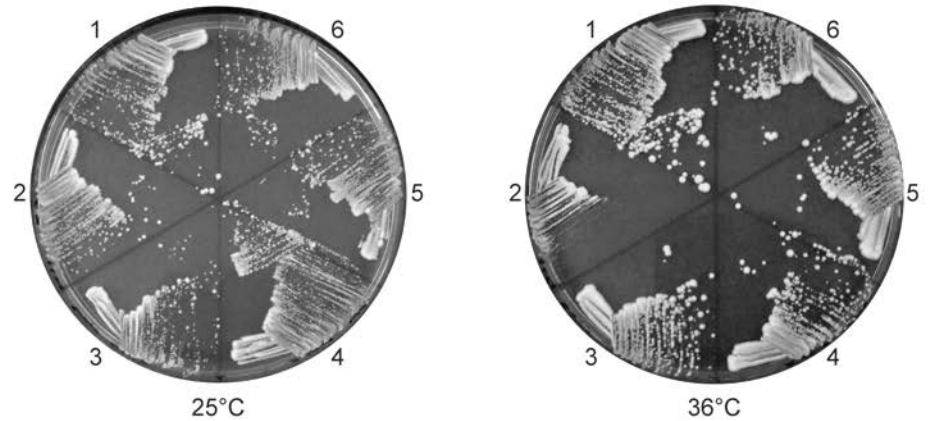
Key: 1: *stn1⁺/stn1⁺-ura4⁺ rqh1Δ/rqh1Δ*
      2: *stn1-75/rqh1Δ* (haploid)
      3: *stn1⁺/stn1-75 rqh1Δ/rqh1Δ*, nr1

4: *stn1⁺/stn1-75 rqh1Δ/rqh1Δ*, nr2
5: *stn1⁺/stn1-99 rqh1Δ/rqh1Δ*, nr1
6: *stn1⁺/stn1-99 rqh1Δ/rqh1Δ*, nr2

B Percentage (%) survival of ts strains with increasing MMS conc. at 25°C and 36°C
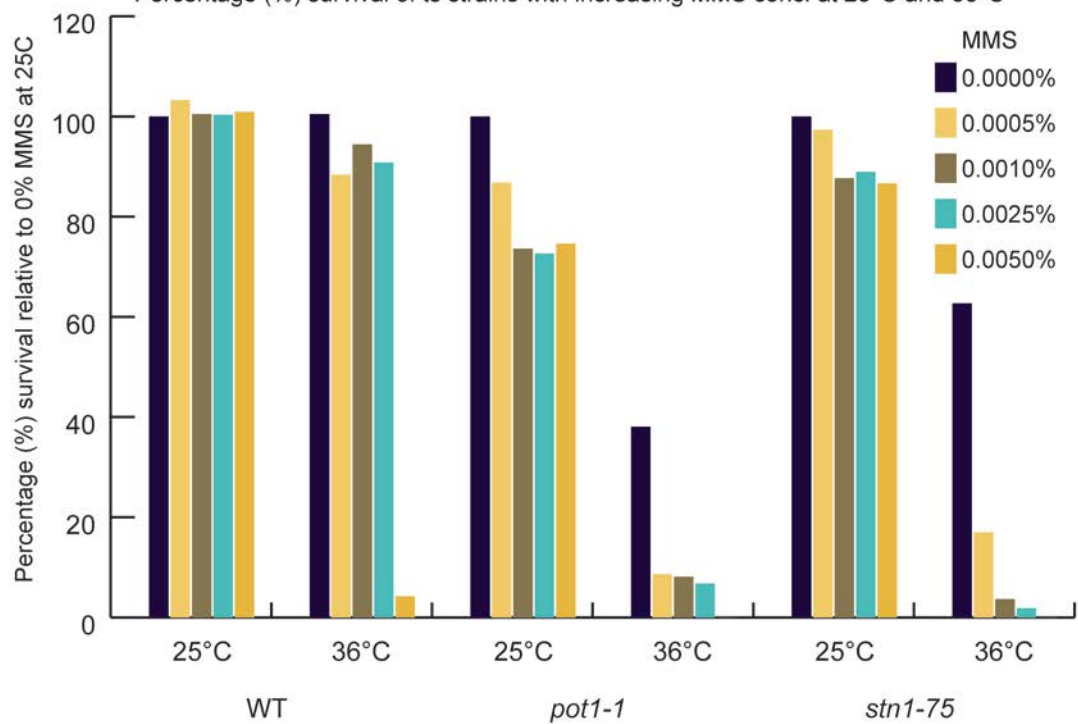
6.2.3 Cloning and testing of a *stn1+* covering plasmid

As a positive control for the suppressor screen, a *stn1*$^+$ covering plasmid could not be overlooked. This would provide not just the ability to use a positive control in a suppressor screen, but also the ability to suppress the *stn1-75* allele during further strain construction, allowing the use of higher temperatures to accelerate the process.

In order to construct a covering plasmid, the endogenous *stn1*$^+$ locus from a wild-type strain was amplified using primers Pstn1-SacII-Sp and Tstn1-KpnI-Sp in a high fidelity PCR reaction. This 3291bp PCR product included 1151bp of the promoter region, upstream of the START codon and 932bp of the terminator region, downstream of the STOP codon. This PCR product was then cloned into pFY116 using the unique SacI and KpnI restriction sites. The result was a plasmid containing the *ura4*$^+$ marker cassette as well as an *ars3002* yeast origin to allow stable maintenance in an *S. pombe* strain [Fig 6.2A].

To test whether this pSpStn1-U plasmid was functional, it was transformed into the *stn1-75* strain. The transformants, along with appropriate controls were streaked on YES + Phloxine B plates and incubated at 25°C, 33.5°C and 36°C for several days. The growth and colouration of the colonies was then assessed [Fig 6.2B].

The Phloxine B test indicated that the covering plasmid only partially suppressed the *stn1-75* allele. The colour of the *stn1*$^+$-*ura4*$^+$ strain at all temperatures remained white while the colour of the *pot1-1* control became a deep pink at the non-permissive temperatures, as expected. The colour of the *stn1-75* strain with the covering plasmid, however, was a slight shade of pink by comparison to the controls. The covering plasmid, however, does appear to prevent the full temperature-sensitivity phenotype from becoming apparent. This judgement is based on a comparison of the colouration of the colonies of the *stn1-75* strain transformed with the covering plasmid and those transformed with the empty vector. A deep pink colour develops in the colonies of the *stn1-75* strain containing the empty vector at 33.5°C and 36°C, while the

stn1-75 strain containing the covering plasmid remained the same slight shade of pink at all temperatures. This implies that the cells were no less healthy at the non-permissive temperatures than at the permissive temperature. Given these results, this plasmid could function as a positive control for the suppressor screen as many suppressors are likely to be partial. However, this plasmid would not be as useful for suppressing the *stn1-75* allele in any further strain construction due to the risk of telomere uncapping.

Figure 6.2: **Construction and testing of a *stn1$^+$* covering plasmid (following page).**

(A) Construction of the pSpStn1-U *stn1* covering plasmid. **(i)** The *stn1* chromosomal locus was amplified using the primers: Pstn1-SacII-Sp and Tstn1-KpnI-Sp in a high-fidelity PCR. The amplicon included the wild-type *stn1$^+$* ORF (purple), 1152bp of the upstream promoter (P*stn1*) region and 932bp of the downstream terminator (T*stn1*) region. **(ii)** The PCR product contains SacII and KpnI restriction sites which are used to clone the product into the same sites in pFY116. **(iii)** The final pSpStn1-U covering plasmid consists of the wild-type *stn1$^+$* ORF (purple) as well as promoter (P*stn1*) and terminator (T*stn1*) regions (blue). In addition, a *ura4$^+$* marker (red) is present under the control of the wild-type promoter (P*ura4*) and terminator (T*ura4*) shown in green. The *ars3002* replication origin sequence is also present to enable maintenance in *S. pombe*. **(B)** Covering plasmid test. The pSpStn1-U plasmid was transformed into the *stn1-75* strain. The pFY116 empty vector was separately transformed into the same strain. Two isolates from each transformation (nr1 and nr2) were streaked with controls on YES + Phloxine B and incubated at 25°C, 33.5°C and 36°C. The colour of the *stn1$^+$-ura4$^+$* control strain remained white at all temperatures. The colour of the *pot1-1* control strain switched from white to a deep pink colour at 33.5°C and 36°C. The *stn1-75* strain containing the covering plasmid (pSpStn1-U) became a slight shade of pink, compared to the controls but not to the same extent as the *stn1-75* strain containing the empty vector. This indicated at least a partial suppression of the temperature-sensitivity phenotype.

A

i: High-fidelity PCR of genomic *stn1* locus

Pstn1-SacII-Sp

Pstn1   stn1+   Tstn1

Tstn1-KpnI-Sp

ii: PCR product

Pstn1   stn1+   Tstn1   pFY116

SacII   KpnI

SacI-KpnI   SacI-KpnI

iii: pSpStn1-U

Pstn1   stn1+   Tstn1

SacII   KpnI

ars3002   Pura4   ura4+   Tura4

B   Stn1 Covering Plasmid Test

25C   33.5C   36C

Key: 1: *stn1+-ura4+*   4: *stn1-75* + pSpStn1-U, nr2
        2: *pot1-1* + Empty Vector   5: *stn1-75* + Empty Vector, nr1
        3: *stn1-75* + pSpStn1-U, nr1   6: *stn1-75* + Empty Vector, nr2

6.2.4 Small scale screening test using pSpStn1-U covering plasmid as a control

An *S. pombe* genomic library containing in excess of 100 000 clones and based in a vector containing an *ura4⁺* marker was provided by the Carr lab (Barbet *et al.*, 1992). Using this library and the pSpStn1-U covering plasmid, a test screen was carried out. Two methods were used. One to take advantage of the synthetic lethal phenotype generated in an rqh1Δ background and the other to take advantage of the MMS sensitivity of the *stn1-75* allele.

The *stn1-75* and *stn1-75 rqh1Δ* strains were, therefore, each transformed with 1µg of the library and separately with 1µg of the pSpStn1-U covering plasmid. The *stn1-75 rqh1Δ* transformations were plated onto YNG –Ura on a series of 6 plates, the first 4 containing approximately 20% of the transformation mixture each and the final two containing 10%. These two plates were incubated at 25°C. The remaining plates were incubated at 33.5°C and 36°C (2 plates at each temperature). For the *stn1-75* transformations, YES + 0.0025% MMS plates were used to take advantage of the acute viability phenotype at this concentration of MMS. Similarly to the first set of transformations, two of six plates received 10% of the transformation mixture and were incubated at 25°C to check transformation efficiency. The remaining transformation mixture was plated on the same plates, 20% per plate. These were incubated at 33.5C and 36°C.

After 5 days, colony formation on the 25°C plates was observed. However, for both the covering plasmid and the library transformation into the *stn1-75 rqh1Δ* strain, a lawn of cells was found indicating that the transformation efficiency was higher than expected. The transformations ought to be diluted such that not more than 1000 clones are screened per plate to allow separation and identification of individual clones. As a result, it was not possible to determine the transformation efficiency with these specific series of plates. Therefore, it was not surprising that on checking the YNG –Ura plates incubated at 33.5°C and 36°C, it was found that no single colonies were visible for either the library or the covering plasmid.

The 0.0025% MMS plates, on the other hand, were more promising. The two plates incubated at 25°C contained 776 and 796 colonies for the library transformation while the covering plasmid transformation plates contained 412 and 287 colonies. Given that 10% of the transformation mix was plated on each of these plates, it would indicate that approximately 8000 clones were successfully transformed from the library as well as 3500 individual pSpStn1-U covering plasmid molecules. The plates incubated at 33.5C revealed 23 colonies for the covering plasmid transformations. No colonies were found on the plates incubated at 36°C. This is much fewer than would be expected from a covering plasmid that would fully suppress the *stn1-75* allele indicating again that it is likely only a partially suppressor.

Several colonies were found for the library transformations on 0.0025% MMS, 12 colonies on the plates incubated at 33.5°C and 3 colonies on the plates at 36°C. It is reasonable to predict that some of these may be false positives, given that it has been established that *stn1-75* can form colonies on 0.0025% MMS, albeit a very small percentage of the total plated and also that the covering plasmid positive control did not form any colonies at 36°C. Nevertheless, these colonies were streaked to YNG –Ura plates at 25°C to check for and maintain the presence of a library plasmid clone and also on 0.0025% MMS plates, incubated at 33.5°C and 36°C [Fig 6.3].

Not all the candidates streaked on YNG –Ura grew to single colonies, indicating that they may false positives which had survived the initial dose of MMS received. On 0.0025% MMS, however, the Ura$^+$ strains as well as several Ura$^-$ grew at 36°C. This would indicate that some of these strains may have developed internal suppressors. Identifying these would require whole genome sequencing to be carried out. All the Ura$^+$ candidates, however, also grew on MMS. The library clones from these candidates could be more easily isolated and identified than those requiring whole genome sequencing. Presently these candidates, numbers 4, 6, 11 and 12, are being further analysed and prepared for plasmid recovery.
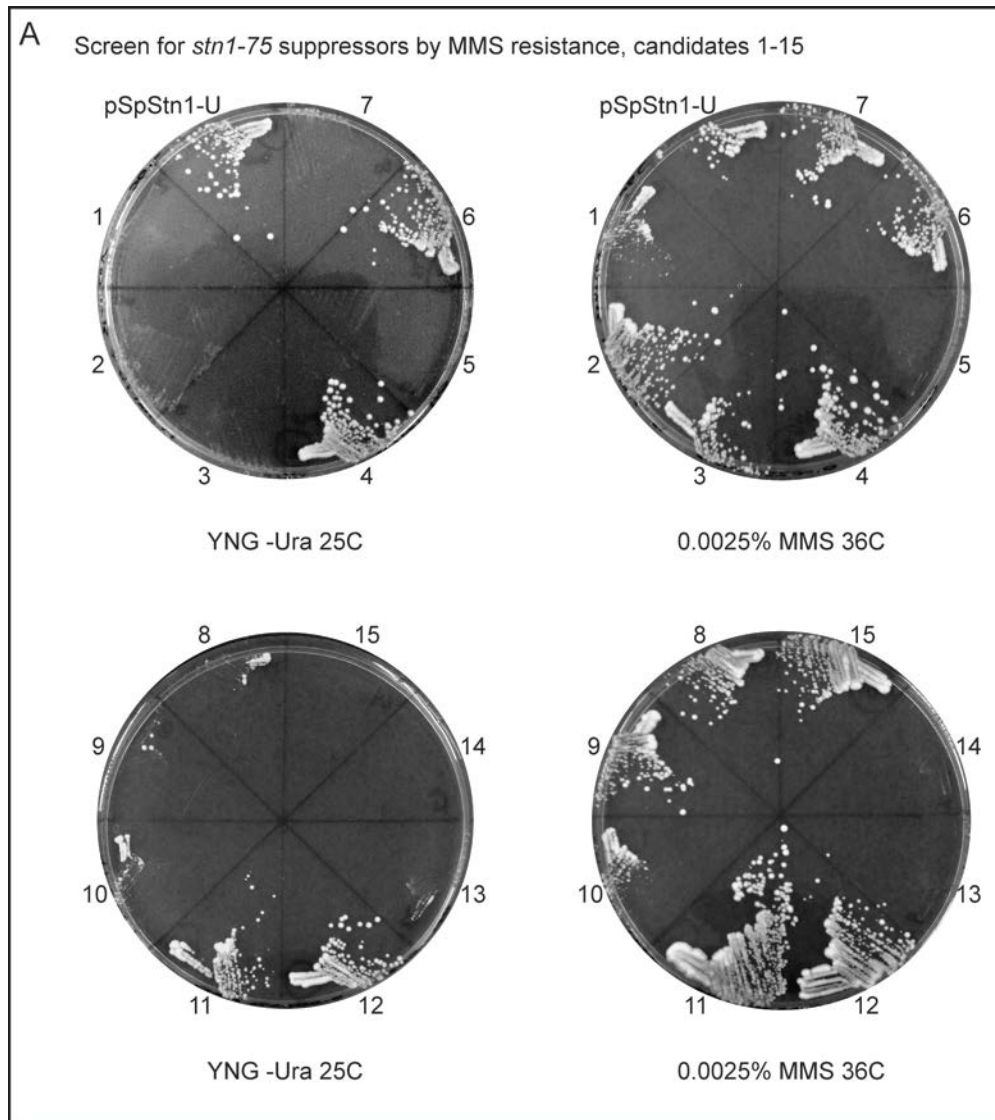
Figure 6.3: Streaks of *stn1-75* suppressor candidates from MMS resistant colonies in a small scale screen.

(A) Streaks of *stn1-75* suppressor candidates. The *stn1-75* strain was transformed with an *S. pombe* genomic library with >10 000 clones in a *ura4*[+] vector. Suppressor candidates were selected on YES + 0.0025% MMS agar. Of approximately 8000 clones screened, a total of 15 candidates were identified as MMS resistant. These were streaked to YNG –Ura as well as fresh YES + 0.0025% MMS with *stn1-75* + pSpStn1-U covering plasmid as a positive control. Growth of the positive control is seen on both YNG –Ura at 25°C and 0.0025% MMS at 36°C. Of the 15 candidates, four were found to grow to single colonies on YNG –Ura, nr4, 6, 11 and 12. These were also found to be 0.0025% MMS resistant at 36°C. Of the remaining 11 candidates, none grew on YNG –Ura but seven of these showed growth on 0.0025% MMS at 36°C indicating that they may have developed internal suppressors of the *stn1-75* allele.

6.3 Summary

The *stn1-75* and *stn1-99* alleles provided a suitable tool to search for a Cdc13, or CTC1 orthologue in *S. pombe*. Previous characterisation identified two phenotypes which could be used to develop an optimal screening method. Firstly, the *rqh1Δ* background, first used to identify the two *stn1* temperature-sensitive alleles, provided a suitable synthetic lethal phenotype that could be used for the screen. Secondly, the *stn1-75* allele was found to be acutely sensitive to MMS, more so than *stn1-99*. These characteristics made *stn1-75* a suitable allele for the screening process.

One aspect of the *stn1-75* allele that had not been investigated, however, was whether a dominant-negative phenotype is produced. If this were the case, even a full wild-type *stn1*⁺ mutant would not suppress the temperature-sensitivity. Therefore, to test this, diploid strains were generated which expressed both wild-type and temperature-sensitive alleles of *stn1*. By combining these with *rqh1Δ*, it was possible to determine whether a wild-type allele could fully suppress the *stn1-75* and *stn1-99* alleles. Streaks on YES agar at 25°C and 36°C indicated that the *stn1-75* and *stn1-99* alleles did not generate a dominant-negative phenotype, as seen by growth at 36°C, which otherwise would have produced the synthetic lethal phenotype. This meant that the *stn1* alleles could, indeed, be used for screening.

To determine the optimal concentrations of MMS to use with the *stn1-75* allele, a quantitative cell viability assay was conducted. A known number of cells from wild-type, *pot1-1* and *stn1-75* strains were plated onto media containing MMS at a range of concentrations. By calculating the percentage of viable colonies formed at each concentration, relative to the number of colonies formed by the wild-type strain at 25°C without MMS, it was possible to determine that a concentration of 0.0025% MMS could be used to screen for suppressors. Though some background growth was present using this concentration of MMS, given that a higher dose produced general cytotoxicity in all strains, use of a higher concentration was not an option.

Any screening method would benefit from the use of a positive control that could be used to determine the optimum stringency for selection of suppressors. Given that expression of a wild-type *stn1*[+] was sufficient to complement the temperature-sensitive alleles, a *stn1*[+] covering plasmid was constructed. This consisted of 1151bp of the *stn1* upstream promoter region and 932bp of the downstream terminator region. Testing this covering plasmid in the *stn1-75* strain determined it was sufficient to at least partially suppress the allele. This made it a useful control to use for partial suppressors in the screen, though further characterisation of the covering plasmid would be useful, for example, the effect it has on telomere length compared to the modified promoter context in which the *stn1-75* allele resides.

With a suitable set of conditions and a positive control plasmid in tow, a small scale screen was conducted. Both methods of screening were employed, selecting for suppressors by growth in an *rqh1Δ* background and separately by resistance to MMS. However, the use of the *rqh1Δ* background did not produce any candidates even though the apparent efficiency of the transformations was much higher than expected. The MMS resistance screen, on the other hand, did produce a number of candidates, 15 out of approximately 8000 clones screened. Of these, four appeared to be real positives while a further seven appeared to be MMS resistant due to internal suppressors. The remaining appeared to be false positives in the initial screen. The library clones from the four positive candidates now await isolation and identification while the internal suppressors require whole genome sequencing for identification.

With the apparent high stringency of selection with the methods used so far and the generation of what appear to be many internal suppressors, modifications need to be considered. Further characterisation of the *stn1* alleles may also assist in the development of alternative and more efficient methods of screening.

Chapter 7

Discussion and future directions

7.1 The role of Poz1 in the *S. pombe* telomeric complex

It is challenging to reliably study specific subunits of the telomeric complex, given the interdependence for functionality between the proteins. A two-state model of telomerase recruitment predicts that telomerase access to the telomere can be modulated by the telomeric complex in a manner that is dependent on the relative strengths of the inhibition and promotive signals (Jun *et al.*, 2013). If inhibitive signals are stronger, as predicted when telomeres are longer, telomerase would not able to act on the telomere. However, if the inhibitive signal is sufficiently weakened, as predicted on shorter telomeres, telomerase would be able to act on telomeres. The core complex is hypothesised to switch from one state to the other, possibly through a structural transition that is dependent on the relative quantities and activity levels of inhibitive and permissive components.

With multiple interactions between the proteins forming the core complex, null alleles can have acute phenotypes. For example, if Taz1, the double-stranded DNA-binding protein, is deleted, a complete loss of telomerase inhibition occurs. This then complicates the study of any aspect of losing Taz1 functionality that does not involve telomerase inhibition (Cooper *et al.*, 1997).

This appears to also be true for Poz1, without which, a similar loss of telomerase inhibition is observed, resulting in telomeres that are extended to lengths in excess of 3kb. This has been shown in previous studies and was shown here once again (Jun *et al.*, 2013, Miyoshi *et al.*, 2008). In order to study more subtle effects of disruption, or functions aside from telomerase

inhibition, it is prudent to attempt to disrupt specific interactions, rather than removing or depleting whole subunits altogether.

The aim of this study was, therefore, to investigate the roles and significance of the known protein-protein interactions of Poz1 with its binding partners, Rap1 and Tpz1, through the generation of specific separation of function alleles. It was hypothesised that these interactions may be responsible for keeping the telomeric complex in the proposed closed, telomerase-inhibitive state. Disruption of these interactions could, therefore, result in modified telomerase recruitment or activation.

7.1.1 The use of a reverse yeast 2-hybrid system in the screening for separation of function alleles

In order to screen for separation of function alleles, the reverse 2-hybrid system developed by the Thorburn lab was employed (Thomas *et al.*, 2002). This system allowed the integration of bait protein constructs into the *TRP* and *URA* loci of the *S. cerevisiae* LY26 strain for consistent and predictable expression of the bait proteins in different screening strains and individual clones. Selection of transformants expressing *ADE2* and *HIS3* using this system allowed the isolation of clones that had lost a specific interaction but maintained a second specific interaction. Using this method also provided the ability to screen a large number of mutagenised prey clones for the specific phenotypes desired.

Although taking a systematic approach to making amino acid substitutions throughout Poz1 may have revealed specific regions important for specific interactions, there would have been no guarantee that single amino acid substitutions would have been sufficient. In that case, generating and screening all combinations of multiple substitutions would have been unnecessarily slow and inefficient. The vast majority of these substitutions would likely not result in the desired phenotype but still would have required individual transformations and

testing to confirm. Using PCR-based random mutagenesis of the *poz1* ORF, followed by bulk transformations of the PCR product, a vast number of clones, with mutations ranging from single to multiple amino acid substitutions, could be and were screened. Indeed, a Rap1-interaction disruption candidate, Poz1-mut17, was isolated from the screen relatively easily. Isolating a Tpz1-disruption candidate was, however, more difficult.

One of the main drawbacks of using the reverse 2-hybrid system, or indeed any yeast 2-hybrid screening system, however, is the likelihood of finding false positives; especially in a complex reporter system such as the one used in these strains [Fig 3.2]. This was an issue that was encountered during this screen, specifically; the screening of Poz1-Tpz1 interaction disruption candidates using screening strain number 3 resulted in multiple false positives. In hindsight this was not surprising, given the selective pressure applied to the strains during the screen. When screening thousands of clones, a relatively small number of cells containing random mutations that affect the reporter genes could produce a high background of false positives.

To combat this possibility, the Thorburn lab designed the strains such that they could be mated with the LacZ reporter strains, Y190 and DY6877 (Thomas *et al.*, 2002). This would allow the interactions between baits and prey molecules to be tested in a forward yeast 2-hybrid assay with a reporter that was not present during the initial screen. In theory, this would identify false positives in just a few additional steps. Indeed, the assay did identify several clear false positives; however, many of the others, based on further tests appeared to be Poz1 clones with weakened interaction with Tpz1, rather than complete loss. This indicated that the reverse 2-hybrid system was allowing partial disruptors through the screening process. Systematic forward 2-hybrid tests using the PJ69-4A strain on a number of these candidates were then able to identify a full Tpz1-interaction disruption clone that was identified as Poz1-mut23.

In hindsight, however, initial forward 2-hybrid assays using truncated forms of wild-type Poz1, would have permitted the identification of likely minimal interaction patches for Poz1-Rap1 and Poz1-Tpz1. This would then have made a systematic approach to making substitutions more manageable.

7.1.2 Sequence analysis of the Rap1- and Tpz1-interaction disruption *poz1* alleles

Two mutants, Poz1-mut17 (Rap1 disruption) and Poz1-mut23 (Tpz1 disruption) were identified from the screen. Sequencing of these identified multiple nucleotide mutations in the ORFs and in both cases these caused five amino acid substitutions with no obvious clusters. Therefore, it was not possible just from the location of the substitutions to determine which residues were functionally important for Rap1 and Tpz1 interactions. However, the $poz1^+$ ORF had been modified with this possibility in mind. Additional restriction sites had been engineered into the ORF to allow separation of multiple mutations [Fig 3.7].

Due to being isolated first, the mutations in the ORF of Poz1-mut17 (Rap1 disruption) were separated by use of the BamHI site engineered into the nucleotide sequence. This separated the mutations into two clusters, three toward the N-terminus and two further toward the C-terminus. These were then tested by forward 2-hybrid analysis to determine which amino acid substitutions were sufficient for Rap1-interaction disruption. Of the two new mutants, named Poz1-mut19 and Poz1-mut20, and five substitutions, it was possible to determine that the C143R and L157P substitutions in Poz1-mut20 were sufficient to display the Rap1 disruption phenotype Fig 3.12 and 3.13]. Poz1-mut20 was then subject to further analysis.

Separation of the mutations in Poz1-mut23 (Tpz1 disruption), however, was not straightforward. With the five substitutions, F18Y, F65I, I89M, L95H and M243R, spread throughout the ORF, separating these into smaller clusters would require multiple cloning steps (see section 3.2.10). To avoid unnecessary cloning, it was, therefore, prudent to analyse

these substitutions further to select candidates most likely to cause the interaction disruption. The two most C-terminal substitutions, L95H and M243R, are substantial changes, from small hydrophobic residues to large, positively charged, hydrophilic residues. This, in theory, made them good candidates, unlike the three N-terminal substitutions, which were minimal changes. However, if specific residues are highly conserved, even minor substitutions could generate disruptive phenotypes. This is based on the theory that functionally important residues would be more likely to be evolutionarily conserved. Therefore, the peptide sequence of wild-type Poz1 from *S. pombe* was aligned to its closest relatives, *S. octosporus*, *S. cryophilus* and *S. japonicas*, all members of the *Schizosaccharomyces* genus, using Clustal Omega. Also, in the absence of a crystal structure, the *S. pombe* Poz1 peptide sequence was used to make a secondary structure prediction using the PSIPRED webserver. The locations of the substitutions in both Poz1-mut20 (Rap1 disruption) and Poz1-mut23 (Tpz1 disruption) were then mapped onto this alignment to determine the conservation of the residues affected in the two mutants [Fig 3.15]. Finally, the likelihood that the substitutions would be tolerable or intolerable was then predicted using the SIFT webserver [Table 3.5]. This takes into account the alignment of the residues in determining whether specific substitutions, even if they are disruptive in the local structure, are likely to be tolerable.

The sequence alignments and predictions allowed several interesting observations to be made. Firstly, the Poz1 peptide sequence, as a whole, is fairly well conserved in the *Schizosaccharomyces* genus, with 37.77% sequence identity between *S. pombe* Poz1 and *S. octosporus* Poz1. However, the position of one of the most potentially disruptive substitutions in Poz1-mut23, M243R, was found to be in the poorly conserved far C-terminus of the protein. Given the conservation throughout the rest of the protein, this makes M243 unlikely to contribute to Tpz1 interaction, though this does not remove the possibility that the substitution brings a structural change in the C-terminus that occludes a conserved Tpz1-binding site. Without solving the Poz1 crystal structure, however, this is difficult to determine

with any confidence. Certainly it would be easier to just separate this substitution from the rest in Poz1-mut23 and test it for Tpz1-disruption.

Another interesting observation is that many of the substitutions, a total of five out of seven, map to residues that are fully conserved in at least the three most closely related Poz1 sequences, *S. pombe*, *S. octosporus* and *S. cryophilus*. These are L157P in Poz1-mut20 (Rap1 disruption) and F18Y, F65I, I89M and L95H in Poz1-mut23. This could just be coincidence, with *S. pombe* Poz1 having more 37% sequence identity with both of these sequences. However, the highest concentrations of conserved residues between *S. pombe* and all three other sequences are mostly found clustered around predicted helices while the regions between helices in *S. pombe* are not as well conserved. This is especially apparent between the predicted α2- and α-7 helices where residues conserved in *S. pombe* tend to be found only in the predicted helices, leaving many non-conserved residues in the regions between them. This would suggest that the residues in these predicted helix structures could be functionally important, more so than the unstructured regions between them.

The SIFT predictions are also quite interesting. Neither substitution in Poz1-mut20 (Rap1 disruption) is predicted to be sufficiently disruptive in the context of the level of conservation as to be intolerable. This could mean that both substitutions are required to disrupt the interaction with Rap1. As another suitable restriction site is not available, this could be tested by making single point mutations in the *poz1* ORF by site-directed mutagenesis and comparing individual substitutions to Poz1-mut20 and wild-type Poz1 in a forward 2-hybrid assay. For the two most disruptive substitutions in Poz1-mut23 (Tpz1 disruption), L95H, being a disruptive substitution at a well conserved residue, is, indeed, predicted to be intolerable. Unsurprisingly, based on the poor conservation, M243R is predicted to be tolerable. This indicates that M243 is not likely to be important in the interaction with Tpz1, but does not rule out the possibility that it introduces some structural change at the C-terminus that hinders the interaction. Of the

three relatively minor substitutions, however, F65I was predicted to be intolerable while the others, F18Y and I89M, were predicted to be tolerable. This appears to be due to the conservation of Phenylalanine 65, which is fully conserved in all four sequences. This would suggest that it may be conserved due to functional importance. Both F65I and L95H, therefore, would make good candidates to separate and test individually for a Tpz1-disruption phenotype. Separating these by restriction digest would unfortunately leave them with one additional substitution in each case, F18Y + F65I and I89M + L95H respectively. As a result, these are the subject of ongoing work to introduce the substitutions by site-directed mutagenesis.

7.1.3 The *poz1* separation of function alleles have an elongated telomere phenotype

An *S. pombe* base strain was designed to allow integration of these disruption alleles by Recombinase-Mediated Cassette Exchange (RMCE) (Watson *et al.*, 2008) and to act as *poz1Δ* control strain. This involved the integration of lox recombination sites at the *poz1* locus, including a loxP site 0.6kb upstream of the START codon. It was thought that this would be sufficiently distant from the START codon so as not to interfere with the expression of integrated *poz1* alleles. However, upon comparing the telomere lengths of *S. pombe* strains containing fully wild-type *poz1⁺* (no lox sites), the wild-type Poz1-FL2 (with lox sites), Poz1-mut20 and Poz1-mut23, a telomere length phenotype was found.

The loxP-Poz1-FL2 strain with the modified promoter initially showed an increase in telomere length of 0.3-0.4kb compared to the full wild-type strain [Fig 3.18]. This was after allowing the strain to equilibrate telomere length by streaking to single colonies 8 times. Streaking this strain to single colonies a further 8 times allowed the loxP-Poz1-FL2 strain to further equilibrate telomere length to a more acceptable length, close to wild-type [Fig 3.20]. However, the addition of 10xMyc epitope tags to the strains for expression and telomere

recruitment analysis resulting in an increase in telomere length once again. The addition of the 10xMyc epitope tag to the full wild-type strain resulted in an increase of telomere length of approximately 0.3-0.4kb. This effect was further exaggerated in the loxP-Poz1-FL2 strain [Fig 3.20].

Expression analysis by western blot indicated that the increase in telomere length of the loxP-Poz1-FL2 strain could be due to slightly reduced expression, relative to the tagged wild-type strain [Fig 3.19]. In addition to this, a second, fainter band is visible in the western blot. This is slightly smaller than the size of a 10xMyc-tagged Poz1 protein (43kDa) which is not present in lanes with untagged Poz1 and so would imply that the tagged protein is susceptible to protease action. Whether the 10xMyc tag is being truncated or Poz1 cannot be discerned with just these strains. It would, perhaps, be possible if an alternative epitope tag were used, such as a Flag tag, and the two compared. A similar truncation in a Flag-tagged Poz1 would indicate that Poz1 is the target of protease action. On the other hand, it is possible the addition of any tag, be it Myc, Flag or otherwise, may contribute to Poz1 being targeted for protease cleavage.

The separation of function mutants, Poz1-mut20 and Poz1-mut23, were found to have very elongated telomeres [Fig 3.18 and 3.20]. The smears on the southern blots, where EcoRI-digested genomic DNA was used, ranged from 1.5kb to at least 5kb. The highest concentration of signal is found at approximately 4kb. This indicated that most telomeres in these strains were within the same range as produced by a *poz1Δ* allele.

The implication from this, therefore, is that disruption of either Poz1 binding partner results in the inability to inhibit telomerase. Based on the closed versus open complex model proposed, this would mean the complex in these strains is left permanently in the open conformation, permissive to telomerase activity.

7.1.4 Localisation of the *poz1* separation of function alleles to the telomere

To determine whether Poz1 is still localised to the telomeres with these separation of function alleles, ChIP samples were taken from the tagged strains using anti-myc antibody. The recruitment to telomeres was assessed by slot blot using the same telomere probe as used in telomere length assays as well as by quantitative PCR using a TAS1 chromosomal amplicon, proximal to the telomeres [Table 3.6 and Fig 3.21].

The signal achieved through the slot blot was much lower than expected, considering the signal achieved in the telomere length assays using the same telomere-specific probe. As a result, it was not possible to quantitate the signal intensities. However, based on a visual comparison, the intensities of the bands for the samples derived from the loxP-Poz1-FL2 strain appeared reduced compared to the full wild-type control. The intensities of the bands from both interaction disruption strains were further reduced, if visible at all. These results indicated that the recruitment of Poz1 to telomeres may be reduced when the gene is expressed in the context of the modified promoter and further reduced when interaction with either binding partner is disrupted.

The results of the qPCR agree with the visual analysis of the slot blot. Recruitment of Poz1 from the loxP-Poz1-FL2 strain appeared reduced compared to a full wild-type. Recruitment of Poz1 from the interaction disruption strains appeared reduced to background levels, almost identical to the untagged Poz1 negative control. Although these data agreed with what would be predicted, based on the telomere lengths, that Poz1 function is compromised, the reliability of the data from the qPCR is questionable. As explained in section 3.2.17 of the chapter, the large size of the telomeres would make accurate quantification of Poz1 recruitment problematic due to the location of the qPCR amplicon upstream of the telomere. Even the use of low sonication conditions, as used in these tests, may not have been sufficient to avoid separating the amplicon from the majority of the telomere. If the issue of the long telomeres

cannot be overcome for reliable qPCR, then at least the slot blot protocol could and would need to be optimised to reduce background and increase signal intensity. Quantification of the band intensities would then allow the levels of Poz1 recruitment to the telomeres to be determined in these strains and any others generated in the future.

If, for a moment, the ChIP/Slot Blot and ChIP/qPCR test results were considered to be reliable, they may also indicate that the interaction disruption alleles, once integrated and expressed in *S. pombe*, have reduced interaction with both binding partners, rather than just the one specified. This could be due to a number of factors. The reduced expression would result in less Poz1 being available to be recruited to telomeres. This could be solved by integrating the alleles in a wild-type locus. There may also be unexpected differences in protein folding between the 2-hybrid assays, where GBD and GAD fusion proteins are used, and these *S. pombe* strains, where the proteins are only epitope tagged.

Therefore, rather than relying on yeast 2-hybrid data, co-immunoprecipitation tests could be used to ensure that the correct interaction disruption phenotypes were still present in *S. pombe*. Co-immunoprecipitation could also be used to determine if any of the existing substitutions in the alleles are located in specific binding sites and the extent of the binding sites through systematic substitutions in residues that are in proximity to each existing substitution.

7.1.5 Further observations and future directions

According to data from a recent publication on Tpz1 function, disruption of the interaction between Tpz1 and Poz1 by mutating residues on Tpz1 results in a telomere elongation phenotype. However, the length of these telomeres is not quite equivalent to a full *poz1Δ* (Jun *et al.*, 2013). This implies that another, separable function of Poz1, other than Tpz1-

interaction, contributes towards the inhibition of telomerase. It is possible that this is though the interaction with Rap1. However, it may also be another, unknown function or interaction.

This discrepancy in telomere length between the alleles generated in this study and the *tpz1* allele generated by Jun *et. al.* (2013) may be due to reduced *poz1* expression in the *S. pombe* strains used in this study. Use of the RMCE method of integration was, perhaps, not the best way to study a gene with such an acute null phenotype. By transferring both the Tpz1- and Rap1-interaction disruption alleles into a wild type locus, it may be possible recover wild-type expression and see the same difference in telomere length between the Tpz1-Poz1 disruption and *poz1Δ* alleles observed in the Tpz1 study. The Rap1-disruption might then reveal a weaker telomere length phenotype which could be additive to a Tpz1-disruption phenotype and make up the difference in length to a *poz1Δ* strain. If this were the case, then a Poz1 allele containing substitutions for both Tpz1- and Rap1-interaction disruption (dual-disruption) would have an identical phenotype to a *poz1Δ*. Though this would not be straightforward to test as presumably the loss of both Tpz1 and Rap1 interaction would prevent Poz1 from associating with the telomere. Therefore, Poz1 would need to be tethered to the telomere artificially, for example, by using a LacO-LacI system as has been used previously to show that human TPP1 is able to recruit telomerase to a non-telomeric location (Zhong *et al.*, 2012). However, if neither the Rap1-disruption, nor the dual-disruption strains were to result in a *poz1Δ* phenotype, the presence of an unknown function or interaction of Poz1, independent of Rap1 or Tpz1 interaction, would be indicated.

Given that Threonine 93 phosphorylation of Ccq1 has been shown to be required for telomerase recruitment, the discrepancy in telomere lengths between a Tpz1-Poz1 disruption and *poz1Δ* could be due to the loss of a specific kinase inhibition role of Poz1, as previously implied by deletion studies (Moser *et al.*, 2011, Yamazaki *et al.*, 2012). However, the Ccq1-hyperphosphorylation phenotype observed in the deletion studies could have been a result of

more than just the general inability to form a closed, telomerase-inhibitory, telomeric complex. They do not exclude the possibility of a specific, unknown function or interaction unobservable in null mutants. Indeed, TIN2, the human Shelterin counterpart to Poz1, has been implicated in supporting the inhibition of ATM and ATR kinases at the telomere through two methods, supporting the function of TRF2 and stabilising POT1-TPP1 binding to the telomere (Takai *et al.*, 2011).

Further speculation regarding an unknown function for Poz1 at the moment, without knowing the actual effect of the alleles in a wild-type locus, is premature. The integration of the existing alleles at a wild-type locus, both individually and combined as a dual-disruption, is, therefore, the priority in the immediate future of this study.

7.2 The search for a CTC1/Cdc13 homologue by yeast 2-hybrid

The Stn1 and Ten1 proteins in *S. pombe* as well as CTC1, STN1 and TEN1 in humans, mice and plants have all been identified in recent years. As a result, rather than being considered a unique feature of *S. cerevisiae* telomeres while POT1 played an analogous role in other eukaryotes, the RPA-like complex of CST is now thought of as a more universal feature, playing a complementing role to POT1 (Price *et al.*, 2010). It has been shown to be important in telomere capping as well as replication, where it has a role in promoting lagging-strand synthesis. In humans, this is thought it be a genome-wide, rather than a telomere-specific feature (Stewart *et al.*, 2012). It is, therefore, curious that in the six years since the identification of Stn1 and Ten1 in fission yeast, a third component, a CTC1 or Cdc13 homologue, has not been found.

Finding the components of Shelterin and CST has required a variety of techniques to be employed including bioinformatics sequence similarity searches, yeast 2-hybrid screens, co-immunoprecipitation, mass spectrometry and temperature-sensitivity suppressor screens (Grandin *et al.*, 2001, Grandin *et al.*, 1997, Houghtaling *et al.*, 2004, Kim *et al.*, 1999, Li *et al.*, 2000, Liu *et al.*, 2004, Martín *et al.*, 2007, Miyake *et al.*, 2009). Fission yeast Stn1 and Ten1 were identified by sequence similarities to the budding yeast counterparts that indicated the presence of OB folds (Martín *et al.*, 2007). Though both budding yeast Cdc13 and human CTC1 contain multiple OB folds, it would appear a similar protein in fission yeast was not identified (Chen and Lingner, 2013). A consistent pattern with regard to the largest subunit of CST, however, is the lack of overall sequence conservation. Indeed, the mammalian and plant CTC1 proteins are not necessarily thought of as true homologues of Cdc13 (Price *et al.*, 2010). Though CTC1 and Cdc13 could both be descended from an RPA ancestor protein, likely the largest subunit, they could have been generated by independent events and the structural similarities produced as a result of convergent evolution. If, however, they do share a common

ancestor, the sequence would appear to have diverged quite substantially (Miyake *et al.*, 2009, Surovtseva *et al.*, 2009).

To investigate the possibility of an as yet unidentified homologue of CTC1 or Cdc13 in *S. pombe*, it was decided that a yeast 2-hybrid approach could be successful. This approach has been used to identify a number of Shelterin components in the past including RAP1, TIN2 and TPP1 (Kim *et al.*, 1999, Li *et al.*, 2000, Liu *et al.*, 2004). It was, therefore, hypothesised that, should a homologue be present in *S. pombe*, a screen dependent on a physical interaction with the most likely binding partner, Stn1, would have the best chance of success.

7.2.1 Use of a forward yeast 2-hybrid system to screen for a CTC1/Cdc13 homologue in *S. pombe*

Unlike the reverse yeast 2-hybrid system employed to generate interaction disruption alleles of *poz1*, the forward yeast 2-hybrid system, based on the strain PJ69-4A, is much less complex. Indeed, it proved to be a more reliable indicator of interaction, or lack thereof, between Poz1 and its binding partners, Rap1 and Tpz1, than the Ly26 reverse 2-hybrid strain [Fig 3.9]. This may have been due to its use being limited to investigating interactions between specific fusion proteins, for example, GBD-SpTpz1 and GAD-SpPoz1 Tpz1-Poz1-disruption candidates [Fig 3.11]. However, reporter system in a forward 2-hybrid strain, like PJ69-4A, is much more straightforward. Only two fusion proteins are tested; one bait and one prey, whereas three fusion proteins had to be expressed in the reverse 2-hybrid; two baits and one prey [Compare Fig 3.2 and 4.1]. The bait and prey plasmids used in the forward 2-hybrid system were also based on well-established commercial plasmids from the Clontech Matchmaker system, pGBKT7 and pGADT7, and, therefore, had already been extensively tested. Indeed, in-house testing of these plasmids with other known *S. pombe* telomeric proteins had shown the system to be easily adaptable and the stringency modifiable (data not shown).

7.2.2 Screening of an *S. pombe* cDNA library using the forward yeast 2-hybrid system

In principle, the use of this forward 2-hybrid system to screen an *S. pombe* cDNA library, pTN-TH7, for a CTC1/Cdc13 homologue, or another novel Stn1 or Ten1 interaction, was expected to be relatively straightforward compared to the reverse 2-hybrid screening process. However, it was hampered with unexpected technical issues. The detection of Stn1-Ten1 interaction itself was only just within the threshold of the system, with only 10-15% recovery of positive controls in tests [Table 4.1]. The study in which *S. pombe* Stn1 and Ten1 were first identified appeared to indicate the same relatively weak interaction in the interaction tests (Martín *et al.*, 2007). It was unlikely, therefore, that an interaction with a novel protein, which may have been even weaker than Stn1-Ten1, would be detected. However, with a sufficiently large and high throughput screen, it may well have been possible had there not been background from *S. pombe ade6⁺* and *his5⁺* producing many false positives [Fig 4.6]. Indeed, if *ade6⁺* and *his5⁺* could have been eliminated from the library, a reduced level of stringency could have been used, making it easier for weaker interactors to be pulled out.

As already stated in Chapter 4, given that the number of *S. pombe* protein coding genes is quite small relative to the size of the library (approximately 5000 relative to a library size of 1 million clones), it was likely that most, if not all, proteins would have already been screened at least once using the procedure detailed in Fig 4.5. This does not, however, take into account variations in clones of the same gene. Indeed, several different *ade6⁺* and *his5⁺* clones were pulled from the library, complicating their exclusion from further testing.

7.2.3 Further observations and future directions

Moving forward, given the failure to pull out novel Stn1 or Ten1 interactors, or indeed Stn1 or Ten1 themselves, the temperature-sensitivity suppressor screen was adopted as an alternative. However, a recent study was able to identify novel interactions of Stn1 with Tpz1

in *S. pombe* (Chang *et al.*, 2013). Unlike the 2-hybrid screen or tests done in-house between Stn1 and, separately, Ten1 with components of the *S. pombe* telomeric complex (data not shown), this recent study used a forward yeast 3-hybrid approach. In this type of system, two bait proteins are used, rather than one. However, they are both expressed under the same type of promoter, on the same plasmid and only one bait protein, in this case Stn1, is fused to the Gal4-DBD. As a result, the GBD-fusion bait protein, GBD-SpStn1, can bind to its known partner, Ten1, which may help stabilise any interactions with a prey plasmid, in this case GAD-SpTpz1. This, therefore, assigned a function to the central region of Tpz1. The N-terminal OB fold is known to bind Pot1, the far C-terminal region is known to bind Poz1 and Ccq1, and the central region is now known to bind the Stn1-Ten1 complex (Chang *et al.*, 2013, Jun *et al.*, 2013, Moser *et al.*, 2011, Nandakumar and Cech, 2012).

In terms of the search for a CTC1 or Cdc13 homologue in *S. pombe*, this finding, that both Stn1 and Ten1 are required for Tpz1 interaction, is quite promising. It would suggest that a screen based on a forward yeast 3-hybrid setup could be more successful in pulling out Stn1-Ten1 interactors from the cDNA library. This would require modifications to the pGBKT7 plasmid used in order to incorporate both Stn1 and Ten1 under the same type of promoter. However, a new screen would benefit from having Tpz1 as a known Stn1-Ten1 interacting protein, a stronger positive control interaction than Stn1-Ten1 alone. A new yeast 3-hybrid screen would, therefore, be quite viable.

In addition, a systematic set of tests could be repeated using the 3-hybrid setup to search for novel interactions with the other components of the telomeric complex, as well as, non-telomeric proteins. Specifically, one possibility that has not yet been discussed is that, given the low sequence conservation of Cdc13/CTC1 across species and the remarkable structural similarities between RPA and the CST complex, the position of the third subunit of *S. pombe* CST may be taken by the equivalent RPA protein, Ssb1 (also known as Rad11) (Casteel *et al.*,

2009, Martín *et al.*, 2007, Miyake *et al.*, 2009). With a 3-hybrid approach, this could be specifically tested.

7.3 The generation, characterisation and use of *S. pombe stn1* temperature-sensitive alleles in the search of a CTC1/Cdc13 homologue

Given that the yeast 2-hybrid approach had not been successful, an alternative approach was selected to search for the elusive Cdc13/CTC1 homologue in *S. pombe*. A temperature-sensitivity suppressor screen was selected as this alternative. Indeed, similar screens have been used in the past to identify the *S. cerevisiae* Stn1 and Ten1 proteins (Grandin *et al.*, 2001, Grandin *et al.*, 1997). To identify Stn1, the *cdc13-1* temperature-sensitive allele was used and found to be suppressed up to 30°C by the novel Stn1 protein. Similarly, Ten1 was identified as a suppressor of the *stn1-13* temperature-sensitive allele at temperatures up to 37°C. Unlike the yeast 2-hybrid approach, a suppressor screen, being based in *S. pombe*, also had the added benefit of potentially identifying suppressors that did not bind Stn1 directly. This brought up the interesting possibility of finding novel regulatory pathways, in addition to novel interactors, which may act on other proteins to indirectly suppress the phenotype of a dysfunctional Stn1. But first a suitable *stn1* temperature-sensitive allele was required.

7.3.1 Identification of an appropriate genetic background to provide a synthetic lethal phenotype for a temperature-sensitivity suppressor screen

In many organisms, deletion or depletion of a protein required to cap the telomere results in activation of the DNA damage response pathways and leads to telomere-loss, chromosome end-to-end fusions and eventually replicative senescence or apoptosis (O'Sullivan and Karlseder, 2010, Palm and de Lange, 2008). In *S. pombe*, however, due to the presence of only three chromosomes, telomere deprotection can lead to chromosome circularisation in a small percentage of cells. These cells may be unhealthy, but remain largely viable and grow similarly to wild-type cells, making them difficult to distinguish once established (Nakamura *et al.*, 1998). They have been found to use the SSA or, in some cases, NHEJ pathways for intra-

chromosomal fusions (Wang and Baumann, 2008). Some cells are also able to maintain linear chromosomes through recombination-based pathways. HAATI cells are dependent on Ccq1 and Pot1 to maintain and cap the chromosome termini. In these cells, sub-telomeric sequences or rDNA from Chromosome III is spread to and amplified on all chromosome termini. If Ccq1 is lost, rather than using the HAATI pathway, another recombination-based pathway is able to maintain linear chromosomes (Jain *et al.*, 2010, Tomita and Cooper, 2008).

These methods of survival pose a potential problem for a suppressor screen. They afford the growth of cells that have undergone telomere deprotection, thereby increasing the background in a screen. Using a more stringent level of suppressor selection might reduce the background, but it would also reduce the likelihood of identifying partial suppressors in a screen. Therefore, a genetic background that would result in a more acute loss of viability when undergoing telomere deprotection was required. This background would need to either inhibit the formation of circularised chromosomes or prevent their maintenance. This would also simplify the identification of a suitable *stn1* temperature-sensitive allele.

The majority of cells that survive when Pot1 is lost do so by maintaining circular chromosomes. Given that previous studies had indicated that the phenotypes of *pot1Δ* and *stn1Δ* strains were indistinguishable (Martín *et al.*, 2007), the temperature-sensitive allele, *pot1-1*, was used as a stand-in for a *stn1* allele to identify a suitable genetic background that would enhance the phenotype. The *pot1-1* had been well characterised and known to lose all detectable telomeres within one cell cycle of being shifted to a non-permissive temperature (Pitt and Cooper, 2010).

Several genetic backgrounds had previously been shown to be incompatible with the *pot1Δ* allele and, therefore, were tested for synthetic lethality with the *pot1-1* allele. It was expected that deletion of *rad16⁺* and *lig4⁺*, combined with *pot1-1*, would result in synthetic lethality. Rad16, the homologue of human XPF, had previously been shown to be required for survival of

pot1Δ cells through the SSA pathway while Lig4 contributed in a limited context through NHEJ (Wang and Baumann, 2008). However, spot tests on single, double and triple mutants indicated that, although there was a reduction in viability, some cells were able to survive the shift to the non-permissive temperature of 36°C, similar to the *pot1-1* single mutant strain [Fig 5.2A]. The mechanism of this survival is unknown. Speculation suggests this may be through a circularisation pathway that is not dependent on SSA or that some cells are maintaining linear chromosomes through a recombination pathway. It is possible that HAATI survivors arise due to sufficient function of Pot1 remaining, even at the non-permissive temperature, and possibly that prevention of circularisation through both SSA and NHEJ results in selection of HAATI survivors.

An alternative background was, therefore, required. There were several other alleles that could be used, however, *rqh1Δ* took precedence. Deletion of *rqh1+* was synthetic lethal in combination with *pot1Δ* (Wang and Baumann, 2008), however, this was later found to not be through the prevention of circularisation. Instead, *rqh1Δ* cells were found to be capable of forming circularised chromosomes, but not maintaining them. It is thought that is due to Rqh1 being required for prevention of crossover events between circular chromosomes, which would otherwise lead to the formation of chromosome dimers that were incapable of correct segregation. As such, the synthetic lethality of an *rqh1Δ* in combination with Pot1 depletion is not immediate, but occurs after several generations (Nanbu *et al.*, 2013). It was also speculated that allowing cells to initially form circularised chromosomes would not select for other types of survivors.

The *rqh1Δ* was, therefore, combined with the *pot1-1* allele and tested for synthetic lethality [Fig 5.2B-D]. As expected, spot assays showed a dramatic loss of viability at the non-permissive temperature thereby confirming that an *rqh1Δ* could be used to help identify *stn1* temperature-sensitive mutants as well as enhance a telomere deprotection phenotype.

7.3.2 Generation of *S. pombe stn1* temperature-sensitive alleles

Error-prone PCR-based mutagenesis was used to generate randomly mutagenised alleles of *stn1*. These were transformed in bulk into an *rqh1Δ* base strain and integrated by RMCE, as had been done previously for Poz1. On screening the resulting transformants for a viability phenotype, two temperature-sensitive strains were found, candidates 75 and 99 [Fig 5.6].

The two strains, containing alleles later designated *stn1-75* and *stn1-99*, appeared to have very similar phenotypes. Both were viable and healthy at the permissive temperature of 25°C and not viable at the non-permissive temperature of 36°C. However, later study of the temperature-sensitivity range indicated that *stn1-75* produced a more acute phenotype [Fig 5.13]. It showed some sensitivity at 30°C, based on the formation of smaller, rougher edged colonies compared to control strains at this temperature. At 33.5°C and, therefore, 36°C it appeared to completely lose viability, indicated by the lack of any visible colony formation [Fig 5.13]. The second allele, on the other hand, allowed the formation of small, rough-edged colonies at 33.5°C, but also lost viability at 36°C.

Sensitivity at a lower temperature would have been preferred. Given that, in *S. cerevisiae*, the Stn1 protein was only able to suppress the phenotype of the *cdc13-1* allele up to 30°C implies that the likelihood of pulling out suppressors at higher temperatures could be reduced (Grandin *et al.*, 1997).

A number of other candidates were also tested for temperature-sensitivity. However, none of these were synthetic-lethal at any temperature up to 36°C. Nevertheless, in hindsight, given that only two synthetic-lethal strains were found, it may have been beneficial to have studied some of the other candidates further. At the very least, an analysis of the amino acid substitutions could have revealed regions of the Stn1 protein that do not tolerate changes, especially if the substitutions producing phenotypes were found clustered in particular regions. Given the hypothesis that functionally important residues would be conserved, it also

would have been interesting to compare the location of these substitutions to the location of conserved residues in Stn1. Should the screen for *stn1* temperature-sensitive alleles be repeated in the future, it would, therefore, be beneficial to retain and analyse strains with less acute sensitivities.

7.3.3 Sequence analysis of the *stn1-75* and *stn1-99* temperature-sensitive alleles

After the isolation of two temperature-sensitive strains, an analysis of each allele was carried out to determine the locations of any amino acid substitutions as well as the likely effects of these substitutions. The *stn1-75* allele was found to contain two nucleotide substitutions, of which only one led to an amino acid substitution. Given that codon usage bias tends to be correlated to gene expression levels, the codon changed in the silent mutation was also checked against *S. pombe* codon usage data to ensure this was not a rarely used codon (Hiraoka *et al.*, 2009). The single amino acid substitution in *stn1-75* was found to be L198S. The second allele, *stn1-99*, was found to contain just a single nucleotide mutation leading to a single amino acid substitution, L236I, which at first glance appears to be a very minor change. Both Leucine and Isoleucine are similar, small hydrophobic residues. However, a small change at a highly conserved residue could still destabilise a protein.

The location of these substitutions in the Stn1 protein was determined by a comparison to a sequence alignment of Stn1 proteins from a previous study (Sun *et al.*, 2009). They were both identified to be located in the C-terminus of Stn1. In the previous study by Sun *et al.* (2009), the crystal structure of the Stn1 N-terminus was been solved and compared between several species. The C-terminus of *S. cerevisiae* Stn1 was also solved. No crystal structure for the C-terminus of Stn1 in *S. pombe*, however, was available. Therefore, the likely structure affected by the substitutions had to be inferred from using other structures as templates.

The C-terminus of *S. cerevisiae* Stn1 had previously been found to contain two tandem winged-Helix-Turn-Helix (WH1 and WH2) motifs (Sun *et al.*, 2009). The peptide sequence of these motifs had been aligned to Stn1 from various species as well as human RPA32. This had allowed the identification of a number of highly conserved hydrophobic residues. Interestingly, when the *S. pombe* Stn1 C-terminal sequence was compared to Stn1 from the other species in the *Schizosaccharomyces* genus as well as this previous alignment, the location of the substitutions from *stn1-75* and *stn1-99* mapped to two of the conserved hydrophobic residues of WH1 [Fig 5.9]. Indeed, the L236I substitution mapped to one of the most well conserved residues in the alignment indicating that it may well be functionally important.

A prediction of the *S. pombe* Stn1 WH1 motif secondary structure was generated using PSIPRED and compared to the known structure of *S. cerevisiae* Stn1 and *H. sapiens* RPA32, which are, based on the alignment, the most closely related solved structures. The prediction identified canonical winged-Helix-Turn-Helix structures that were conserved in both *S. cerevisiae* Stn1 and RPA32 [Fig 5.10]. This added confidence to the alignment generated with the peptide sequence. Given that a crystal structure was not available for the *S. pombe* Stn1 C-terminus, the *S. cerevisiae* Stn1 and *H. sapiens* RPA32 C-terminal structures were used to model the locations of the *stn1-75* and *stn1-99* substitutions. L198 and L236 were found to be located on the hydrophobic surfaces of the α1- and α3-helices respectively in both model structures [Fig 5.11].The locations of equivalent residues were also identified in the WH1 and WH2 motifs of *H. sapiens* STN1 [Fig 5.12]. This produced accurate results for residues equivalent to *S. pombe* Stn1 L236 that agreed with the *S. cerevisiae* Stn1 and *H. sapiens* RPA32 structures; however, the same could not be said for the L198 residue. In this case, considering the locations in the other structures, an alignment of the WH1 and WH2 motif sequences did not agree with the expected position on the crystal structure. The alignment, however, indicates multiple insertions in both WH1 and WH2, when compared to *S. pombe* Stn1. It is,

therefore, likely to have some discrepancies. The positions of residues equivalent to *S. pombe* Stn1 L198, therefore, had to be approximated.

The identification of equivalent residues on multiple model structures allowed the use of protein stability prediction tools to calculate the likely effects of the specific substitutions found in *S. pombe* [Table 5.2]. Two of these tools, the SDM and mCSM webservers, are able to use the PDB files associated with each structure to calculate the change in Gibbs free energy difference between wild-type and mutant structures (ΔΔG), which can be thought of a stability score. A negative ΔΔG indicates a destabilising effect while a positive ΔΔG indicates a stabilising effect. SDM consistently predicted a destabilising effect of substituting the residue equivalent to *S. pombe* Stn1 L198 to a Serine for each structure. In most of the structures it also predicted an increase in solvent accessibility, indicating that there would be a structural change in that region. The mCSM server largely agreed with these data, though it was unable to process the *H. sapiens* RPA32 structures due to the presence of multiple models in the file, a limitation of the tool. On the other hand, the data from the two tools did not agree for the substitutions involving the residue equivalent to *S. pombe* Stn1 L236. SDM predicted a minimal ΔΔG in each structure as well as much smaller changes in solvent accessibility compared to the first set. All substitutions from Leucine to Isoleucine were, therefore, not predicted to be destabilising. The mCSM server data, however, disagreed with this, predicting a larger ΔΔG for each substitution than SDM and scoring them as destabilising. The two tools use different methods to calculate the value of ΔΔG so some discrepancy is to be expected. It is not surprising that minimal changes at the residues equivalent to S. pombe Stn1 L236 to Isoleucine are predicted to produce a marginal effect. However, as stated earlier, taking into account the high level of conservation at this position, a small change could produce a larger effect than expected. Indeed, it is the sole amino acid substitution in an *S. pombe* temperature-sensitive *stn1* allele and these data are based on homologous structures, not the *S. pombe* Stn1 C-terminus. Therefore, predicted and actual effects of substitutions should be expected to differ.

The existing studies of *S. pombe* Stn1 have established that the N-terminal OB fold is required for Ten1-interaction (Sun *et al.*, 2009). If *S. cerevisiae* Stn1 is used as a guide, it would suggest that these C-terminal WH motifs are responsible for interactions with a Cdc13 homologue, which might be disrupted in *stn1-75* and *stn1-99*. On the other hand, given the predicted similarity in structure to *H. sapiens* RPA32 C-terminus, it may instead be the N-terminal OB fold that interacts with a Cdc13 homologue. This would leave open the possibility that these *S. pombe* Stn1 WH motifs, rather than the OB fold, are used in DNA binding or other protein interactions, such as the recruitment of lagging-strand replication machinery. Determination of specific DNA-binding properties of these motifs would be aided by solving the crystal structure of the *S. pombe* Stn1 C-terminus. Indeed, the C-terminal crystal structure of *S. cerevisiae* Stn1 helped determine that the precise orientation of the two WH motifs would allow protein-protein interactions, but prevent direct DNA interaction (Sun *et al.*, 2009).

Although the function of the WH1 and WH2 motifs may differ in *H. sapiens* STN1, compared to *S. cerevisiae* Stn1, these residues may still be good candidates for targeted substitutions. In *S. cerevisiae* the WH motifs are required for interaction with the C-terminus of Cdc13 as well as Pol12 (Grossi *et al.*, 2004, Puglisi *et al.*, 2008). In *H. sapiens*, however, it is the N-terminal OB fold that is required for interaction with the CTC1 C-terminus, though the presence of the C-terminus of STN1 is still required for the formation of the CST complex (Chen *et al.*, 2012, Miyake *et al.*, 2009). Currently the specific function of the *H. sapiens* STN1 WH motifs remains a mystery, but it is possible that they may contribute to stabilisation of the CST complex, ssDNA binding, recruitment of Pol-α/primase or other protein interactions. If the level of conservation is an indication of importance in the structure of these motifs, substitutions at the identified conserved residues may result in STN1 that is less stable towards the C-terminus. Indeed, given the destabilising nature of the substitutions in *S. pombe*, these substitutions in *H. sapiens* have the potential to affect the stability of the CST complex or any one or more of its functions.

7.3.3 Initial characterisation of the *stn1-75* and *stn1-99* alleles

Following the initial isolation of the *stn1-75* and *stn1-99* strains, strains were generated that contained the alleles in an *rqh1⁺* background. The cell morphology and growth rate at permissive and non-permissive temperatures was then observed [Fig 5.15]. The two *stn1* temperature-sensitive alleles, when transferred to an *rqh1⁺* background, appeared visually to be quite healthy at the permissive temperature of 25°C. After shifting to the non-permissive temperature of 36°C for 6 hours, however, cell elongation is observed, similar to the *pot1-1* strain. This is typically indicative of cell cycle arrest in *S. pombe*. After 24 hours additional incubation at 36°C, however, elongated cells become few and far between. Many cells evidently had managed to undergo cell division. Based on the images, at this point, approximately half of the cells in culture appeared to be non-viable, as shown by rough textured cell membranes. Again, these characteristics were very similar to the *pot1-1* strain reflecting the similarities between *pot1Δ* and *stn1Δ*.

Despite the morphological similarities of the strains, differences were observed in the growth rates between the *stn1* alleles and *pot1-1*. At the permissive temperature of 25°C, the growth rates of both *stn1* temperature-sensitive strains and the *pot1-1* strain were very similar to the wild-type control. When shifted to 36°C, however, the *stn1-75* and *stn1-99* strains initially continued to grow at the same rate as wild-type with a doubling time of approximately 3-4 hours, while the *pot1-1* strain grew more slowly with a population doubling time of approximately 9 hours. This would suggest that the shift to the non-permissive temperature in the *pot1-1* strain had an immediate effect, agreeing with data from the study that initially generated this *pot1-1* allele where telomere deprotection and loss was observed within one cell cycle. With the *stn1-75* and *stn1-99* strains, continuing to grow at a similar rate to wild type would point to a delayed or less acute effect of shifting temperatures. Interestingly, the *stn1-75*, *stn1-99*, *pot1-1* and wild-type strains reached a plateau in growth at approximately the same time. None of these strains, however, reached the typical saturation density for *S.*

pombe indicating that this plateau in growth rate was not due to excessive cell numbers. Indeed, it is certainly possible to culture wild-type cells for several days at lower temperatures and to densities in excess of $6x10^7$ cells/ml compared to the plateau at approximately $2.5x10^7$ cells/ml observed in this test. This is probably due to an excessive amount of time at 36°C, resulting in a rate of cell death equalling the rate of cell division. This probably would have masked any delayed responses to Stn1 dysfunction in the *stn1-75* and *stn1-99* strains as well as any later recovery in any of these temperature-sensitive strains.

A 48 hour time course using duplicate samples to the growth rate assay appear to confirm that there is a delayed response to Stn1 dysfunction in these strains. Southern blot analysis shows a very gradual reduction in telomere signal intensity without shortening over the course of 48 hours, which, as seen in the growth curve, equates to multiple cell divisions before plateauing [Fig 5.16]. A difference in the signal intensity between the *stn1-75* and *stn1-99* strains is apparent by 36 hours, however, this may be misleading due to reduced DNA in the *stn1-75* 36hr and 48hr time points. This, therefore, called into question whether these strains were circularising chromosomes in response to telomere deprotection or were synthetic lethal with *rqh1Δ* for another reason.

Strains that maintain circularised chromosomes are known to be MMS sensitive whereas cells which retain linear chromosomes, even HAATI cells, remain resistant (Jain *et al.*, 2010). MMS spot tests, therefore, appeared to point to circularisation, as seen by an acute sensitivity of the *stn1-75* and *stn1-99* strains, similar to or more so than *pot1-1* [Fig 5.17]. The *stn1-75* strain appears to be sensitive to MMS at 33.5°C where *stn1-99* and *pot1-1* are not. This is likely due to the more acute temperature-sensitivity characteristic of this allele, relative to the others. However, given that neither *stn1-99* nor *pot1-1* are as MMS sensitive as *stn1-75* at their non-permissive temperature of 36°C, speculation would suggest that a function other than telomere deprotection may be affected in *stn1-75*.

MMS is known to cause replication stress through methylation of DNA and, in humans, the CST complex has been implicated in a fork-restart function throughout the genome. The possibility exists that the *stn1-75* allele results in a Stn1 protein that is dysfunctional in fork restart function, possibly due to a compromised ability to recruit Pol-α/primase to stalled forks. This could be compatible with the synthetic lethality observed when these alleles are combined with *rqh1Δ*. In addition to being required in the prevention of chromosome dimer formation, Rqh1 is implicated in replication slowing and fork stability in response to replication stress (Murray *et al.*, 1997, Nanbu *et al.*, 2013, Willis and Rhind, 2009). Stn1 unable to contribute to fork restart combined with Rqh1 unable to slow replication could lead to genomic instability. This could be instead of or in addition to a telomere deprotection phenotype of *stn1-75* and thus requires further investigation.

7.3.4 Further characterisation of and speculation regarding the *stn1-75* and *stn1-99* alleles

There are quite a number of further tests to do to properly characterise these *stn1-75* and *stn1-99* alleles. The first of these should be a pulsed-field gel using chromosomal DNA from samples of *stn1-75* and *stn1-99* strains incubated at permissive and non-permissive temperatures. This would confirm whether or not these alleles result in chromosome circularisation.

At this point, it would also be prudent to look at the context of the *stn1* alleles. There is a slight telomere length phenotype that appears to be a result of the modified promoter (addition of loxP and restriction sites), as seen for the Poz1 strains discussed in Chapter 3. Elongated telomeres, as seen in these *stn1* strains [Fig 5.4 and 5.16], would imply that some telomerase regulation functionality of Stn1 may be compromised. If so, it is possible that this has some ability to mask the full effects of the *stn1-75* and *stn1-99* alleles. Therefore, the alleles ideally

ought to be transferred to a wild-type *stn1+* locus. This could be done by several methods, but one of the most straightforward would be to construct a *stn1+/stn1Δ::ura4+* diploid strain and integrate the *stn1-75* and *stn1-99* ORFs directly into the *stn1Δ::ura4+* locus by recombination, counter-selecting for the *ura4+* marker.

The interaction between Stn1 and Ten1 could also be investigated in these *stn1* alleles. The yeast 2-hybrid system would allow any changes in Stn1-Ten1 interaction to be detected by growth on selective plates at a range of temperatures. Switching to a yeast 3-hybrid system, as suggested earlier, would also allow the known interaction with Tpz1 to be tested as well as any other interactions that may be identified in a yeast 3-hybrid screen or systematic tests.

After shifting to the non-permissive temperature, there is no evidence of telomere shortening in *stn1-75* or *stn1-99*, much like *pot1-1*. Combining the *stn1* alleles with a *taz1Δ*, known for elongated telomeres (Nakamura *et al.*, 1998), could to make any reduction in length more easily visible. The evidence is also debatable regarding whether the *stn1-75* and *stn1-99* strains do lose telomeres with continued incubation at the non-permissive temperature. Certainly a repetition of the time course would be required.

Under the assumption that the pulsed-field gel does show that the chromosomes are circularising, the pathway used, which is likely to be SSA, ought to be confirmed. Using separate southern blot probes for the G-rich and C-rich strands, native gels, where the genomic DNA has not been denatured, could be used to compare relative levels of telomeric G-rich overhang as cells are shifted from permissive to non-permissive temperatures. In the use of SSA in circularisation, substantial resection of the C-rich strand is expected (Wang and Baumann, 2008). This allows the sub-telomeric homology regions to be exposed for use as substrates in chromosome end annealing. Use of a native gel, therefore, could show whether there is a dramatic increase in single-stranded DNA on shifting the *stn1-75* and *stn1-99* strains to the non-permissive temperature, as has been shown for *pot1-1* (Pitt and Cooper, 2010).

Indeed, this could also be used to look for the cell cycle dependence for chromosome circularisation, as shown for *pot1-1*, by comparing G-rich overhang signals of cells held in G1 by nitrogen starvation and cells allowed to move through S phase on release.

Finally, confirmation of SSA usage could be found by PCR amplification of the junction where the chromosomes join using the primer pairs specified in the study by Wang *et al.* (2008). Sequencing of these PCR products would then indicate whether the sub-telomeric homology regions used in circularisation by SSA were present.

Further speculation on the direction of future investigations without knowing some of the data from the proposed experiments may be premature. The immediate priority would be to confirm whether or not the chromosomes in these *stn1-75* and *stn1-99* strains circularise.

7.3.5 Using the *stn1-75* and *stn1-99* alleles in a screen for suppressors

The initial characterisation of the *stn1-75* and *stn1-99* alleles determined that they were both synthetic lethal when combined with *rqh1Δ* as well as MMS sensitive at the non-permissive temperature of 36°C. However, of the two alleles, *stn1-75* displayed a more acute phenotype in both cases. The *stn1-75 rqh1Δ* strain was found to be noticeably more sensitive to temperature, being synthetic lethal at 33.5°C [Fig 5.13 and 5.14]. It was also noticeably more sensitive to MMS at this temperature [Fig 5.17]. This made it a better allele for use in a suppressor screen as a lower non-permissive temperature could be used if required.

Having established appropriate conditions, a small scale screen was carried out, transforming an *S. pombe* genomic library based in a *ura4⁺* plasmid, using the *rqh1Δ* background and, separately, MMS selection (Barbet *et al.*, 1992). A *stn1⁺* covering plasmid was used as a positive control [Fig 6.2]. An unexpectedly high amount of background was found in the screen involving the use of the *stn1-75 rqh1Δ* strain at both 33.5°C and 36°C. This was initially thought

to perhaps have been due to an error in dilution or unexpectedly high transformation efficiency; however, given the sensitivity of this strain in previous tests, it seems unlikely that so many library transformants would suppress the temperature-sensitivity so easily. Indeed, 36°C was expected to provide very stringent selection of suppressors. It is possible that, between the initial tests and this screen, an internal suppressor had developed. If this were the case, the strain would need to be constructed again from parent strains.

The second method of selection, use of MMS, was more successful. Of approximately 8000 library clones screened, fifteen colonies formed between the transformations incubated at 33.5°C and 36°C. Of these, several did not appear to retain the library clone, as indicated by no growth on YNG –Ura agar. These too appeared to have developed MMS resistance as a result of internal suppressors. As the entire transformation was not affected, it can be presumed that these arose during the MMS selection. Of the fifteen candidates, however, four did grow on YNG –Ura agar, indicating the presence of a library plasmid. On streaking to fresh MMS agar, these four candidates, as well as seven out of the eleven candidates with internal suppressors, retained their resistance to MMS. These candidates are now the subject of further analysis. The four $ura4^+$ candidates will have the library plasmid recovered, sequenced and retested while the candidates with internal suppressors would require whole-genome sequencing.

7.3.6 Further observations and future directions for the suppressor screen

It is interesting how the development of bioinformatics methods has changed the way novel proteins are identified. However, the identification of the components of CST in various species has mostly required methods that involve the detection of a physical interaction. This may be due to limitations in current bioinformatics tools that mean they have been unable to identify components of CST by sequence alone. In the case of an *S. pombe* CTC1/Cdc13 homologue, it is possible that a yeast 3-hybrid assay, using both Stn1 and Ten1 as baits could

pull out a novel interacting protein. It may also pull out a subunit of RPA, as previously suggested, and it would be expected to pull out Tpz1, given that this interaction was recently identified (Chang *et al.*, 2013). In a suppressor screen, however, more than just direct physical interactors could be identified. Proteins involved in the regulation of Stn1-Ten1 activity could be pulled out of the genomic library. Or perhaps, the identification of the internal suppressors will reveal mutations in proteins that have a regulatory or antagonistic role over Stn1-Ten1.

The screening process, however, could be improved. The harsh selection used in both methods would likely mean that many partial suppressors would be missed, even with selection at the lower temperature of 33.5°C. It may be possible to optimise the conditions used so far; however, alternative methods of screening should also be considered. For example, it was established that these *stn1-75 rqh1[+]* and *stn1-99 rqh1[+]* strains grow with a deep pink colouration at non-permissive temperatures compared to permissive temperatures on YES agar plates containing Phloxine B [Fig 5.17]. Taking advantage of this, candidates could be screened by colour at permissive and non-permissive temperatures. A far higher dilution of the transformation mixture would be required to allow individual colonies to grow unhindered. However, then it would then be possible to compare replica colonies from plates incubated at a range of temperatures to identify suppressors based on colour as well as colony morphology.

It is also possible that the phenotype of the *stn1* alleles could be enhanced by combining the amino acid substitutions found in each. It may not be possible to predict the phenotype of such an allele; however, there is a chance that it could display a temperature-sensitive phenotype at temperatures lower than 33.5°C. Transfer of the alleles to a wild-type *stn1* locus (no lox sites or restriction sites) could also help lower the permissive/non-permissive temperature threshold by reducing telomere lengths back down to the wild-type range.

Current and future work with these *stn1* temperature-sensitive alleles, therefore, involves a number of directions and possibilities. Additional characterisation of the alleles may help in

optimising conditions for a suppressor screen. By determining whether or not these alleles result in chromosome circularisation as well as identifying any novel interactors by yeast 3-hybrid, it would be possible to speculate on whether a non-telomeric function may also be affected. The Stn1-Ten1 dimer may have a function restricted to telomeres, specifically at the end of S phase, as a study has recently indicated (Chang *et al.*, 2013). However, upon binding a third component, perhaps the Ssb1 subunit of *S. pombe* RPA, it may then switch to a more genome-wide function in replication fork stabilisation. Not only would this be consistent with data from human cells, which implies that CST has a genome-wide function (Stewart *et al.*, 2012), but it would also be consistent with the synthetic lethality when the *stn1* alleles are combined with *rqh1Δ* as well as their sensitivity to DNA damage by MMS.

References

ABAD, J., DE PABLOS, B., OSOEGAWA, K., DE JONG, P., MARTÍN-GALLARDO, A. & VILLASANTE, A. 2004a. Genomic Analysis of Drosophila Melanogaster Telomeres: Full-Length Copies of Het-a and Tart Elements at Telomeres. *Molecular Biology and Evolution,* 21**,** 1613-1619.

ABAD, J., DE PABLOS, B., OSOEGAWA, K., DE JONG, P., MARTÍN-GALLARDO, A. & VILLASANTE, A. 2004b. Tahre, a Novel Telomeric Retrotransposon from Drosophila Melanogaster, Reveals the Origin of Drosophila Telomeres. *Molecular Biology and Evolution,* 21**,** 1620-1624.

ABREU, E., ARITONOVSKA, E., REICHENBACH, P., CRISTOFARI, G., CULP, B., TERNS, R., LINGNER, J. & TERNS, M. 2010. Tin2-Tethered Tpp1 Recruits Human Telomerase to Telomeres in Vivo. *Molecular and Cellular Biology,* 30**,** 2971-2982.

AMIARD, S., DOUDEAU, M., PINTE, S., POULET, A., LENAIN, C., FAIVRE-MOSKALENKO, C., ANGELOV, D., HUG, N., VINDIGNI, A., BOUVET, P., PAOLETTI, J., GILSON, E. & GIRAUD-PANIS, M.-J. 2007. A Topological Mechanism for Trf2-Enhanced Strand Invasion. *Nature Structural & Molecular Biology,* 14**,** 147-154.

ARAT, N. & GRIFFITH, J. 2012. Human Rap1 Interacts Directly with Telomeric DNA and Regulates Trf2 Localization at the Telomere. *The Journal of Biological Chemistry,* 287**,** 41583-41594.

BAE, N. & BAUMANN, P. 2007. A Rap1/Trf2 Complex Inhibits Nonhomologous End-Joining at Human Telomeric DNA Ends. *Molecular Cell,* 26**,** 323-334.

BARBET, N., MURIEL, W. & CARR, A. 1992. Versatile Shuttle Vectors and Genomic Libraries for Use with Schizosaccharomyces Pombe. *Gene,* 114**,** 59-66.

BAROUDY, B., VENKATESAN, S. & MOSS, B. 1982. Incompletely Base-Paired Flip-Flop Terminal Loops Link the Two DNA Strands of the Vaccinia Virus Genome into One Uninterrupted Polynucleotide Chain. *Cell,* 28**,** 315-324.

BAUMANN, P. & CECH, T. 2000. Protection of Telomeres by the Ku Protein in Fission Yeast. *Molecular Biology of the Cell,* 11**,** 3265-3275.

BAUMANN, P. & CECH, T. 2001. Pot1, the Putative Telomere End-Binding Protein in Fission Yeast and Humans. *Science (New York, N.Y.),* 292**,** 1171-1175.

BEAUD, G. 1995. Vaccinia Virus DNA Replication: A Short Review. *Biochimie,* 77**,** 774-779.

BEERNINK, H., MILLER, K., DESHPANDE, A., BUCHER, P. & COOPER, J. 2003. Telomere Maintenance in Fission Yeast Requires an Est1 Ortholog. *Current Biology : CB,* 13**,** 575-580.

BERMAN, H., WESTBROOK, J., FENG, Z., GILLILAND, G., BHAT, T., WEISSIG, H., SHINDYALOV, I. & BOURNE, P. 2000. The Protein Data Bank. *Nucleic Acids research,* 28**,** 235-242.

BIANCHI, A. & SHORE, D. 2008. How Telomerase Reaches Its End: Mechanism of Telomerase Regulation by the Telomeric Complex. *Molecular Cell,* 31**,** 153-165.

BIANCHI, A., SMITH, S., CHONG, L., ELIAS, P. & DE LANGE, T. 1997. Trf1 Is a Dimer and Bends Telomeric DNA. *The EMBO Journal,* 16**,** 1785-1794.

BIESSMANN, H., CARTER, S. & MASON, J. 1990. Chromosome Ends in Drosophila without Telomeric DNA Sequences. *Proceedings of the National Academy of Sciences of the United States of America,* 87**,** 1758-1761.

BIFFI, G., TANNAHILL, D., MCCAFFERTY, J. & BALASUBRAMANIAN, S. 2013. Quantitative Visualization of DNA G-Quadruplex Structures in Human Cells. *Nature Chemistry,* 5**,** 182-186.

BILAUD, T., BRUN, C., ANCELIN, K., KOERING, C., LAROCHE, T. & GILSON, E. 1997. Telomeric Localization of Trf2, a Novel Human Telobox Protein. *Nature Genetics,* 17**,** 236-239.

BISHOP, D., PARK, D., XU, L. & KLECKNER, N. 1992. Dmc1: A Meiosis-Specific Yeast Homolog of E. Coli Reca Required for Recombination, Synaptonemal Complex Formation, and Cell Cycle Progression. *Cell,* 69**,** 439-456.

BLASCO, M. 2005. Telomeres and Human Disease: Ageing, Cancer and Beyond. *Nature reviews. Genetics,* 6**,** 611-622.

BLOW, J. & DUTTA, A. 2005. Preventing Re-Replication of Chromosomal DNA. *Nature reviews. Molecular Cell Biology,* 6**,** 476-486.

BONETTI, D., CLERICI, M., ANBALAGAN, S., MARTINA, M., LUCCHINI, G. & LONGHESE, M. 2010. Shelterin-Like Proteins and Yku Inhibit Nucleolytic Processing of Saccharomyces Cerevisiae Telomeres. *PLoS Genetics,* 6.

BOSOY, D., PENG, Y., MIAN, I. & LUE, N. 2003. Conserved N-Terminal Motifs of Telomerase Reverse Transcriptase Required for Ribonucleoprotein Assembly in Vivo. *The Journal of Biological Chemistry,* 278**,** 3882-3890.

BOX, J., BUNCH, J., TANG, W. & BAUMANN, P. 2008. Spliceosomal Cleavage Generates the 3' End of Telomerase Rna. *Nature,* 456**,** 910-914.

BRENNAN, R. 1993. The Winged-Helix DNA-Binding Motif: Another Helix-Turn-Helix Takeoff. *Cell,* 74**,** 773-776.

BROCCOLI, D., SMOGORZEWSKA, A., CHONG, L. & DE LANGE, T. 1997. Human Telomeres Contain Two Distinct Myb-Related Proteins, Trf1 and Trf2. *Nature Genetics,* 17**,** 231-235.

BRYAN, C., RICE, C., HARKISHEIMER, M., SCHULTZ, D. & SKORDALAKES, E. 2013. Structure of the Human Telomeric Stn1-Ten1 Capping Complex. *PloS One,* 8.

BRYAN, T., GOODRICH, K. & CECH, T. 2000. Telomerase Rna Bound by Protein Motifs Specific to Telomerase Reverse Transcriptase. *Molecular Cell*.

BUCHAN, D., MINNECI, F., NUGENT, T., BRYSON, K. & JONES, D. 2013. Scalable Web Services for the Psipred Protein Analysis Workbench. *Nucleic Acids Research,* 41**,** 57.

BUDD, M. & CAMPBELL, J. 2013. Dna2 Is Involved in Ca-Strand Resection and Nascent Lagging Strand Completion at Native Yeast Telomeres. *The Journal of Biological Chemistry*.

BURGERS, P. 2009. Polymerase Dynamics at the Eukaryotic DNA Replication Fork. *The Journal of Biological Chemistry,* 284**,** 4041-4045.

CAPPER, R., BRITT-COMPTON, B., TANKIMANOVA, M., ROWSON, J., LETSOLO, B., MAN, S., HAUGHTON, M. & BAIRD, D. 2007. The Nature of Telomere Fusion and a Definition of the Critical Telomere Length in Human Cells. *Genes & Development,* 21**,** 2495-2508.

CARR, A. 2002. DNA Structure Dependent Checkpoints as Regulators of DNA Repair. *DNA Repair*, 1**,** 983-994.

CASPARI, T. & CARR, A. 2002. Checkpoints: How to Flag up Double-Strand Breaks. *Current Biology*, 12**,** R105-R107.

CASPARI, T., DAHLEN, M. & KANTER-SMOLER, G. 2000. Characterization of Schizosaccharomyces Pombe Hus1: A Pcna-Related Protein That Associates with Rad1 and Rad9. *Molecular and Cellular Biology*, 20**,** 1254-1262.

CASTEEL, D., ZHUANG, S., ZENG, Y., PERRINO, F., BOSS, G., GOULIAN, M. & PILZ, R. 2009. A DNA Polymerase-{Alpha}{Middle Dot}Primase Cofactor with Homology to Replication Protein a-32 Regulates DNA Replication in Mammalian Cells. *The Journal of Biological Chemistry,* 284**,** 5807-5818.

CAVERO, S., CHAHWAN, C. & RUSSELL, P. 2007. Xlf1 Is Required for DNA Repair by Nonhomologous End Joining in Schizosaccharomyces Pombe. *Genetics,* 175**,** 963-967.

CESARE, A., J. , QUINNEY, N., WILLCOX, S., SUBRAMANIAN, D. & GRIFFITH, J., D. 2003. Telomere Looping in P.Sativum (Common Garden Pea). *The Plant Journal,* 36**,** 271-279.

CHACONAS, G. & KOBRYN, K. 2010. Structure, Function, and Evolution of Linear Replicons in Borrelia. *Annual Review of Microbiology,* 64**,** 185-202.

CHAI, W., SFEIR, A., HOSHIYAMA, H., SHAY, J. & WRIGHT, W. 2006. The Involvement of the Mre11/Rad50/Nbs1 Complex in the Generation of G-Overhangs at Human Telomeres. *EMBO Reports,* 7**,** 225-230.

CHAN, S. & BLACKBURN, E. 2003. Telomerase and Atm/Tel1p Protect Telomeres from Nonhomologous End Joining. *Molecular Cell,* 11**,** 1379-1387.

CHAN, S. & BLACKBURN, E. 2004. Telomeres and Telomerase. *Philosophical transactions of the Royal Society of London. Series B, Biological Sciences,* 359**,** 109-121.

CHANDRA, A., HUGHES, T., NUGENT, C. & LUNDBLAD, V. 2001. Cdc13 Both Positively and Negatively Regulates Telomere Replication. *Genes & Development,* 15**,** 404-414.

CHANG, Y.-T., MOSER, B. & NAKAMURA, T. 2013. Fission Yeast Shelterin Regulates DNA Polymerases and Rad3(Atr) Kinase to Limit Telomere Extension. *PLoS Genetics,* 9.

CHEN, J.-L. & GREIDER, C. 2004. An Emerging Consensus for Telomerase Rna Structure. *Proceedings of the National Academy of Sciences of the United States of America,* 101**,** 14683-14684.

CHEN, L.-Y. & LINGNER, J. 2013. Cst for the Grand Finale of Telomere Replication. *Nucleus (Austin, Tex.),* 4**,** 227-282.

CHEN, L.-Y., REDON, S. & LINGNER, J. 2012. The Human Cst Complex Is a Terminator of Telomerase Activity. *Nature,* 488**,** 540-544.

CHEN, Y., YANG, Y., VAN OVERBEEK, M., DONIGIAN, J., BACIU, P., DE LANGE, T. & LEI, M. 2008. A Shared Docking Motif in Trf1 and Trf2 Used for Differential Recruitment of Telomeric Proteins. *Science (New York, N.Y.),* 319**,** 1092-1096.

CHONG, L., VAN STEENSEL, B., BROCCOLI, D., ERDJUMENT-BROMAGE, H., HANISH, J., TEMPST, P. & DE LANGE, T. 1995. A Human Telomeric Protein. *Science (New York, N.Y.),* 270**,** 1663-1667.

CONG, Y.-S., WRIGHT, W. & SHAY, J. 2002. Human Telomerase and Its Regulation. *Microbiology and Molecular Biology reviews : MMBR,* 66**,** 407.

COOPER, J., NIMMO, E., ALLSHIRE, R. & CECH, T. 1997. Regulation of Telomere Length and Function by a Myb-Domain Protein in Fission Yeast. *Nature,* 385**,** 744-747.

CRABBE, L., VERDUN, R., HAGGBLOM, C. & KARLSEDER, J. 2004. Defective Telomere Lagging Strand Synthesis in Cells Lacking Wrn Helicase Activity. *Science (New York, N.Y.),* 306**,** 1951-1953.

DE JONG, R. & VAN DER VLIET, P. 1999. Mechanism of DNA Replication in Eukaryotic Cells: Cellular Host Factors Stimulating Adenovirus DNA Replication. *Gene,* 236**,** 1-12.

DE LANGE, T. 2004. T-Loops and the Origin of Telomeres. *Nature reviews. Molecular Cell Biology,* 5**,** 323-329.

DE LANGE, T. 2009. How Telomeres Solve the End-Protection Problem. *Science (New York, N.Y.),* 326**,** 948-952.

DEHÉ, P.-M. & COOPER, J. 2010. Fission Yeast Telomeres Forecast the End of the Crisis. *FEBS letters,* 584**,** 3725-3733.

DING, H., SCHERTZER, M., WU, X., GERTSENSTEIN, M., SELIG, S., KAMMORI, M., POURVALI, R., POON, S., VULTO, I., CHAVEZ, E., TAM, P., NAGY, A. & LANSDORP, P. 2004. Regulation of Murine Telomere Length by Rtel: An Essential Gene Encoding a Helicase-Like Protein. *Cell,* 117**,** 873-886.

EGAN, E. & COLLINS, K. 2012. Biogenesis of Telomerase Ribonucleoproteins. *RNA (New York, N.Y.),* 18**,** 1747-1759.

FAIRALL, L., CHAPMAN, L., MOSS, H., DE LANGE, T. & RHODES, D. 2001. Structure of the Trfh Dimerization Domain of the Human Telomeric Proteins Trf1 and Trf2. *Molecular Cell,* 8**,** 351-361.

FENG, J., FUNK, W., WANG, S., WEINRICH, S. & AVILION…, A. 1995. The Rna Component of Human Telomerase. *Science*, 269**,** 1236-1241.

FERREIRA, M. & COOPER, J. 2001. The Fission Yeast Taz1 Protein Protects Chromosomes from Ku-Dependent End-to-End Fusions. *Molecular Cell,* 7**,** 55-63.

FERREIRA, M. & COOPER, J. 2004. Two Modes of DNA Double-Strand Break Repair Are Reciprocally Regulated through the Fission Yeast Cell Cycle. *Genes & Development,* 18**,** 2249-2254.

FIELDS, S. & SONG, O. 1989. A Novel Genetic System to Detect Protein-Protein Interactions. *Nature,* 340**,** 245-246.

FIKES, J., BECKER, D., WINSTON, F. & GUARENTE, L. 1990. Striking Conservation of Tfiid in Schizosaccharomyces Pombe and Saccharomyces Cerevisiae. *Nature,* 346**,** 291-294.

FISHER, T. & ZAKIAN, V. 2005. Ku: A Multifunctional Protein Involved in Telomere Maintenance. *DNA Repair,* 4**,** 1215-1226.

FLECK, O. & NIELSEN, O. 2004. DNA Repair. *Journal of Cell Science,* 117**,** 515-517.

FLICEK, P., AHMED, I., AMODE, M. R., BARRELL, D., BEAL, K., BRENT, S., CARVALHO-SILVA, D., CLAPHAM, P., COATES, G., FAIRLEY, S., FITZGERALD, S., GIL, L., GARCIA-GIRON, C., GORDON, L., HOURLIER, T., HUNT, S., JUETTEMANN, T., KAHARI, A. K., KEENAN, S., KOMOROWSKA, M., KULESHA, E., LONGDEN, I., MAUREL, T., MCLAREN, W. M., MUFFATO, M., NAG, R., OVERDUIN, B., PIGNATELLI, M., PRITCHARD, B., PRITCHARD, E., RIAT, H. S., RITCHIE, G. R. S., RUFFIER, M., SCHUSTER, M., SHEPPARD, D., SOBRAL, D., TAYLOR, K., THORMANN, A., TREVANION, S., WHITE, S., WILDER, S. P., AKEN, B. L., BIRNEY, E., CUNNINGHAM, F., DUNHAM, I., HARROW, J., HERRERO, J., HUBBARD, T. J. P., JOHNSON, N., KINSELLA, R., PARKER, A., SPUDICH, G., YATES, A., ZADISSA, A. & SEARLE, S. M. J. 2012. Ensembl 2013. *Nucleic Acids Research,* 41**,** D41-D55.

FLORY, M., CARSON, A., MULLER, E. & AEBERSOLD, R. 2004. An Smc-Domain Protein in Fission Yeast Links Telomeres to the Meiotic Centrosome. *Molecular Cell,* 16**,** 619-630.

FORSBURG, S. 1999. The Best Yeast? *Trends in Genetics : TIG,* 15**,** 340-344.

FORSBURG, S. & RHIND, N. 2006. Basic Methods for Fission Yeast. *Yeast (Chichester, England),* 23**,** 173-183.

FU, D. & COLLINS, K. 2007. Purification of Human Telomerase Complexes Identifies Factors Involved in Telomerase Biogenesis and Telomere Length Regulation. *Molecular Cell,* 28**,** 773-785.

FUJITA, I., TANAKA, M. & KANOH, J. 2012. Identification of the Functional Domains of the Telomere Protein Rap1 in Schizosaccharomyces Pombe. *PloS One,* 7.

FULCHER, N., DERBOVEN, E., VALUCHOVA, S. & RIHA, K. 2013. If the Cap Fits, Wear It: An Overview of Telomeric Structures over Evolution. *Cellular and Molecular Life Sciences : CMLS*.

GAO, G., WALSER, J.-C., BEAUCHER, M., MORCIANO, P., WESOLOWSKA, N., CHEN, J. & RONG, Y. 2010. Hiphop Interacts with Hoap and Hp1 to Protect Drosophila Telomeres in a Sequence-Independent Manner. *The EMBO Journal,* 29**,** 819-829.

GAO, H., CERVANTES, R., MANDELL, E., OTERO, J. & LUNDBLAD, V. 2007. Rpa-Like Proteins Mediate Yeast Telomere Function. *Nature Structural & Molecular Biology,* 14**,** 208-214.

GARVIK, B., CARSON, M. & HARTWELL, L. 1995. Single-Stranded DNA Arising at Telomeres in Cdc13 Mutants May Constitute a Specific Signal for the Rad9 Checkpoint. *Molecular and Cellular Biology,* 15**,** 6128-6138.

GELINAS, A., PASCHINI, M., REYES, F., HÉROUX, A., BATEY, R., LUNDBLAD, V. & WUTTKE, D. 2009. Telomere Capping Proteins Are Structurally Related to Rpa with an Additional Telomere-Specific Domain. *Proceedings of the National Academy of Sciences of the United States of America,* 106**,** 19298-19303.

GIRAUD-PANIS, M.-J., TEIXEIRA, M., GÉLI, V. & GILSON, E. 2010. Cst Meets Shelterin to Keep Telomeres in Check. *Molecular Cell,* 39**,** 665-676.

GOUJON, M., MCWILLIAM, H., LI, W., VALENTIN, F., SQUIZZATO, S., PAERN, J. & LOPEZ, R. 2010. A New Bioinformatics Analysis Tools Framework at Embl-Ebi. *Nucleic Acids Research,* 38**,** 9.

GRANDIN, N., DAMON, C. & CHARBONNEAU, M. 2001. Ten1 Functions in Telomere End Protection and Length Regulation in Association with Stn1 and Cdc13. *The EMBO Journal,* 20**,** 1173-1183.

GRANDIN, N., REED, S. & CHARBONNEAU, M. 1997. Stn1, a New Saccharomyces Cerevisiae Protein, Is Implicated in Telomere Size Regulation in Association with Cdc13. *Genes & Development,* 11**,** 512-527.

GREIDER, C. & BLACKBURN, E. 1989. A Telomeric Sequence in the Rna of Tetrahymena Telomerase Required for Telomere Repeat Synthesis. *Nature*, 337**,** 331-337.

GRIFFITH, J., COMEAU, L., ROSENFIELD, S., STANSEL, R., BIANCHI, A., MOSS, H. & DE LANGE, T. 1999. Mammalian Telomeres End in a Large Duplex Loop. *Cell,* 97**,** 503-514.

GROSSI, S., PUGLISI, A., DMITRIEV, P., LOPES, M. & SHORE, D. 2004. Pol12, the B Subunit of DNA Polymerase Alpha, Functions in Both Telomere Capping and Length Regulation. *Genes & Development,* 18**,** 992-1006.

GU, P., MIN, J.-N., WANG, Y., HUANG, C., PENG, T., CHAI, W. & CHANG, S. 2012. Ctc1 Deletion Results in Defective Telomere Replication, Leading to Catastrophic Telomere Loss and Stem Cell Exhaustion. *The EMBO Journal,* 31**,** 2309-2321.

HARLEY, C., FUTCHER, A. & GREIDER, C. 1990. Telomeres Shorten During Ageing of Human Fibroblasts. *Nature,* 345**,** 458-460.

HE, H., MULTANI, A., COSME-BLANCO, W., TAHARA, H., MA, J., PATHAK, S., DENG, Y. & CHANG, S. 2006. Pot1b Protects Telomeres from End-to-End Chromosomal Fusions and Aberrant Homologous Recombination. *The EMBO Journal,* 25**,** 5180-5190.

HENSON, J., NEUMANN, A., YEAGER, T. & REDDEL, R. 2002. Alternative Lengthening of Telomeres in Mammalian Cells. *Oncogene,* 21**,** 598-610.

HIRAOKA, Y., KAWAMATA, K., HARAGUCHI, T. & CHIKASHIGE, Y. 2009. Codon Usage Bias Is Correlated with Gene Expression Levels in the Fission Yeast Schizosaccharomyces Pombe. *Genes to cells : Devoted to Molecular & Cellular Mechanisms,* 14**,** 499-509.

HOCKEMEYER, D., PALM, W., ELSE, T., DANIELS, J.-P., TAKAI, K., YE, J., KEEGAN, C., DE LANGE, T. & HAMMER, G. 2007. Telomere Protection by Mammalian Pot1 Requires Interaction with Tpp1. *Nature Structural & Molecular Biology,* 14**,** 754-761.

HOEIJMAKERS, J. 2001. Genome Maintenance Mechanisms for Preventing Cancer. *Nature,* 411**,** 366-374.

HOUGHTALING, B., CUTTONARO, L., CHANG, W. & SMITH, S. 2004. A Dynamic Molecular Link between the Telomere Length Regulator Trf1 and the Chromosome End Protector Trf2. *Current Biology : CB,* 14**,** 1621-1631.

HSU, H., GILLEY, D., GALANDE, S., HANDE, M., ALLEN, B., KIM, S., LI, G., CAMPISI, J., KOHWI-SHIGEMATSU, T. & CHEN, D. 2000. Ku Acts in a Unique Way at the Mammalian Telomere to Prevent End Joining. *Genes & Development,* 14**,** 2807-2812.

HUBER, M., DUQUETTE, M., SHIELS, J. & MAIZELS, N. 2006. A Conserved G4 DNA Binding Domain in Recq Family Helicases. *Journal of Molecular Biology,* 358**,** 1071-1080.

HUG, N. & LINGNER, J. 2006. Telomere Length Homeostasis. *Chromosoma,* 115**,** 413-425.

HUISINGA, K., BROWER-TOLAND, B. & ELGIN, S. 2006. The Contradictory Definitions of Heterochromatin: Transcription and Silencing. *Chromosoma,* 115**,** 110-122.

ISHIKAWA, F. 2013. Portrait of Replication Stress Viewed from Telomeres. *Cancer Science,* 104**,** 790-794.

JAIN, D. & COOPER, J. 2010. Telomeric Strategies: Means to an End. *Annual Review of Genetics,* 44**,** 243-269.

JAIN, D., HEBDEN, A., NAKAMURA, T., MILLER, K. & COOPER, J. 2010. Haati Survivors Replace Canonical Telomeres with Blocks of Generic Heterochromatin. *Nature,* 467**,** 223-227.

JAMES, P., HALLADAY, J. & CRAIG, E. 1996. Genomic Libraries and a Host Strain Designed for Highly Efficient Two-Hybrid Selection in Yeast. *Genetics,* 144**,** 1425-1436.

JONES, D. 1999. Protein Secondary Structure Prediction Based on Position-Specific Scoring Matrices. *Journal of Molecular Biology,* 292**,** 195-202.

JUN, H.-I., LIU, J., JEONG, H., KIM, J.-K. & QIAO, F. 2013. Tpz1 Controls a Telomerase-Nonextendible Telomeric State and Coordinates Switching to an Extendible State Via Ccq1. *Genes & Development,* 27**,** 1917-1931.

KANOH, J. & ISHIKAWA, F. 2003. Composition and Conservation of the Telomeric Complex. *Cellular and Molecular Life Sciences : CMLS,* 60**,** 2295-2302.

KERSEY, P., STAINES, D., LAWSON, D., KULESHA, E., DERWENT, P., HUMPHREY, J., HUGHES, D., KEENAN, S., KERHORNOU, A., KOSCIELNY, G., LANGRIDGE, N., MCDOWALL, M., MEGY, K., MAHESWARI, U., NUHN, M., PAULINI, M., PEDRO, H., TONEVA, I., WILSON, D., YATES, A. & BIRNEY, E. 2012. Ensembl Genomes: An Integrative Resource for Genome-Scale Data from Non-Vertebrate Species. *Nucleic Acids Research,* 40**,** 7.

KIM, S.-H., BEAUSEJOUR, C., DAVALOS, A., KAMINKER, P., HEO, S.-J. & CAMPISI, J. 2004. Tin2 Mediates Functions of Trf2 at Human Telomeres. *The Journal of Biological Chemistry,* 279**,** 43799-43804.

KIM, S., KAMINKER, P. & CAMPISI, J. 1999. Tin2, a New Regulator of Telomere Length in Human Cells. *Nature Genetics,* 23**,** 405-412.

KISHI, S., ZHOU, X., ZIV, Y., KHOO, C., HILL, D., SHILOH, Y. & LU, K. 2001. Telomeric Protein Pin2/Trf1 as an Important Atm Target in Response to Double Strand DNA Breaks. *The Journal of Biological Chemistry,* 276**,** 29282-29291.

KROGH, B. & SYMINGTON, L. 2004. Recombination Proteins in Yeast. *Annual Review of Genetics,* 38**,** 233-271.

KUMAR, P., HENIKOFF, S. & NG, P. 2009. Predicting the Effects of Coding Non-Synonymous Variants on Protein Function Using the Sift Algorithm. *Nature Protocols,* 4**,** 1073-1081.

KUMARI, S., BUGAUT, A., HUPPERT, J. & BALASUBRAMANIAN, S. 2007. An Rna G-Quadruplex in the 5' Utr of the Nras Proto-Oncogene Modulates Translation. *Nature Chemical Biology,* 3**,** 218-221.

LABIB, K. 2010. How Do Cdc7 and Cyclin-Dependent Kinases Trigger the Initiation of Chromosome Replication in Eukaryotic Cells? *Genes & Development,* 24**,** 1208-1219.

LAMBERT, S. & CARR, A. 2005. Checkpoint Responses to Replication Fork Barriers. *Biochimie,* 87**,** 591-602.

LANGER, S., GHAFOORI, A., BYRD, M. & LEINWAND, L. 2002. A Genetic Screen Identifies Novel Non-Compatible Loxp Sites. *Nucleic Acids Research,* 30**,** 3067-3077.

LANGERAK, P., MEJIA-RAMIREZ, E., LIMBO, O. & RUSSELL, P. 2011. Release of Ku and Mrn from DNA Ends by Mre11 Nuclease Activity and Ctp1 Is Required for Homologous Recombination Repair of Double-Strand Breaks. *PLoS Genetics,* 7.

LANSDORP, P., VERWOERD, N., VAN DE RIJKE, F., DRAGOWSKA, V., LITTLE, M., DIRKS, R., RAAP, A. & TANKE, H. 1996. Heterogeneity in Telomere Length of Human Chromosomes. *Human Molecular Genetics,* 5**,** 685-691.

LATRICK, C. & CECH, T. 2010. Pot1-Tpp1 Enhances Telomerase Processivity by Slowing Primer Dissociation and Aiding Translocation. *The EMBO Journal,* 29**,** 924-933.

LAUD, P., MULTANI, A., BAILEY, S., WU, L., MA, J., KINGSLEY, C., LEBEL, M., PATHAK, S., DEPINHO, R. & CHANG, S. 2005. Elevated Telomere-Telomere Recombination in Wrn-Deficient, Telomere Dysfunctional Cells Promotes Escape from Senescence and Engagement of the Alt Pathway. *Genes & Development,* 19**,** 2560-2570.

LEGOURAS, I., XOURI, G., DIMOPOULOS, S., LYGEROS, J. & LYGEROU, Z. 2006. DNA Replication in the Fission Yeast: Robustness in the Face of Uncertainty. *Yeast (Chichester, England),* 23**,** 951-962.

LEI, M., PODELL, E. & CECH, T. 2004. Structure of Human Pot1 Bound to Telomeric Single-Stranded DNA Provides a Model for Chromosome End-Protection. *Nature Structural & Molecular Biology,* 11**,** 1223-1229.

LEONARDI, J., BOX, J., BUNCH, J. & BAUMANN, P. 2008. Ter1, the Rna Subunit of Fission Yeast Telomerase. *Nature Structural & Molecular Biology,* 15**,** 26-33.

LEWIS, K. & WUTTKE, D. 2012. Telomerase and Telomere-Associated Proteins: Structural Insights into Mechanism and Evolution. *Structure (London, England : 1993),* 20**,** 28-39.

LI, B. & DE LANGE, T. 2003. Rap1 Affects the Length and Heterogeneity of Human Telomeres. *Molecular Biology of the Cell,* 14**,** 5060-5068.

LI, B., OESTREICH, S. & DE LANGE, T. 2000. Identification of Human Rap1: Implications for Telomere Evolution. *Cell,* 101**,** 471-483.

LI, P., LI, J., LI, M., DOU, K., ZHANG, M.-J., SUO, F. & DU, L.-L. 2012. Multiple End Joining Mechanisms Repair a Chromosomal DNA Break in Fission Yeast. *DNA Repair,* 11**,** 120-130.

LI, X., STITH, C., BURGERS, P. & HEYER, W.-D. 2009. Pcna Is Required for Initiation of Recombination-Associated DNA Synthesis by DNA Polymerase Delta. *Molecular Cell,* 36**,** 704-713.

LILLARD-WETHERELL, K., MACHWE, A., LANGLAND, G., COMBS, K., BEHBEHANI, G., SCHONBERG, S., GERMAN, J., TURCHI, J., ORREN, D. & GRODEN, J. 2004. Association and Regulation of the Blm Helicase by the Telomere Proteins Trf1 and Trf2. *Human Molecular Genetics,* 13**,** 1919-1932.

LIMBO, O., CHAHWAN, C., YAMADA, Y., DE BRUIN, R., WITTENBERG, C. & RUSSELL, P. 2007. Ctp1 Is a Cell-Cycle-Regulated Protein That Functions with Mre11 Complex to Control Double-Strand Break Repair by Homologous Recombination. *Molecular Cell,* 28**,** 134-146.

LIN, J. & ZAKIAN, V. 1996. The Saccharomyces Cdc13 Protein Is a Single-Strand Tg1–3 Telomeric DNA-Binding Protein in Vitro That Affects Telomere Behavior in Vivo. *Proceedings of the National Academy of Sciences of the United States of America,* 93, 13760-13765.

LIPPS, H. & RHODES, D. 2009. G-Quadruplex Structures: In Vivo Evidence and Function. *Trends in Cell Biology,* 19**,** 414-422.

LIU, D., SAFARI, A., O'CONNOR, M., CHAN, D., LAEGELER, A., QIN, J. & SONGYANG, Z. 2004. Ptop Interacts with Pot1 and Regulates Its Localization to Telomeres. *Nature Cell Biology,* 6**,** 673-680.

LOAYZA, D., PARSONS, H., DONIGIAN, J., HOKE, K. & DE LANGE, T. 2004. DNA Binding Features of Human Pot1: A Nonamer 5'-Tagggttag-3' Minimal Binding Site, Sequence Specificity, and Internal Binding to Multimeric Sites. *The Journal of Biological Chemistry,* 279**,** 13241-13248.

LU, W., ZHANG, Y., LIU, D., SONGYANG, Z. & WAN, M. 2013. Telomeres-Structure, Function, and Regulation. *Experimental Cell Research,* 319**,** 133-141.

LUKE-GLASER, S., POSCHKE, H. & LUKE, B. 2012. Getting in (and out of) the Loop: Regulating Higher Order Telomere Structures. *Frontiers in Oncology,* 2**,** 180.

MAHANEY, B., MEEK, K. & LEES-MILLER, S. 2009. Repair of Ionizing Radiation-Induced DNA Double-Strand Breaks by Non-Homologous End-Joining. *The Biochemical Journal,* 417**,** 639-650.

MARINGELE, L. & LYDALL, D. 2002. Exo1-Dependent Single-Stranded DNA at Telomeres Activates Subsets of DNA Damage and Spindle Checkpoint Pathways in Budding Yeast Yku70delta Mutants. *Genes & Development,* 16**,** 1919-1933.

MARTÍN, V., DU, L.-L., ROZENZHAK, S. & RUSSELL, P. 2007. Protection of Telomeres by a Conserved Stn1-Ten1 Complex. *Proceedings of the National Academy of Sciences of the United States of America,* 104**,** 14038-14043.

MASER, R. & DEPINHO, R. 2004. Telomeres and the DNA Damage Response: Why the Fox Is Guarding the Henhouse. *DNA Repair,* 3**,** 979-988.

MASON, J., FRYDRYCHOVA, R. & BIESSMANN, H. 2008. Drosophila Telomeres: An Exception Providing New Insights. *BioEssays : News and Reviews in Molecular, Cellular and Developmental Biology,* 30**,** 25-37.

MASUDA-SASA, T., POLACZEK, P., PENG, X., CHEN, L. & CAMPBELL, J. 2008. Processing of G4 DNA by Dna2 Helicase/Nuclease and Replication Protein a (Rpa) Provides Insights into the Mechanism of Dna2/Rpa Substrate Recognition. *The Journal of Biological Chemistry,* 283**,** 24359-24373.

MCVEY, M. & LEE, S. 2008. Mmej Repair of Double-Strand Breaks (Director's Cut): Deleted Sequences and Alternative Endings. *Trends in Genetics : TIG,* 24**,** 529-538.

MITCHELL, J., CHENG, J. & COLLINS, K. 1999a. A Box H/Aca Small Nucleolar Rna-Like Domain at the Human Telomerase Rna 3' End. *Molecular and Cellular Biology,* 19**,** 567-576.

MITCHELL, J., WOOD, E. & COLLINS, K. 1999b. A Telomerase Component Is Defective in the Human Disease Dyskeratosis Congenita. *Nature,* 402**,** 551-555.

MITCHELL, M., SMITH, J., MASON, M., HARPER, S., SPEICHER, D., JOHNSON, F. & SKORDALAKES, E. 2010. Cdc13 N-Terminal Dimerization, DNA Binding, and Telomere Length Regulation. *Molecular and Cellular Biology,* 30**,** 5325-5334.

MIYABE, I., KUNKEL, T. & CARR, A. 2011. The Major Roles of DNA Polymerases Epsilon and Delta at the Eukaryotic Replication Fork Are Evolutionarily Conserved. *PLoS Genetics,* 7.

MIYAKE, Y., NAKAMURA, M., NABETANI, A., SHIMAMURA, S., TAMURA, M., YONEHARA, S., SAITO, M. & ISHIKAWA, F. 2009. Rpa-Like Mammalian Ctc1-Stn1-Ten1 Complex Binds to Single-Stranded DNA and Protects Telomeres Independently of the Pot1 Pathway. *Molecular Cell,* 36**,** 193-206.

MIYOSHI, T., KANOH, J., SAITO, M. & ISHIKAWA, F. 2008. Fission Yeast Pot1-Tpp1 Protects Telomeres and Regulates Telomere Length. *Science (New York, N.Y.),* 320**,** 1341-1344.

MOL, C., HOSFIELD, D. & TAINER, J. 2000. Abasic Site Recognition by Two Apurinic/Apyrimidinic Endonuclease Families in DNA Base Excision Repair: The 3' Ends Justify the Means. *Mutation Research,* 460**,** 211-229.

MOSER, B., CHANG, Y.-T., KOSTI, J. & NAKAMURA, T. 2011. Tel1atm and Rad3atr Kinases Promote Ccq1-Est1 Interaction to Maintain Telomeres in Fission Yeast. *Nature Structural & Molecular Biology,* 18**,** 1408-1413.

MOYER, S., LEWIS, P. & BOTCHAN, M. 2006. Isolation of the Cdc45/Mcm2-7/Gins (Cmg) Complex, a Candidate for the Eukaryotic DNA Replication Fork Helicase. *Proceedings of the National Academy of Sciences of the United States of America,* 103**,** 10236-10241.

MUÑOZ-JORDÁN, J., CROSS, G. & DE, T. 2001. T-Loops at Trypanosome Telomeres. *The EMBO Journal*, 20**,** 579-588.

MURRAY, J., LINDSAY, H., MUNDAY, C. & CARR, A. 1997. Role of Schizosaccharomyces Pombe Recq Homolog, Recombination, and Checkpoint Genes in Uv Damage Tolerance. *Molecular and Cellular Biology,* 17**,** 6868-6875.

MURTI, K. & PRESCOTT, D. 1999. Telomeres of Polytene Chromosomes in a Ciliated Protozoan Terminate in Duplex DNA Loops. *Proceedings of the National Academy of Sciences of the United States of America,* 96**,** 14436-14439.

NAITO, T., MATSUURA, A. & ISHIKAWA, F. 1998. Circular Chromosome Formation in a Fission Yeast Mutant Defective in Two Atm Homologues. *Nature Genetics,* 20**,** 203-206.

NAKAMURA, T. & CECH, T. 1998. Reversing Time: Origin of Telomerase. *Cell,* 92**,** 587-590.

NAKAMURA, T., COOPER, J. & CECH, T. 1998. Two Modes of Survival of Fission Yeast without Telomerase. *Science (New York, N.Y.),* 282**,** 493-496.

NAKAMURA, T., MORIN, G., CHAPMAN, K., WEINRICH, S., ANDREWS, W., LINGNER, J., HARLEY, C. & CECH, T. 1997. Telomerase Catalytic Subunit Homologs from Fission Yeast and Human. *Science (New York, N.Y.),* 277**,** 955-959.

NANBU, T., TAKAHASHI, K., MURRAY, J., HIRATA, N., UKIMORI, S., KANKE, M., MASUKATA, H., YUKAWA, M., TSUCHIYA, E. & UENO, M. 2013. Fission Yeast Recq Helicase Rqh1 Is Required for the Maintenance of Circular Chromosomes. *Molecular and Cellular Biology,* 33**,** 1175-1187.

NANDAKUMAR, J., BELL, C., WEIDENFELD, I., ZAUG, A., LEINWAND, L. & CECH, T. 2012. The Tel Patch of Telomere Protein Tpp1 Mediates Telomerase Recruitment and Processivity. *Nature,* 492**,** 285-289.

NANDAKUMAR, J. & CECH, T. 2012. DNA-Induced Dimerization of the Single-Stranded DNA Binding Telomeric Protein Pot1 from Schizosaccharomyces Pombe. *Nucleic Acids Research,* 40**,** 235-244.

NANDAKUMAR, J. & CECH, T. 2013. Finding the End: Recruitment of Telomerase to Telomeres. *Nature reviews. Molecular Cell Biology,* 14**,** 69-82.

NG, P. & HENIKOFF, S. 2006. Predicting the Effects of Amino Acid Substitutions on Protein Function. *Annual Review of Genomics and Human Genetics,* 7**,** 61-80.

NOSEK, J., DINOUËL, N., KOVAC, L. & FUKUHARA, H. 1995. Linear Mitochondrial Dnas from Yeasts: Telomeres with Large Tandem Repetitions. *Molecular & General Genetics : MGG,* 247**,** 61-72.

NUGENT, C., HUGHES, T., LUE, N. & LUNDBLAD, V. 1996. Cdc13p: A Single-Strand Telomeric DNA-Binding Protein with a Dual Role in Yeast Telomere Maintenance. *Science (New York, N.Y.),* 274, 249-252.

NURSE, P. 1997. Regulation of the Eukaryotic Cell Cycle. *European Journal of Cancer (Oxford, England : 1990),* 33, 1002-1004.

O'CONNOR, M., SAFARI, A., XIN, H., LIU, D. & SONGYANG, Z. 2006. A Critical Role for Tpp1 and Tin2 Interaction in High-Order Telomeric Complex Assembly. *Proceedings of the National Academy of Sciences of the United States of America,* 103, 11874-11879.

O'SULLIVAN, R. & KARLSEDER, J. 2010. Telomeres: Protecting Chromosomes against Genome Instability. *Nature reviews. Molecular Cell Biology,* 11, 171-181.

OKAZAKI, R., OKAZAKI, T., SAKABE, K., SUGIMOTO, K. & SUGINO, A. 1968. Mechanism of DNA Chain Growth. I. Possible Discontinuity and Unusual Secondary Structure of Newly Synthesized Chains. *Proceedings of the National Academy of Sciences of the United States of America,* 59, 598-605.

OPRESKO, P., OTTERLEI, M., GRAAKJAER, J., BRUHEIM, P., DAWUT, L., KØLVRAA, S., MAY, A., SEIDMAN, M. & BOHR, V. 2004. The Werner Syndrome Helicase and Exonuclease Cooperate to Resolve Telomeric D Loops in a Manner Regulated by Trf1 and Trf2. *Molecular Cell,* 14, 763-774.

OPRESKO, P., VON KOBBE, C., LAINE, J.-P., HARRIGAN, J., HICKSON, I. & BOHR, V. 2002. Telomere-Binding Protein Trf2 Binds to and Stimulates the Werner and Bloom Syndrome Helicases. *The Journal of Biological Chemistry,* 277, 41110-41119.

PALM, W. & DE LANGE, T. 2008. How Shelterin Protects Mammalian Telomeres. *Annual Review of Genetics,* 42, 301-334.

PALM, W., HOCKEMEYER, D., KIBE, T. & DE LANGE, T. 2009. Functional Dissection of Human and Mouse Pot1 Proteins. *Molecular and Cellular Biology,* 29, 471-482.

PALZKILL, T. & NEWLON, C. 1988. A Yeast Replication Origin Consists of Multiple Copies of a Small Conserved Sequence. *Cell,* 53, 441-450.

PÂQUES, F. & HABER, J. 1999. Multiple Pathways of Recombination Induced by Double-Strand Breaks in Saccharomyces Cerevisiae. *Microbiology and Molecular Biology Reviews : MMBR,* 63, 349-404.

PARDUE, M.-L. & DEBARYSHE, P. 2003. Retrotransposons Provide an Evolutionarily Robust Non-Telomerase Mechanism to Maintain Telomeres. *Annual Review of Genetics,* 37, 485-511.

PIRES, D., ASCHER, D. & BLUNDELL, T. 2013. Mcsm: Predicting the Effects of Mutations in Proteins Using Graph-Based Signatures. *Bioinformatics (Oxford, England)*, 30, 335-342.

PITT, C. & COOPER, J. 2010. Pot1 Inactivation Leads to Rampant Telomere Resection and Loss in One Cell Cycle. *Nucleic Acids Research,* 38, 6968-6975.

POULET, A., BUISSON, R., FAIVRE-MOSKALENKO, C., KOELBLEN, M., AMIARD, S., MONTEL, F., CUESTA-LOPEZ, S., BORNET, O., GUERLESQUIN, F., GODET, T., MOUKHTAR, J., ARGOUL,

F., DÉCLAIS, A.-C., LILLEY, D., IP, S., WEST, S., GILSON, E. & GIRAUD-PANIS, M.-J. 2009. Trf2 Promotes, Remodels and Protects Telomeric Holliday Junctions. *The EMBO Journal,* 28**,** 641-651.

PRICE, C., BOLTZ, K., CHAIKEN, M., STEWART, J., BEILSTEIN, M. & SHIPPEN, D. 2010. Evolution of Cst Function in Telomere Maintenance. *Cell Cycle (Georgetown, Tex.),* 9**,** 3157-3165.

PRINGLE, J. R. & HARTWELL, L. H. 1981. The *Saccharomyces Cerevisiae* Cell Cycle. *In:* STRATHERN, J. N., JONES, E. W. & BROACH, J. R. (eds.) *Molecular Biology of the Yeast Saccharomyces: Life Cycle and Inheritance.* Cold Spring Harbor, NY: Cold Spring Harbor Laboratory.

PRITCHARD, L., CORNE, D., KELL, D., ROWLAND, J. & WINSON, M. 2005. A General Model of Error-Prone Pcr. *Journal of Theoretical Biology,* 234**,** 497-509.

PUGLISI, A., BIANCHI, A., LEMMENS, L., DAMAY, P. & SHORE, D. 2008. Distinct Roles for Yeast Stn1 in Telomere Capping and Telomerase Inhibition. *The EMBO Journal,* 27**,** 2328-2339.

QI, H. & ZAKIAN, V. 2000. The Saccharomyces Telomere-Binding Protein Cdc13p Interacts with Both the Catalytic Subunit of DNA Polymerase Alpha and the Telomerase-Associated Est1 Protein. *Genes & Development,* 14**,** 1777-1788.

RADHAKRISHNAN, S., JETTE, N. & LEES-MILLER, S. 2014. Non-Homologous End Joining: Emerging Themes and Unanswered Questions. *DNA Repair*.

RAFFA, G., RAIMONDO, D., SORINO, C., CUGUSI, S., CENCI, G., CACCHIONE, S., GATTI, M. & CIAPPONI, L. 2010. Verrocchio, a Drosophila Ob Fold-Containing Protein, Is a Component of the Terminin Telomere-Capping Complex. *Genes & Development,* 24**,** 1596-1601.

RAFFA, G., SIRIACO, G., CUGUSI, S., CIAPPONI, L., CENCI, G., WOJCIK, E. & GATTI, M. 2009. The Drosophila Modigliani (Moi) Gene Encodes a Hoap-Interacting Protein Required for Telomere Protection. *Proceedings of the National Academy of Sciences of the United States of America,* 106**,** 2271-2276.

RAJI, H. & HARTSUIKER, E. 2006. Double-Strand Break Repair and Homologous Recombination in Schizosaccharomyces Pombe. *Yeast (Chichester, England),* 23**,** 963-976.

RASHKOVA, S., ATHANASIADIS, A. & PARDUE, M. L. 2003. Intracellular Targeting of Gag Proteins of the Drosophila Telomeric Retrotransposons. *Journal of Virology,* 77**,** 6376-6384.

REICHENBACH, P., HÖSS, M., AZZALIN, C., NABHOLZ, M., BUCHER, P. & LINGNER, J. 2003. A Human Homolog of Yeast Est1 Associates with Telomerase and Uncaps Chromosome Ends When Overexpressed. *Current Biology : CB,* 13**,** 568-574.

REKOSH, D., RUSSELL, W., BELLET, A. & ROBINSON, A. 1977. Identification of a Protein Linked to the Ends of Adenovirus DNA. *Cell,* 11**,** 283-295.

RIBES-ZAMORA, A., INDIVIGLIO, S., MIHALEK, I., WILLIAMS, C. & BERTUCH, A. 2013. Trf2 Interaction with Ku Heterotetramerization Interface Gives Insight into C-Nhej Prevention at Human Telomeres. *Cell Reports,* 5**,** 194-206.

RICHARD, P., DARZACQ, X., BERTRAND, E., JÁDY, B., VERHEGGEN, C. & KISS, T. 2003. A Common Sequence Motif Determines the Cajal Body-Specific Localization of Box H/Aca Scarnas. *The EMBO Journal,* 22**,** 4283-4293.

RIETHMAN, H., AMBROSINI, A. & PAUL, S. 2005. Human Subtelomere Structure and Variation. *Chromosome Research : an international journal on the molecular, supramolecular and evolutionary aspects of chromosome biology,* 13**,** 505-515.

ROBERTSON, A., KLUNGLAND, A., ROGNES, T. & LEIROS, I. 2009. DNA Repair in Mammalian Cells: Base Excision Repair: The Long and Short of It. *Cellular and Molecular Life Sciences : CMLS,* 66**,** 981-993.

ROST, B., YACHDAV, G. & LIU, J. 2004. The Predictprotein Server. *Nucleic Acids Research,* 32**,** 6.

RUDIN, N. & HABER, J. 1988. Efficient Repair of Ho-Induced Chromosomal Breaks in Saccharomyces Cerevisiae by Recombination between Flanking Homologous Sequences. *Molecular and Cellular Biology,* 8**,** 3918-3928.

SABATINOS, S. & FORSBURG, S. 2010. Molecular Genetics of Schizosaccharomyces Pombe. *Methods in Enzymology,* 470**,** 759-795.

SEGURADO, M., DE LUIS, A. & ANTEQUERA, F. 2003. Genome-Wide Distribution of DNA Replication Origins at a+T-Rich Islands in Schizosaccharomyces Pombe. *EMBO Reports,* 4**,** 1048-1053.

SHAY, J., ZOU, Y., HIYAMA, E. & WRIGHT, W. 2001. Telomerase and Cancer. *Human Molecular Genetics,* 10**,** 677-685.

SIEVERS, F., WILM, A., DINEEN, D., GIBSON, T., KARPLUS, K., LI, W., LOPEZ, R., MCWILLIAM, H., REMMERT, M., SÖDING, J., THOMPSON, J. & HIGGINS, D. 2011. Fast, Scalable Generation of High-Quality Protein Multiple Sequence Alignments Using Clustal Omega. *Molecular Systems Biology,* 7**,** 539.

SIPICZKI, M. 2000. Where Does Fission Yeast Sit on the Tree of Life? *Genome Biology,* 1.

SLIJEPCEVIC, P. & AL-WAHIBY, S. 2005. Telomere Biology: Integrating Chromosomal End Protection with DNA Damage Response. *Chromosoma,* 114**,** 275-285.

SOGO, J., LOPES, M. & FOIANI, M. 2002. Fork Reversal and Ssdna Accumulation at Stalled Replication Forks Owing to Checkpoint Defects. *Science (New York, N.Y.),* 297**,** 599-602.

SONG, X., LEEHY, K., WARRINGTON, R., LAMB, J., SUROVTSEVA, Y. & SHIPPEN, D. 2008. Stn1 Protects Chromosome Ends in Arabidopsis Thaliana. *Proceedings of the National Academy of Sciences of the United States of America,* 105**,** 19815-19820.

STANSEL, R., DE LANGE, T. & GRIFFITH, J. 2001. T-Loop Assembly in Vitro Involves Binding of Trf2 near the 3' Telomeric Overhang. *The EMBO Journal,* 20**,** 5532-5540.

STELLWAGEN, A., HAIMBERGER, Z., VEATCH, J. & GOTTSCHLING, D. 2003. Ku Interacts with Telomerase Rna to Promote Telomere Addition at Native and Broken Chromosome Ends. *Genes & Development,* 17**,** 2384-2395.

STEWART, J., WANG, F., CHAIKEN, M., KASBEK, C., CHASTAIN, P., WRIGHT, W. & PRICE, C. 2012. Human Cst Promotes Telomere Duplex Replication and General Replication Restart after Fork Stalling. *The EMBO Journal,* 31**,** 3537-3549.

STILLMAN, B. 2008. DNA Polymerases at the Replication Fork in Eukaryotes. *Molecular Cell,* 30**,** 259-260.

SUGAWARA, N., IRA, G. & HABER, J. 2000. DNA Length Dependence of the Single-Strand Annealing Pathway and the Role of Saccharomyces Cerevisiae Rad59 in Double-Strand Break Repair. *Molecular and Cellular Biology,* 20**,** 5300-5309.

SUGAWARA, N., PÂQUES, F., COLAIÁCOVO, M. & HABER, J. 1997. Role of Saccharomyces Cerevisiae Msh2 and Msh3 Repair Proteins in Double-Strand Break-Induced Recombination. *Proceedings of the National Academy of Sciences of the United States of America,* 94**,** 9214-9219.

SUGIYAMA, T., CAM, H., SUGIYAMA, R., NOMA, K.-I., ZOFALL, M., KOBAYASHI, R. & GREWAL, S. 2007. Shrec, an Effector Complex for Heterochromatic Transcriptional Silencing. *Cell,* 128**,** 491-504.

SUN, J., YANG, Y., WAN, K., MAO, N., YU, T.-Y., LIN, Y.-C., DEZWAAN, D., FREEMAN, B., LIN, J.-J., LUE, N. & LEI, M. 2011. Structural Bases of Dimerization of Yeast Telomere Protein Cdc13 and Its Interaction with the Catalytic Subunit of DNA Polymerase A. *Cell Research,* 21**,** 258-274.

SUN, J., YU, E., YANG, Y., CONFER, L., SUN, S., WAN, K., LUE, N. & LEI, M. 2009. Stn1-Ten1 Is an Rpa2-Rpa3-Like Complex at Telomeres. *Genes & Development,* 23**,** 2900-2914.

SUNG, P. & KLEIN, H. 2006. Mechanism of Homologous Recombination: Mediators and Helicases Take on Regulatory Functions. *Nature reviews. Molecular Cell Biology,* 7**,** 739-750.

SUROVTSEVA, Y., CHURIKOV, D., BOLTZ, K., SONG, X., LAMB, J., WARRINGTON, R., LEEHY, K., HEACOCK, M., PRICE, C. & SHIPPEN, D. 2009. Conserved Telomere Maintenance Component 1 Interacts with Stn1 and Maintains Chromosome Ends in Higher Eukaryotes. *Molecular Cell,* 36**,** 207-218.

SZOSTAK, J., ORR-WEAVER, T., ROTHSTEIN, R. & STAHL, F. 1983. The Double-Strand-Break Repair Model for Recombination. *Cell,* 33**,** 25-35.

TAKAI, K., KIBE, T., DONIGIAN, J., FRESCAS, D. & DE LANGE, T. 2011. Telomere Protection by Tpp1/Pot1 Requires Tethering to Tin2. *Molecular Cell,* 44**,** 647-659.

TAKEDA, D. & DUTTA, A. 2005. DNA Replication and Progression through S Phase. *Oncogene,* 24**,** 2827-2843.

TAMARU, H. 2010. Confining Euchromatin/Heterochromatin Territory: Jumonji Crosses the Line. *Genes & Development,* 24**,** 1465-1478.

TANG, W., KANNAN, R., BLANCHETTE, M. & BAUMANN, P. 2012. Telomerase Rna Biogenesis Involves Sequential Binding by Sm and Lsm Complexes. *Nature,* 484**,** 260-264.

THOMAS, L., STILLMAN, D. & THORBURN, A. 2002. Regulation of Fas-Associated Death Domain Interactions by the Death Effector Domain Identified by a Modified Reverse Two-Hybrid Screen. *The Journal of Biological Chemistry,* 277**,** 34343-34348.

TOMASKA, L., MAKHOV, A., GRIFFITH, J. & NOSEK, J. 2002. T-Loops in Yeast Mitochondria. *Mitochondrion,* 1**,** 455-459.

TOMASKA, L., WILLCOX, S., SLEZAKOVA, J., NOSEK, J. & GRIFFITH, J. 2004. Taz1 Binding to a Fission Yeast Model Telomere: Formation of Telomeric Loops and Higher Order Structures. *The Journal of Biological Chemistry,* 279**,** 50764-50772.

TOMITA, K. & COOPER, J. 2008. Fission Yeast Ccq1 Is Telomerase Recruiter and Local Checkpoint Controller. *Genes & Development,* 22**,** 3461-3474.

TOMITA, K., KIBE, T., KANG, H.-Y., SEO, Y.-S., URITANI, M., USHIMARU, T. & UENO, M. 2004. Fission Yeast Dna2 Is Required for Generation of the Telomeric Single-Strand Overhang. *Molecular and Cellular Biology,* 24**,** 9557-9567.

TOMITA, K., MATSUURA, A., CASPARI, T., CARR, A., AKAMATSU, Y., IWASAKI, H., MIZUNO, K.-I., OHTA, K., URITANI, M., USHIMARU, T., YOSHINAGA, K. & UENO, M. 2003. Competition between the Rad50 Complex and the Ku Heterodimer Reveals a Role for Exo1 in Processing Double-Strand Breaks but Not Telomeres. *Molecular and Cellular Biology,* 23**,** 5186-5197.

TRUONG, L., LI, Y., SHI, L., HWANG, P., HE, J., WANG, H., RAZAVIAN, N., BERNS, M. & WU, X. 2013. Microhomology-Mediated End Joining and Homologous Recombination Share the Initial End Resection Step to Repair DNA Double-Strand Breaks in Mammalian Cells. *Proceedings of the National Academy of Sciences of the United States of America,* 110**,** 7720-7725.

UNTERGASSER, A., CUTCUTACHE, I., KORESSAAR, T., YE, J., FAIRCLOTH, B., REMM, M. & ROZEN, S. 2012. Primer3--New Capabilities and Interfaces. *Nucleic Acids Research,* 40.

VAN STEENSEL, B., SMOGORZEWSKA, A. & DE LANGE, T. 1998. Trf2 Protects Human Telomeres from End-to-End Fusions. *Cell,* 92**,** 401-413.

VANNIER, J.-B., PAVICIC-KALTENBRUNNER, V., PETALCORIN, M., DING, H. & BOULTON, S. 2012. Rtel1 Dismantles T Loops and Counteracts Telomeric G4-DNA to Maintain Telomere Integrity. *Cell,* 149**,** 795-806.

VENTEICHER, A., ABREU, E., MENG, Z., MCCANN, K., TERNS, R., VEENSTRA, T., TERNS, M. & ARTANDI, S. 2009. A Human Telomerase Holoenzyme Protein Required for Cajal Body Localization and Telomere Synthesis. *Science (New York, N.Y.),* 323**,** 644-648.

VENTEICHER, A. & ARTANDI, S. 2009. Tcab1: Driving Telomerase to Cajal Bodies. *Cell Cycle (Georgetown, Tex.),* 8**,** 1329-1331.

VERDUN, R. & KARLSEDER, J. 2007. Replication and Protection of Telomeres. *Nature,* 447**,** 924-931.

WANG, F., PODELL, E., ZAUG, A., YANG, Y., BACIU, P., CECH, T. & LEI, M. 2007. The Pot1-Tpp1 Telomere Complex Is a Telomerase Processivity Factor. *Nature,* 445**,** 506-510.

WANG, F., STEWART, J., KASBEK, C., ZHAO, Y., WRIGHT, W. & PRICE, C. 2012. Human Cst Has Independent Functions During Telomere Duplex Replication and C-Strand Fill-In. *Cell Reports,* 2**,** 1096-1103.

WANG, X. & BAUMANN, P. 2008. Chromosome Fusions Following Telomere Loss Are Mediated by Single-Strand Annealing. *Molecular Cell,* 31**,** 463-473.

WATSON, A., GARCIA, V., BONE, N., CARR, A. & ARMSTRONG, J. 2008. Gene Tagging and Gene Replacement Using Recombinase-Mediated Cassette Exchange in Schizosaccharomyces Pombe. *Gene,* 407**,** 63-74.

WEBB, C. & ZAKIAN, V. 2008. Identification and Characterization of the Schizosaccharomyces Pombe Ter1 Telomerase Rna. *Nature Structural & Molecular Biology,* 15**,** 34-42.

WEBB, C. & ZAKIAN, V. 2012. Schizosaccharomyces Pombe Ccq1 and Ter1 Bind the 14-3-3-Like Domain of Est1, Which Promotes and Stabilizes Telomerase-Telomere Association. *Genes & Development,* 26**,** 82-91.

WEBER, J. 2009. Proteinshader: Illustrative Rendering of Macromolecules. *BMC Structural Biology,* 9**,** 19.

WELLINGER, R. 2009. The Cst Complex and Telomere Maintenance: The Exception Becomes the Rule. *Molecular Cell,* 36**,** 168-169.

WILLIAMS, G., LEES-MILLER, S. & TAINER, J. 2010. Mre11-Rad50-Nbs1 Conformations and the Control of Sensing, Signaling, and Effector Responses at DNA Double-Strand Breaks. *DNA Repair,* 9**,** 1299-1306.

WILLIS, N. & RHIND, N. 2009. Mus81, Rhp51(Rad51), and Rqh1 Form an Epistatic Pathway Required for the S-Phase DNA Damage Checkpoint. *Molecular Biology of the Cell,* 20**,** 819-833.

WINTJENS, R. & ROOMAN, M. 1996. Structural Classification of Hth DNA-Binding Domains and Protein-DNA Interaction Modes. *Journal of Molecular Biology,* 262**,** 294-313.

WIXON, J. 2002. Featured Organism: Schizosaccharomyces Pombe, the Fission Yeast. *Comparative and Functional Genomics,* 3**,** 194-204.

WOOD, V., GWILLIAM, R., RAJANDREAM, M. A., LYNE, M., LYNE, R., STEWART, A., SGOUROS, J., PEAT, N., HAYLES, J., BAKER, S., BASHAM, D., BOWMAN, S., BROOKS, K., BROWN, D., BROWN, S., CHILLINGWORTH, T., CHURCHER, C., COLLINS, M., CONNOR, R., CRONIN, A., DAVIS, P., FELTWELL, T., FRASER, A., GENTLES, S., GOBLE, A., HAMLIN, N., HARRIS, D., HIDALGO, J., HODGSON, G., HOLROYD, S., HORNSBY, T., HOWARTH, S., HUCKLE, E., HUNT, S., JAGELS, K., JAMES, K., JONES, L., JONES, M., LEATHER, S., MCDONALD, S., MCLEAN, J., MOONEY, P., MOULE, S., MUNGALL, K., MURPHY, L., NIBLETT, D., ODELL, C., OLIVER, K., O'NEIL, S., PEARSON, D., QUAIL, M., RABBINOWITSCH, E., RUTHERFORD, K., RUTTER, S., SAUNDERS, D., SEEGER, K., SHARP, S., SKELTON, J., SIMMONDS, M., SQUARES, R., SQUARES, S., STEVENS, K., TAYLOR, K., TAYLOR, R., TIVEY, A., WALSH, S., WARREN, T., WHITEHEAD, S., WOODWARD, J., VOLCKAERT, G., AERT, R., ROBBEN, J., GRYMONPREZ, B., WELTJENS, I., VANSTREELS, E., RIEGER, M., SCHÄFER, M., MÜLLER-AUER, S., GABEL, C., FUCHS, M., DÜSTERHÖFT, A., FRITZC, C., HOLZER, E., MOESTL, D., HILBERT, H., BORZYM, K., LANGER, I., BECK, A., LEHRACH, H., REINHARDT, R., POHL, T., EGER, P., ZIMMERMANN, W., WEDLER, H., WAMBUTT, R., PURNELLE, B., GOFFEAU, A.,

CADIEU, E., DRÉANO, S. & GLOUX, S. 2002. The Genome Sequence of Schizosaccharomyces Pombe. *Nature,* 415**,** 871-880.

WOOD, V., HARRIS, M., MCDOWALL, M., RUTHERFORD, K., VAUGHAN, B., STAINES, D., ASLETT, M., LOCK, A., BÄHLER, J., KERSEY, P. & OLIVER, S. 2012. Pombase: A Comprehensive Online Resource for Fission Yeast. *Nucleic Acids Research,* 40**,** 9.

WORTH, C., PREISSNER, R. & BLUNDELL, T. 2011. Sdm--a Server for Predicting Effects of Mutations on Protein Stability and Malfunction. *Nucleic Acids Research,* 39**,** 22.

WRIGHT, W., TESMER, V., HUFFMAN, K., LEVENE, S. & SHAY, J. 1997. Normal Human Chromosomes Have Long G-Rich Telomeric Overhangs at One End. *Genes & Development,* 11**,** 2801-2809.

WU, L., MULTANI, A., HE, H., COSME-BLANCO, W., DENG, Y., DENG, J., BACHILO, O., PATHAK, S., TAHARA, H., BAILEY, S., DENG, Y., BEHRINGER, R. & CHANG, S. 2006. Pot1 Deficiency Initiates DNA Damage Checkpoint Activation and Aberrant Homologous Recombination at Telomeres. *Cell,* 126**,** 49-62.

WU, P., TAKAI, H. & DE LANGE, T. 2012. Telomeric 3' Overhangs Derive from Resection by Exo1 and Apollo and Fill-in by Pot1b-Associated Cst. *Cell,* 150**,** 39-52.

WU, Y., MITCHELL, T. & ZHU, X.-D. 2008. Human Xpf Controls Trf2 and Telomere Length Maintenance through Distinctive Mechanisms. *Mechanisms of Ageing and Development,* 129**,** 602-610.

WU, Y., XIAO, S. & ZHU, X.-D. 2007. Mre11-Rad50-Nbs1 and Atm Function as Co-Mediators of Trf1 in Telomere Length Control. *Nature Structural & Molecular Biology,* 14**,** 832-840.

XU, Y.-J., DAVENPORT, M. & KELLY, T. 2006. Two-Stage Mechanism for Activation of the DNA Replication Checkpoint Kinase Cds1 in Fission Yeast. *Genes & Development,* 20**,** 990-1003.

YAMAZAKI, H., TARUMOTO, Y. & ISHIKAWA, F. 2012. Tel1(Atm) and Rad3(Atr) Phosphorylate the Telomere Protein Ccq1 to Recruit Telomerase and Elongate Telomeres in Fission Yeast. *Genes & Development,* 26**,** 241-246.

YANG, D., HE, Q., KIM, H., MA, W. & SONGYANG, Z. 2011. Tin2 Protein Dyskeratosis Congenita Missense Mutants Are Defective in Association with Telomerase. *J Biol Chem,* 286**,** 23022-30.

YE, J., HOCKEMEYER, D., KRUTCHINSKY, A., LOAYZA, D., HOOPER, S., CHAIT, B. & DE LANGE, T. 2004. Pot1-Interacting Protein Pip1: A Telomere Length Regulator That Recruits Pot1 to the Tin2/Trf1 Complex. *Genes & Development,* 18**,** 1649-1654.

ZAHLER, A., WILLIAMSON, J., CECH, T. & PRESCOTT, D. 1991. Inhibition of Telomerase by G-Quartet DNA Structures. *Nature,* 350**,** 718-720.

ZEGERMAN, P. & DIFFLEY, J. 2009. DNA Replication as a Target of the DNA Damage Checkpoint. *DNA Repair,* 8**,** 1077-1088.

ZHANG, Y., CHEN, L.-Y., HAN, X., XIE, W., KIM, H., YANG, D., LIU, D. & SONGYANG, Z. 2013. Phosphorylation of Tpp1 Regulates Cell Cycle-Dependent Telomerase Recruitment.

Proceedings of the National Academy of Sciences of the United States of America, 110**,** 5457-5462.

ZHAO, Y., SFEIR, A., ZOU, Y., BUSEMAN, C., CHOW, T., SHAY, J. & WRIGHT, W. 2009. Telomere Extension Occurs at Most Chromosome Ends and Is Uncoupled from Fill-in in Human Cancer Cells. *Cell,* 138**,** 463-475.

ZHONG, F., BATISTA, L., FREUND, A., PECH, M., VENTEICHER, A. & ARTANDI, S. 2012. Tpp1 Ob-Fold Domain Controls Telomere Maintenance by Recruiting Telomerase to Chromosome Ends. *Cell,* 150**,** 481-494.

ZHONG, Z., SHIUE, L., KAPLAN, S. & DE LANGE, T. 1992. A Mammalian Factor That Binds Telomeric Ttaggg Repeats in Vitro. *Molecular and Cellular Biology,* 12**,** 4834-4843.

ZONNEVELD, B. & VAN DER ZANDEN, A. 1995. The Red Ade Mutants of Kluyveromyces Lactis and Their Classification by Complementation with Cloned Ade1 or Ade2 Genes from Saccharomyces Cerevisiae. *Yeast (Chichester, England),* 11**,** 823-827.

"We've done the impossible, and that makes us mighty."

- Sergeant Malcolm "Mal" Reynolds, *Firefly*[1]

[1] "Serenity." *Firefly* (2002), Writ. Joss Whedon. Dir. Joss Whedon. Perf. Nathan Fillion. 20th Century Fox Television (USA), 20 December 2002.